A STUDY OF THE ELECTRICAL AND OPTICAL PROPERTIES OF UNHYDROGENATED NEON-SPUTTERED AMORPHOUS SILICON

by

SALEM AL-ABD ABO-NAMOUS
M.Sc. (Univ. of L'pool)

A Thesis submitted to the Faculty of Science at the University of Aston in Birmingham for the Degree of

Doctor of Philosophy

JULY 1984

The University of Aston in Birmingham

A STUDY OF THE ELECTRICAL AND OPTICAL PROPERTIES OF UNHYDROGENATED NEON-SPUTTERED AMORPHOUS SILICON

Salem Al-Abd Abo-Namous

Submitted for the Degree of Doctor of Philosophy (1984)

ABSTRACT

Films of amorphous silicon (a-Si) were prepared by r.f. sputtering in a Ne plasma without the addition of hydrogen or a halogen. The d.c. dark electrical conductivity, the optical gap and the photoconductivity of the films were investigated for a range of preparation conditions, the sputtering gas pressure, P, the target-substrate spacing, d, the self-bias voltage, V_{sb}, on the target and the substrate temperature, T_s. The dependence of the electrical and optical properties on these conditions showed that various combinations of P, d and V_{sb}, at a constant T_s, giving the same product (Pd/V_{sb}) result in films with similar properties, provided that P, d and V_{sb} remain within a certain range.

Variation of Pd/V_{sb} between about 0.2 and 0.8 mTorr.cm/V varied the dark conductivity over about 4 orders of magnitude, the optical gap by 0.5 eV and the photoconductivity over 4-5 orders of magnitude. This is attributed to controlling the density-of-states distribution in the mobility gap. The temperature-dependence of photoconductivity and the photoresponse of undoped films are in support of this conclusion. Films prepared at relatively high (Pd/V_{sb}) values and T_s=300 °C exhibited low dark-conductivity and high thermal activation energy, optical gap and photoresponse, characteristic properties of a low density-of-states material.

P-type doping with group-III elements (Al, B and Ga) by sputtering from a composite target or from a predoped target (B-doped) was investigated. The systematic variation of room-temperature conductivity over many orders of magnitude and a Fermi-level shift of about 0.7 eV towards the valence-band edge suggest that substitutional doping had taken place. The effects of preparation conditions on doping efficiency were also investigated.

The post-deposition annealing of undoped and doped films were studied for a temperature range from 250 °C to 470 °C. It was shown that annealing enhanced the doping efficiency considerably, although it had little effect on the basic material (a-Si) prepared at the optimum conditions (Pd/V_{sb}=0.8 mTorr.cm/V and T_s=300 °C).

Preliminary experiments on devices imply potential applications of the present material, such as p-n and MS junctions.

KEY WORDS: Ne-Sputtering, a-Si, Electrical & Optical Properties.

بسم الله الرحمن الرحيم

الحمد لله رب العالمين

TO

MY MOTHER

THE SOUL OF MY FATHER

MY BROTHERS AND SISTERS

MY WIFE AND CHILDREN FOR THEIR LOSS OF MY LEISURE HOURS

ACKNOWLEDGEMENTS

Many thanks are due to Dr. R.W.Fane for his supervision and continuous encouragement during the course of this work. I acknowledge valuable comments made on the manuscript by Mr. J.Sullivan and Mr. Y.Zaka. My thanks are also due to Mr. R.S.Bassi and Mr. A.Abbot for technical assistance. I have appreciated the friendly atmosphere of various groups in the Physics Department which has helped to sustain me during my postgraduate studies.

I acknowledge the receipt of a grant from Kuwait Institute for Scientific Research (KISR), without which this work could not have been undertaken. The moral support and encouragement of Dr. H.A.Ghalib of KISR are greatly appreciated.

CONTENTS

LIST OF FIGURES

LIST OF TABLES

LIST OF SYMBOLS

$N(\epsilon)$	Density of states at energy ϵ
ϵ_c	Conuction-band edge
ϵ_v	Valence-band edge
ϵ_F	Fermi level
ϵ_A	Band tail edge
$\Delta\epsilon_F$	Shift in Fermi level
p^+	Positive charge density
n^-	Negative charge density
n_d	Density of substitutional atoms
n_d^+	Density of ionised donors
n_i	Density of incorporsted impurity
f	Doping efficiency
σ	Electrical dark conductivity
σ_{RT}	Room-temperature dark conductivity
σ_{Ph}	Photoconductivity
i_{Ph}	Photocurrent
δ	Temperature coefficient (of energy)
ΔE_a	Thermal activation energy of dark conductivity
σ_h	Hopping conductivity
W	Hopping energy
R	Reflectivity
α	Absorption coefficient
a^{-1}	Spatial extent of electron wavefunction at The Fermi energy
Tr	Transmittance
t	Film thickness
E_o	Optical gap
$\hbar\omega$	Photon energy
μ_c	The electron mobility at ϵ_c
e	Electronic charge
G	Photocarrier generation rate
K_1, K_2	The recombination constant in bimolecular and monomolecular recombination processes respectively
n_A, P_y	The total densities of electrons and holes during the illumination at ϵ_A and ϵ_y respectively
n_c	The total density of electrons in the conduction band

F	Light intensity
γ	Exponent factor determining the type of recombination process
μ_D	The electron drift mobility
T_R	The response time for photocurrent
η	The quantum efficiency for photocarrier generation
E_o^{Ph}	The optical gap determined from the photocurrent measurements
ΔE_a^{Ph}	Thermal activation energy at room temperature, determined from the photocurrent measurements (Photoconductive threshold)
T_s	Substrate temperature
P	Sputtering gas pressure
d	Target-substrate spacing
V_{sb}	Self-bias voltage on the target
A	Cross sectional areas of the gap cell configuration
I	Current
V	Voltage
L	Width of the gap cell configuration
λ	Wavelength
π_{Si}, π_{Al}	Photoionisation cross sections of Si and Al respectively
λ_{Si}, λ_{Al}	Electron escape depths for Si and Al respectively
I_{Si}, I_{Al}	Intensities of Si and Al photopeaks respectviely
N_{Al}/N_{Si}	The atomic ratio of Al to Si
Y_{Al}, Y_{Si}	Ne-sputtering yield of Al and Si respectively
T_a	Annealing temperature
t_a	Annealing time

CHAPTER ONE

INTRODUCTION

During the last decade, extensive work on amorphous silicon (a-Si) has been carried out in many laboratories to optimise the preparation conditions and study the detailed properties of this material. Hydrogenated amorphous silicon (a-Si:H) prepared by glow-discharge (GD) decomposition of silane was found to have a low density of unwanted defect-states in the mobility gap (e.g. Spear and LeComber, 1972), which made it possible to be n- or p-type doped from the gas phase (Spear and LeComber, 1975) or by ion implantation (Müller et al, 1977). Reactive sputtering of Si with hydrogen in Ar plasma has been found to produce a-Si:H (Paul et al, 1976) with similar properties to that of GD material. Unhydrogenated Ar-sputtered and evaporated a-Si are believed to possess a relatively high overall density-of-states in the gap, (e.g. Madan et al, 1976; Spear and LeComber,1979), making doping impossible.

It is worth mentioning that a-Si:H is a material with, intrinsically, a high density-of-states. These states can be reduced by dangling-bonds termination using H atoms. Therefore, the effusion of hydrogen (e.g. Tsai et al, 1977) makes the thermal stability of this material questionable. In recent years, attempts have been made to produce a-Si, with intrinsically a low density-of-states, without the addition of hydrogen or a halogen, by sputtering at high Ar pressure, which could be doped by co-sputtering with the dopant (e.g. Suzuki et al, 1980). Although doping has taken place in this material the

doping efficiency seems to be very low compared with that achieved by other known techniques, in particular the lack of success in doping by co-sputtering with Al, the main dopant in the present work, is noted. In addition, there has been some evidence of porosity in a-Si films prepared by sputtering at high Ar pressure. A more detailed survey of the previous work on a-Si is presented in chapter 2.

More recently, the production of a low defect-density a-Si by r.f. sputtering in Ne gas has been reported (Fane , 1981), where doping by co-sputtering from Al/Si composite target has proved possible. The present work is an extension to the work of Fane (1981). The main aims of this work are summarised in the following.

(i) To try to understand the mechanism of film deposition by studying combinations of deposition parameters such as Ne gas pressure, the target-substrate distance, the self-bias voltage on the target and the substrate temperature, which control the optical and electronic properties of a-Si.

(ii) To study the effect of the preparation conditions on the quality of the films, by carrying out three types of measurements; namely, dark conductivity, photoconductivity and optical absorption, to remove the possible ambiguities in interpreting the data.

(iii) To find the optimum preparation conditions for a-Si.

(iv) To investigate the doping possibility and efficiency of a-Si by group-III elements and attempt to establish better

conditions to enhance the doping efficiency.

A detailed investigation of the electronic and optical properties of undoped a-Si, as a function of the preparation conditions is presented and discussed in chapter 5. Chapter 6 is devoted to the doping possibility by group-III elements. Possible further improvement of the doping efficiency, by post-deposition annealing at relatively high temperatures, is demonstrated in chapter 7. The results are discussed in the light of the available theory outlined in chapter 3. The experimental details are explained in chapter 4, where appropriately referred to throughout the thesis.

In summary, the present work could be considered a feasibility study of the production of a dopable a-Si, for semiconductor and possibly photovoltaic applications, without the introduction of hydrogen or a halogen; i.e. to obtain a-Si with intrinsically a low density-of-defect-states without the need for any dangling-bond terminator.

CHAPTER TWO

SURVEY OF PREVIOUS WORK

2.1. INTRODUCTION

The aim of this chapter is to briefly summarise previous work on amorphous silicon (a-Si) including preparation techniques and electrical and optical properties of this material. Amorphous silicon has been receiving an increasing amount of attention in many places around the world. The history of amorphous materials dates back nearly 50 years, though it has only been in the last 7-9 years that interest in these materials has increased enormously. The increased interest in a-Si can be realised from the increase in publications on this material as illustrated in Fig. 2-1 (Abo-Namous and Sayigh, 1982; INSPEC-EMIS group, U.K.). Interest has further increased since the limited supply of the present conventional energy sources has become apparent; and crystalline silicon (c-Si) is limited in terms of cost reduction (DOE, U.S., 1980) when making solar cells or semiconductor devices. Recent advances in a-Si technology have made it plausible that this material may replace or at least compete with c-Si for some devices. In fact recently an efficiency of 7.5% has been reported for a-Si solar cells with 100 cm^2 area (Kuwano and Ohnishi, 1981). More recently, Matsushita et al (1984) reported that solar cells with 8.05% efficiency can be produced.

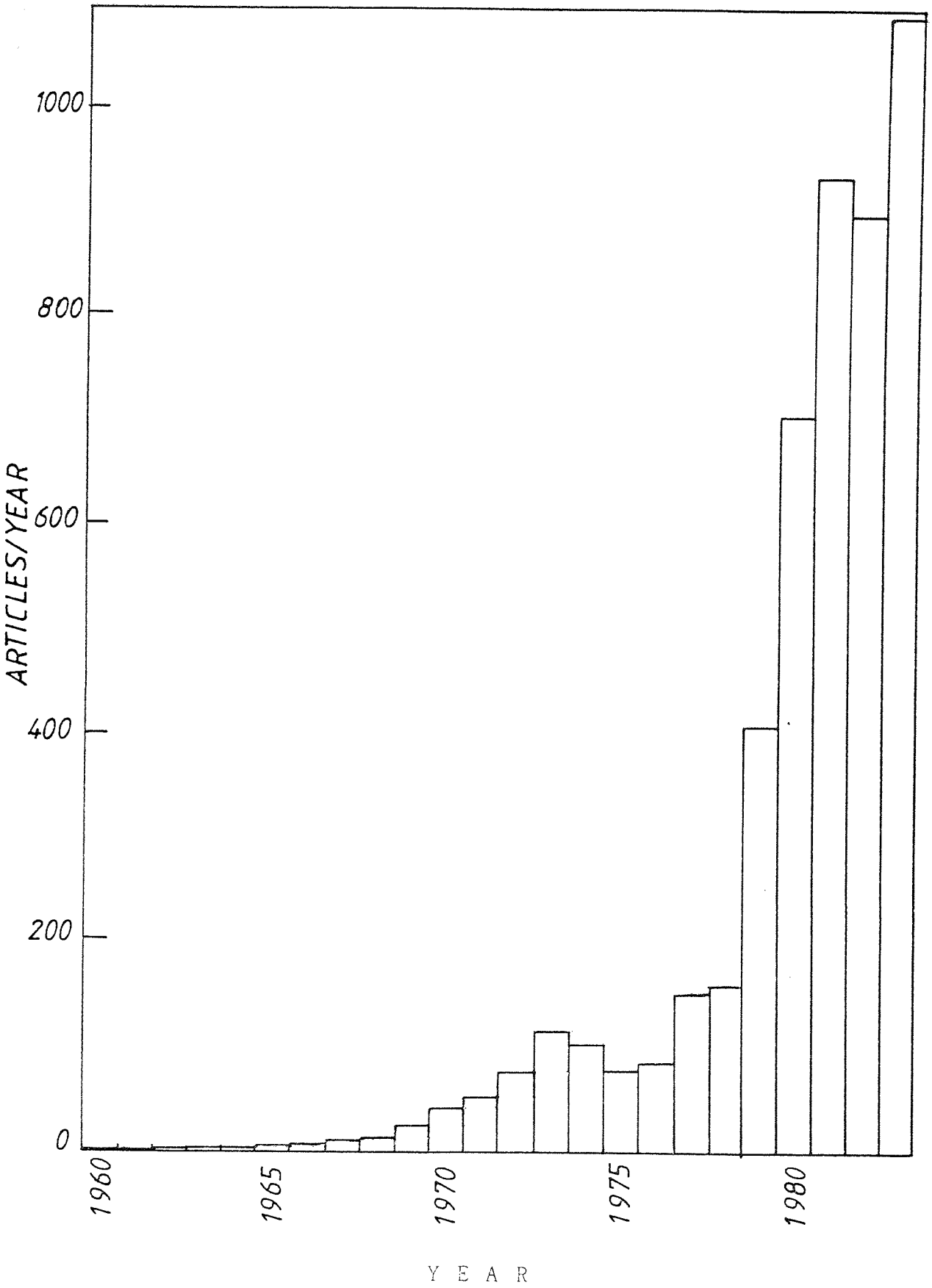

Fig. 2-1: A histogram showing the growing interest in a-Si in the period 1960 - 1983. 1960-1979 (Abo-Namous and Sayigh, 1982), 1980-1983 (INSPEC-EMIS group, U.K.)

Relatively little work has been carried out on the production of pure a-Si with a low density-of-states and consequently it was considered to be a valuable area of research. The relatively detailed survey of hydrogenated amorphous silicon (a-Si:H) in the following pages is presented to enable a comparison to be made between the unhydrogenated a-Si, which is the material of interest, and the well established properties of a-Si:H.

2.2. DEVELOPMENT OF PREPARATION TECHNIQUES

There are many techniques that produce amorphous silicon, although the literature shows that only a few methods have received much attention. These methods can be summarised in the following.

(1) Thermal evaporation (EV), in which the Si is thermally heated under vacuum to the melting point (about 1400 ^{o}C), and then evaporation takes place and the material is deposited onto the appropriate substrate. Heating could be supplied either electrically through a graphite boat or by an electron beam gun (e.g. Bahl et al, 1973). It has been reported that EV a-Si could be hydrogenated by subsequent heat treatment in a hydrogen plasma (Kaplan et al, 1978), or by introducing hydrogen during the evaporation process (Iselborn et al, 1983; Jang et al, 1980; Malhotra et al, 1976).

(2) Chemical vapour deposition (CVD) in which films of a-Si are deposited by the pyrolytic decomposition of silane

(SiH_4) or silicon tetrachloride ($SiCl_4$) onto the appropriate substrate in a horizontal, heated, atmospheric pressure reactor. A typical carrier gas is helium. This technique has been widely investigated by Seraphin's group at the University of Arizona (USA) (e.g. Janai et al, 1979; Booth et al, 1979).

(3) Reactive sputtering (SP) of c-Si in Ar/H_2 plasma ; was developed by Paul et al (1976). In this technique, Ar plasma is initiated by radio-frequency (r.f.) power, and the argon ions are accelerated through the plasma sheath to sputter Si atoms from the silicon target, which are then deposited on a substrate.

(4) Glow discharge (GD) decomposition of SiH_4 or SiH_4/Ar gas mixture with the aid of plasma discharge produced by either d.c. or r.f. power. This technique was first developed at Harlow by Sterling and Swann (1965).

The last two techniques have been employed mainly for the photovoltaic and semiconductor devices (e.g. Snell et al, 1981; Carasco and Spear, 1983; Hamakawa, 1981, Carlson,1980). This is due to the possibility of effective doping of a-Si produced by these techiques, since this material possesses a low density-of-states in the mobility gap. On the other hand, CVD and EV a-Si have the property of high optical absorption in the solar spectrum region, which extends to long wavelengths. For this reason, these two types of a-Si could be suitable for solar photothermal absorbers. However,

hydrogenation of EV a-Si proved to make doping of this material possible (e.g. Jang et al, 1980; Beyer et al, 1980; 1979).

Fig. 2-2 compares the absorption coefficient, α , of c-Si (Carlson and Wronski, 1976) and two types of a-Si, one prepared by thermal evaporation (Wakim et al, 1982) and the other prepared by glow discharge (Gibson et al, 1978). The figure also includes a linear plot of the AM1 solar spectrum (e.g. Treble, 1977). It can be seen from the figure that for amorphous silicon, α is up to about an order of magnitude higher than that of the crystalline in the region of interest. This means that for the same absorbed energy , amorphous solar-cells and thermal collectors can be appreciably thinner than the crystalline devices, with a consequent saving in material.

Although work with amorphous materials dates back to 1930, relatively little progress was made untill about 1975, when the Dundee University group demonstrated the possibility of gas phase (phosphine or diborane) doping of a-Si:H prepared by glow-discharge decomposition of SiH_4 (Spear and LeComber, 1975). Since that date, there has been renewed interest in using "thin" films of a-Si for cheap photovoltaic and semiconductor devices. Consequently, several universities and companies in the United States, Britain, Japan, France and Germany, have started the investigation of GD a-Si. This was followed immediately by reported attempts of the Harvard

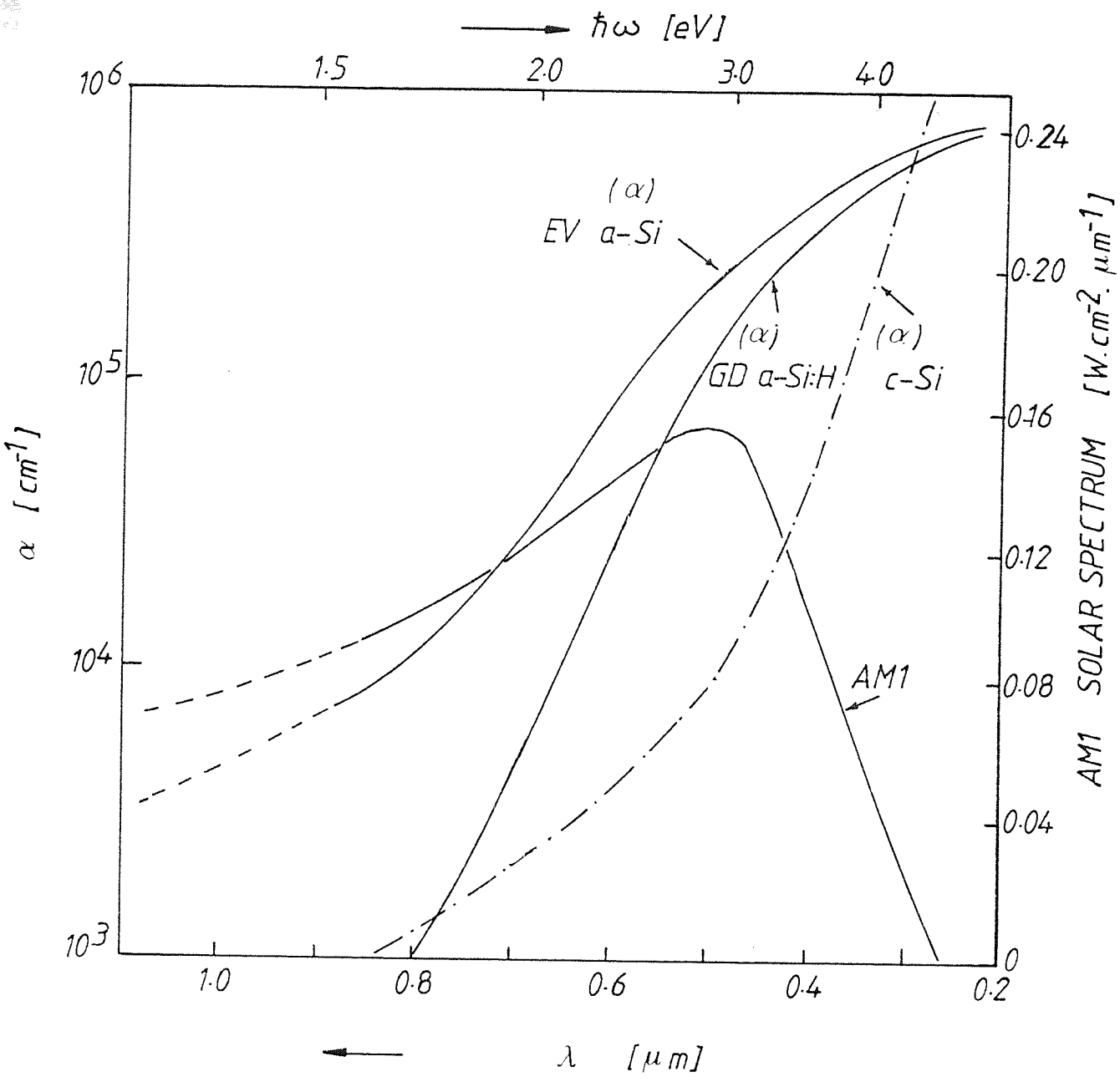

Fig. 2-2: Absorption coefficient α of amorphous and crystalline silicon as functions of wavelength λ of the incident light. EV a-Si (Wakim et al., 1982), GD a-Si:H (Gibson et al, 1978), c-Si (Carlson and Wronski, 1976), AM1 (e.g. Treble, 1977).

group (Paul et al, 1976) and others (Thompson et al, 1978; McGill et al. 1979). Doping from the gas phase introducing phosphine or diborane (Paul et al, 1976) and from the solid phase by co-sputtering with the dopant or by sputtering a predoped target (Thompson et al, 1978) have proved possible, although some results demonstrated a modification of the a-Si:H network by co-sputtering Al (Thompson and Reinhard, 1980), Ga or In (Xu et al, 1984) with Si rather than true doping effects.

In recent years, attempts have been made to produce a pure stable a-Si having the major fundamental properties of GD and SP a-Si:H (such as low density of gap states and hence low conductivity and high thermal activation energy) by means of a more simple and safe method. Pawlewicz (1978) investigated the dependence of the properties of unhydrogenated Ar-sputtered a-Si on preparation conditions such as Ar pressure, the target-substrate spacing and the substrate temperature (see section 2.3.2.1.). He found that the electronic and optical properties could be influenced considerably by changing the preparation conditions and that these could be optimised to produce material with a low density-of-states in the mobility gap. A Japanese group (Shimizu et al, 1979; Suzuki et al, 1980) has investigated the production of a-Si without hydrogen by sputtering in high Ar pressure (up to 0.2 Torr) and/or high target-substrate distance (up to 4.5 cm). They reported a high resistivity a-Si (about $10^8\ \Omega$cm) and high thermal activation

energy (about 0.8 eV). Substitutional doping by co-sputtering B or P with silicon under high Ar pressure has been reported (Suzuki et al, 1980). It seems from these results, especially the conductivity and thermal activation energy values, that doping efficiency is low compared to that in the case of other known techniques. Furthermore it seems that there has been a lack of success in doping by co-sputtering Al with Si in Ar. The same group has also shown that a-Si produced by negative biasing of the substrate and/or by magnetron sputtering in Ar is promising (Suzuki et al, 1982).

Sputtering Si in Ne without the addition of hydrogen, to our knowledge, has not been seriously investigated previously. Recently, the Aston University group demonstrated that r.f. sputtering of Si in a Ne gas plasma could be an alternative technique to produce dopable a-Si without hydrogen (Fane , 1981). It has been shown that sputtering at high Ne gas pressure may produce material with a low density of defect-states in the mobility gap. This has been demonstrated by the high resistivity ($\gtrsim 10^8\ \Omega$ cm) and high thermal activation energy (about 0.6 eV). The low density-of-states made it possible to n- or p-dope this material by co-sputtering with Ta (Fane and Zaka, 1983) or with Al (Fane and Abo-Namous, 1983) respectively. Doping with other group-III elements has demonstrated the same effect (chapter 6).

2.3. PROPERTIES OF a-Si

The electronic and optical properties of unhydrogenated and hydrogenated a-Si have been extensively investigated. Several extensive reviews of the development in the technology of a-Si and the study of its properties are available in the literature (e.g. Spear, 1977, Moustakas, 1979). The characterisation of GD a-Si:H is reviewed by Fritzsche (1980). The properties of a-Si:H prepared by r.f. sputtering in Ar/H_2 mixture are reviewed by Paul and Anderson (1981) and Moustakas (1979). For further information the reader is refered to articles in Volume 36 of Topics in Applied Physics (Brodsky, 1979), to the Physics of Amorphous Silicon and Its Applications (Joannopoulous and Lucovsky, 1983), to article in Photoconductivity and Related Phenomena (Mort and Pai, 1976), to the comprehensive book by Mott and Davis (1979), to the Proceedings of 13th IEEE Photovoltaic Specialists Conference (1978) and to the 7th, 8th and 9th Proceedings of the International conference on Amorphous and Liquid semiconductors, 1977 , 1979 and 1981 respectively. For more references on a-Si the reader is refered to the classified bibliography by Mahan and Stone (1981,1982 and 1984).

A considerable amount of conflicting data has been reported on the properties of a-Si, making it very difficult to specify the properties of a typical sample (e.g. Zemek et al, 1980; Paul and Anderson, 1981). However, by careful study

of the literature, it has become apparent that the electronic and optical properties of a-Si depend markedly on the method of preparation and the detailed conditions during deposition.

2.3.1. HYDROGENATED AMORPHOUS SILICON (a-Si:H)

2.3.1.1. GLOW-DISCHARGE a-Si:H

It has been established that in a-Si:H prepared by the glow-discharge technique, the properties of the films are mainly determined by the substrate temperature during deposition (e.g. LeComber et al, 1972; Fritzsche, 1980). Hydrogen in the amorphous silicon network is believed to have a major role in controlling the optical gap by satisfying the dangling bonds (Tsai and Fritzsche, 1979). On the other hand Cody et al (1981) consider that the optical gap is determined by the degree of disorder in the lattice rather than by hydrogen content. It has been found that a-Si:H films with good electronic properties contain one to two orders of magnitude more hydrogen than is needed for the compensation of dangling bonds (Title et al, 1977; Wronski and Carlson, 1977; Moustakas et al, 1977). This suggests that the role of hydrogen is far more complicated than simply passivating dangling bonds. However, the exact role of hydrogen in a-Si:H is still uncertain and requires further investigation.

Spear et al (1980) reported that without adding dopants, variations in deposition conditions produce a-Si:H samples with thermal activation energy, ΔE_a, in the range $0.6 \lesssim \Delta E_a \lesssim 0.9$ eV. The optical gap E_o of a-Si:H has been found to vary, according to the preparation conditions (especially the substrate temperature), from 1.5 eV to about 1.9 eV.

The Dundee University group were the first to dope GD a-Si:H from the gas phase (Spear and LeComber, 1975). The doping effect has been demonstrated through the control of dark conductivity over about 10 orders of magnitude and the shift of Fermi level over a range of about 1.2 eV. The above authors claimed that one in three P atoms acts as a donor centre in the gas phase doping. However, lower values of doping efficiency for B from the gas phase (1/10) have been announced (e.g. Müller et al , 1977). The doping efficiencies of 1/500, 1/100 and 1/200 for P-, alkali- and B-implantations respectively have been reported (LeComber et al, 1980), which reflect the lower doping efficiency of the implantation process compared to gas phase doping. Fig. 2-3 illustrates a comparison of doping efficiencies of various dopants using different doping techniques. The comparison is made through the room-temperature dark conductivity as a function of the dopant concentration in a-Si:H.

Extensive photoconductivity measurements on a-Si:H prepared

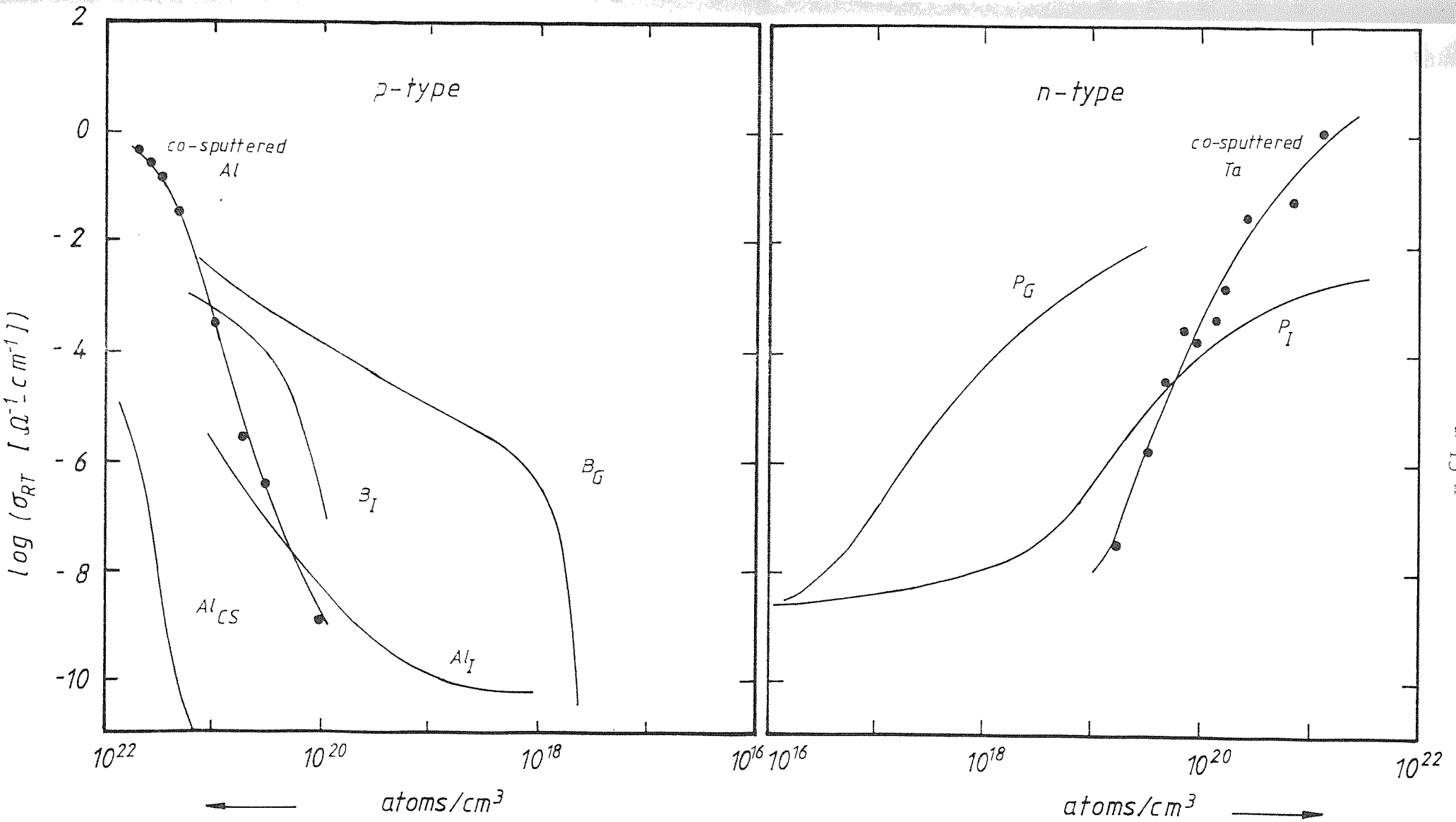

Fig. 2-3: The dark conductivity as a function of dopanat concentration for different n- and p-type doping using various techniques. B_G and P_G are for B- and P-doping from gas phase, B_I and P_I are for B- and P-doping by ion implantation (LeComber et al, 1980), Al_{cs} is for doping with Al by co-sputtering in Ar/H_2 (Thompson and Reinhard, 1980), Al and Ta represent co-sputtering in Ne reported by Fane and Abo-Namous (1983) and Fane and Zaka (1983) respectively.

by glow discharge have been reported by Loveland et al (1973/74) and Spear et al (1974). It has been shown that the photoconductive response depends critically on the preparation conditions; through the control of the density-of-states distribution in the mobility gap. The spectral dependence of the photoresponse has been used to determine the optical gap, E_o, and the photoconductive threshold . These measurements provide confirmation of the values of the optical gap and the thermal activation energy obtained from the direct transmission technique and the dark conductivity measurements respectively.

The dependence of the photocurrent of a-Si:H on the temperature indicates the position of the band-tail edge in the mobility gap (Spear et al, 1974). For further details the reader is refered to a review article by Spear and LeComber (1976). Recent photoconductive measurements on GD a-Si:H (Ray et al,1983) are in support of the above results.

The intensity dependence (Spear et al, 1974) and the temperature dependence (Ray et al, 1983: Spear et al,1974) of photoconductivity indicate that, at room temperature, monomolecular recombination is dominating at low light intensities and a bimolecular process at high intensities. Spear et al (1974) argued that the monomolecular recombination transition most likely results from transitions

from localised tail states at ϵ_A to the states at the Fermi energy ϵ_F. On the other hand the bimolecular recombination is believed to take place as a result of transition between ϵ_A and the density-of-states maximum at ϵ_y, about 1.2 eV below the conduction-band edge (see Fig. 3-3). Furthermore, it has been suggested by the above authors that the photocurrent is mainly carried by electrons (LeComber and Spear, 1970).

2.3.1.2. REACTIVE SPUTTERED a-Si:H

Although a-Si:H prepared by r.f. sputtering in Ar/H_2 gas mixture may have similar properties to that prepared by glow-discharge decomposition of silane, it has been argued that the two materials have different structures, due to the hydrogen bonding into the silicon network in different configurations (e.g. Brodsky et al, 1977; Fritzsche, 1980; Paul and Anderson, 1981). However, it has been reported that the optical absorption of a-Si:H prepared by Ar/H_2 sputtering is shifted to higher energies with increasing hydrogen concentration in the plasma. A variation in the optical gap between 1.4 eV and 2.1 eV has been reported (Paul and Anderson, 1981). However, it seems that a high hydrogen partial pressure may introduce additional states into the gap of a-Si:H prepared by r.f. sputtering. The density of these states could be sufficient to completely dominate the electronic properties. The conductivity activation energy, ΔE_a, has been varied from about 0.7 eV to

about 1.0 eV depending on the hydrogen partial pressure in the plasma (e.g. Anderson et al, 1977; Paul and Anderson , 1981).

N- and p-type doping proved to be successful from the gas phase, where the Fermi level is shifted towards the conduction or valence band, accompanied by a control of the conductivity over many orders of magnitude (Anderson, 1978) in a similar way to that reported for the glow discharge case (e.g. Spear, 1977).

The Harvard University group studied the photoconductive properties of the sputtered a-Si:H and found similar properties to those of the glow-discharge a-Si:H . They developed a model to extract the optical-absorption coefficient as a function of energy at low photon energies (1.2-1.8 eV) from the measurements of photoconductivity (Moddel et al, 1980). This model is used in the present work to study the absorption coefficients at low energies, and to study semiquantitatively the density-of-states distribution in the mobility gap (see section 3.6.3.). The photoconductive, electrical and optical properties of the r.f. sputtered hydrogenated amorphous silicon are reviewed extensively by Paul and Anderson (1981) and Moustakas (1979).

The modification of the electrical and optical properties by co-sputtering from composite targets incorporating aluminium has been reported by Thompson and Reinhard (1980).

The "doping" effects were suggested by the control of conductivity over several orders of magnitude (see Fig. 2-3) and a shift in the Fermi level position of about 0.4 eV towards the valence band. However, the authors reported a reduction in the band gap for the higher Al concentrations in the silicon which was attributed to modification in the silicon band structure, suggesting that an alloying effect had taken place rather than a true doping effect. The modification of the structure of a-Si:H by co-sputtering transition elements has also been reported (e.g. Ovshinsky, 1977; Yacobi et al, 1980).

More recently, Xu et al (1984) reported doping effects of Ga and In in a-Si:H prepared by r.f. co-sputtering in Ar/H_2 mixture. They reported that 5.2 at.% Ga or 22 at.% In in a-Si gave a conductivity of about 10^{-5} $\Omega^{-1}cm^{-1}$, accompanied by shifting the Fermi level to about 0.4 eV from the valence band edge. However, higher content of Ga or In showed a sudden increase in conductivity with zero thermal activation energy, indicating the alloying effect. Niu et al (1984) reported that 25 at.% Al in a-Si:H, prepared by co-sputtering in Ar/H_2 mixture, produced an a-Si:Al:H alloy with conductivity of 10^{-5} $\Omega^{-1}cm^{-1}$. However, Niu et al (1984) reported that annealing the a-Si:Al:H films at about 600 ^{o}C increased the conductivity by 5 orders of magnitude for films containing more than 6 at.% Al, for films with less than 6 at.% Al no annealing effect was observed.

2.3.2. UNHYDROGENATED a-Si

2.3.2.1. Ar-SPUTTERED a-Si

The work of Pawlewicz (1978) showed that the eleectrical, optical and photoconductive properties of Ar-sputtered unhydrogenated a-Si films are related systematically to deposition parameters. Sputtering at high Ar pressure and/or relatively high target-substrate spacing produced films with resistivity of about 10^7 Ω-cm, and significantly reduced the density of states in the mobility gap. The latter property was deduced from the optical absorption measurements and the high photoconductive response. The above author also reported that film properties were independent of deposition rate. The above technique was based on deposition conditions (gas pressure, target-substrate distance and substrate temperature) which were believed to minimise the plasma interaction with the film and maximise thermal reorganisation (Pawlewicz , 1978). Remarkably good electrical and optical properties for unhydrogenated a-Si resulted. The influence of substrate temperature on the film properties was attributed to annealing of collision-induced defects during film growth, or to a decrease in the density of microvoids (Paul et al, 1976).

In recent years, the Kanazawa University group in Japan, have attempted to produce a-Si without hydrogen by r.f.

sputtering at high Ar pressure. They found that the overall density-of-states in the gap depended on the preparation conditions (Shimizu et al, 1979). For instance upon increasing the product (Pd) of the pressure P and target-substrate distance d, to about 1 Torr.cm, the density of defect-centres was reduced by one order of magnitude. Accordingly the dark conductivity decreased from about 10^{-2} $\Omega^{-1}cm^{-1}$ to about 10^{-8} $\Omega^{-1}cm^{-1}$. Upon annealing the films the conductivity changed from about 10^{-4} $\Omega^{-1}cm^{-1}$ to about 10^{-10} $\Omega^{-1}cm^{-1}$ as (Pd) product approaches 1 Torr.cm. This was accompanied by an increase in the thermal activation energy up to about 0.9 eV. The authors reported that Ar content in the films decreased with increasing Ar pressure which was attributed to the decrease in kinetic energy of Ar particles hitting the substrate. It is worth mentioning that a-Si films prepared at high Ar pressure were reported to have a porous structure (Suzuki et al, 1980), where oxygen was found to be introduced into the film by exposing it to air after preparation. However, the authors attributed the low conductivity of these films to the low density of dangling-bonds (Shimizu et al, 1980).

More recently, Batabyal et al (1984) studied the effect of the sputtering pressure and substrate temperature on the properties of a-Si films prepared by magnetron sputtering in Ar. They found that variation of the pressure from 3 mTorr to 40 mTorr, varied the dark conductivity from 3.4×10^{-1} $\Omega^{-1}cm^{-1}$ to 1.2×10^{-7} $\Omega^{-1}cm^{-1}$ and the optical gap

from 1.3 eV to 1.7 eV. This was attributed to a reduction in the density of defect states and microvoids as the pressure is increased, where low deposition rate means allowing more time for atoms to orient themselves, and Ar^+ and neutrals have lower energy due to scattering. Batabyal et al (1984) showed that variation of substrate temperature from 240 °C to 350 °C resulted in reducing the conductivity from $10^{-2}\ \Omega^{-1}cm^{-1}$ to $10^{-5}\ \Omega^{-1}cm^{-1}$. This was attributed to high mobility of atoms on the surface at high substrate temperatures, and to the possibility of some annealing of microvoids. It was claimed (Batabyal et al, 1984) that a sputtering at a pressure of 40 mTorr resulted in films with photoconductivity to conductivity ratio of 10 under 20 $mW.cm^{-2}$ white light illumination.

The conductivity control over 6 orders of magnitude, by doping with B or P for Ar-co-sputtered films was reported (Suzuki et al, 1980). This was accompanied by a shift in the Fermi level position over about 1 eV. A slight increase in the conductivity upon doping with Al was attributed to modification of a-Si network as evidenced by the decrease of the optical gap as Al content was increased . The annealing effects on undoped Ar-sputtered a-Si were studied by Suzuki et al (1982). They reported that the room-temperature conductivity was reduced by about one order of magnitude upon annealing at 600 °C. Negative bias of the substrate and the use of a magnetron target have been reported to produce a-Si with a reduced density-

of-states in the mobility gap (10^{18} $cm^{-3}eV^{-1}$) and increased thermal stability up to about 500 ^{o}C (Suzuki et al, 1982).

2.3.2.2. Ne-SPUTTERED a-Si

It has been suggested (Grigorovici, 1969) that an a-Si with a truncated tetrahedral structure, where all the bonds are satisfied, is possible. Polk (1971) developed a moel, based on a concept proposed by Zachariasen (1932), in which a continuous random network, might be constructed with pureley tetrahedral coordination. According to this model, a-Si atoms are organised in a tetrahedral structure with all the atoms having four neighbours, i.e. all bonds are satisfied, provided that a slight variation in the bond angle is allowed. Recently, at the University of Aston, attempts have been made to produce a high-resistivity a-Si with high thermal activation energy, without hydrogen, by sputtering in Ne plasma. It is believed that the type and energy of the plasma species hitting the film during deposition play an important role in determining the properties of the produced films. A-Si films with high resistivity (10^{8} Ωcm) and high thermal activation energy ($\sim$0.6 eV) have been produced (Fane, 1981). A preliminary study of doping by co-sputtering with Al showed that 2% (target area ratio) of Al moved the Fermi level by more than 0.45 eV and increased the conductivity by about 6 orders of magnitude, indicating that doping had taken place. The doping was not as efficient as gas-phase doping.

The author suggests that deposition conditions might need to be optimised. However, further investigation of the deposition conditions, such as gas pressure, target-substrate distance, self-bias voltage on the target and substrate temperature, showed that a-Si with conductivity as low as $10^{-9}\ \Omega^{-1}cm^{-1}$, activation energy of 0.85 and photoconductivity of $10^{-6}\ \Omega^{-1}cm^{-1}$ can be produced (Abo-Namous et al, 1983).

The present work is an extension to the work of Fane (1981) where more detailed investigations of the deposition conditions and the electronic and optical properties of Ne-sputtered a-Si, as well as the doping efficiency of this technique, are carried out.

CHAPTER THREE

THEORETICAL BACKGROUND

3.1. INTRODUCTION

For the interpretation of various properties of amorphous semiconductors, such as electrical conduction, optical absorption and photoconductivity, it is necessary to understand the band structure and the nature and density of electronic states in the mobility gap between the conduction and the valence bands. This chapter summarises the available theoretical concepts which are used in interpreting the data described in this thesis.

3.2. BAND MODEL

Experimental data of electrical transport and optical absorption can only be properly interpreted if a model for the electronic structure is available. In this section an outline is given of the approach to a model which is thought to be relevant to the experimental results presented in this thesis. It is well known that for crystalline semiconductors, the main feature of the energy distribution of the density of electronic states $N(\epsilon)$ is the well-defined band-edges. This means a well defined structure in the valence and conduction bands, and abrupt terminations at the valence-band maximum and conduction-band minimum (Fig. 3-1). The sharp edges in the density-of-states distribution produce a well-defined forbidden energy gap. The states within the bands are extended, where

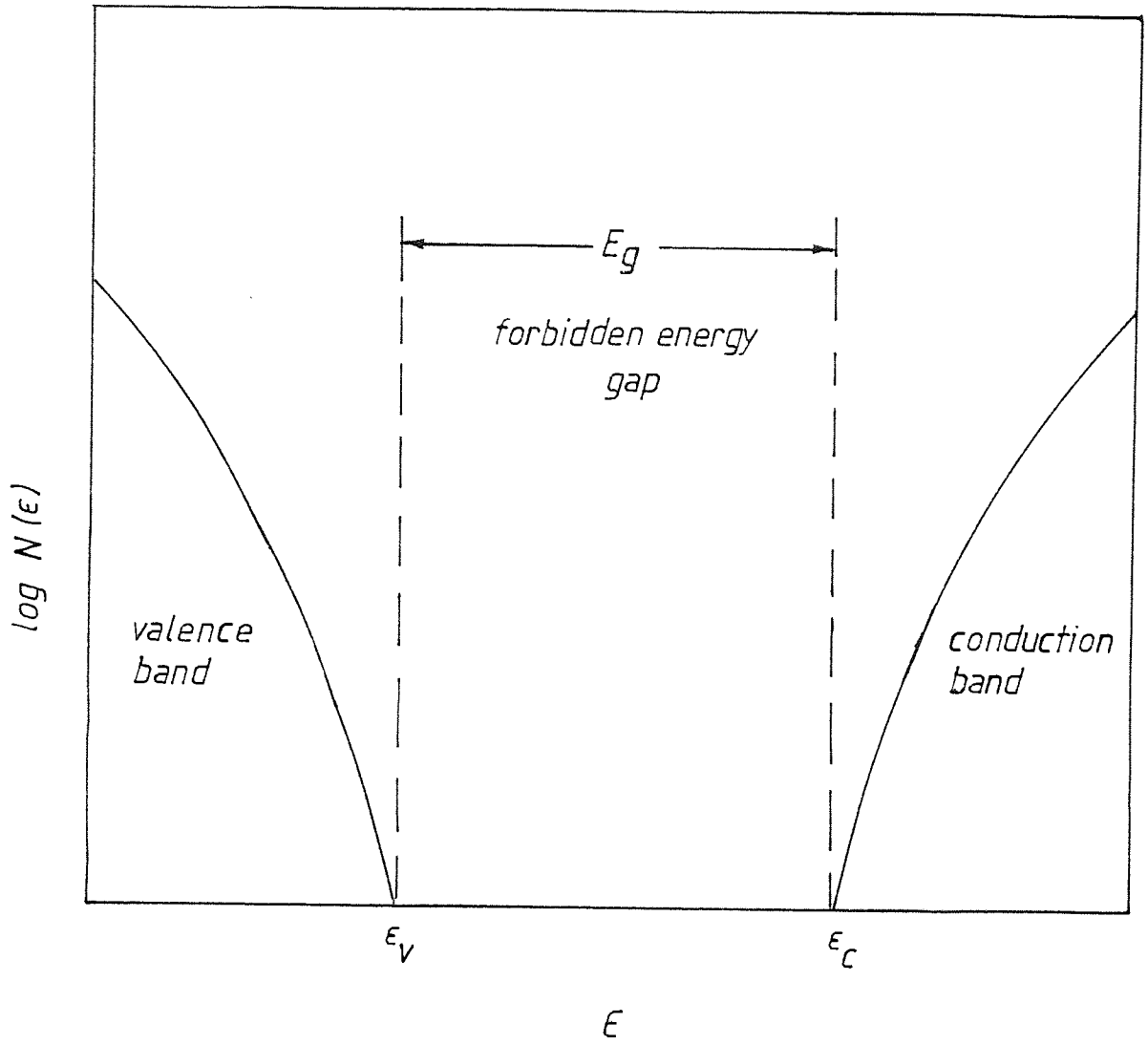

Fig. 3-1: Density-of-states distribution in a crystalline semiconductor. ϵ_c is conduction-band edge; ϵ_v is valence-band edge.

the wavefunctions extend to the entire volume of the solid. These features of the band structure are consequences of the perfect short-range and long-range order of the crystal.

On the other hand, in amorphous solids, the long-range order is destroyed while short-range order is retained over a few atomic spacings. Mott (1970) suggested that fluctuations in the potential caused by the disorder in amorphous materials may lead to the formation of localised states, which do not occupy all the different energies in the band, but rather form a tail above the valence band and another below the conduction band. Furthermore, he states that there should be a sharp boundary between the energy ranges of extended and localised states. The localisation of states means that an electron placed in a region will not diffuse at T=0 ^{o}K to other regions with corresponding potential fluctuations (Mott, 1969).

However several models have been suggested for the band structure of amorphous semiconductors, which are almost the same to the extent that they all consider the concept of localised states in the band tail, although they differ in the extent of this tailing.

Cohen et al (1969) proposed a model refered to as Cohen-Fritzsche-Ovshinsky (CFO) model in which it is assumed that the tail states extend accross the gap in a structureless

distribution as shown in Fig. 3-2. The CFO model considers the overlap of tail states in alloy glasses, where the disorder is sufficiently great that the tails of the conduction and valence bands overlap, leading to an appreciable density-of-states in the middle of the gap. More recently a similar but modified model (Fig. 3-3) was used by the Dundee group (e.g. Madan et al, 1976) which was suggested in the light of field effect measurements on glow-discharge amorphous silicon. This model considers the overlap of defect-states distributions which include dangling and weak bonds. In this model it is suggested that the minimum in the density of states, $N(\epsilon)$, arises from overlapping tails of two distributions of defect centres with their charge states being different. The dotted curves in Fig. 3-3 show $N(\epsilon)$ as if it is divided into two components. Distribution A, which extends from the side of the conduction band edge, ϵ_c, into the gap, contains acceptor-like states. These states are neutral when empty, so that below the the Fermi level, ϵ_F, they will be negatively charged with a charge density n^-. On the other hand, distribution B contains states extending from the opposite side of the mobility gap (valence band edge, ϵ_v), into the gap. These states are neutral when full and therefore provide positively charged donor-like states above ϵ_F, with a charge density p^+.

However, our experimental measurements of conductivity, photoconductivity, optical absorption (chapter 5) and doping effects (chapter 6)

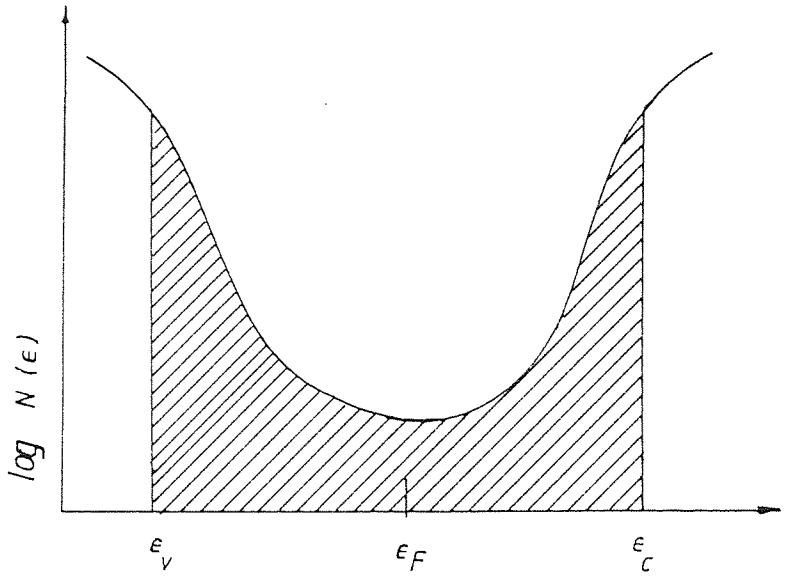

Fig. 3-2: The density-of-states distribution according to Cohen-Fritzsche-Ovshinsky (CFO) model.

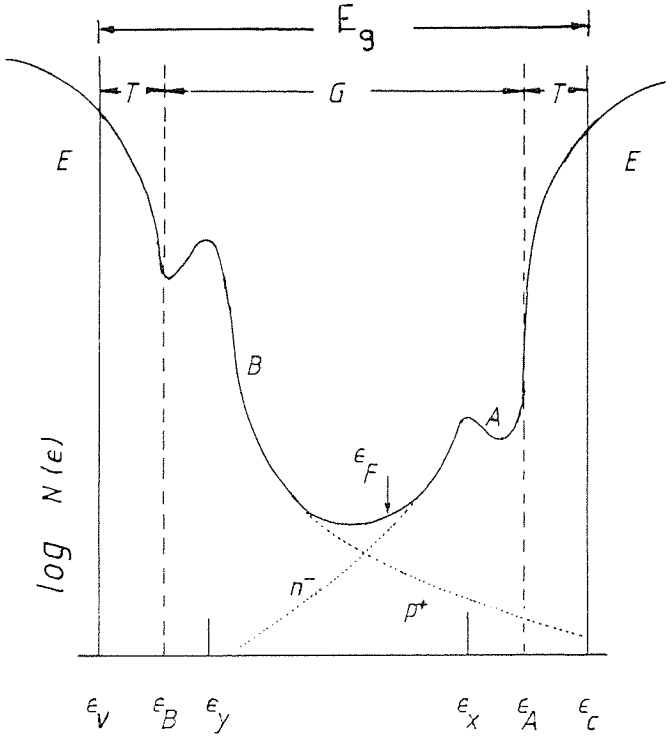

Fig. 3-3: The density-of-states distribution as proposed by the Dundee group. E the extended states, T the tail states, G the gap (defect) states, E_g the optical gap.

can be interpreted consistently by the Dundee group model described above. Therefore the model of Fig. 3-3 will be refered to throughout the thesis as the basis for interpretation of results.

3.3. SUBSTITUTIONAL DOPING IN a-Si

We will now consider the possibility of substitutional doping in a-Si specimens with a density-of-states distribution as described by Fig. 3-3. Following Spear and LeComber (1979), assume a band of n_d substitutional atoms are incorporated into the amorphous semiconductor material leading to donor states between the conduction band edge ϵ_c and the tail states at ϵ_A. Practically all the n_d excess electrons will condense into previously empty gap states above the Fermi level, ϵ_F, shifting ϵ_F towards ϵ_c by an amount $\Delta\epsilon_F$. In amorphous materials, changes in the electrical properties are brought about primarily by changes in the occupation of the gap-states. The new position of ϵ_F, for small changes, is determined by the charge neutrality conditions (Spear and LeComber, 1979)

$$\Delta\epsilon_F \simeq \frac{n_d^+}{N(\epsilon_F)} \qquad (3-1)$$

where $N(\epsilon_F)$ is the density of states around ϵ_F and n_d^+ is the density of the ionised donors. For sensitive doping $N(\epsilon_F)$ should be as low as possible and hence $\Delta\epsilon_F$ would be as large as possible. The above approach applies similarly to the acceptor doping, where a similar expression to (3-1) can be written.

Since the density of donors (or acceptors) in an amorphous semiconductor is not necessarily equal to the incorporated impurity density n_i (e.g. Mott,1969; Mott and Davis, 1979), eq. (3-1) may be written as

$$\Delta\epsilon_F \simeq \frac{f n_i}{N(\epsilon_F)} \qquad (3 - 2)$$

where f is the fraction of impurities that act as ionised donors (or acceptors) and will be refered to as the doping efficiency.

Relation (3-2) has been used by Beyer et al (1979a) to estimate the density-of-states distribution in the mobility gap using the ion-implantation results . Alternatively, if $N(\epsilon_F)$ is calculated, for example , from the dark conductivity measurements at low temperatures (section 3-4), f can be determined for doped samples . However in this approximate method of calculation the following assumptions are made;

(i) f is essentially independent of the doping concentration. Practically this assumption could be valid at relatively low dopant concentrations since the Fermi level is still in the vicinity of the density-of-states minimum. As the Fermi level moves towards the rapidly rising density-of-states in the mobility gap, the doping efficiency is reduced.

(ii) The gap density is not significantly modified by the doping procedure. Our results, as well as the results of others (Anderson et al, 1980), show that at high doping levels, more defect states are created in the mobility gap.

However the above two assumptions could be considered a reasonable approximation for low doping levels since a negligible variation in the density of states is then expected.

3.4. ELECTRICAL CONDUCTION IN AMORPHOUS SEMICONDUCTORS

It was seen in section 3.2. that the main feature of an amorphous semiconductor, such as a-Si, is that there is a continuous distribution of localised states within the energy gap as shown in Fig. 3-3. It can be shown that the conductivity, σ, due to electrons excited beyond the mobility edge, ϵ_c, into the extended states is given by (e.g. Mott and Davis, 1979)

$$\sigma = \sigma_o \exp\left[-\frac{(\epsilon_c - \epsilon_F)_0}{kT}\right] \qquad (3 - 3)$$

where ϵ_F is the Fermi level and σ_o is a pre-exponent parameter containing the density of states, $N(\epsilon_c)$, and the electron mobility, μ_c, both at ϵ_c, and a linear dependence on temperature, T. A similar expression can be written for the hole conduction in the extended states,

$$\sigma = \sigma'_o \exp\left[-\frac{(\epsilon_F - \epsilon_v)_0}{kT}\right] \qquad (3 - 4)$$

The optical absorption mesurements made on amorphous semiconductors (e.g. Freeman and Paul, 1979) have shown that the optical gap decreases with increasing temperature. Therefore $(\epsilon_c - \epsilon_F)$ and $(\epsilon_F - \epsilon_v)$ will show a similar behaviour. Assuming a linear temperature dependence,

$$(\epsilon_c - \epsilon_F)_T = (\epsilon_c - \epsilon_F)_0 - \delta T \qquad (3 - 5a)$$

and

$$(\epsilon_F - \epsilon_v)_T = (\epsilon_F - \epsilon_v)_0 - \delta T \qquad (3 - 5b)$$

where δ is a temperature coefficient, and $(\epsilon_c - \epsilon_F)_0$ and $(\epsilon_F - \epsilon_v)_0$ are energy differences at T=0 °K. In general $\epsilon_c - \epsilon_F$ and $\epsilon_F - \epsilon_v$ are called thermal activation energies for dark conductivity and will be denoted by ΔE_a. This type of thermally activated conduction is believed to be dominant at room- and higher temperatures (Spear et al, 1980), for relatively low density-of-states semiconductors, or when ΔE_a is small (Mott and Davis, 1979). However, Anderson and Paul (1982) argue that thermally activated conduction in the extended states tends to dominate at temperatures higher than 150 °C.

If the wavefunctions are localised, as is the case in the band tails, then the conduction is expected to occur only by thermally activated hopping. Every time an electron moves from one localised state to another it will exchange energy with a phonon. The conductivity, σ_h, in the tail states, when hopping takes place from one site to an adjacent site (Fig. 3-4a) is given by (Mott and Davis, 1979)

$$\sigma_h = \sigma_{oh} \exp\left[- \frac{\epsilon_A - \epsilon_F + W}{k T} \right] \qquad (3 - 6)$$

where W is the hopping energy and σ_{oh} is a pre-exponent

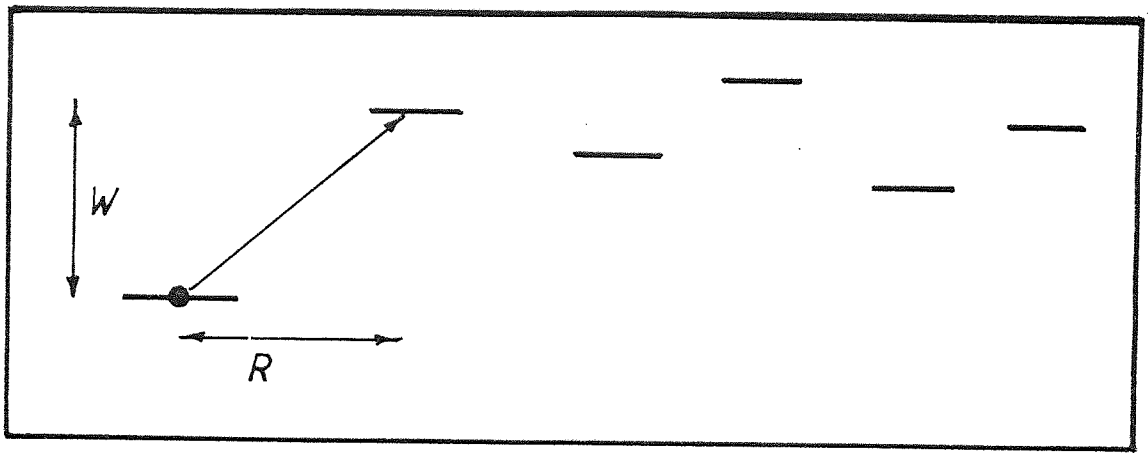

Fig. 3-4: (a) Hopping from a localised state at one site to an adjacent site (nearest neighbour hopping). (LeComber,1979).

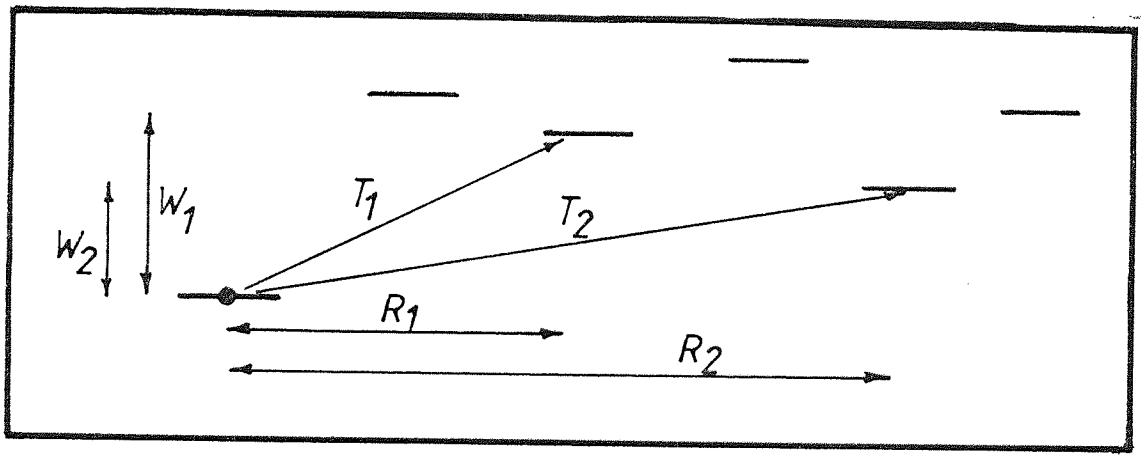

Fig. 3-4: (b) Variable-range hopping at various low temperatures. $T_2 < T_1$; $W_2 < W_1$ and $R_2 > R_1$. (LeComber,1979).

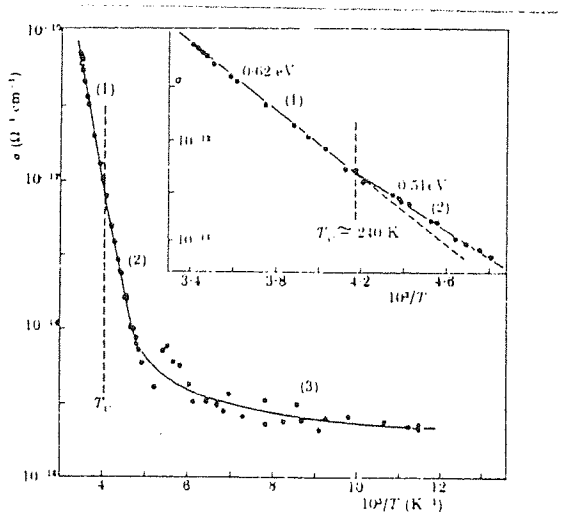

Fig. 3-4: (c) Log σ vs 1000/T for a-Si:H. (1) Thermally activated conduction the extended states; (2) Phonon-assisted hopping conduction; (3) Variable-range hopping conduction. (LeComber and Spear, 1970)

parameter containing the distance covered in one hop .

Mott (1969) has suggested that at low temperatures, rather than hop a given distance to the nearest neighbour site, for which the electron needs to gain an energy W from the lattice, it may prove more likely that the electron will hop a longer distance if this involves a smaller energy jump (Fig. 3-4b). This process has been called variable-range hopping. When it occurs via localised states around the Fermi level it leads to an expression for the conductivity of the form (Mott, 1969)

$$\sigma_h = \sigma_{oh} \exp \left[- \frac{T_o}{T} \right]^{1/4} \qquad (3 - 7)$$

where σ_{oh} and T_o in this case are parameters both involving $N(\epsilon_F)$ and the spatial extent, a^{-1}, of the electron wave-functions at the Fermi energy, where

$$T_o \simeq \frac{16\, a^3}{k\, N(\epsilon_F)} \qquad (3 - 8)$$

Equations (3-7) and (3-8) can be used to evaluate $N(\epsilon_F)$ if a reasonable guess is made for a^{-1}.

Finally, it is worth mentioning that various current paths, such as extended-states conduction and conduction through the localised states, may contribute to the observed conductivity simultaneously (e.g. LeComber, 1979). However, at a given temperature range, it can be assumed that one path predominates, so that the interpretation of the results becomes simple. Fig. 3-4c shows $\log \sigma$ vs 1000/T for a-Si:H

(LeComber and Spear, 1970), where the temperature range is divided into three regions with different conduction mechanisms.

3.5. OPTICAL ABSORPTION

The measurements of the optical properties have played a significant role in understanding the structural and electronic properties of amorphous silicon (e.g. Pierce and Spicer, 1972; Gibson et al, 1978; Yamasaki et al, 1982). In fact, the optical absorption does not give an exact representation of the density of states in the valence band (e.g. Moddel et al, 1980). Nevertheless, like photoemission (e.g. Von Roedern et al, 1979), it exhibits the major features of the band, where it represents the initial-final states coupling.

It is normally assumed that the densities of states just beyond the mobility edges (extended states) can be represented by power laws, similar to the case for crystalline material. When a parabolic shape of the conduction- and valence-band edges are assumed, the desired extended-extended optical transitions can be described by the relation (Tauc, 1970)

$$\alpha = \beta (\hbar\omega - E_o)^2 / \hbar\omega \qquad (3 - 9)$$

where α is the absorption coefficient, $\hbar\omega$ is the photon energy, E_o is the optical gap, which is arbitrarily defined as $(\epsilon_c - \epsilon_v)$ (see Fig. 3-3), and β is a constant. The absorption coefficient, α, can be deduced from the transmittance, Tr, data with a reasonable accuracy for $\alpha \gtrsim 10^3$ cm^{-1}, using the relation

$$Tr = (1-R) \exp(-\alpha t) \qquad (3 - 10)$$

where (1-R) is the transmittance at long wavelengths and t is the thickness of the film.

In the light of experimental results the optical absorption in amorphous semiconductors can be divided into three regions (Connell, 1979) as shown schematically in Fig. 3-5, which shows α vs $\hbar\omega$. Regions I and II represent extended-extended transitions partly perturbed by defects, while region III is believed to arise from transitions involving the defect states directly. The absorption edge at regions II and III represents a defect-induced tail at the lowest energies, an exponential region at intermediate energies resulting from lack of long-range order, and a power-law region at the highest energies . In the latter region , α is described by eq. (3-9).

The direct absorption measurements, however, proved to have large uncertainty in the energy range well below the optical gap, E_o, because of the weak absorption signal in that range. Another method to measure the optical absorption in this range is by photoconductivity measurements and is described in section 3.6.3..

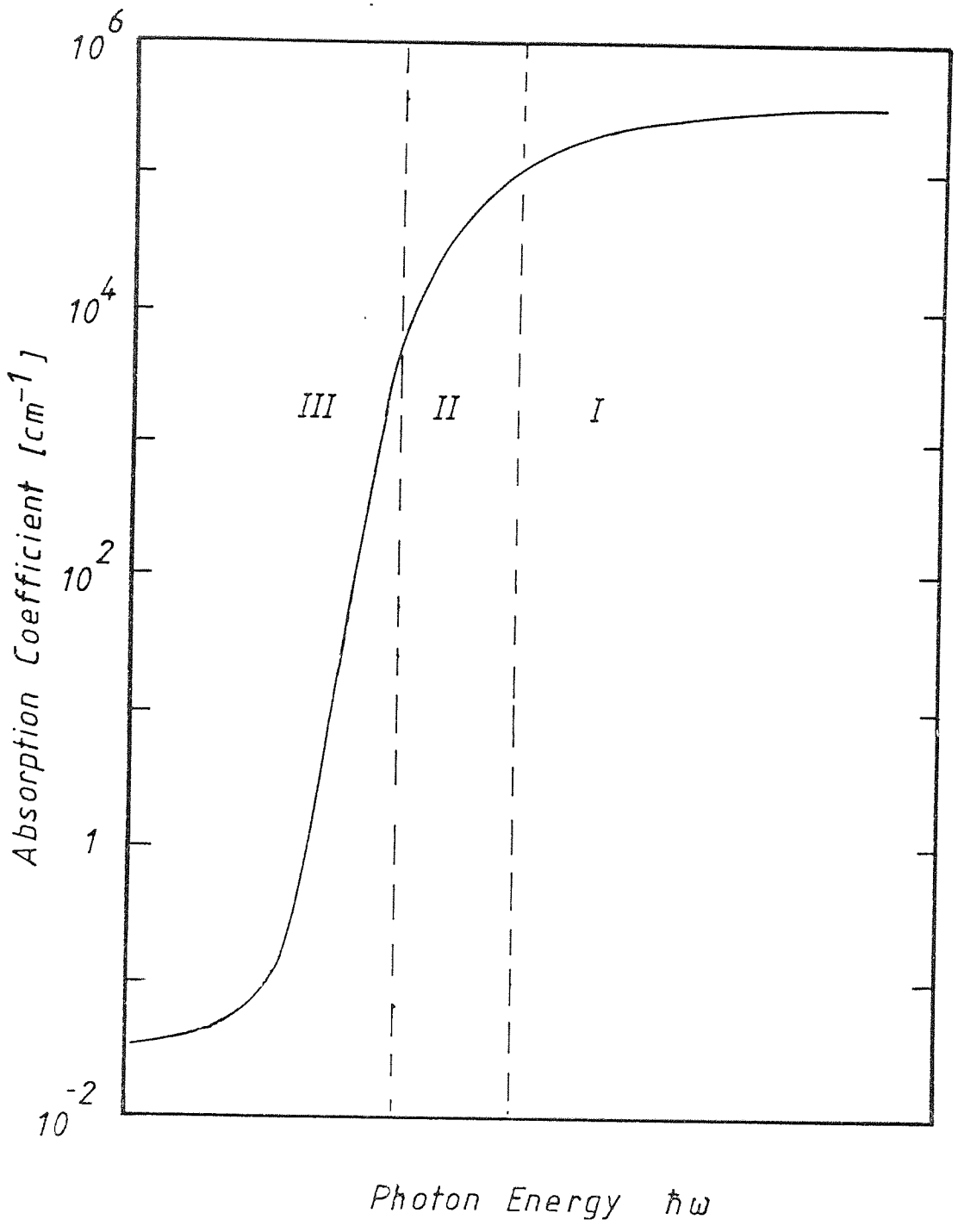

Fig. 3-5: Schematic representation of the absorption coefficient vs photon energy, $\hbar\omega$, of amorphous semiconductors. (Connell, 1979).

3.6. PHOTOCONDUCTIVITY

3.6.1. TEMPERATURE AND LIGHT INTENSITY DEPENDENCE OF PHOTOCONDUCTIVITY

The photocurrent, i_{Ph}, is defined as the difference between the current measured under illumination and the dark current. It has been established that at room-temperature, electrical transport occurs predominantly through the electron extended states at ϵ_c. Spear et al (1974) suggested that the localised states in the regions ϵ_A, ϵ_x, ϵ_y and ϵ_F, in the density-of-states distribution of Fig. 3-3 play an important role in the recombination processes of the photogenerated electrons and holes in a-Si, where recombination proceeds from the localised tail states at ϵ_A. The photoconductivity data presented in section(5.2.3.) suggests that at low light intensities the electrons recombine via the states at the Fermi level, ϵ_F, whereas at high light intensities recombination proceeds via holes trapped in the density-of-states feature at ϵ_y above the valence band edge. The following expressions for photoconductivity, σ_{Ph}, in the above two cases have been derived by Spear et al (1974) to explain their results for the temperature dependence of the photoconductivity of GD a-Si:H films. It will be shown that these expressions apply to the light-intensity as well as temperature dependence of photoconductivity of Ne-sputtered a-Si (sections 5.2.4.2. and 5.2.4.3.)

3.6.1.1. RECOMBINATIONS VIA HOLES TRAPPED AT ϵ_y

For the electronic conduction at ϵ_c, σ_{Ph} can be written as

$$\sigma_{Ph} = n_c e \mu_c \qquad (3 - 11)$$

where n_c is the carrier density at ϵ_c and μ_c is the mobility at ϵ_c. In the steady state, the generation rate, G, of electron-hole pairs created by photon excitation (illumination) is given by

$$G = K_1 n_A p_y \qquad (3 - 12)$$

where K_1 is the recombination constant and n_A and p_y are the total densities of electrons and holes at ϵ_A and ϵ_y respectively during illumination. If we assume that the electron densities at ϵ_c and ϵ_A are in quasi-thermal equilibrium, we can write

$$\frac{n_c}{n_A} = \frac{N(\epsilon_c)}{N(\epsilon_A)} \exp\left[- \frac{\epsilon_c - \epsilon_A}{kT} \right] \qquad (3 - 13)$$

where $N(\epsilon_c)$ and $N(\epsilon_A)$ are the effective densities of states at ϵ_c and ϵ_A respectively. When the density of the photogenerated carriers at ϵ_c (and ϵ_v) is larger than that in the dark, then the condition for charge neutrality will give $n_A \simeq p_y$, since $n_A \gg n_c$ and the photoexcited holes are assumed to be rapidly trapped at ϵ_y. Using this charge neutrality condition, eq. (3-12) can be rewritten as

$$G = K_1 n_A^2 \qquad (3 - 14)$$

Combining eqs. (3-11), (3-13) and (3-14) the photoconductivity can be given by

$$\sigma_{Ph} = e \mu_c (G/K_1)^{\frac{1}{2}} \frac{N(\epsilon_c)}{N(\epsilon_A)} \exp\left[- \frac{\epsilon_c - \epsilon_A}{kT} \right] \qquad (3 - 15)$$

Since the generation rate, G, of the electron-hole pairs, at a given excitation energy, is proportional to the light intensity, F, eq. (3-15) would lead us to expect that the photoconductivity of a specimen under the above conditions would increase as the square root of the light intensity at a given temperature. This type of recombination process is called a bimolecular process and occurs either at high light intensities or at sufficiently low temperature.

3.6.1.2. RECOMBINATION VIA STATES AT ϵ_F

We still assume the conduction to occur in the electron extended states. Assume that recombination takes place from states at ϵ_A via states at the Fermi level. In a similar way to the above case (eq. (3-12)), the photogeneration rate of electron-hole pairs, in the steady state, is

$$G = K_2 n_A N(\epsilon_F, T) \qquad (3 - 16)$$

where K_2 is the recombination constant in this case, and

$N(\epsilon_F,T)$ is the effective density of states at the Fermi energy, which is given by

$$N(\epsilon_F,T) = N(\epsilon_F)\,kT \qquad (3-17)$$

Combining eqs. (3-11), (3-13) and (3-16) we find that

$$\sigma_{Ph} = \frac{e\mu_c}{kT}\left(\frac{G}{K_2}\right)\frac{N(\epsilon_c)}{N(\epsilon_F)N(\epsilon_A)}\exp\left[-\frac{\epsilon_c-\epsilon_A}{kT}\right] \qquad (3-18)$$

Eq. (3-18) indicates that at a fixed temperature, under the above conditions, the photoconductivity would increase linearly with the light intensity. This type of recombination is called a monomolecular process and normally occurs at low light intensity levels, or at high temperatures.

From eqs. (3-15) and (3-18) we can draw a general relation between photoconductivity and light intensity at a given temperature, in the form

$$\sigma_{Ph} = C\,F^{\gamma} \qquad (3-19)$$

where C is a constant. The exponent γ varies between 0.5 and 1 depending on the dominant recombination process. Furthermore the thermal activation of the photoconductivity is expected to give the position of the tail-states edge, ϵ_A, with respect to the conduction-band edge at ϵ_c.

3.6.2. PHOTORESPONSE

Assuming that only electrons in the extended states are

contributing to the photocurrent (LeComber and Spear,1970), the photoconductivity can be given by the following expression

$$\sigma_{Ph} = e F (1-R) [1 - \exp (-\alpha t)] \eta \mu_D T_R / t \qquad (3 - 20)$$

where F(1-R) is the number of photons falling on 1 cm^2 of the specimen per second, corrected for the surface reflection. η is the quantum efficiency for photocarrier generation, μ_D is the electron drift mobility, T_R is the response time for photocurrent, which is a function of recombination lifetime, and t is the thickness of the film. In the weak absorption region (low photon energies), and for thin films $\alpha t \ll 1$, therefore eq. (3-20) may become

$$\sigma_{Ph} / e F (1-R) \simeq \alpha \eta \mu_D T_R \qquad (3 - 21)$$

This equation suggests that the photoconductivity results, especially at energies around and lower than the optical gap, could be used as a sensitive measure of the absorption below the optical energy gap. This is valid if we can assume constant η , μ_D and T_R. The validity of these assumptions is discussed in section 3.6.3..

The photoresponse represented by $i_{Ph} / e F (1-R)$ can be used to determine the optical gap, E_o^{Ph}, from the intercept of the plot of $[i_{Ph} \hbar\omega / e F (1-R)]^{\frac{1}{2}}$ vs excitation energy, $\hbar\omega$, with the $\hbar\omega$ axis. Furthermore from the plots, the photoconductive threshold, ΔE_a^{Ph}, (thermal activation energy at room temperature) can be determined by

extrapolating the "tail" of the curve at low energies to the zero value of $[i_{Ph}\hbar\omega/eF(1-R)]^{\frac{1}{2}}$.

3.6.3 LOW-ENERGY OPTICAL-ABSORPTION FROM PHOTOCONDUCTIVITY

It has been found that for energies not far below the optical gap, the absorption signal of a-Si films is strong enough to be detected and subsequently α values with significant accuracy can be obtained. In a-Si the thin film geometry limits the accuracy of α from direct transmission techniques to $\alpha \gtrsim 10$ cm^{-1} (e.g. Moddel et al, 1980). The values of α as low as this correspond to energies well below the optical gap, where the absorption signal is not strong enough and uncertainty in reflection is relatively high. Moreover in our samples the technique used to measure the transmittance is limited to $\hbar\omega \gtrsim 1.4$ eV (section 4.5.). Information about states in the gap requires the measurements of low α . Therefore another complementary technique is used. The Harvard group (Moddel et al, 1980) have developed a model in which the absorption coefficient, α, at low photon energies, can be derived from the photocurrent spectral distribution (i_{Ph} vs $\hbar\omega$) at these energies. The relative absorption coefficient (α/α_o) can be given by

$$\frac{\alpha(\hbar\omega)}{\alpha_o} = \frac{F_o}{F}\left[\frac{i_{Ph}(\hbar\omega,F)}{i_{Ph0}}\right]^{1/\gamma} \qquad (3-22)$$

where F_o is a reference photon flux, α_o is a reference absorption coefficient, i_{Ph0} is a corresponding reference photocurrent and γ is an empirical exponent in eq. (3-19) where $0.5 \lesssim \gamma \lesssim 1$ for a given excitation energy, $\hbar\omega$, and a given α . Relation (3-22) instead of considering i_{Ph} as a function of the incident flux, as in eq. (3-19), relates the dependence of i_{Ph} on the absorbed photons in the film. In this case i_{Ph} would be a function of both the incident photon flux, F, and the absorption coefficient, $\alpha(\hbar\omega)$.

In deriving eq. (3-22) the following assumptions were made.

(i) The illumination and electron-hole generation are uniform throughout the material. This is met by using thin film samples so that $\alpha t \ll 1$ and subsequently eq. (3-20) leads to eq. (3-21).

(ii) Reflectivity does not vary with $\hbar\omega$ at energies below the optical gap, and the interference resulting from the front and back surfaces is ignored.

(iii) Only one type of photocarriers is contributing to photocurrent with drift mobility μ_D independent of $\hbar\omega$ over the excitation energy range of interest. However, it has been established that the electrons are the dominant photocarriers in a-Si (LeComber and Spear, 1970). The plots of α/α_o vs $\hbar\omega$ at different temperatures (Fig. 3-6) show that within the experimental error, there is no marked

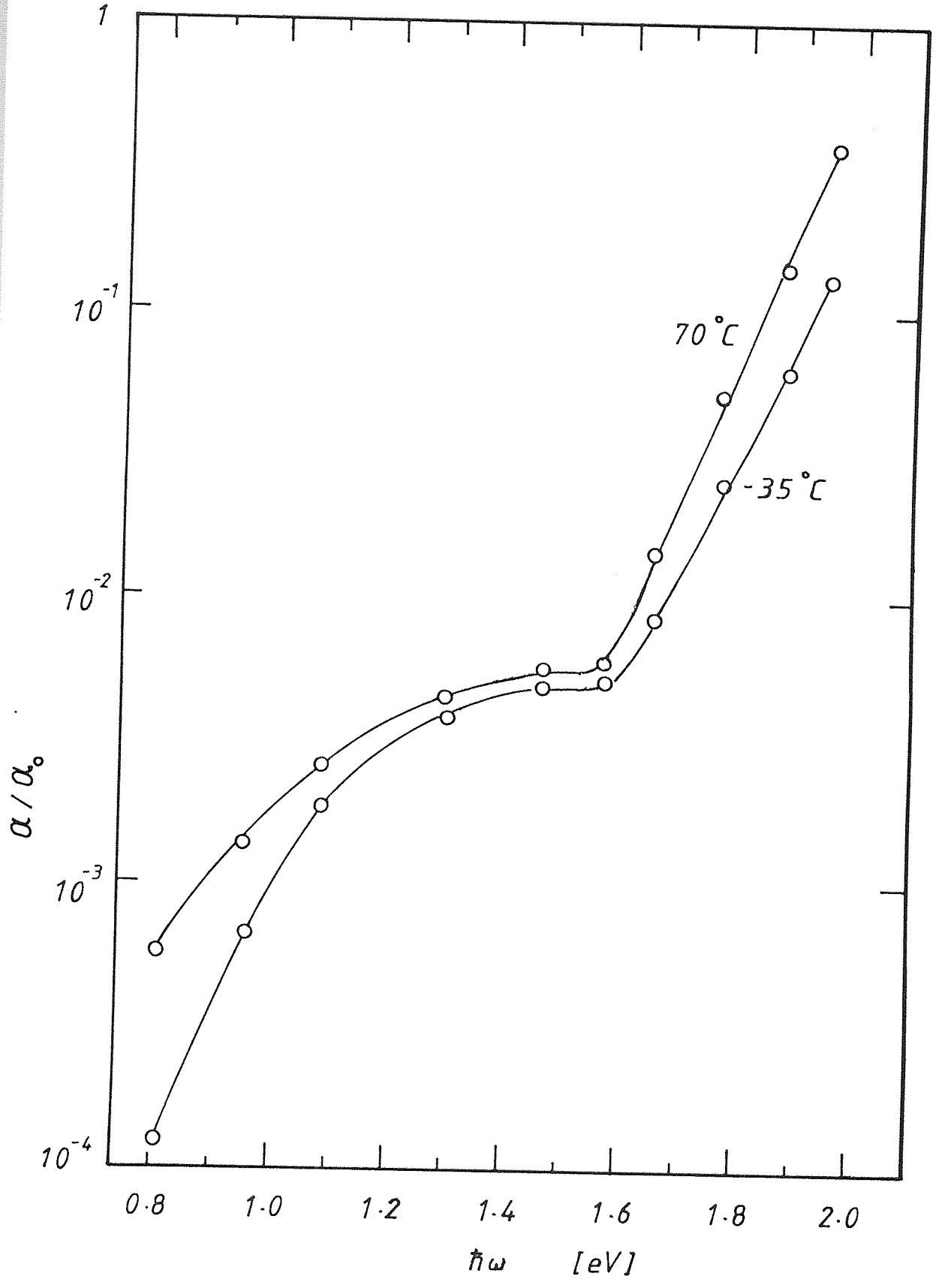

Fig. 3-6: The relative absorption coefficient (α/α_o) vs photon energy, $\hbar\omega$, at two different temperatures.

change in the shape of the curves for energies above 1 eV. Thermal activation behaviour of μ_D has been reported (e.g. Moustakas and Paul, 1977; Spear et al, 1974). Therefore if μ_D depends on the excitation energy, α/α_o curves would be expected to show strong dependence on the temperature. The similarities in curves of Fig. 3-6 indicate that μ_D is independent of excitation energy. The horizontal shift in the curve with temperature is expected because of the temperature dependence of the absorption edge (e.g. Freeman and Paul, 1979)

(iv) The exponent γ in eq. (3-19) does not vary with $\hbar\omega$. This assumption can be justified experimentally (Fig. 3-7). The figure shows the measured i_{Ph} plotted against the light flux, F, at different $\hbar\omega$ values. It can be seen that the γ values are independent of the excitation energy .

(v) The response time, T_R, of photocurrent and the quantum efficiency, η , for the photocarriers generation are assumed to be independent of $\hbar\omega$ in the energy range under consideration. The measurements of photocurrent decay after the light is switched off (Moddel et al, 1980) showed that the response time, T_R, in the energy range considered depends on the density of photocarriers in the material rather than on the excitation energy. The independence of the exponent factor γ on the excitation energy (Fig. 3-7), could be another justification for this assumption, since γ is an indication of the rate of rise of the

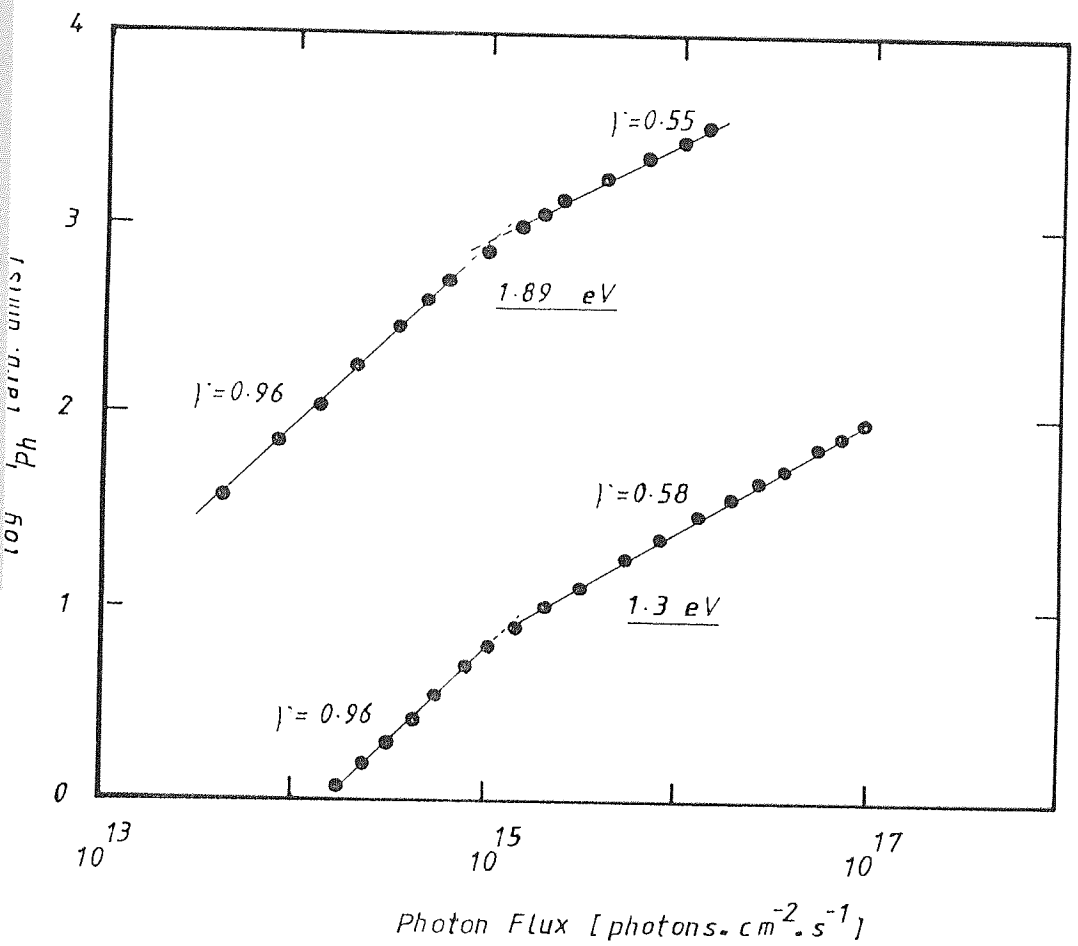

Fig. 3-7: The light intensity dependence of photocurrent, i_{Ph}, in a-Si for two exciting photon energies. γ is the exponent factor in the relation $i_{Ph} \propto F^{\gamma}$.

photocurrent. Finally Carasco and Spear (1983) have argued that the quantum efficiency, η, should decrease as the excitation energy becomes lower than the optical gap. On the other hand, it has been suggested that at room temperature, the excitons dissociate thermally, which is evidenced by the absence of luminescence structure corresponding to the exciton recombination (Paesler and Paul, 1980). However we must deal with this assumption with caution, where assuming constant η would reduce the derived α at lower energies to less than its true value. Therefore the α values derived from photocurrent measurements particularly at low $\hbar\omega$ will be regarded as the lower limit of α .

Using the above method, absorption coefficients as low as about 10^{-1} cm^{-1} may be reliably determined (e.g. LeComber et al, 1973: Anderson et al, 1979). The details of the results which are analysed in the light of this model will be discussed in section 5.2 .4.4.. However, it should be emphasised that the absorption spectra cannot determine an absolute value for the density of states in the mobility gap, but they are reliable for comparison of samples prepared under different conditions and they can be used as a check on other types of direct measurements of the density of states such as field effect measurements (e.g. Madan et al, 1976).

CHAPTER FOUR

EXPERIMENTAL DETAILS

4.1. INTRODUCTION

In this chapter the sputtering system which was used for preparing the films is described. Also the preparation procedure of the specimens is described in some detail. Various measurements, such as dark electrical current , photocurrent, optical absorption and film composition are explained.

4.2. SPUTTERING SYSTEM

A schematic diagram of the radio-frequency diode sputtering system which was used during the course of this work is shown in Fig. 4-1. The system was originally designed and built by Newman (1972). It comprises three main components; the sputtering chamber, the vacuum system and the radio frequency (r.f.) power supply. The sputtering chamber consists of a target (cathode) and substrates holder in plane-parallel arrangement with a rotatable shutter between them. The target-holder assembly is shown in Fig. 4-2. The single-crystal wafer target of electronic grade silicon was about 7 cm in diameter with a grounded shielding bracket usually positioned around the backing electrode, typically, at a spacing of about 2 mm to prevent neon plasma coming into contact with the backing electrode, therefore stabilising the plasma conditions and preventing the sputtering of the target holder. The target was glued with a high thermally-

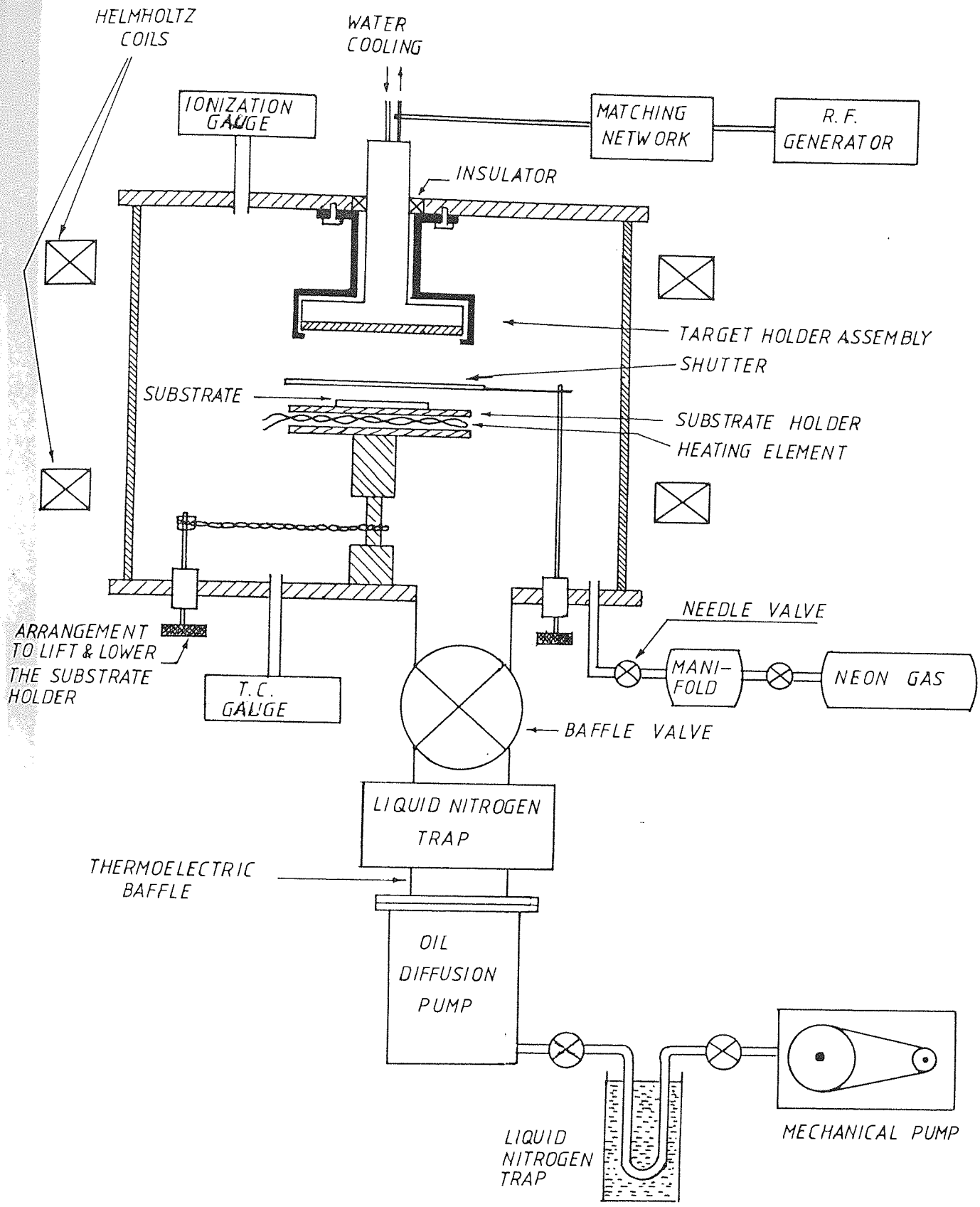

Fig. 4-1: A schematic diagram of the rf-sputtering system.

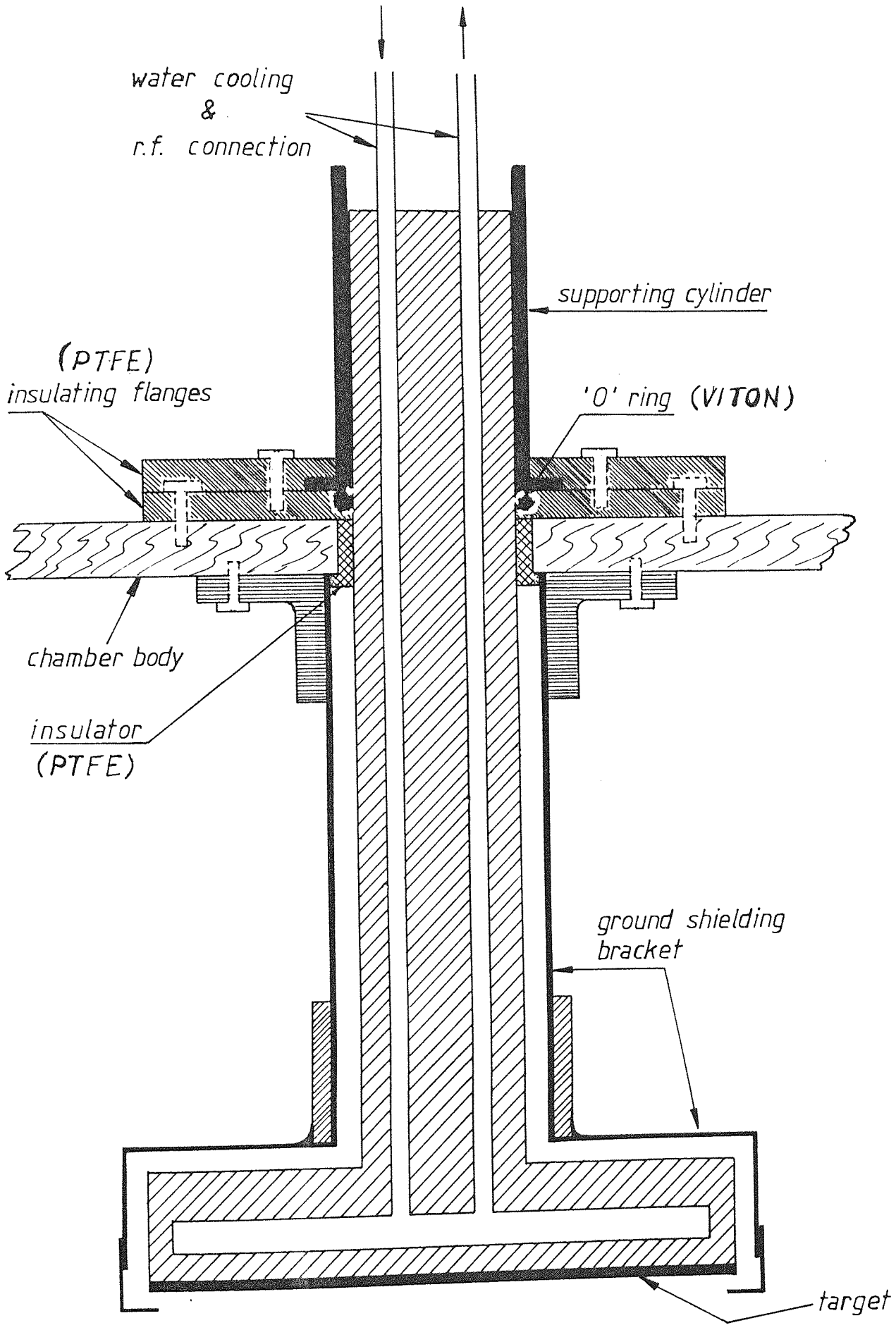

Fig. 4-2: Target holder assembly.

conductive epoxy (silicone 732-DOW CORNING) to the water cooled target-holder. However, recently a more practical target holder was designed and used, which is similar to that of Fig. 4-2 except that it is more convenient since the target, instead of being glued, could be placed on the target holder with a thermal grease between them, and then screwed in. The target was connected via the target holder to a r.f. generator and matching network (Fig. 4-1) which was tuned for minimum reflected power. The substrate was placed on a grounded copper substrate-holder which could be electrically heated using a Nichrome ribbon resistor (3.63 Ohm/meter). The substrate temperature was measured with two chromel-alumel thermocouples, one at a corner of the substrate holder and another at the opposite corner. The agreement between the two thermocouples was good. The target-substrate distance could be adjusted using a gear. To confine the plasma to the space between the target and the substrate, a Helmholtz pair of coils was mounted around the chamber to provide a uniform magnetic field in the centre of the plasma.

The sputtering chamber is mounted on a conventional high vacuum system consisting of a 6" SPEEDIVAC E04 oil diffusion pump with a liquid nitrogen cooled-trap and a thermoelectric baffle to prevent backstreaming of oil vapour into the sputtering chamber. The diffusion pump is backed by a mechanical rotary pump and another liquid nitrogen trap as shown in Fig. 4-1. The sputtering chamber was outgassed by an electrical heating tape around it. With this aid, the background pressure prior to a sputtering run was always of

the order of 10^{-7} Torr, measured by an ionisation guage.

During the run, the sputtering chamber was isolated from the vacuum system by a butterfly baffle valve, which together with a needle valve on the gas supply line was used to control the gas flow to achieve the required gas pressure in the chamber which was measured by a SPEEDIVAC DCB6 thermocouple (T.C.) guage.

4.3. DEPOSITION PROCEDURE

Cleaning of the substrates and the sputtering chamber before the film deposition has been found to be very important in order to obtain good adhesion between the film and the substrate, as well as pinhole free films. For this purpose Corning 7059 glass substrates were ultrasonically cleaned in a detergent for about 15 minutes, rinsed thoroughly in distilled water, washed ultrasonically in distilled water for a few minutes and then boiled in isopropyl alcohol before placing in the sputtering chamber. The chamber was evacuated to a pressure of 5×10^{-7} Torr as described in section 4.2.. The sputtering chamber was outgassed by baking overnight at about 150^{o}C. The substrate was electrically heated to the appropriate temperature in the range up to 500 ^{o}C. The target was a single crystal wafer of electronic grade silicon, kindly supplied by Mullard Limited.

For the purpose of doping, a composite target was used where the dopant material was fixed on the centre of the

silicon target. In the case of Al doping, a disc cut from an aluminium sheet (99.99%) was used, while for boron doping a pellet was prepared by compressing boron powder (99.9%) in a die. Since gallium has a low melting temperature a small ingot of Ga was rubbed against the centre of the silicon target. This helped Ga to stick to the target . However, during the sputtering, the gallium piece melted and formed a small ball at the centre of the target. In some cases, the target was a highly B-predoped target, kindly supplied by Mullard.

Neon gas (99.999%) was admitted into the chamber via a needle valve, thus by controlling the flow rate the desired pressure could be achieved. The deposition pressure ranged between 40 and 200 mTorr. The target-substrate distance was varied from 2 to 5.3 cm. The radio-frequency field was applied to start the plasma resulting in a self-bias voltage on the target in the range between 600 V and about 1000 V. The self-bias voltage was measured using a circuit similar to that of Rock and Smith (1975). A Helmholtz pair of coils gave a field of about 0.01 T at the centre of the discharge. The target was pre-sputtered prior to deposition for a few minutes to remove any possible contamination on the target.

As will be demonstrated in chapter Five, combinations of the above prearation conditions resulted in films with a wide range of deposition rates (Fig. 5-3) , electronic and optical properties (see section 5.2.).

The film thickness, with an estimated uncertainty of $\pm$ 10%, was measured using multiple beam interferometry (HILGER & WATTS interfero meter) on an edge produced by masking and overlayed with evaporated-aluminium. The film thickness ranged from 0.3 to 1.5 μm. The thick-of some of the films was also measured by a TALYSURF surface profiling instrument and a good agreement between the two methods was obtained. The thickness uniformity throughout the film was within the experimental uncertainty.

4.4. D.C. CONDUCTIVITY AND PHOTOCONDUCTIVITY

The d.c. electrical dark conductivity was measured in the temperature range between -150 ^{o}C and 150 ^{o}C under vacuum using the arrangement shown in Fig. 4-3. Aluminium surface cell electrodes, 2 mm wide and with typically 1 mm gap, were thermally evaporated onto the top surface of the a-Si specimens, prepared by sputtering in Ne gas as described in section 4.3.. A stainless steel mask was used. A Keithley 610C Electrometer was used for the measurements of current, I, as a function of temperature, T, with a fixed applied field of 10^2 V.cm^{-1}, using the circuit shown in Fig. 4-4. The electrical leads and copper-constantan thermocouple used for measuring the specimen temperature were attached to the specimen surface by a DU PONT high temperature silve paste. The current-voltage characteristics for each specimen were checked for linear behaviour in electric fields up to about $5x10^2$ V.cm^{-1} at room temperature and at a number of higher and lower temperatures during the run. Al electrodes proved to make good ohmic contacts, both with undoped and p-type doped a-Si within the range of the

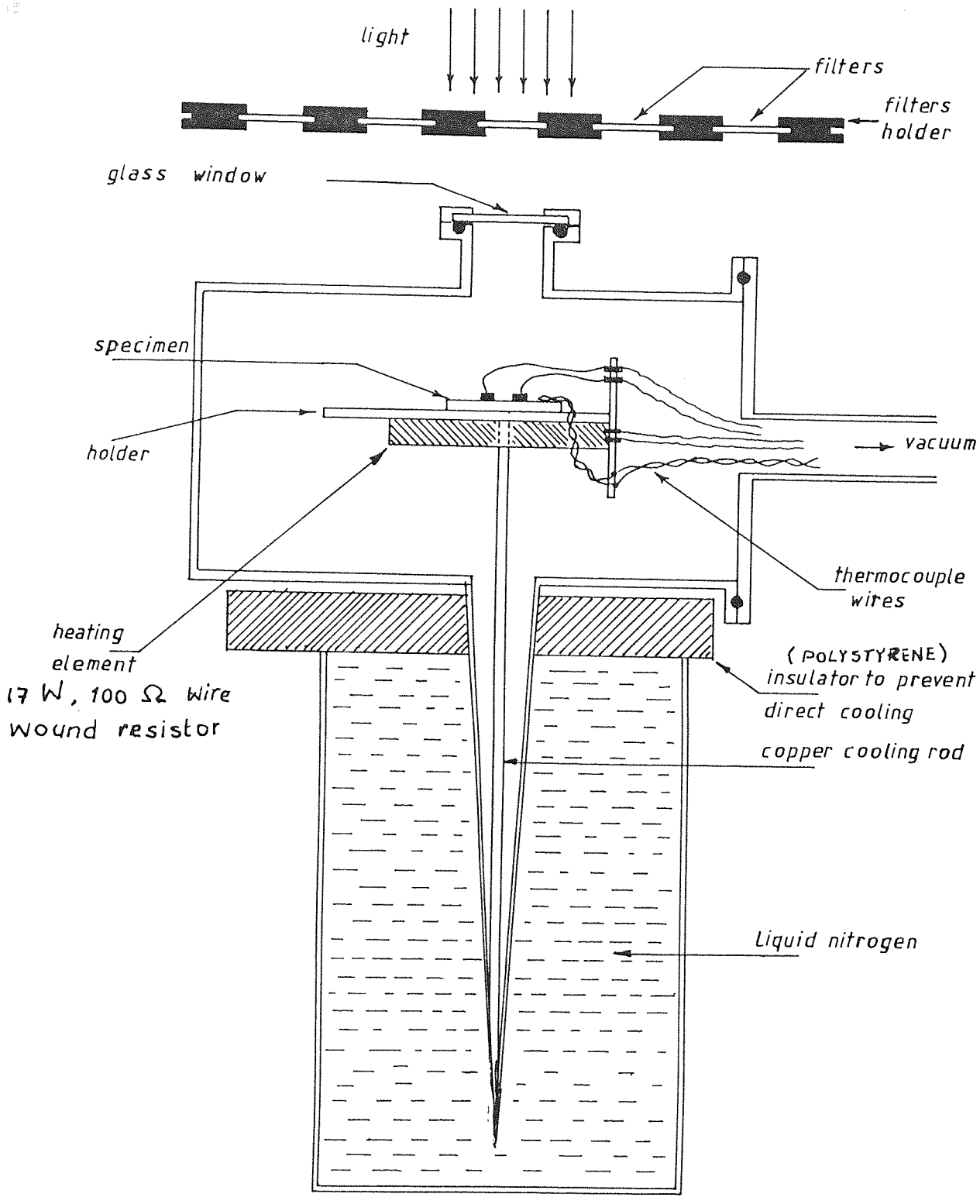

Fig. 4-3: An arrangement for dark-conductivity and photoconductivity measurements.

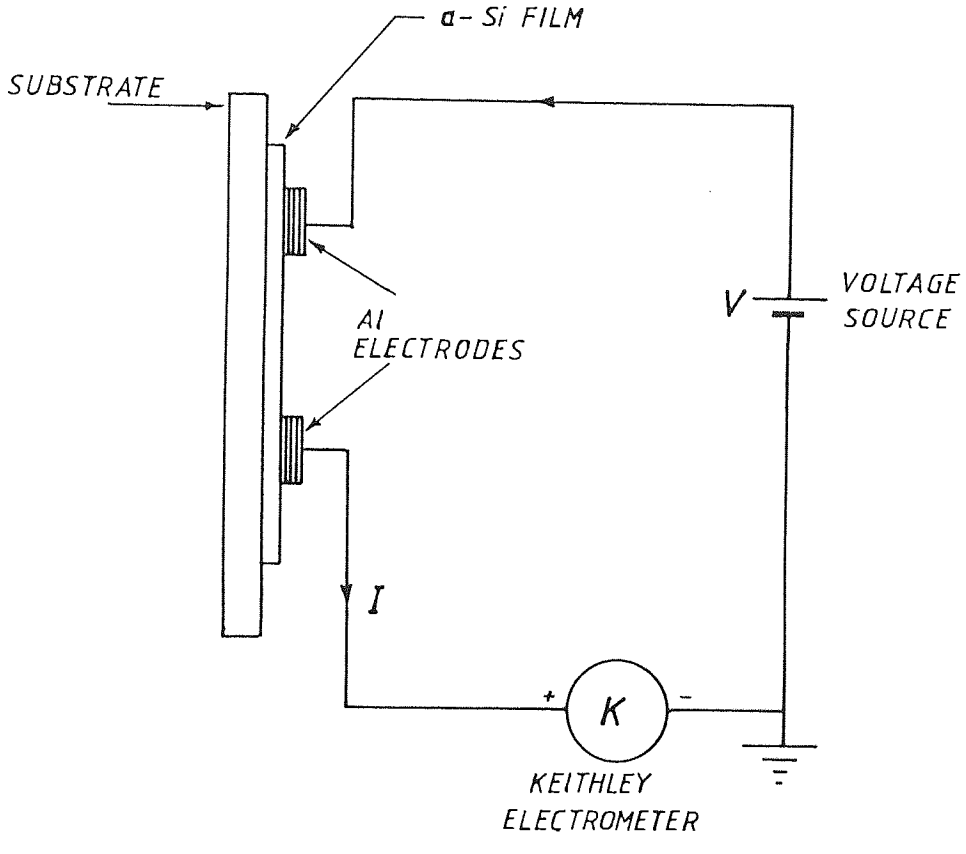

Fig. 4-4: The circuit used for conductivity and photoconductivity measurements.

applied fields at the various temperature ranges. However more recently, further investigation showed that Al makes good ohmic contacts with a-Si in a field range up to about 10^4 V.cm^{-1} as shown in Fig. 4-5.

The dark conductivity, σ, was calculated from the relation

$$\sigma = LI/AV \qquad (4 - 1)$$

wher L is the width of the cell gap, A is the cross sectional area and V is the applied voltage.

The conduction type of randomly chosen undoped and doped films was readily determined from the polarity of the room-temperature thermopower sign observed by the hot-probe technique. The tested undoped samples were all n-type; while the doped samples were p-type.

The photoconductivity experiments were carried out on the same gap-cell configurations as for the dark conductivity measurements. The steady photocurrent, defined as the difference between the current measured under illumination and the dark current, was measured for the applied field of 10^2 V.cm^{-1}. A 300 W rated tungsten lamp was used as a light source, and was mounted on a stand for a vertical incidence of light on the specimen.

For spectral photoresponse, a group of BALZERS selected interference filters were mounted on a rotatable disc above the specimen

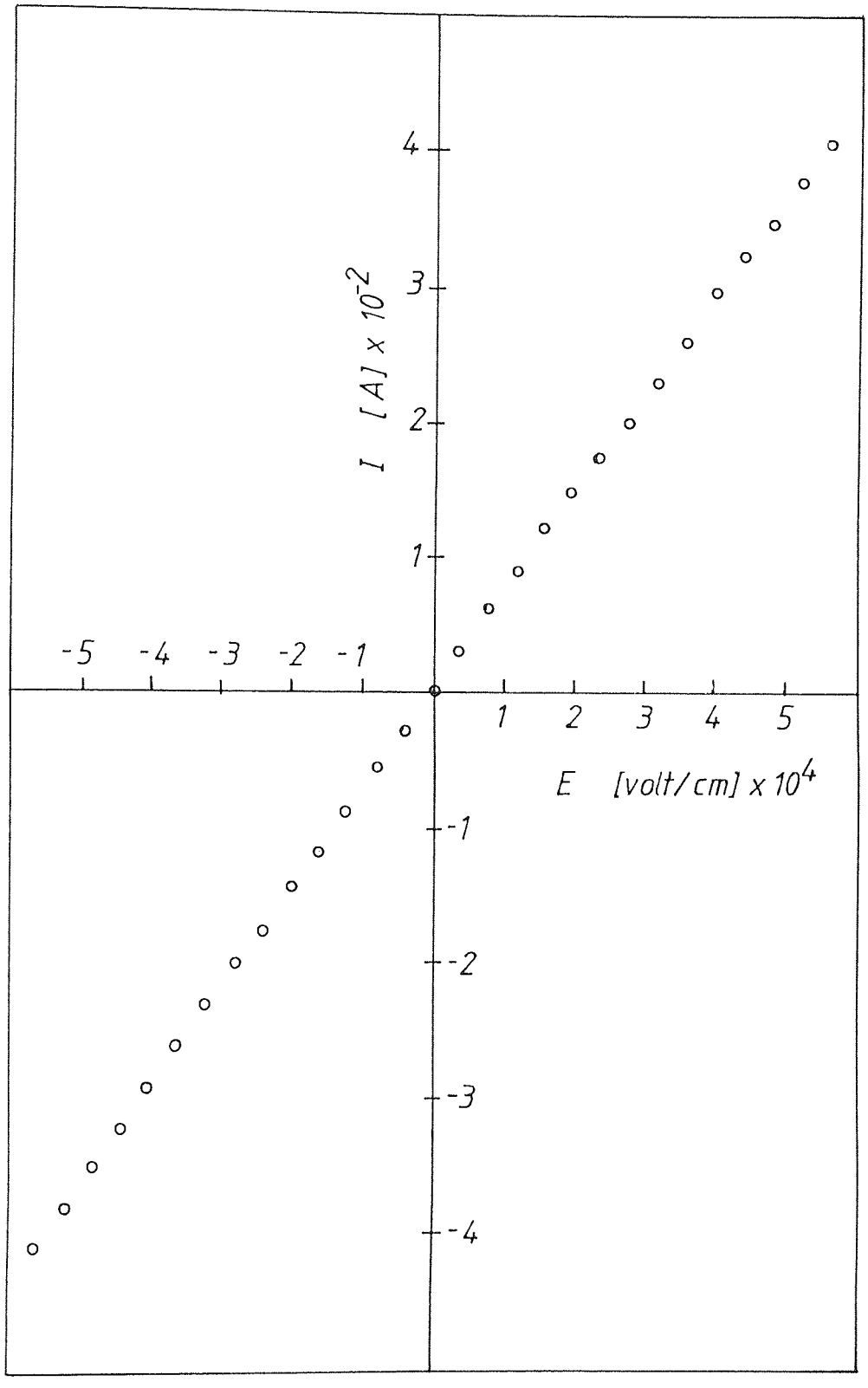

Fig. 4-5: I-V characteristic curve of a typical Al/a-Si/Al junction, at room temperature.

(see Fig. 4-3). The band width of the filters is typically about 10 nm as specified by the manufacturer. The transmission band-shape of a typical filter is shown in Fig. 4-6. However, the band width of the filters is negligibly small compared both to the "monochromatic" light wavelength and to the breadth of the photoresponse spectra as seen from Fig. 4-7. the output light intensity of these filters was calibrated using an EPPLEY PSP pyranometer, rated 9.98×10^{-6} $V.W^{-1}.m^2$, which was in turn checked against a NEC GLG2058 He-Ne laser beam of 6328 nm wavelength and 0.7 mW. The measured rating of the pyranometer was 7.88×10^{-6} $V.W^{-1}.m^2$.

Due to difficulties in adjusting the specimens for normal light incidence, they were displaced horizontally to give the maximum photoresponse. This was considered to correspond to normal incidence. However, the dislocation of the centre of the specimen with an angle of about 0.7° from the normal, caused a change in the photocurrent of less than 3%.

To have a wide range of light intensities, the voltage across the tungsten lamp was varied up to about 240 V. The variation of the light intensity with the applied voltage for two wavelengths is shown in Fig. 4-8.

The intensity dependence of the photoconductivity was measured using mainly two filters (1.89 eV and 1.3 eV), for the light flux intensity in the range from about 10^{13} to about 10^{17} photons.$cm^{-2}.s^{-1}$. The dependence of photo-conductivity on temperature was measured in the temperature

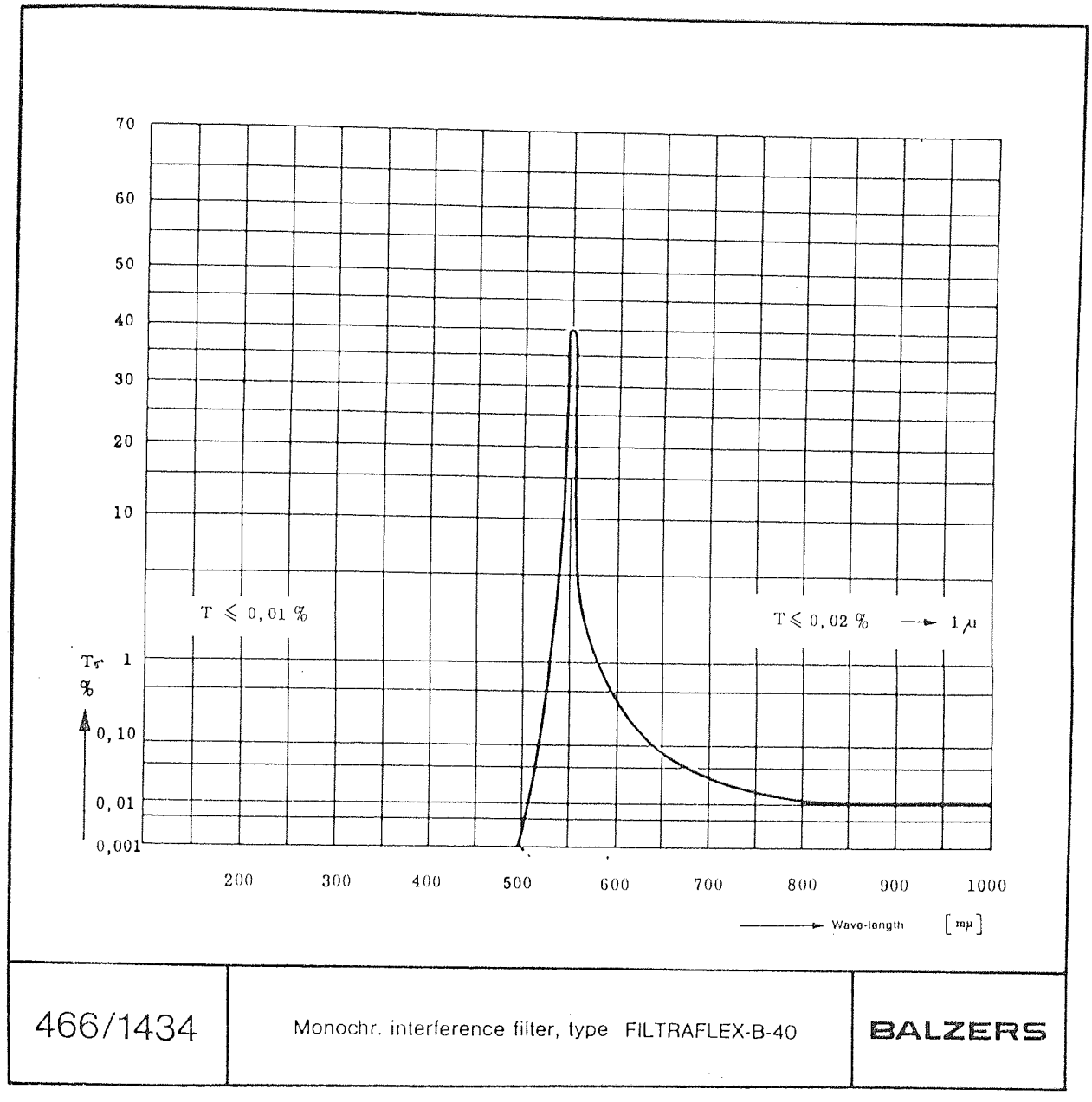

Fig. 4-6: The transmission band-shape of a typical interference filter.

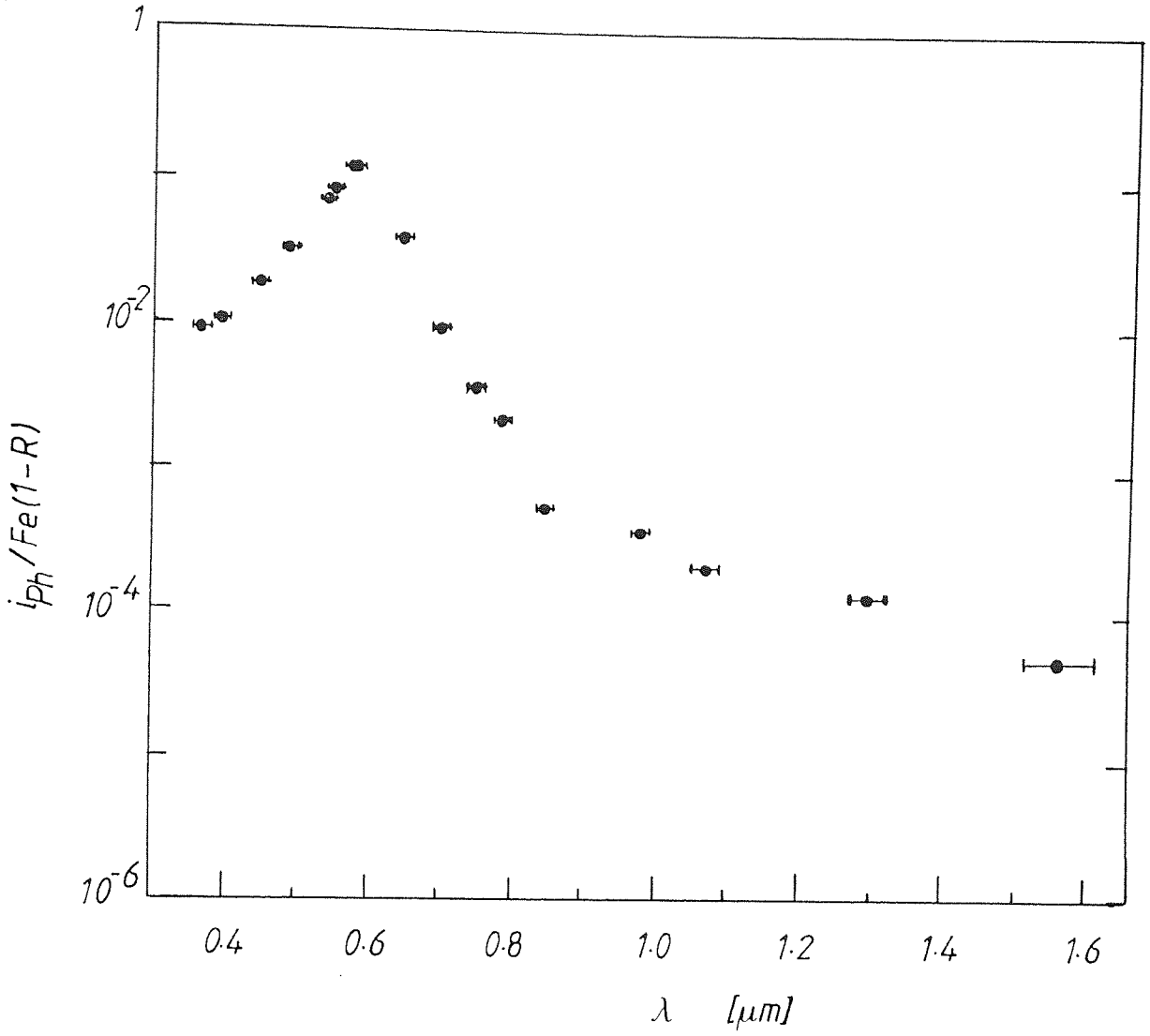

Fig. 4-7: The photoresponse of a typical a-Si film as a function of wavelength.

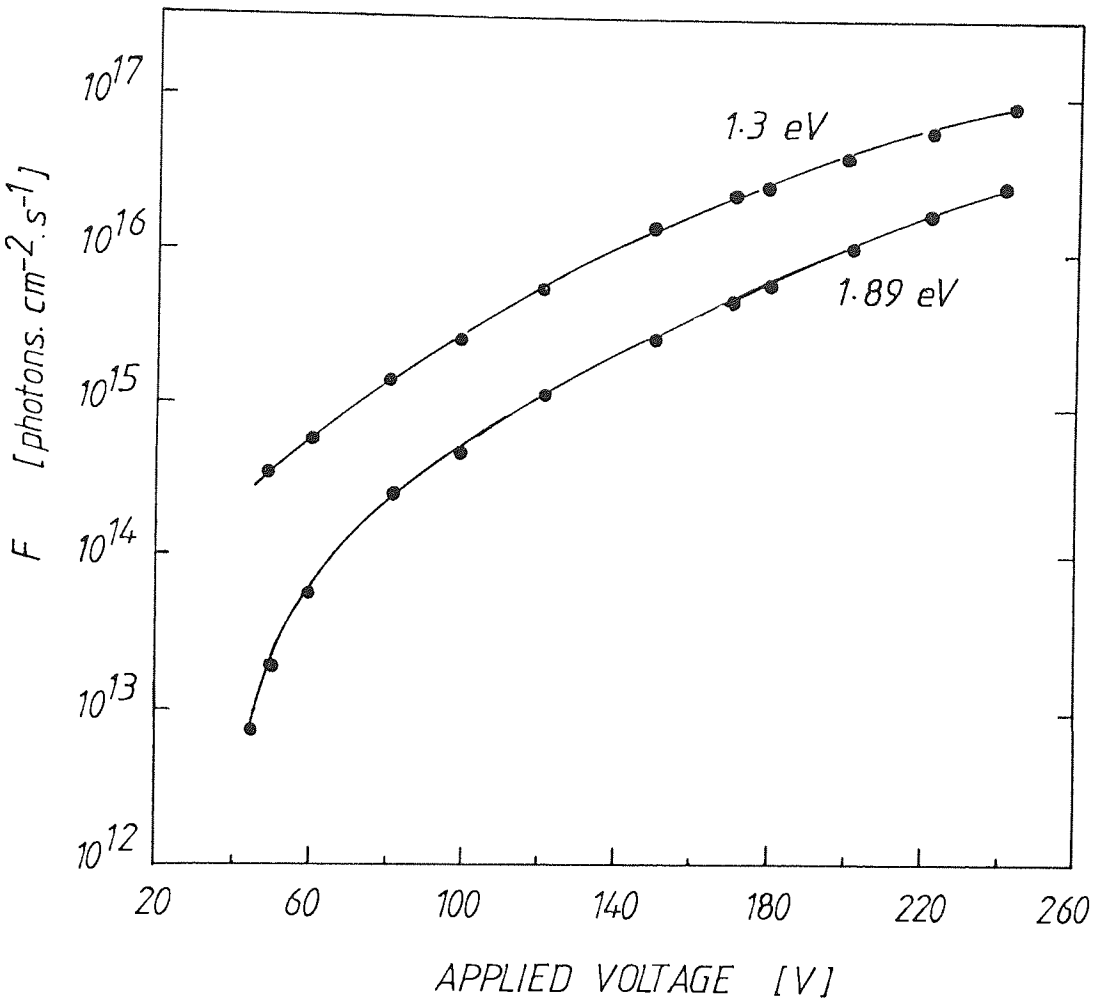

Fig. 4-8: Calibration of the light intensity for two photon energies, 1.89 eV and 1.3 eV, against the applied voltage to the lamp. The lamp was at a distance of 40 cm from the radiometer.

range from about -40 °C to about 140 °C. The same arrangement shown in Fig. 4-3 was used for these experiments.

4.5. OPTICAL ABSORPTION

Optical transmission in the wavelength range from about 400 nm to about 900 nm was measured for samples deposited on glass substrates, using a UNICAM spectrophotometer. These wavelengths cover the visible range and part of the ultraviolet range. To calculate the absorption coefficient α, it has been assumed that reflection is constant with wavelength at long wavelengths where this is justified when α is not small. The approximate relation for transmittance, Tr,

$$Tr \simeq (1-R) \exp(-\alpha t) \qquad (4-2)$$

was used for calculating α, where t is the film thickness and (1-R) is the value of Tr at which the interference averaged transmittance levels off at higher wavelengths. The uncertainty in the calculated α for $\alpha \gtrsim 10^3$ cm^{-1} was found to be less than 10%.

4.6. CLEANLINESS OF FILMS

Infrared absorption was used to check for any oxide contamination in the films. No absorption corresponding to Si-O vibrational mode was detected. As another check for the presence of contamination in the films, photoemission spectroscopy was used. The measurements were

taken by a KRATOS XAMS-800 spectrometer, using Mg $K\alpha$ x-ray excitation. The photoemission spectra showed no sign of chemical shifts due to silicon oxides. However oxygen photopeaks could be detected before etching the surface of the film. This could be due to the presence of voids in some of the films. Upon etching the surface of the films no oxide or free-oxygen peaks were detected in films prepared at $Pd/V_{sb} \leq 0.8$ mTorr.cm.V^{-1}. P, d and V_{sb} are the sputtering pressure, the target-substrate distance and the self-bias voltage on the target respectively. Furthermore, the presence of a relatively strong surface plasmon of Si(2s) photopeak at the right energy (Fig. 4-9) is another indication of the contamination free surface, at least within the detection limit of this technique. Also, this technique failed to detect Ne traces. The same measurements were taken at different depths in the films by means of ion etching. No change in the spectra shape was indicated. It is worth noting that the XPS measurements were taken at least a few days after deposition.

The absence of both the chemical shifts and Ne photopeaks in the photoemission spectra are indicative of oxide- and Ne-free films within the detection limit of this technique generally accepted as 0.1% (e.g. Usami et al, 1980).

Finally, the appearance of a plasmon loss at an energy almost similar to that in the crystalline silicon (about 17 eV (e.g: Kittel, 1971)) may suggest that the material of the films is close packed.

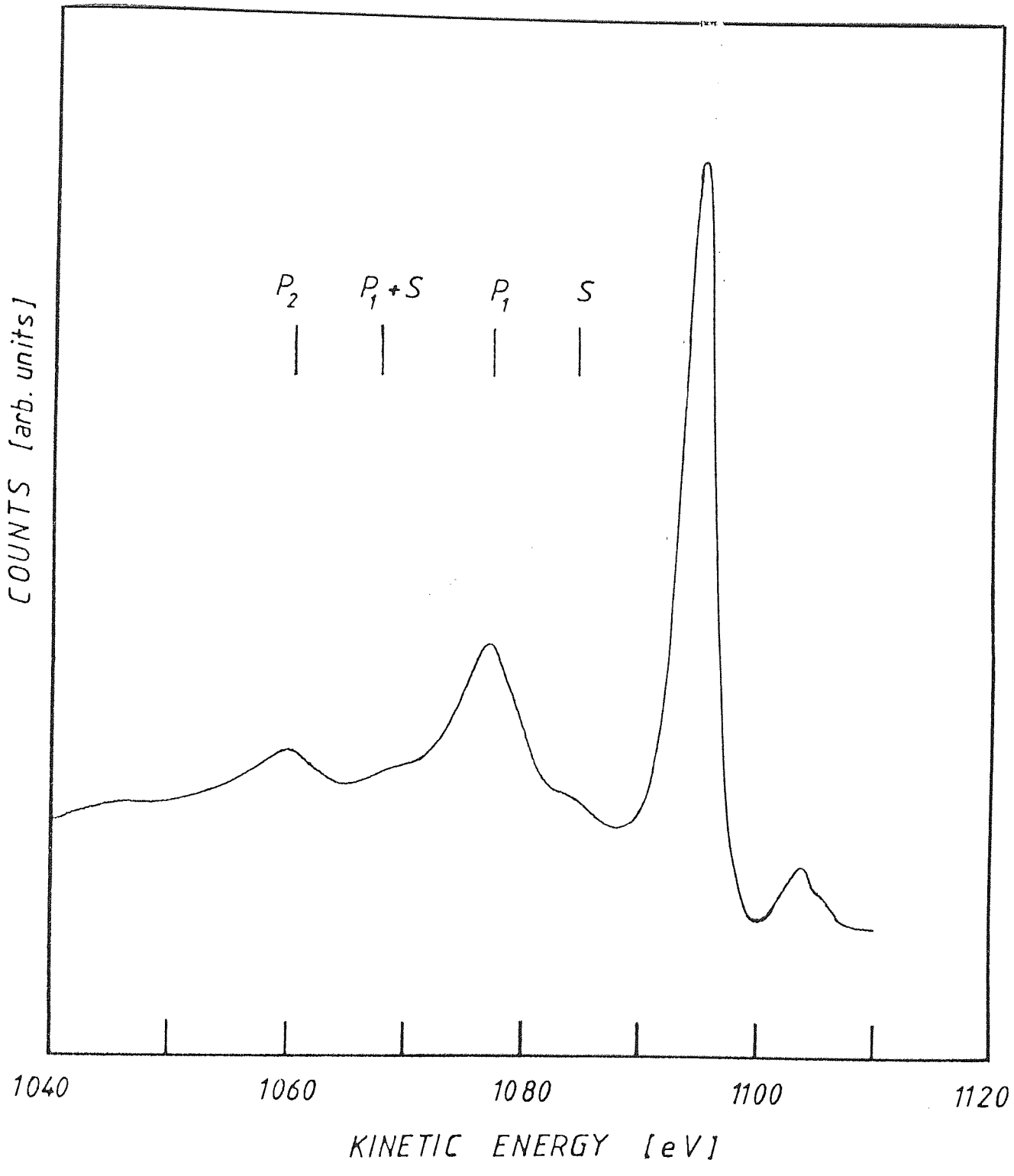

Fig. 4-9: Si(2s) photopeak in the XPS spectra showing the bulk (P) and surface (S) plasmon losses, for a-Si. P_1 first bulk plasmon, P_2 second bulk plasmon , etc.. For clean surface $E_S=E_P/\sqrt{2}$.

4.7. FILM COMPOSITION

The aim of this study was to determine the atomic percentage of the dopant in the a-Si films. Two methods were used as described in the following two sections. Photoemission measurements were used for determining the Al and Ga concentrations, though for the convenience of explanation, Al is mentioned in the equations of section 4.7.1.. Since B(1s) photopeak is superimposed on the plasmon peaks of Si(2p), and B(1s) also has a small ionisation cross-section (Scofield, 1976), the B/Si atomic ratio was difficult to determine by XPS. The etching profile method was used only for Al since information about the sputtering yields of B and Ga are not available. In the light of the reasons given in section 6.2.2., the B/Si target area ratio was considered to represent the upper limit of the B/Si atomic ratio in the films.

4.7.1. PHOTOEMISSION MEASUREMENTS

The atomic percentage of Al in the silicon films was calculated from the photoemission measurements. Al (2p) and Si (2p) photopeaks were choosen to calculate Al percentage in Si since they have similar kinetic energies, so the electron escape depths for these two lines are considered to be approximately equal. However, for more accurate calculations, the electron escape depths reported by Penn (1976) were used. The atomic ratio (N_{Al}/N_{Si}) of Al to Si was calculated from the approximate relation

$$\frac{N_{Al}}{N_{Si}} = \frac{I_{Al} \cdot \pi_{Si} \cdot \lambda_{Si}}{I_{Si} \cdot \pi_{Al} \cdot \lambda_{Al}} \qquad (4 - 3)$$

where I_{Si} and I_{Al} are the intensities of Si(2p) and Al(2p) peaks respectively, π_{Si} and π_{Al} are the photoionisation cross-sections for Si(2p) and Al(2p) respectively, and λ_{Si} and λ_{Al} are the electron escape depths for Si(2p) and Al(2p) respectively. The photoionisation cross-sections were taken from the calculations of Scofield (1976). The atomic percentages of Al in the a-Si films determined by this method are shown in Table 4-1. The atomic ratio of Al to Si was found to be nearly the same at different depths in the films. A similar method to that described above has been followed to determine the atomic ratio of Ga to Si.

4.7.2. ETCHING PROFILE OF THE TARGET

The etching profile of the sputtered Si target was studied as a function of the distance from the centre of the target. The thickness of the target after a long time sputtering was measured at different positions with respect to the centre. The shape of the target after etching is shown in Fig. 4-10, where the target could be divided into two regions. Region A represents a grove-like ring, a result of a higher etching rate near the edges of the target. This could be due to the distortion of the electric field at this region which might effect the angles of incidence of the bombarding ions. However, it has been reported that the sputtering yield

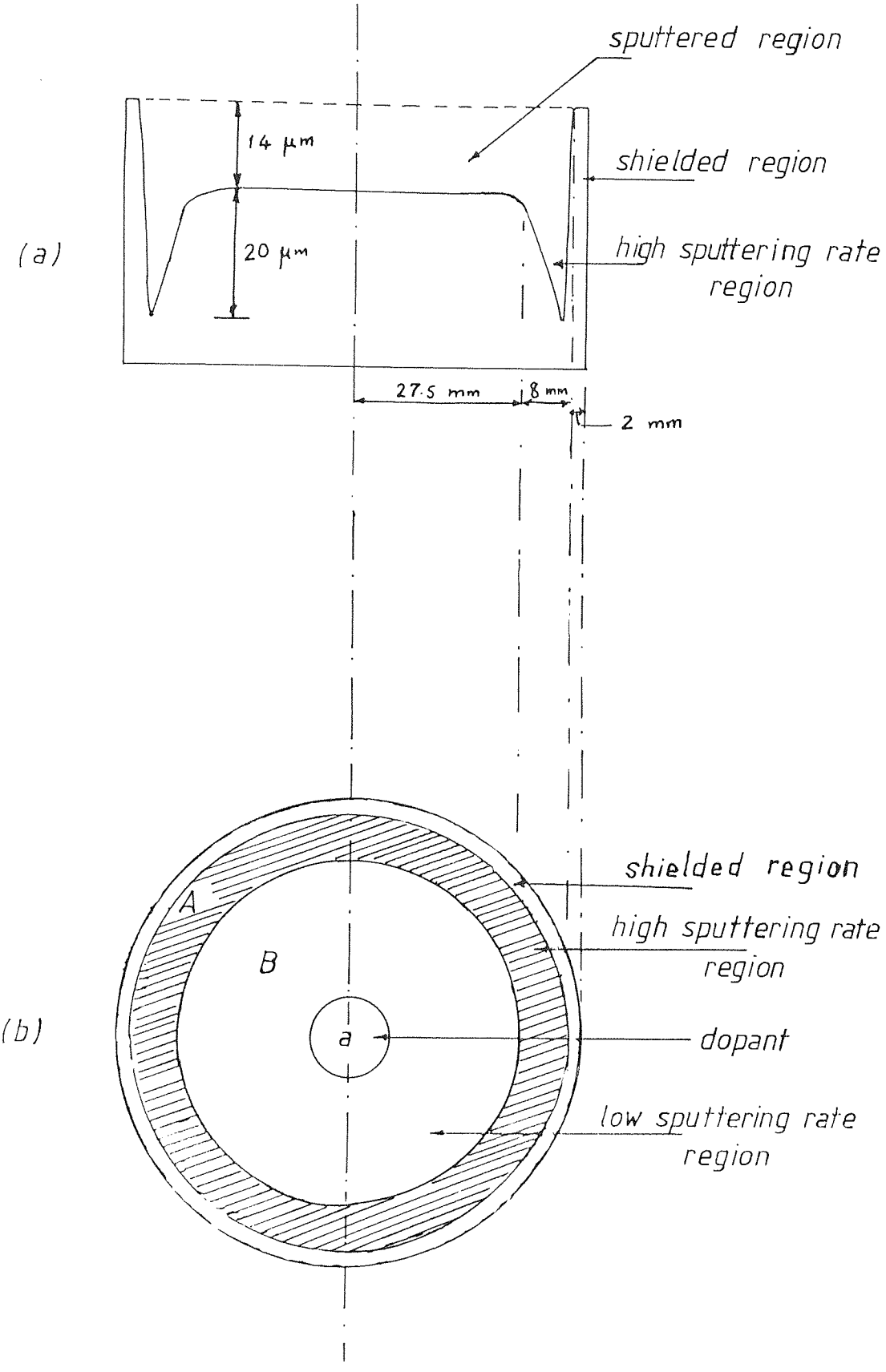

Fig. 4-10: The shape of the target after sputtering for a long time. (a) side view, (b) top view.

(i.e. the number of target atoms emitted per bombarding ion) increases for increasing angle of incidence up to 40^{o} to 80^{o} from the normal (e.g. Jackson, 1970). On the other hand, region B represents a flat disc which had resulted from a uniform sputtering at a lower etching rate. Measurements showed that over 65% of the target area was uniformly sputtered, though this fraction would be larger if the total target areas was larger. The volumes of the sputtered regions, calculated from the dimensions shown in Fig. 4-10a, were used to calculate the sputtering rate of silicon at region A relative to that at region B, which was found to be about 1.56:1. Now with the Al disc of area (a) at the centre of the target (i.e. in region B), the sputtering rate of the Al is given by

$$a.Y_{Al} \qquad (4 - 4)$$

where Y_{Al} is the Ne-sputtering yield for Al. The relative sputtering rate of Si is given by

$$(B-a).Y_{Si} + 1.56\ A.Y_{Si} \qquad (4 - 5)$$

A and B are the areas of regions A and B respectively, and Y_{Si} is the Ne-sputtering yield of Si. From the expressions (4-4) and (4-5), considering the measured values of A and B, the Al/Si atomic ratio is given by

$$\frac{N_{Al}}{N_{Si}} = \frac{Y_{Al} \cdot a}{2326 - Y_{Si} \cdot a} \qquad (4 - 6)$$

the areas being in mm^2. The sputtering yields for different elements were taken from the measured values reported by

Carter and Colligon (1968). The atomic percentages of Al in the films obtained by this method are shown in Table 4-1.

From Table 4-1 we can see a good agreement between the Al atomic percentages obtained from the above two methods, within $\pm$ 5%. These measurements show that the Al/Si atomic ratio is as 1.15 times the Al/Si target area ratio.

4.8. ANNEALING EXPERIMENTS

A CALBOLITE tube furnace was used to anneal some of the specimens. The furnace was electrically heated by a resistance wire wound onto a refractory tube, where the heated length of the tube is 30 cm. The temperature of the furnace was measured by a Pt/Pt 13%Rh thermocouple. The furnacewas facilitated with solid-state controllers to stabilise the temperature. Using an alumel-chromel thermocouple, it was found that the temperature in the vicinity of the specimen was about 10 ^{o}C below the reading of the built-in thermocouple.

As recommended by the manufacturer, prior to annealing, the furnace was run at 800 ^{o}C for 30 minutes to remove moisture and contamination . For annealing, the furnace was switched ON to give the required temperature, the tube was flushed with nitrogen then the specimen was inserted into the tube, while

the nitrogen was kept flowing at a low rate to minimise the temperature gradient between one end of the tube and the other. To cool the specimen the furnace was turned OFF and the nitrogen flow rate increased. The tube was pulled out slightly to get the specimen to the cold region.

A fresh set of Al-electrodes were deposited on the film for the electrical measurements as described in section 4.4..

Table 4-1: The atomic percentage of Al in a-Si films obtained by (a) XPS measurements and (b) etching profile method.

Al/Si (area ratio)	(a) Al/Si %	(b) Al/Si %	average Al/Si%
0.37	0.70	0.69	0.70
0.99	1.31	1.18	1.25
1.85	2.52	2.21	2.37
4.16	5.45	4.94	5.20
6.22	8.30	7.33	7.82
7.41	9.98	8.68	9.33
10.09	13.20	11.69	12.45

CHAPTER FIVE

ELECTRICAL, OPTICAL AND PHOTOCONDUCTIVE PROPERTIES OF UNDOPED a-Si

5.1. INTRODUCTION

In this chapter the possibility of the production of a low density-of-states amorphous silicon (a-Si) without the introduction of hydrogen or a halogen is discussed in the light of the experimental results obtained. This has been investigated through four physical quantities; namely, the d.c. dark electrical conductivity (σ), the steady-state photoconductivity (σ_{Ph}), the optical gap (E_o) and the thermal activation energy (ΔE_a). The measurements on photoconductivity are extended to include the photoresponse spectral distribution and the temperature and light-intensity dependence of photoconductivity. In addition, it will be shown how the photoconductivity could be useful as a double check on physical quantities, such as the optical gap (deduced from the direct transmission measurements) and the thermal activation energy of dark conductivity. Furthermore a qualitative study of the density-of-states in the mobility gap is also shown to be possible using the photoconductivity measurements. The results suggest, consistently, that a material with low density-of-states in the mobility gap can be produced by controlling the preparation conditions.

It has been found that the deposition rate, D_R, decreases almost exponentially with increasing target-substrate

distance, d, (Fig. 5-1a) or the sputtering gas pressure, P, (Fig. 5-1b). Various combinations of P and d proved to give a systematic variation of D_R with the product Pd (Fig. 5-1c) in a similar way to the variation of D_R with P or d. In addition, the self-bias voltage, V_{sb}, on the target has been found to control the deposition rate as shown in Fig. 5-1d. Furthermore, as it will be shown in section 5.2.1., the deposition rate was found to be controlled systematically by the product Pd/V_{sb}. Also, the above observations apply equally well to the control of the electrical and optical properties of the films by the individual parameters (Figs. 5-2a and b) as well as by the product Pd (Fig. 5-2c) or Pd/V_{sb}. The interesting result of this investigation was that different combinations of these preparation conditions, within the considered ranges of P (40 - 220 mTorr), d (2 - 5.3 cm) and V_{sb} (650 - 1100 V), which give the same product (Pd/V_{sb}) resulted in films with the same electronic and optical properties. Consequently, throughout the rest of the text, the preparation conditions will be dealt with as two quantities; the product Pd/V_{sb} and the substrate temperature, T_s.

5.2. RESULTS

5.2.1. DEPENDENCE OF D_R ON Pd/V_{sb} AND T_s

The deposition rate (D_R) of the films was found to decrease with increasing sputtering gas pressure and/or the target-substrate separation, while it was found to

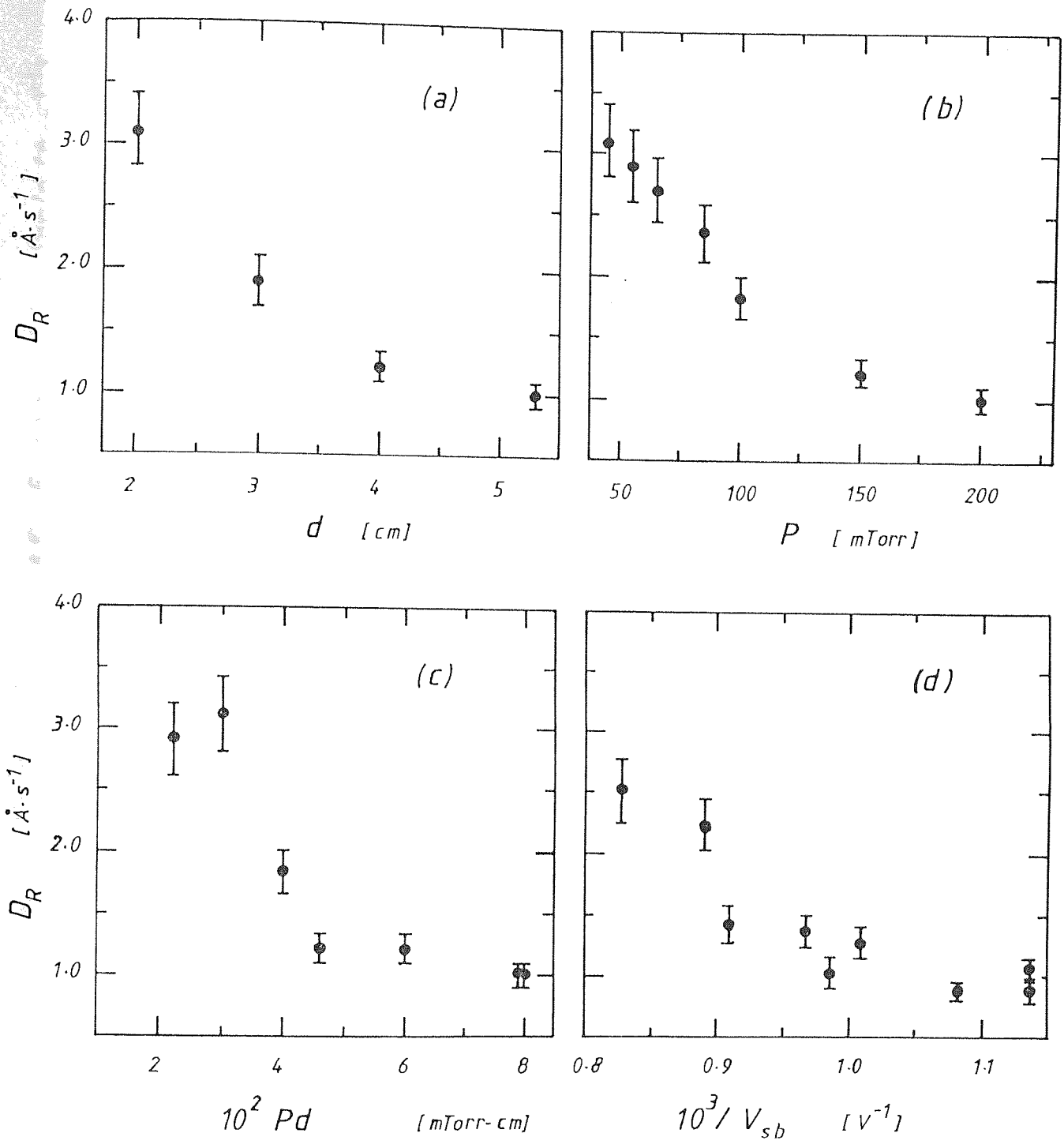

Fig. 5-1: The deposition rate, D_R, of undoped a-Si as a function of (a) the target-substrate distance, d, (b) the sputtering pressure, P, (c) The product Pd and (d) the self-bias voltage, V_{sb}, on the target.

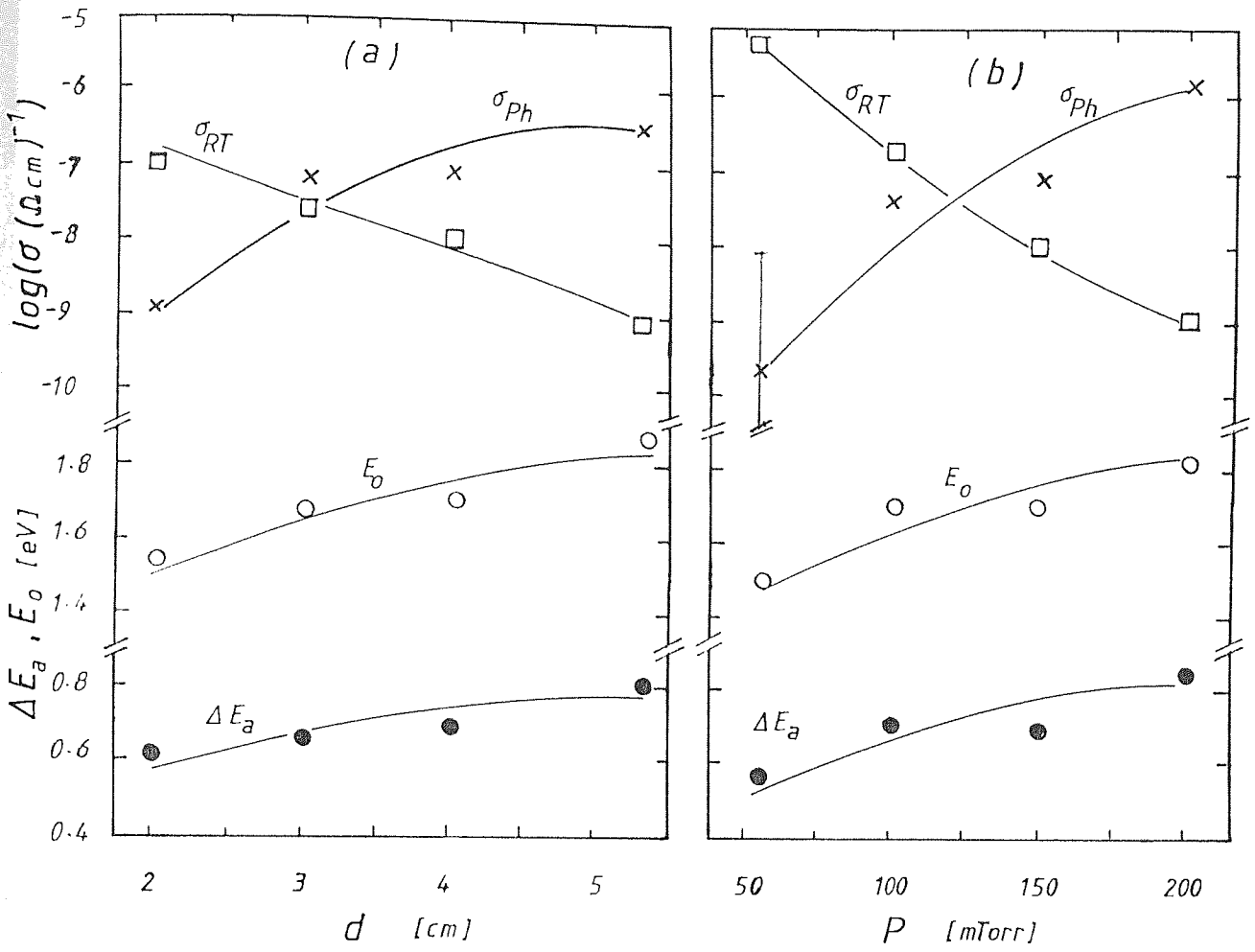

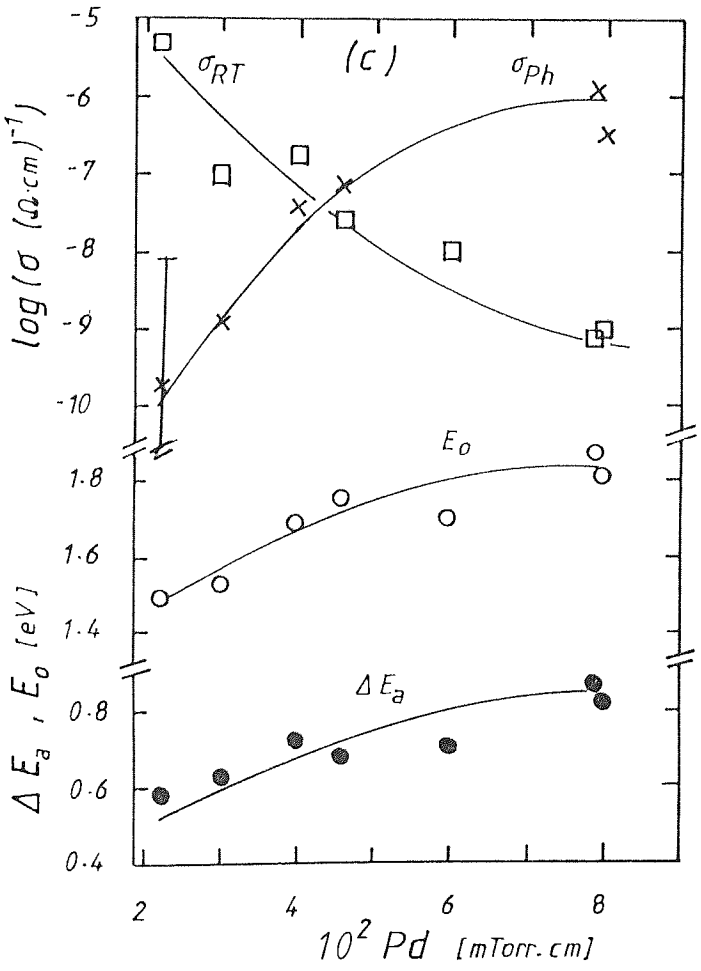

Fig. 5-2:
The room-temperature conductivity, σ_{RT}, optical gap, E_o and thermal activation energy, ΔE_a of undoped a-Si vs (a) target-substrate distance, d, (b) sputtering pressure, P and (c) Pd.

increase upon increasing the self-bias voltage on the target. However, it should be emphasised that there are limits to the above peparation conditions. At the gas pressure $P > 250$ mTorr. sputtering is not possible due to the limit of the mean free path for the Ne gas particles with respect to the distance between the shielding bracket and the target. The target-substrate distance was limited so that $2 > d > 6$ cm due to the limitations of the mean free path and the length of the region of uniform magnetic field. The minimum self-bias voltage on the target to give a reasonable deposition rate was about 650 V.

In the light of the discussion in section 5.1., it will be more convenient to consider D_R as a function of Pd/V_{sb} at a fixed substrate temperature (about 300 ^{o}C). Fig. 5-3 shows D_R as a function of Pd/V_{sb}. It can be seen from this figure that D_R varies almost exponentially from about 4 $\mathring{A}s^{-1}$ for low Pd/V_{sb} to $\lesssim$ 1 $\mathring{A}.s^{-1}$ for high Pd/V_{sb}. This type of variation seems to be consistent with the fact that the number of silicon atoms which reach the substrate without suffering collisions would be expected to be proportional to the exponent of (-Pd). The very slow variation in D_R at high (Pd/V_{sb}) values (Fig. 5-3, range II) would also logically follow from this.

The deposition rate of a-Si was also studied as a function of the substrate temperature (T_s), over the range from $T_s \simeq 150$ ^{o}C to about 470 ^{o}C. The Pd/V_{sb} value was about

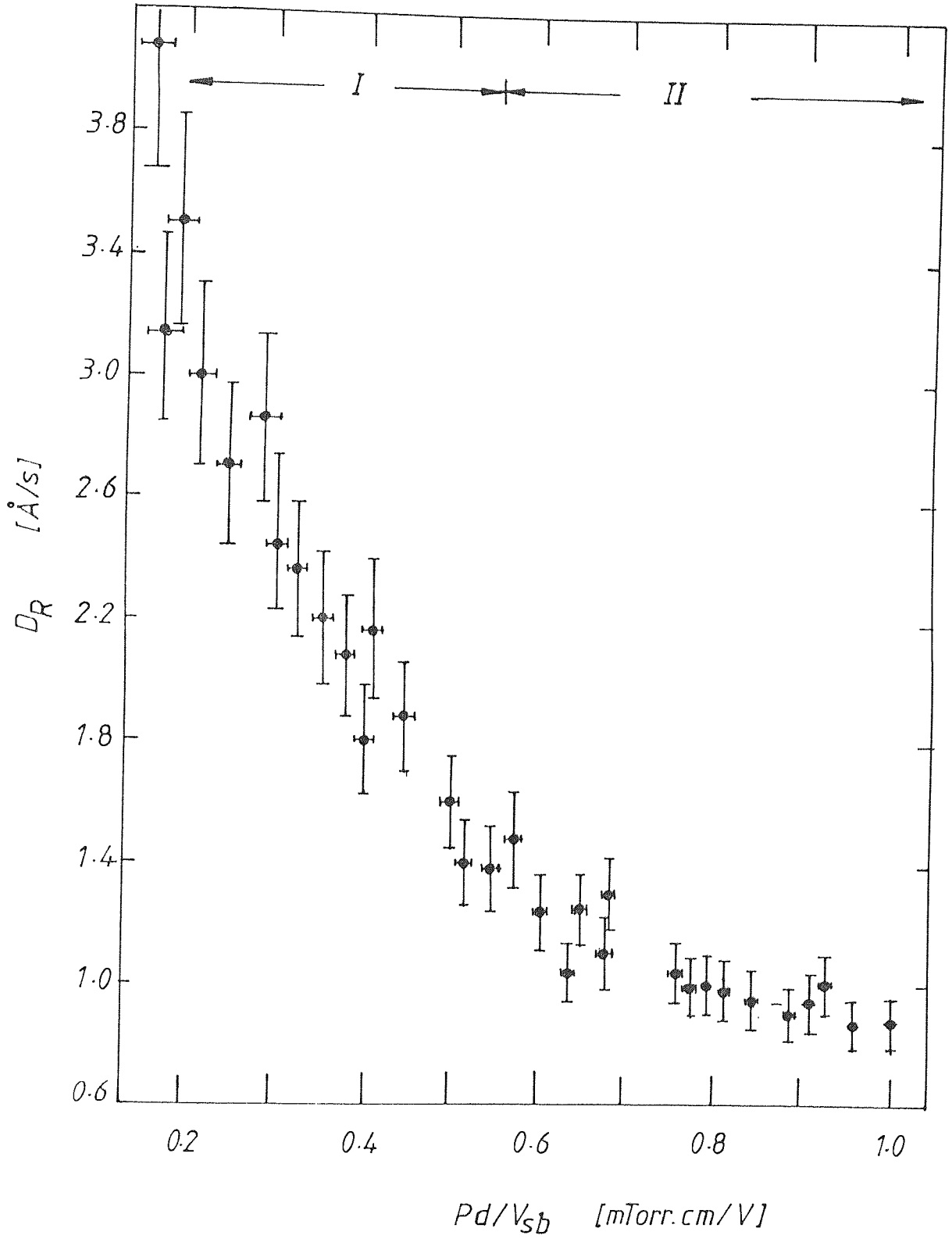

Fig. 5-3: The deposition rate, D_R, as a function of (Pd/V_{sb}). P, d and V_{sb} are gas pressure, target-substrate separation and self-bias voltage respectively.

0.68 mTorr.cm.V^{-1}; a condition in the optimum range (see Fig. 5-5, range II and the details of section 5.2.2.). The deposition rate as a function of T_s is shown in Fig. 5-8a. It can be seen from the figure that D_R decreases from about 1.4 Å.s^{-1} at T_s 300 °C to about 0.8 Å.s^{-1} at T_s = 460 °C. The decrease in D_R with increasing T_s above 300 °C could be due to the low sticking coefficient at high substrate-temperature (e.g. Davidse and Maissel, 1965; Batabyal et al, 1984).

5.2.2. DEPENDENCE OF ELECTRICAL & OPTICAL PROPERTIES ON Pd/V_{sb}

The results of the room-temperature conductivity (σ_{RT}), the thermal activation energy, the optical gap and the steady-state photoconductivity were measured for films prepared at T_s = 300 °C and different values of Pd/V_{sb}. These results are summarised in Table 5-1. In the following, the above quantities will be discussed in more detail.

5.2.2.1. THE D.C. DARK CONDUCTIVITY

The d.c. dark electrical conductivity (σ) was measured as a function of temperature in the temperature range from about -150 °C to about 150 °C, using the method described in section 4.4.. The plots of $\log\sigma$ vs 1000/T are shown in Fig. 5-4. These plots represent films prepared at a range of Pd/V_{sb} values with T_s = 300 °C. It can be seen from the plots that the films prepared at low Pd/V_{sb} have a relatively high conductivity and a low slope, while as

Table 5-1: A summary of various measurements for a-Si films prepared at different Pd/V_{sb} values and T_s=300 °C. D_R deposition rate; σ_{RT} room-temperature conductivity; ΔE_a thermal activation energy of the dark conductivity; σ_{Ph} photoconductivity; E_o optical gap.

specimen	Pd/V_{sb} [mTorr.cm.V^{-1}]	D_R [Å.s^{-1}]	σ_{RT} [Ω.cm]$^{-1}$	ΔE_a [eV]	σ_{Ph} [Ω.cm]$^{-1}$	E_o [eV]
1	0.17	3.14	7.9×10^{-6}	0.51	5.6×10^{-11}	1.41
2	0.19	3.50	——	——	——	1.49
3	0.21	3.00	5.0×10^{-6}	0.58	2.0×10^{-10}	1.49
4	0.25	2.70	7.9×10^{-7}	0.66	2.0×10^{-9}	1.56
5	0.31	2.48	1.3×10^{-7}	0.64	1.4×10^{-9}	1.56
6	0.33	2.37	1.6×10^{-7}	0.58	7.9×10^{-9}	1.66
7	0.36	2.20	6.3×10^{-8}	0.66	——	1.69
8	0.41	1.80	1.0×10^{-7}	0.72	4.0×10^{-8}	1.71
9	0.46	1.90	2.5×10^{-8}	0.68	6.3×10^{-8}	1.68
10	0.50	1.60	1.3×10^{-8}	0.78	2.5×10^{-7}	1.75
11	0.55	1.40	5.6×10^{-9}	——	4.0×10^{-7}	——
12	0.61	1.20	2.5×10^{-9}	0.84	2.2×10^{-7}	1.71
13	0.64	1.00	3.2×10^{-9}	——	6.8×10^{-7}	——
14	0.65	1.30	1.3×10^{-9}	0.77	——	1.90
15	0.68	1.10	1.4×10^{-9}	0.81	4.5×10^{-7}	1.76
16	0.76	1.00	2.2×10^{-9}	0.78	8.5×10^{-7}	1.75
17	0.79	1.00	9.3×10^{-10}	0.86	1.1×10^{-6}	1.81
18	0.81	1.00	7.9×10^{-10}	0.82	3.0×10^{-7}	1.88
19	0.84	0.90	1.1×10^{-9}	0.80	1.1×10^{-6}	1.80
20	0.89	0.90	1.4×10^{-9}	0.75	3.2×10^{-7}	1.74
21	0.92	0.90	2.5×10^{-9}	0.68	1.0×10^{-7}	1.67
22	0.95	0.80	3.2×10^{-9}	0.61	8.9×10^{-8}	1.70

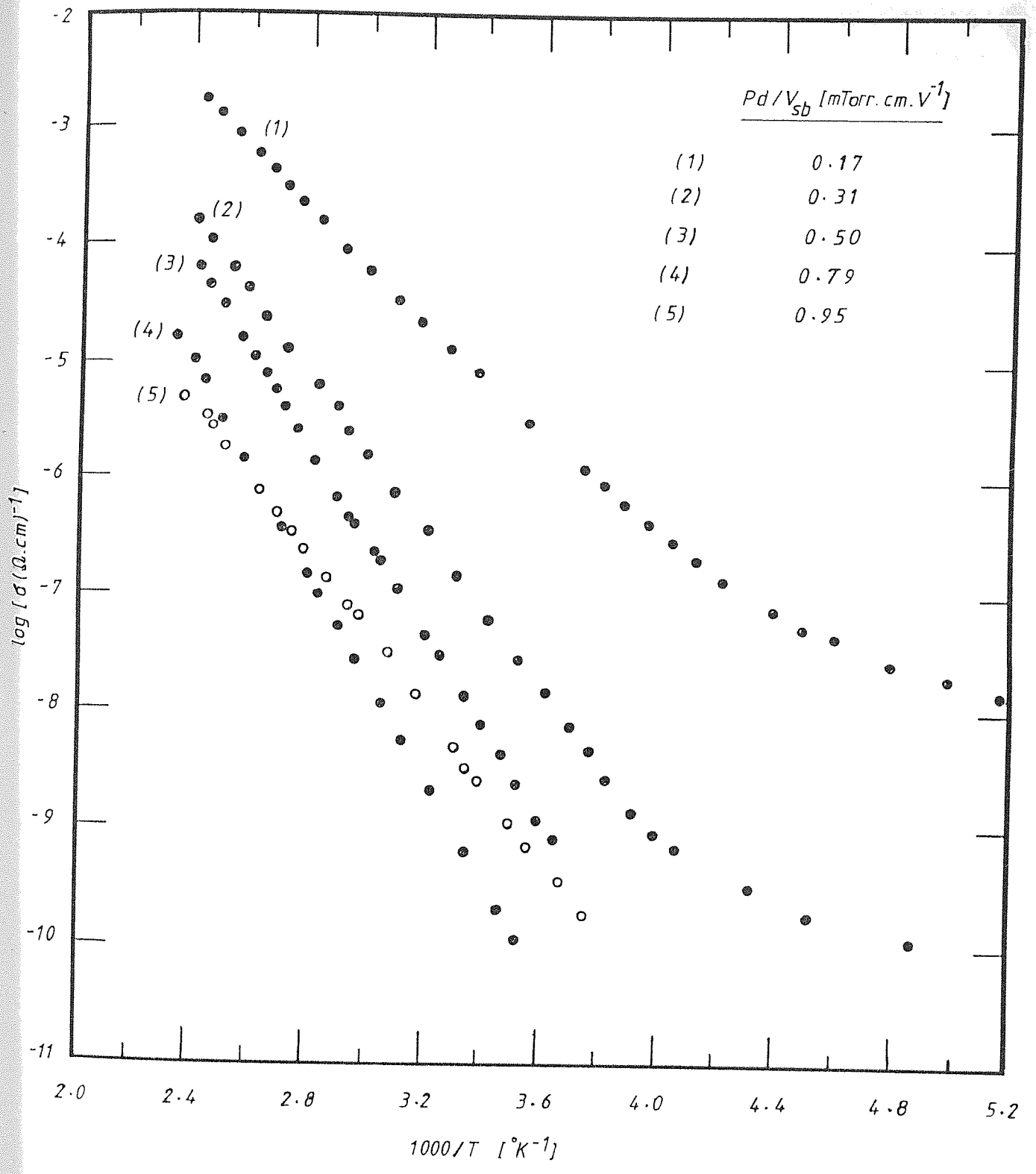

Fig. 5-4: Log σ vs 1000/T for a-Si films prepared at T_s=300 °C and different values of Pd/V_{sb} as indicated.

Pd/V_{sb} increases up to about 0.80 mTorr.cm.V^{-1}, the conductivity decreases and the plots become steeper. The curve marked 0.95 mTorr.cm.V^{-1} represents a film prepared at a very high Pd/V_{sb} value and shows a higher conductivity and lower slope than that of the film prepared at 0.8 mTorr.cm.V^{-1}.

Also, from Fig. 5-4, a change in the slope of the curves can be seen at a temperature which depends on the Pd/V_{sb} value, where below this temperature the current is believed to be carried by a phonon-assisted hopping process described in section 3.4.. The temperature at which hopping conduction occurs, decreases as Pd/V_{sb} is increased up to about 0.80 mTorr.cm.V^{-1}.

From the slope of the plots of Fig. 5-4, around room-temperature, the thermal activation energy (ΔE_a) was deduced according to eq. (3-3). The room-temperatue dark-conductivity (σ_{RT}) and ΔE_a are shown in Fig. 5-5 as functions of Pd/V_{sb}. It can be seen from this figure that σ_{RT} can be varied systematically over more than 4 orders of magnitude, from about 10^{-5} $\Omega^{-1}cm^{-1}$ at about 0.15 mTorr.cm.V^{-1} to about 10^{-9} $\Omega^{-1}cm^{-1}$ at about 0.80 mTorr.cm.V^{-1}. On the other hand, ΔE_a changes with Pd/V_{sb} in a manner consistent with the variation in σ_{RT}, and it approaches a maximum value of nearly 0.85 eV at $Pd/V_{sb} \simeq 0.80$ mTorr.cm.V^{-1}. This latter value is comparable with those values found for samples prepared by glow-discharge (e.g. Spear & LeComber, 1975) and Ar/H_2 sputtering (e.g. Paul et al, 1976) techniques.

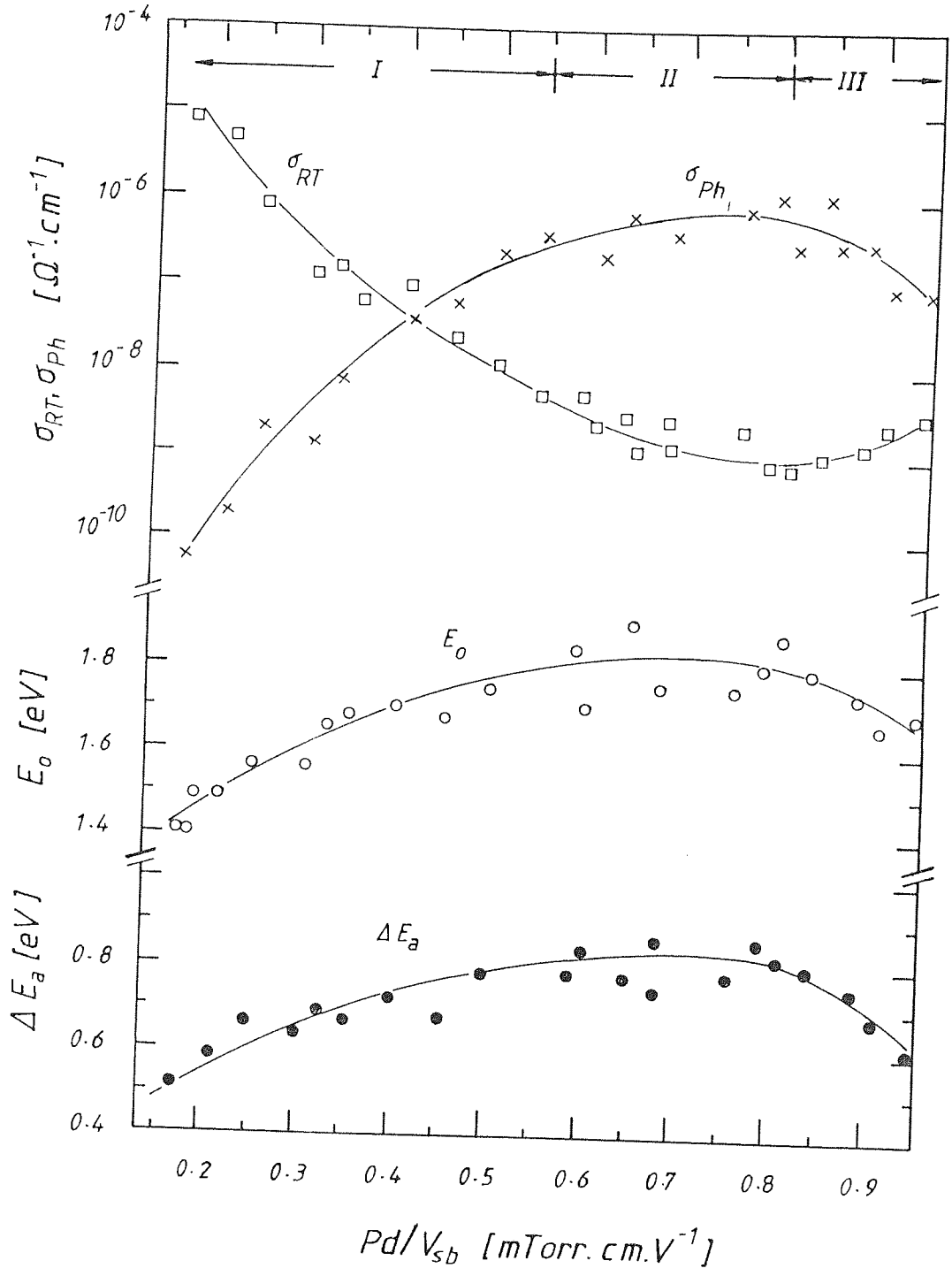

Fig. 5-5: The room-temperature conductivity σ_{RT}, the photoconductivity σ_{Ph}, the thermal activation energy ΔE_a and the optical gap E_o as functions of (Pd/V_{sb}).

At Pd/V_{sb} values higher than 0.80 mTorr.cm.V^{-1} (Fig. 5-5 range III), σ_{RT} increases and ΔE_a decreases with increasing Pd/V_{sb}. This suggests that, with the other preparation conditions being fixed, range II of Fig. 5-5 may represent the optimum Pd/V_{sb} range for preparing a-Si films with a relatively low density-of-states, by Ne sputtering.

The conduction type of randomly chosen undoped films was readily determined from the polarity of the room-temperature thermopower sign observed by the hot-probe technique. All the tested samples were n type.

5.2.2.2. THE OPTICAL GAP

The absorption coefficient (α) was determined from the direct transmittance spectra measured by a UNICAM SP-800 spectrophotometer, as explained in section 4.5.. Eq. (4-2) was used in calculating α, where (1-R) in this equation was considered as the value at which the interference averaged transmittance levels off at longer wavelengths. The transmission and reflection measurements for two samples were made in the Physics Laboratories of Leicester University, using a PERKIN ELMER spectrophotometer; which covered the IR, visible and UV regions of the spectrum. The agreement between the (1-R) values from the two spectrophotometers was good. The uncertainty in α for $\alpha \geq 10^3$ cm^{-1}, due to the error in (1-R) was found to be less than 10%. The plots of $(\alpha\hbar\omega)^{\frac{1}{2}}$ against the photon energy $\hbar\omega$ of films prepared at different values of Pd/V_{sb}, with $T_s \approx 300$ °C, are shown in Fig. 5-6. The optical gap (E_o) of each sample was considered as the intercept of the extrapolation of the straight part of the appropriate curve, with the $\hbar\omega$ axis, according to eq. (3-9). It can be seen that as Pd/V_{sb} increases, the slope β of

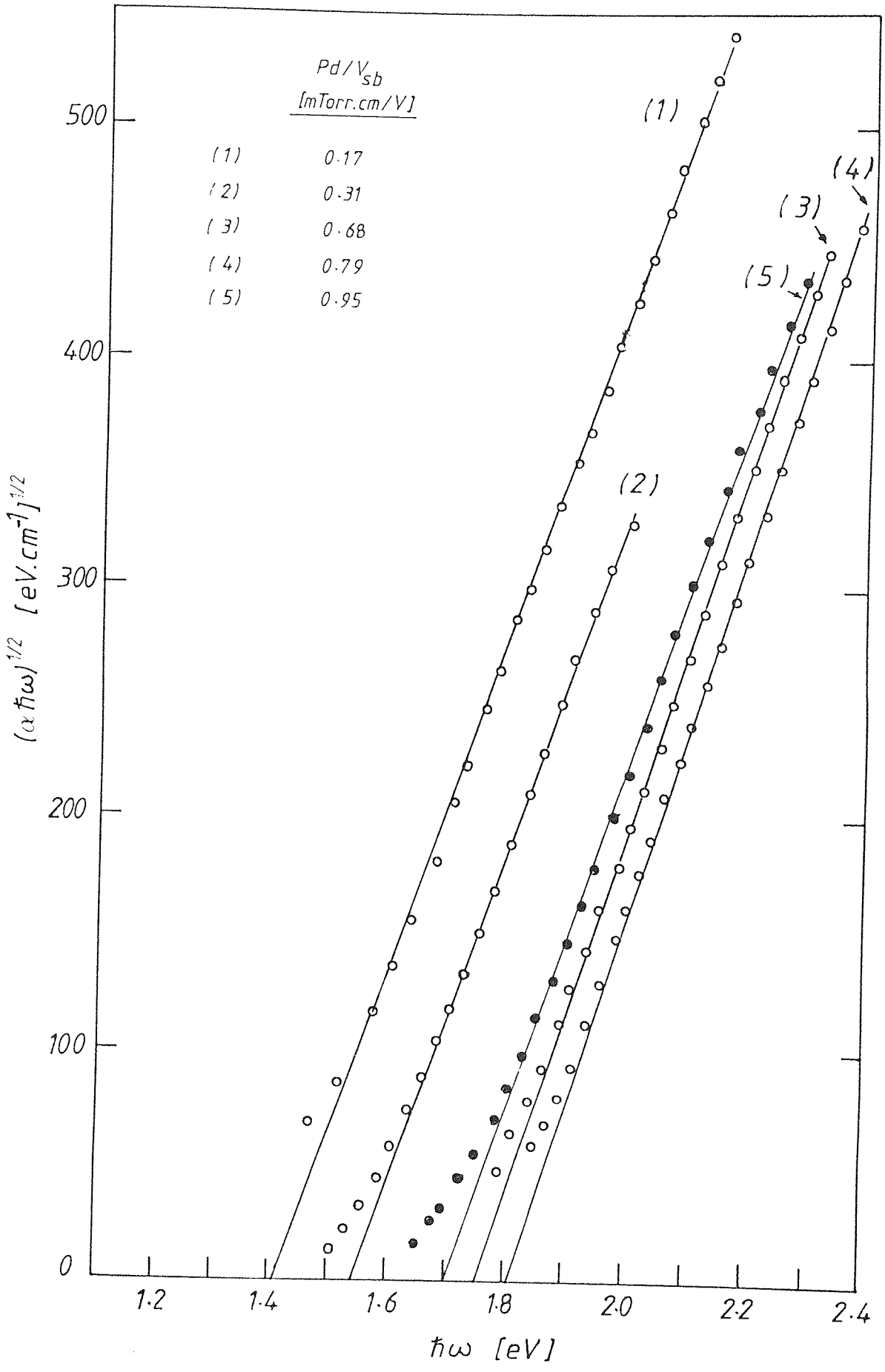

Fig. 5-6: Samples of the plots of $(\alpha\hbar\omega)^{\frac{1}{2}}$ vs $\hbar\omega$ for a-Si films pepared at T_s=300 °C and different values of (Pd/V_{sb}) as indicated.

the curve increases and the curve shifts to higher photon energies. The variation of β with the optical gap seems to be linear as shown in Fig. 5-7.

From Fig. 5-5 it can be seen that E_o increases from about 1.4 eV at low values of Pd/V_{sb} to about 1.85 eV at high Pd/V_{sb} values up to about 0.80 mTorr.cm.V^{-1}. As Pd/V_{sb} increases above this value, the optical gap decreases (Fig. 5-5 range III). This observation will be discussed in section 5.3.1.. The increase of E_o in ranges I and II of Fig. 5-5 with the increase in Pd/V_{sb} is consistent with the decrease in σ_{RT} and the increase in ΔE_a in the same figure.

5.2.2.3. THE STEADY-STATE PHOTOCONDUCTIVITY

In this section it is not intended to discuss the details of the photoconductive properties of a-Si. instead, the variation in the steady-state photoconductivity, at room temperature, with Pd/V_{sb} is presented only for the comparison with the other electrical and optical properties . However, more detailed information about this topic will be found in section 5.2.4..

The steady-state photocurrent, defined as the difference between the current under illumination and the dark current, was measured using the arrangement described in section 4.4.. The films were illuminated by a monochromatic light with energy 1.89 eV and $F \simeq 10^{15}$ photons.$cm^{-2}.s^{-1}$ flux intensity. At room temperature, the photoconductivity (σ_{Ph}) was

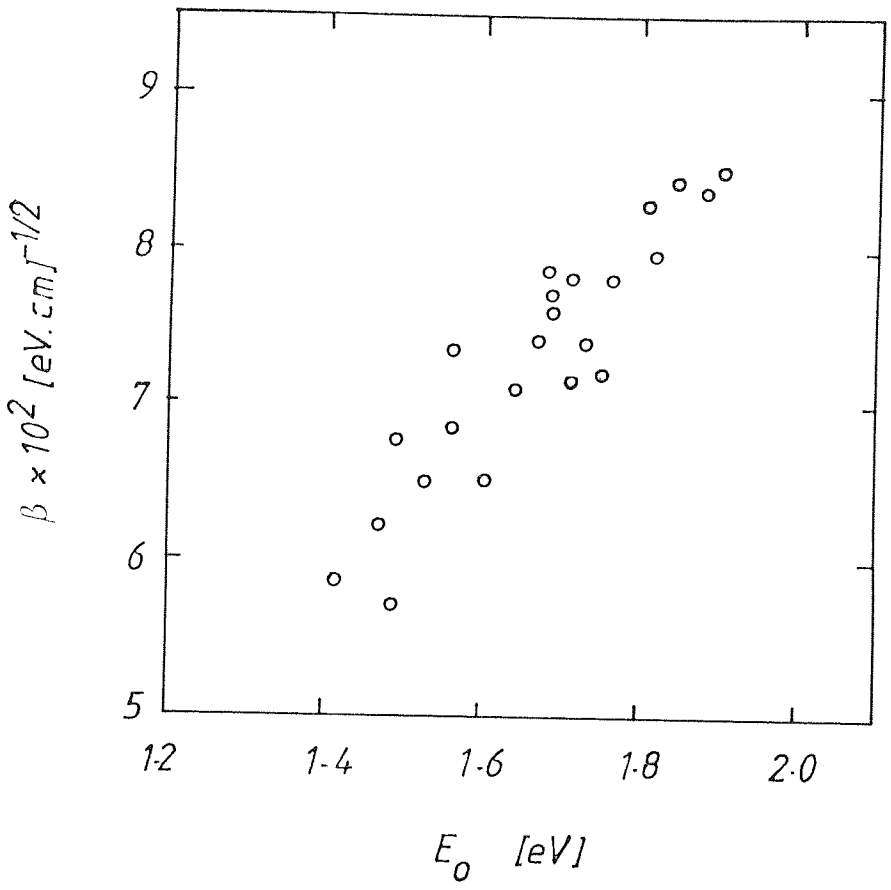

Fig. 5-7: The slope β of the plot $(\alpha\hbar\omega)^{1/2}$ vs $\hbar\omega$, against the optical gap E_o.

measured for films prepared at a range of Pd/V_{sb}; σ_{Ph} is shown as a function of Pd/V_{sb} in Fig. 5-5. It can be seen from this figure that σ_{Ph} increases rapidly as Pd/V_{sb} is increased. An optimum value of about $10^{-6}\ \Omega^{-1}cm^{-1}$ compares well with the photoconductivity of a-Si:H (Moustakas et al, 1977; Spear et al, 1974). It can also be concluded from Fig. 5-5 that σ_{Ph} increases with ΔE_a (i.e. the position of the Fermi level in the mobility gap) in an analogous way to that observed for a-Si:H with low H_2 content (Paul and Anderson, 1981).

5.2.3. DEPENDENCE OF ELECTRICAL AND OPTICAL PROPERTIES ON T_s

The electrical and optical properties of undoped a-Si were studied as functions of the substrate temperature during the deposition. The Pd/V_{sb} value was kept around o.68 $mTorr.cm.V^{-1}$; a condition in the optimum range (Fig. 5-5 range II). The results concerning σ_{RT}, ΔE_a, σ_{Ph} and E_o are summarised in Table 5-2.

5.2.3.1. THE DARK CONDUCTIVITY

The d.c. room-temperature dark-conductivity σ_{RT} vs T_s is shown in Fig. 5-8b, where σ_{RT} decreases with increasing T_s until it approaches a minimum value of about $10^{-9}\ \Omega^{-1}cm^{-1}$ around $T_s \simeq 300\ ^{o}C$. At substrate temperatures higher than 300 ^{o}C, σ_{RT} increases upon increasing T_s. On the other hand, the plots of $\log\sigma$ vs 1/T, shown in Fig. 5-9, for

Table 5-2: A summary of various measurements for a-Si films prepared at different substrate temperatures and Pd/V_{sb}=0.68 mTorr. $cm.V^{-1}$. D_R deposition rate; σ_{RT} room-temperature conductivity; ΔE_a thermal activation energy of the dark conductivity; σ_{Ph} photoconductivity; E_o optical gap.

specimen	T_s [°C]	D_R [Å.s^{-1}]	σ_{RT} [Ω.cm]$^{-1}$	ΔE_a [eV]	σ_{Ph} [Ω.cm]$^{-1}$	E_o [eV]
1	150	1.36	1.3×10^{-8}	0.64	5.6×10^{-8}	1.58
2	195	1.35	1.3×10^{-8}	0.62	——	1.65
3	220	1.34	5.6×10^{-9}	0.68	7.1×10^{-8}	1.73
4	255	1.26	1.0×10^{-8}	0.73	4.5×10^{-8}	——
5	265	1.28	4.0×10^{-9}	0.66	1.4×10^{-7}	1.69
6	295	1.26	2.8×10^{-9}	0.79	2.5×10^{-7}	——
7	298	1.10	1.4×10^{-9}	0.81	4.5×10^{-7}	1.76
8	340	1.06	2.8×10^{-9}	0.79	3.2×10^{-7}	1.67
9	380	0.84	1.4×10^{-8}	0.70	5.0×10^{-7}	1.68
10	390	1.04	1.0×10^{-8}	0.76	1.0×10^{-7}	1.62
11	460	0.85	2.8×10^{-8}	0.64	5.0×10^{-8}	1.53

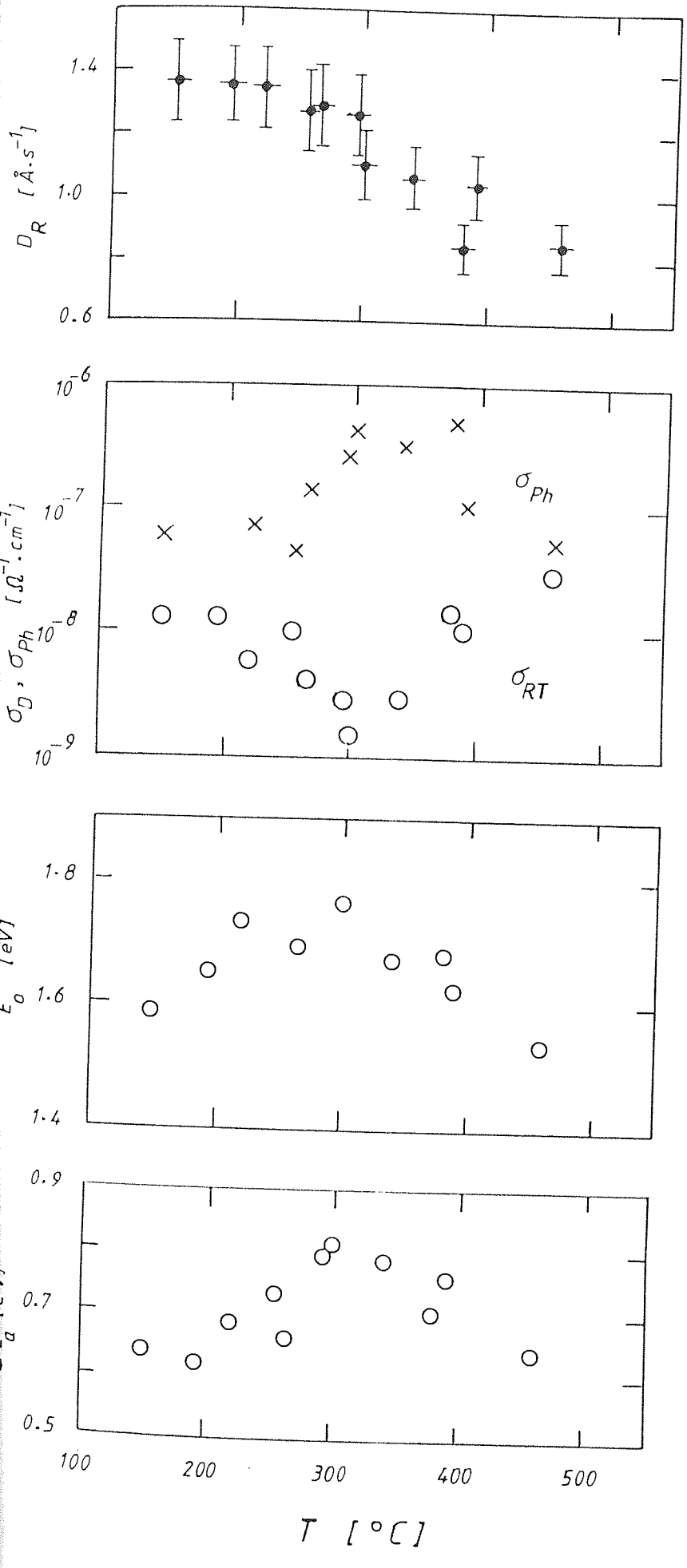

(a) The deposition rate D_R as a function of substrate temperature T_s.

(b) The photoconductivity σ_{Ph} and room-temperature conductivity σ_{RT} as functions of T_s.

(c) The optical gap E_o as a function of T_s.

(d) The thermal activation energy ΔE_a of dark conductivity as a function of T_s.

Fig. 5-8:

films prepared at different ranges of T_s, indicate a variation in the thermal activation energy ΔE_a with T_s. This is shown in Fig. 5-8d, where a maximum in ΔE_a of more than 0.8 eV around $T_s \approx 300$ °C corresponds to the minimum in σ_{RT}. It can be seen from Fig. 5-9 that at a moderate temperature (about 300 °C) the activated conduction in the extended states remains the dominating conduction mechanism even at temperatures well below room temperature.

5.2.3.2. THE OPTICAL GAP

The optical gap (E_o) for the same films as discussed in section 5.2.3.1 was determined in the same way as described in sections 4.5. and 5.2.2.2.. The dependence of E_o on T_s is shown in Fig. 5-8c. It can be seen that E_o increases with increasing the substrate temperature to a maximum value of about 1.8 eV at $T_s \approx 300$ °C. Beyond this temperature E_o decreases as the substrate temperature increases. The maximum E_o is consistent with the maximum in ΔE_a and the minimum in σ_{RT}.

5.2.3.3. THE PHOTOCONDUCTIVITY

The room-temperature photoconductivity, σ_{Ph}, measured in the same way as described in section 4.4., is plotted as a function of T_s in Fig. 5-8b. The variation in σ_{Ph} with T_s is consistent with that in σ_{RT}, ΔE_a and E_o, and the maximum of about $10^{-6}\ \Omega^{-1}cm^{-1}$ in σ_{Ph} at $T_s \approx 300$ °C is consistent with the maximum in ΔE_a and E_o and the minimum in σ_{RT}.

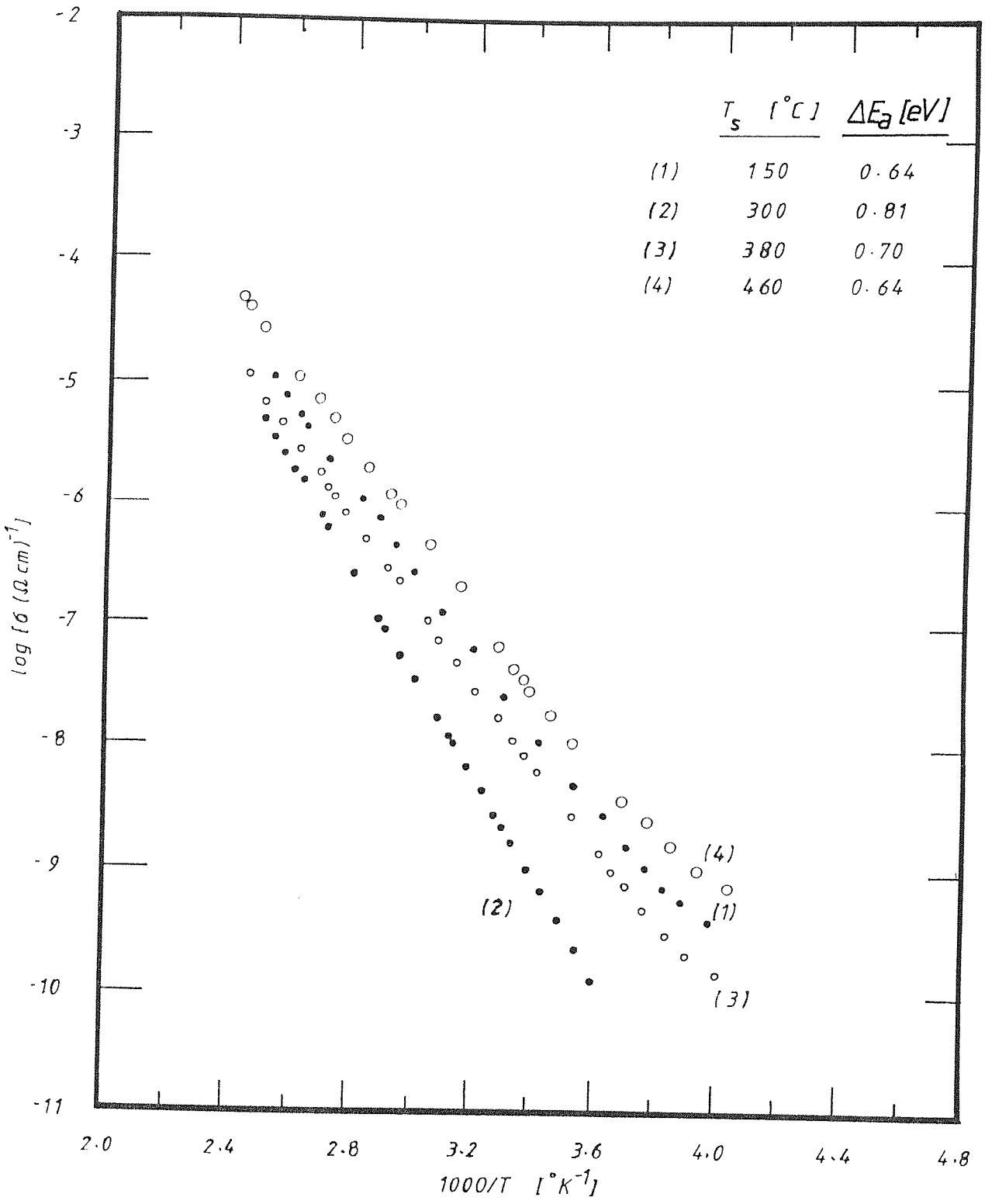

Fig. 5-9: Log σ vs 1000/T for a-Si films prepared at Pd/V_{sb}=0.68 mTorr.cm.V^{-1} and different T_s as indicated.

5.2.4.. THE PHOTOCONDUCTIVE PROPERTIES OF UNDOPED a-Si

The photoconductivity was measured using gap-cell configurations with Al electrodes separated by 1 mm and an applied field of about 10^2 V.cm^{-1}. Selected interference filters, with 10 nm band-width, were used to obtain near monochromatic light of the appropriate photon energy. Further details of the experimental arrangements can be found in chapter 4.

5.2.4.1. THE PHOTORESPONSE SPECTRAL DISTRIBUTION

The steady-state photocurrent (i_{Ph}), at room temperature was measured as a function of photon energy ($\hbar\omega$) for a number of undoped a-Si films deposited at about 300 ^{o}C with a range of Pd/V_{sb} values. Fig. 5-10 shows the steady-state photoresponse, represented as $[i_{Ph}/eF(1-R)]$, as a function of $\hbar\omega$ in the range of $\hbar\omega$ from about 0.8 eV to 3.5 eV. The quantity $[i_{Ph}/eF(1-R)]$ represents the number of charge carriers flowing round the circuit for each photon entering the specimen, and $F(1-R)$ is the number of photons falling on 1 cm^2 of the specimen per second, corrected for surface reflection. The photon flux intensity F was ~ 10^{14} photons. cm^{-2}.s^{-1}. At room temperature it was found that in this range of light intensity the photocurrent was almost proportional to the intensity throughout the spectral range (see section 5.2.4.2.). From Fig. 5-10 we can see the following;

(i) Films prepared at high values of Pd/V_{sb} (~ 0.80 mTorr. cm.V^{-1}) show peaks in the photoresponse between 1.8

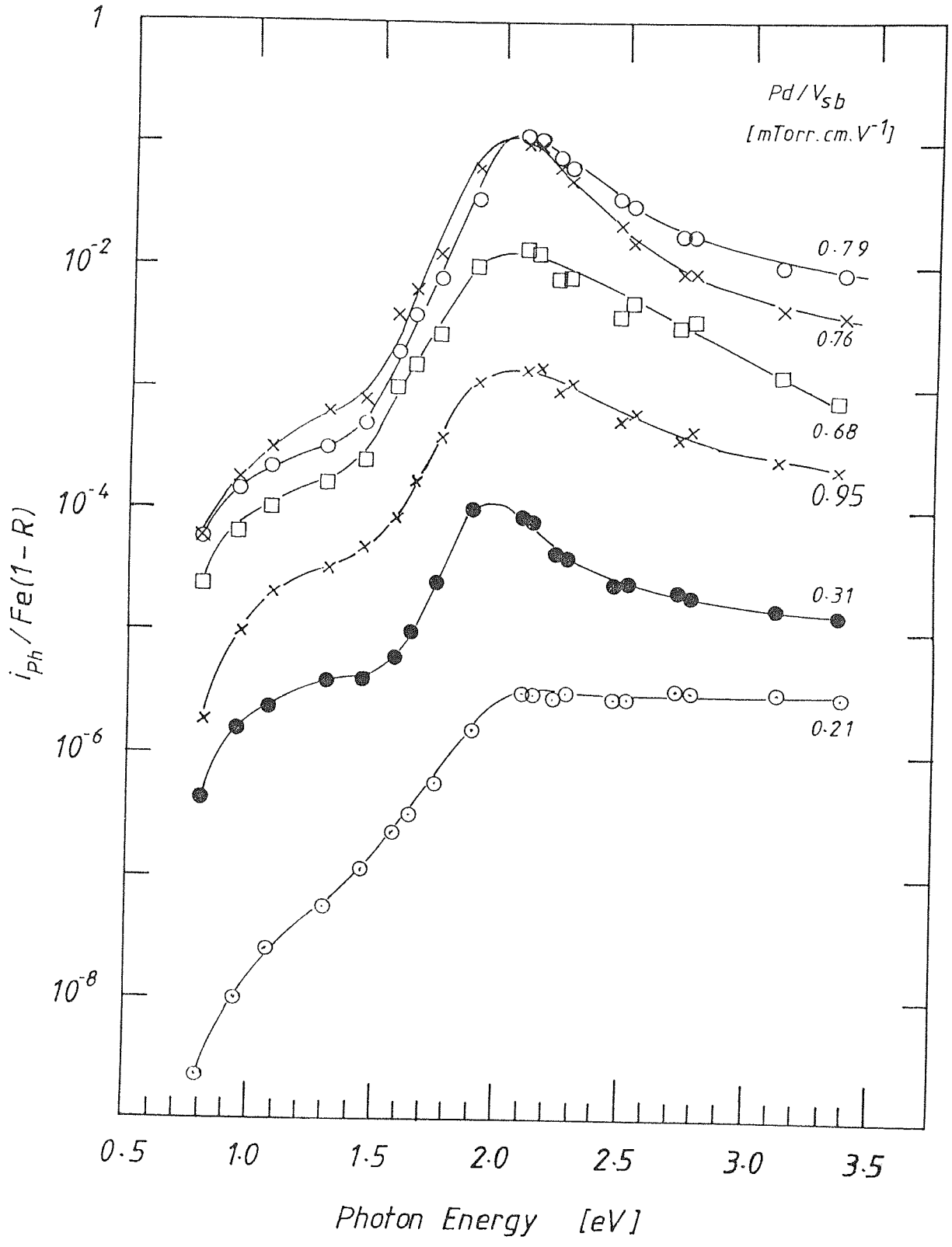

Fig. 5-10: Spectral dependence of the photoresponse in a-Si prepared by Ne sputtering at 300 ^{o}C and Pd/V_{sb} values as indicated. The ordinate represents the number of excess charge carriers flowing around the circuit per photon entering the films.

and 2.15 eV about an order of magnitude below unity but may well approach, or even exceed, unity at higher applied fields. Measurements of I-V characteristics of the films, showed that the current is linearly proportional to applied field up to about 10^4 V.cm^{-1}. Accordingly at this field the photoresponse would be about 2 orders of magnitude higher than that shown in Fig. 5-10.

(ii) Specimens prepared at low values of Pd/V_{sb} exhibit a marked decrease in photoresponse at all photon energies.

(iii) At higher Pd/V_{sb} values than 0.80 mTorr.cm.V^{-1} the photoresponse is reduced at all photon energies; this effect is demonstrated by the curve marked 0.95 mTorr. cm.V^{-1}.

(iv) The photoresponse drops rapidly at energies lower than 0.8 eV.

(v) All the curves show a shoulder around 1.2 eV, followed by a rapid rise in the photoresponse above about 1.6 eV.

The above features in the photoresponse spectra are closely similar to those reported for a-Si:H prepared by glow-discharge decomposition of silane (Loveland et al, 1973/74; Ray et al, 1983).

According to eqs. (3-9) and (3-21), the photoresponse could be used as another technique to determine the optical gap. The quantity $[i_{Ph}\hbar\omega/eF(1-R)]^{\frac{1}{2}}$ is plotted against photon energy $\hbar\omega$ for four samples, prepared at Pd/V_{sb} values of 0.31, 0.68, 0.79 and 0.95 mTorr.cm.V^{-1}. Respectively, these

plots are shown in Figs. 5-11 (a, b, c and d). From these plots two quantities have been deduced; the optical gap E_o^{Ph} and the photoconductive threshold ΔE_a^{Ph}, from the extrapolation of the straight part of the curves and the extrapolation of the curves at low $\hbar\omega$, respectively. The E_o^{Ph} values ranged between about 1.48 eV, for films prepared at low Pd/V_{sb}, and about 1.85 eV for films prepared at relatively high Pd/V_{sb}. ΔE_a^{Ph} varied betweeen 0.52 eV, for low Pd/V_{sb}, and 0.76 eV, for relatively high Pd/V_{sb}.

In fact many undoped specimens were analysed in this way and the results are summarised in Table 5-3. The table shows a good agreement between E_o^{Ph} values obtained from this method and those obtained from the plots of $(\alpha\hbar\omega)^{\frac{1}{2}}$ vs $\hbar\omega$ (section 5.2.2.2.). Also the values of ΔE_a^{Ph} are compared with the thermal activation energies for the dark conductivity (ΔE_a) (section 5.2.2.1.).

Furthermore, the shoulder around 1.2 eV, which is a common feature of the plots of Fig. 5-11, can be seen clearly when the appropriate portion of the curves is expanded as shown in curve (i) (Figs. 5-11a,b,c and d). This shoulder becomes lower in height as the Pd/V_{sb} value is increased up to about 0.80 mTorr.cm.V^{-1}, while it starts to increase in height when Pd/V_{sb} becomes greater than 0.80 mTorr.cm.V^{-1} (Fig. 5-11d).

Table 5-3: Summary of specimen data of a-Si films. P sputtering gas pressure; d target-substrate distance; V_{sb} self-bias on the target; σ_{RT} room-temperature dark conductivity; ΔE_a thermal activation energy of dark conductivity; ΔE_a^{Ph} photoconductive threshold; E_o and E_o^{Ph} optical gap from absorption measurements and photoresponse measurements respectively.

Specimen	Pd/V_{sb} (mTorr.cm/V)	σ_{RT} $(\Omega\ cm)^{-1}$	ΔE_a(eV)	ΔE_a^{Ph}(eV)	E_o(eV)	E_o^{Ph}(eV)
1	0.21	5.0×10^{-6}	0.58	0.52	1.49	1.48
2	0.31	1.2×10^{-7}	0.63	0.56	1.56	1.56
3	0.36	6.3×10^{-8}	0.66	----	1.69	----
4	0.41	10^{-7}	0.72	0.65	1.71	1.68
5	0.46	2.5×10^{-8}	0.67	0.64	1.68	1.70
6	0.51	1.1×10^{-8}	0.70	0.66	1.71	1.71
7	0.65	1.3×10^{-9}	0.75	----	1.85	----
8	0.68	2.8×10^{-9}	0.68	0.64	1.76	1.75
9	0.76	2.2×10^{-9}	0.78	0.70	1.75	1.75
10	0.79	9.3×10^{-10}	0.86	0.72	1.81	1.79
11	0.81	7.9×10^{-10}	0.82	0.76	1.88	1.85
12	0.95	2.5×10^{-9}	0.68	0.63	1.67	1.68

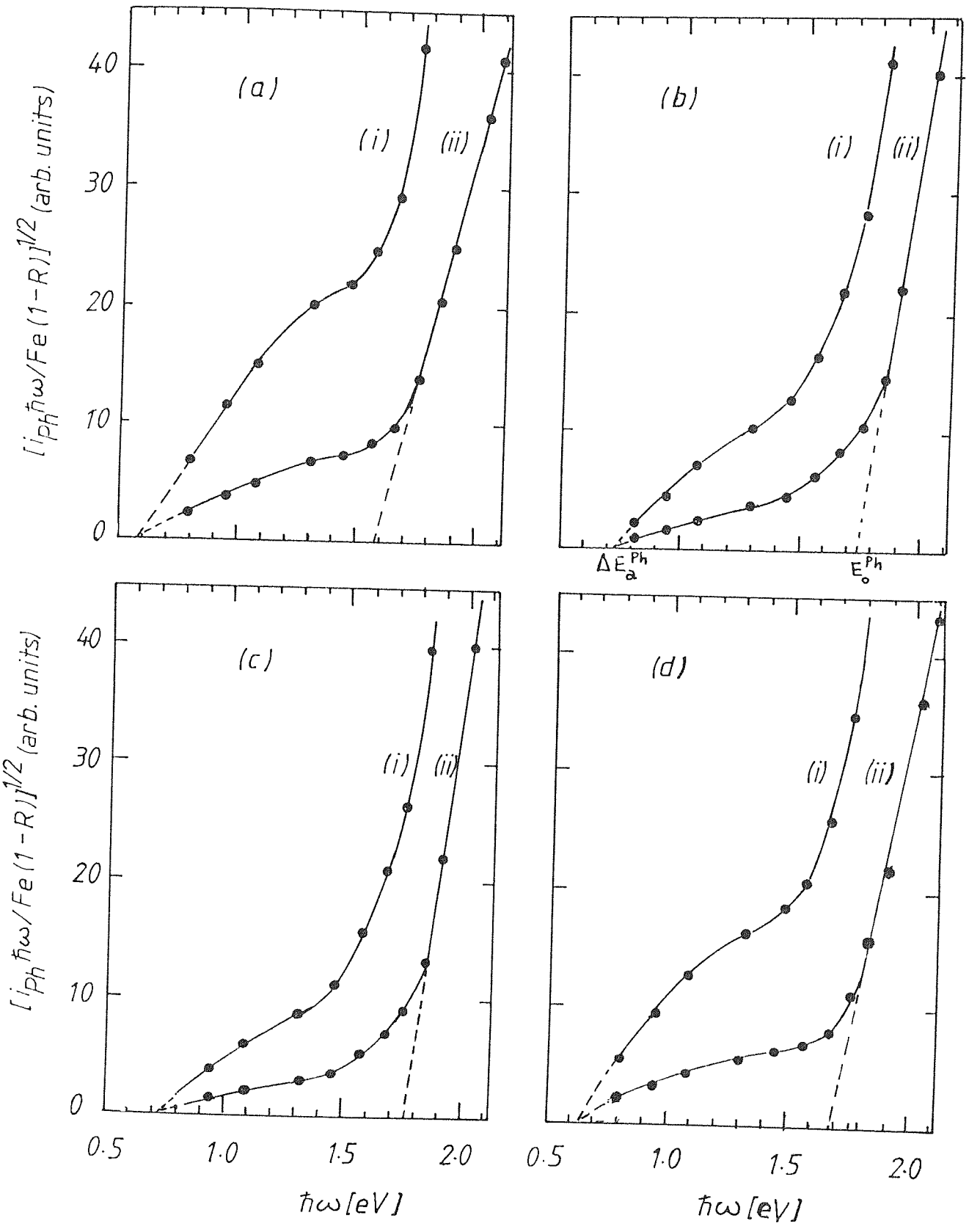

Fig. 5-11: Determination of the optical gap E_o^{Ph} and the photoconductive threshold ΔE_a^{Ph} from the photoconductivity measurements of a-Si prepared at Pd/V_{sb} equal to (a) 0.31, (b) 0.68, (c) 0.79 and (d) 0.95 mTorr.cm.V^{-1}. In each case, curve (i) is part of curve (ii) expanded three times.

5.2.4.2. DEPENDENCE OF PHOTOCONDUCTIVITY ON LIGHT INTENSITY

At room temperature, the photoconductivity was studied as a function of the light intensity for the films listed in Table 5-3. The excitation energy was about 1.9 eV. The dependence of photoconductivity, σ_{Ph}, on the light intensity for some of these films is shown in Fig. 5-12. These films cover the full range of Pd/V_{sb} values considered. It has been found that the intensity dependence of σ_{Ph} may be represented by the relation (3-19) discussed in section 3.6.1.2..

In general, it can be seen from Fig. 5-12 that at low light intensity, the exponent γ in eq. (3-19) is unity, indicating a monomolecular recombination process (section 3.6.1.2.). On the other hand, at high light intensities, γ varies from 1 towards 0.5 indicating that a bimolecular recombination process is dominating in this range of light intensities (section 3.6.1.1.).

It can also be seen from Fig. 5-12 that as the product (Pd/V_{sb}) increases, up to 0.80 mTorr.cm.V^{-1}, the light intensity at which the recombination process changes into bimolecular decreases. This indicates that films with less recombination centres are produced by sputtering at a relatively high (Pd/V_{sb}) values. At very high Pd/V_{sb}, the recombination process changes into bimolecular at

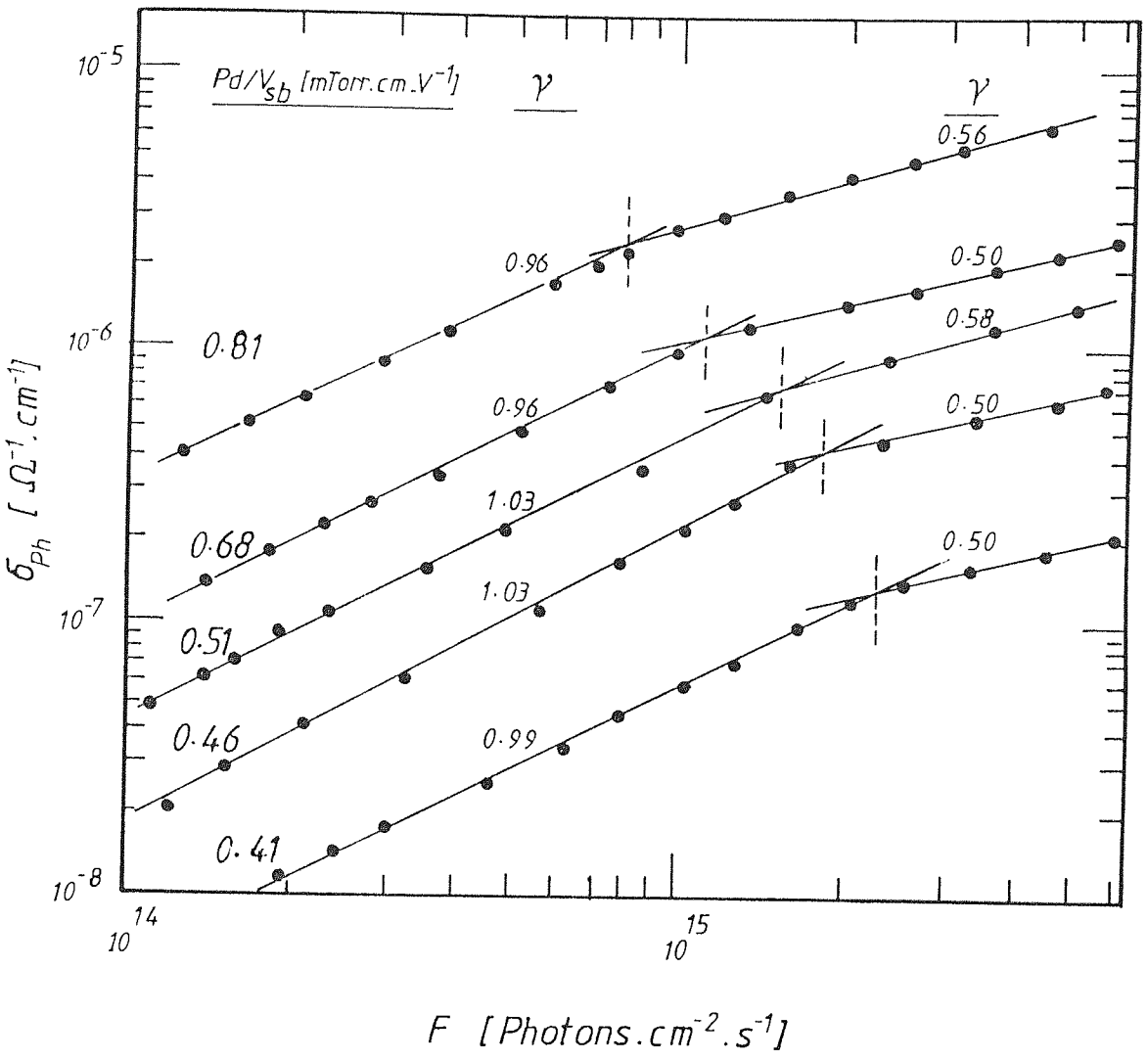

Fig. 5-12: The room-temperature photoconductivity σ_{Ph} vs light intensity F for a-Si films prepared at different Pd/V_{sb} values as indicated. The exponent factor γ in the relation $\sigma_{Ph} \propto F^{\gamma}$ is indicated on each curve.

higher light intensities. These results are consistent with the electrical and optical properties reported in section 5.2.2..

5.2.4.3. TEMPERATURE DEPENDENCE OF PHOTOCONDUCTIVITY

The photoconductivity of several films was measured as a function of temperature in the range from about -30 ^{o}C to about 115 ^{o}C under different intensities of illumination ranging from about 2×10^{12} to 8×10^{14} photons.cm^{-2}.s^{-1}. The excitation energy was about 1.9 eV. Figs. 5-13 (a and b) show σ_{Ph} plotted against 1/T for two films. Fig. 5-13a represents a film prepared at low Pd/V_{sb} value (0.31 mTorr.cm.V^{-1}), while Fig. 5-13b represents another film prepared at a relatively high Pd/V_{sb} value (0.76 mTorr.cm.V^{-1}). For the two films, the dark conductivity (σ) is also included in the figures.

The film of Fig. 5-13a exhibits very low photoconductivity compared to that of Fig. 5-13b. Therefore for the film prepared at low Pd/V_{sb} (Fig. 5-13a) only the photconductivity under high light intensity was measured. In genral at high temperature range the photoconductivity approaches a maximum value. Beyond this temperature range the photocurrent was difficult to measure with reasonable accuracy because $\sigma_{Ph} \ll \sigma$. Accordingly the decreasing part of the photoconductivity curves are not shown. The maximum in photoconductivity has been reported by others for a-Si:H (Spear et al, 1974; Fuhs et al, 1978; Moustakas

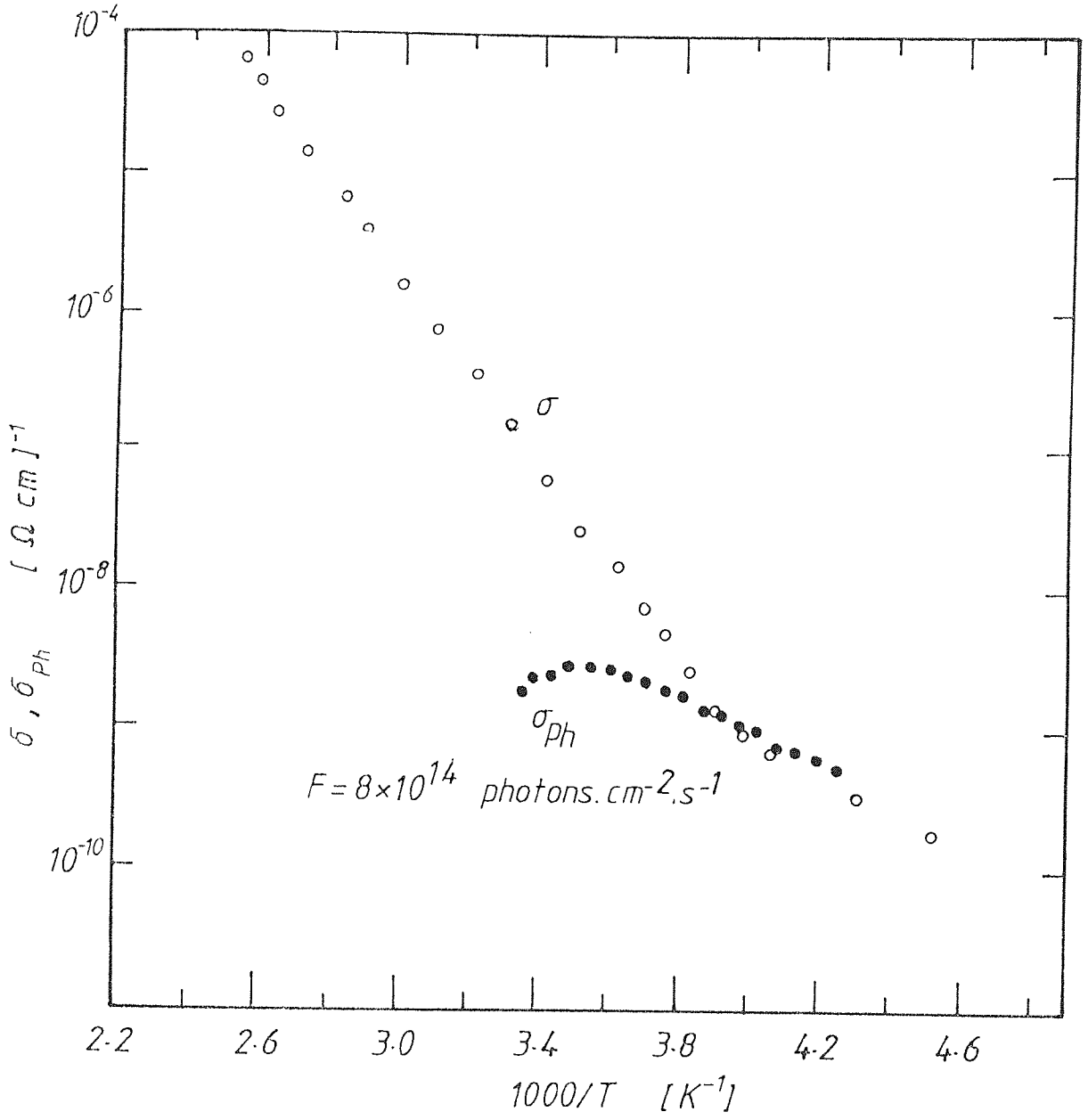

Fig. 5-13 (a) The photoconductivity σ_{Ph} and the dark conductivity σ vs 1000/T for a-Si prepared at T_s=300 °C and Pd/V_{sb}=0.31 mTorr.cm.V^{-1}. The measurements were made at a photon energy of 1.89 eV at the indicated flux intensity.

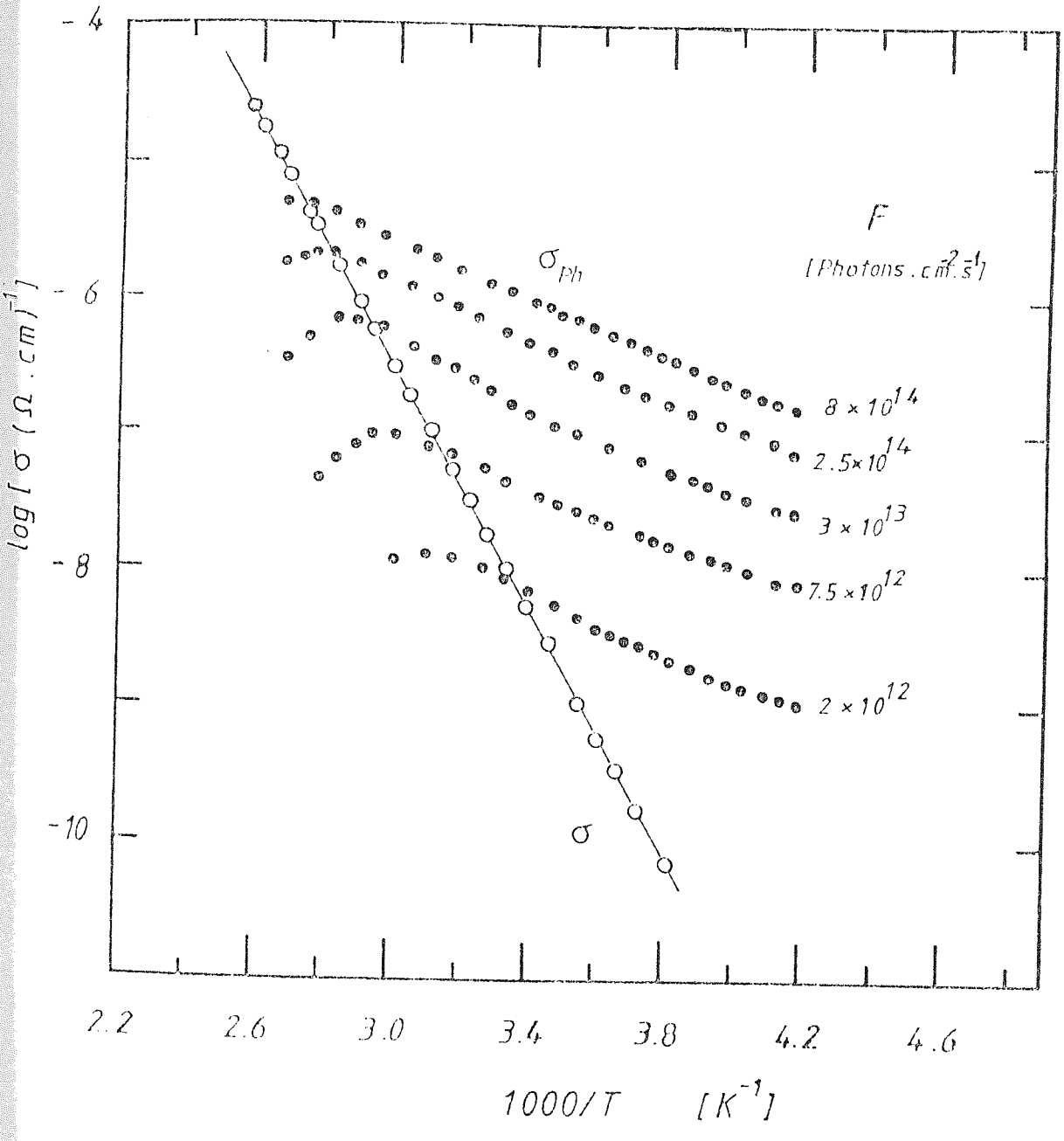

Fig. 5-13 (b) The photoconductivity σ_{Ph} and the dark conductivity vs 1000/T for a-Si prepared at T_s=300 °C and Pd/V_{sb}=0.76 mTorr.cm.V^{-1}. The measurements were made at a photon energy of 1.89 eV with the indicated flux intensities.

1980; Ray et al, 1983). At the lower temperature side of the photoconductivity curves, it was found that the intensity dependence of σ_{Ph} follows eq. (3-19). For instance, for high Pd/V_{sb} films, at about room temperature, the exponent $\gamma \simeq 0.55$ while γ approaches 1 at high temperatures near the maximum, at relatively high light intensities (about 10^{15} photons.cm^{-2}.s^{-1}). The value of $\gamma \simeq 0.55$ indicates that the bimolecular recombination process is dominant, and as the temperature is increased there is a combination of monomolecular and bimolecular recombination processes, as γ increases towards 1. At high temperatures where $\gamma \simeq 1$, monomolecular recombination process is dominating and the photoconductivity becomes much less than the dark conductivity.

The available data of σ_{Ph} vs 1/T suggest a thermally activated photocurrent with an activation energy (at the low temperatures side of the maximum photoconductivity) between 0.15 and 0.2 eV. It is interesting to note that no systematic dependence of the activation energy of the photoconductivity on preparation conditions (especially Pd/V_{sb}) or light intensity was found. Furthermore it was found that the shape of the curve σ_{Ph} vs 1/T is independent of the photon energy in the range between 1 eV and 2 eV. This agrees well with experimental results for a-Si:H observed by others (e.g. Spear et al, 1974).

5.2.4.4. LOW-ENERGY α FROM PHOTOCONDUCTIVITY MEASUREMENTS

It has been seen in section 5.2.2.2. that the absorption coefficient (α) from direct transmission measurements, can be measured with a reasonable accuracy only for $\alpha \gtrsim 10^3$ cm^{-1}. This corresponds to an energy limit of $\hbar\omega \gtrsim 1.5$ eV. To extend the range of $\hbar\omega$ below the optical gap, E_o, eq. (3-22) was used to evaluate the relative absorption coefficient (α/α_o) from the photoconductivity results. The calculated (α/α_o) plotted as a function of $\hbar\omega$ were fitted to the absolute absorption scale at one energy where the two data sets overlap. It has been found that this fit could be made at energy between 1.5 and 1.7 eV. By fitting (α/α_o) to the absolute α scale, the energy range of α was extended down to about 0.8 eV.

The plots of α vs $\hbar\omega$ for films prepared at different values of Pd/V_{sb} are shown in Fig. 5-14. The films represented in Fig. 5-14 are all about the same thickness. Therefore there was no need to correct for the light penetration depth, and direct comparison between these films is valid. Furthermore the thickness was less than 1 μm so that the condition of $\alpha t \ll 1$ for eq. (3-22) to be valid is fulfilled.

It can be seen from Fig. 5-14 that α vs $\hbar\omega$ curves (especially the absorption edge between 10^4 and 10^5 cm^{-1}),

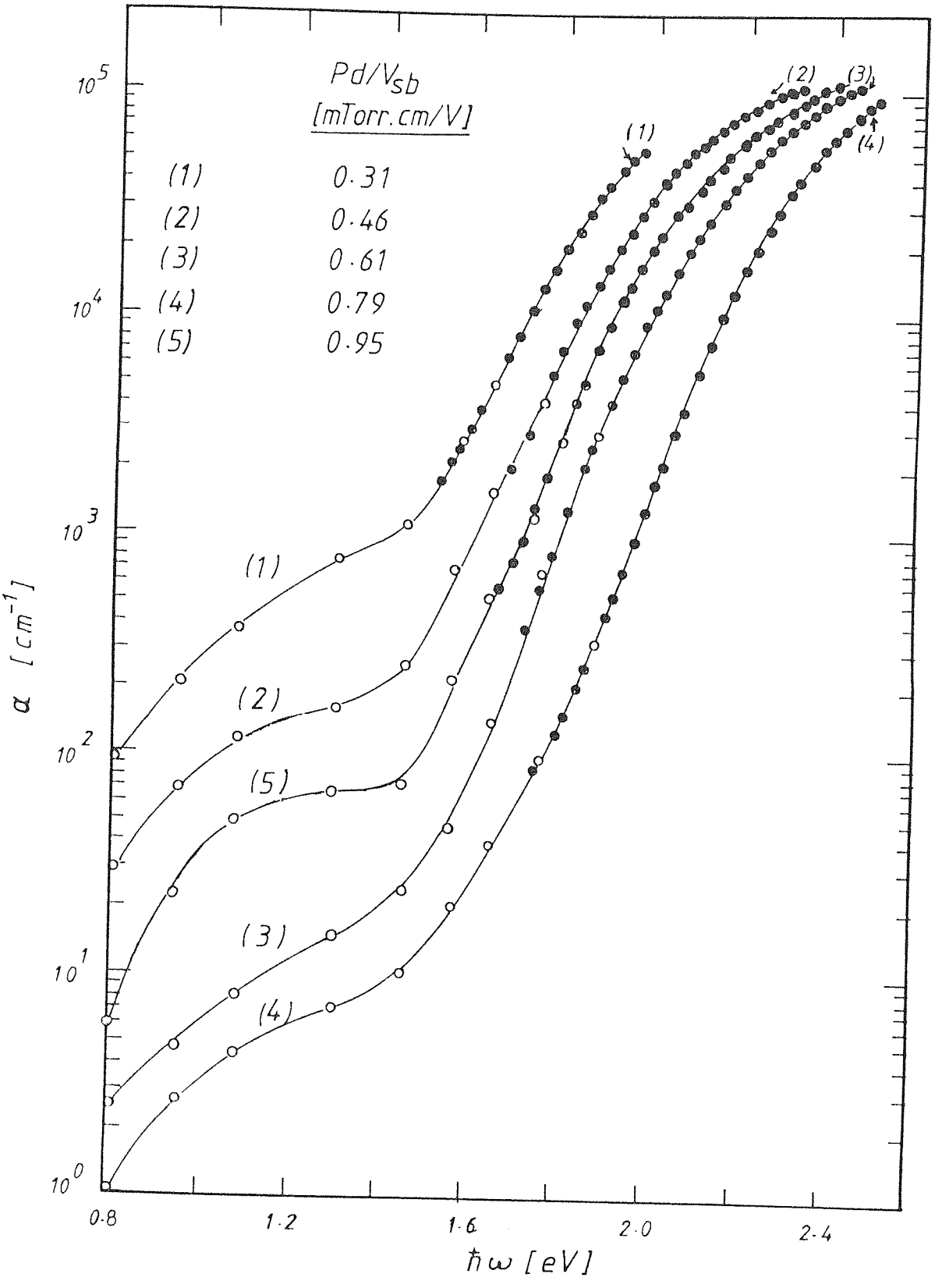

Fig. 5-14: The absorption coefficient α vs photon energy $\hbar\omega$ for a-Si films prepared at different values of Pd/V_{sb} as indicated. The open circles are the values derived from photoconductivity measurements using Harvard group's method (Moddel et al, 1980).

are displaced to higher $\hbar\omega$ values, and the shoulder around 1.2 eV is lowered in intensity with increased Pd/V_{sb} up to 0.80 $mTorr.cm.V^{-1}$, similar to the variations observed for Ar-sputtered a-Si:H films upon increasing H_2 content (Anderson et al, 1980). For Pd/V_{sb} values higher than 0.80 $mTorr.cm.V^{-1}$, the α vs $\hbar\omega$ plot shifts to lower $\hbar\omega$ values and the absorption at energies lower than 1.5 eV is increased. This suggests a control of the localised - defect-states-density by Pd/V_{sb}. These observations, however, are consistent with the variation in the constant β in eq. (3-9) with the optical gap E_o (Fig. 5-7).

5.3. DISCUSSION

In this section, the discussion is divided into two subsections. In section 5.3.1., the results of the electrical and optical properties will be discussed, while section 5.3.2. will be devoted to the discussion of the photoconductive properties.

5.3.1. THE ELECTRICAL AND OPTICAL PROPERTIES

The results described in section 5.2.2. have demonstrated that the electrical and optical properties of undoped a-Si prepared by Ne sputtering can be controlled and varied systematically over a wide range, by variation of the preparation conditions. The similarities between the changes in optical and electrical properties and the deposition rate shown in Figs. 5-5 and 5-3 imply that the deposition rate, D_R,

plays an important role in determining the properties of the films. Upon increasing the product Pd/V_{sb} (Fig. 5-5 ranges I and II), at a fixed substrate-temperature, the decrease in the room-temperature dark-conductivity (σ_{RT}) and the increase in the photoconductivity (σ_{Ph}) are consistent with the increase in both the thermal activation energy of the dark conductivity (ΔE_a) and the optical gap E_o (Fig. 5-5). It is interesting to point out that the increase σ_{Ph} with Pd/V_{sb} (Fig. 5-5 ranges I and II) of these films is qualitatively similar to the increase of σ_{Ph} with increasing hydrogen content in a-Si:H produced by Ar/H_2 sputtering at low hydrogen partial pressure (Paul and Anderson, 1981). The increase in σ_{Ph} has been attributed to reducing the density-of-states in the mobility gap.

The slow change both in the deposition rate (Fig. 5-3, range II) and in the optical and the electronic properties (Fig. 5-5 range II) indicates the optimum range of the parameters V_{sb}, P and d for Ne sputtering. Details of this can be found in section 4.3.. It may be possible, however, to improve further the films by changing some other parameters not examined here. For example negative substrate bias and magnetron sputtering have recently been shown to improve the electronic and optical properties of a-Si (e.g. Suzuki et al,1982; Batabyal et al, 1984).

From the plots of $(\alpha\hbar\omega)^{\frac{1}{2}}$ vs $\hbar\omega$ for various films prepared under different conditions (Fig. 5-6), it can be seen that upon increasing the product Pd/V_{sb} up to about 0.80 mTorr.cm.V^{-1}, the curves are displaced to higher

energies, and the slope β in eq. (3-9) is increased, where β vs E_o (Fig. 5-7) shows a linear relationship similar to the case of glow-discharge (e.g. Cody et al, 1980) and sputtered (Paul and Anderson,1981) a-Si:H. This relation and the shift in the curves may suggest that the increase in the optical gap is due to reduction in the density of the band tail-states or gap-defect states or both (Paul and Anderson, 1981), which in turn might lower the overall density-of-states in the mobility gap. The variation in band tail width means a change in the degree of disorder. This possibility may be excluded, since the temperature dependence of photoconductivity showed that the band tail-width, calculated from the slope of log σ_{ph} vs 1/T, is independent of Pd/V_{sb}. Therefore the variation in the intensity of the shoulder at 1.2 eV in the photoresponse curves and the change in β are more likely due to changes in the density of defects.

Therefore, a conclusion can be drawn that combinations of pressure, target-substrate spacing and self-bias voltage on target that give relatively high values of Pd/V_{sb} (Fig. 5-5, range III) may produce films with low density-of-states in the mobility gap. It can be argued that the deposition rate is controlled by the kinetic energy of the sputtering gas species, ions and neutrals, bombarding the target and the subsequent collisions with the gas, which include Ne-Ne and Si-Ne collisions (both ions and neutrals). In addition, the plasma contains energetic electrons (e.g. Brodie et al, 1969); these electrons strike the substrate. Increasing the Pd product enhances the collisions within the plasma and reduces the

kinetic energy of the particles arriving at the substrate surface. Priestland and Jackson (1968) estimated that with $P = 10^{-3}$ Torr and d = 6 cm, about 60% of the sputtered material will experience collisions with the sputtering gas species during transit from the target to the substrate. Therefore with P=0.15 Torr and d-4 cm, a negligible fraction of the sputtered material is expected to arrive at the substrate surface without suffering any collision. V_{sb} is also expected to play a role in controlling the kinetic energy of the particles arriving at the substrate surface (e.g. Batabyal et al,1984; Suzuki et al, 1982). Therefore moderating the kinetic energy of the Ne species and the sputtered Si particles, by the above quantities (P, d and V_{sb}), will result in less damage in the deposited film in addition to the possibility of re-constructing some weak bonds in the a-Si network (e.g. Suzuki et al, 1981, 1982); so giving the optimum conditions for producing a low density-of-states material .

On the other hand, increasing the product Pd/V_{sb} above the optimum conditions (Fig. 5-5 range III), results in reversing the effect where the arriving particles at the film surface may have less kinetic energy than that required for removing weak bonds. Accordingly higher density-of-states films are expected to be produced by sputtering at very high Pd/V_{sb} product. This is suggested by the reverse changes of σ_{RT}, σ_{Ph}, E_o and ΔE_a (Fig. 5-5 range III), where the increase in σ_{RT} and the reduction in σ_{Ph}, ΔE_a and E_o are indicative of the increase in the density of states in the mobility gap.

Comparison of the influence of the preparation conditions of sputtering in a Ne plasma on film properties with that of sputtering in

Ar plasma (Pawlewicz, 1978) indicates that the former technique produces a material with less defect states. Detailed examination of the sputtering plasma is required to determine the factors which result in an improvement in film quality when using neon as opposed to argon sputtering (Zaka et al, 1984). Thermalisation of the plasma species is important but this may be achieved in either case by using the appropriate Pd/V_{sb}. Other factors may be important. The higher ionisation potential of Ne as compared to Ar (Gray, 1970) means that there is less likelihood of doubly ionised ions which would result in greater damage to the film. For a given energy the smaller stopping distance for argon ions, and possibly neutrals, results in a larger energy dissipation per unit path length and consequently more damage to the growing film. Small atomic size of Ne could also be important in causing less structural deformation. There is a higher probability for clusters of atoms to be sputtered with argon (Wehner and Anderson, 1970) which could result in film inhomogeneity and also lead to lower doping efficiency (Thompson and Reinhard, 1980; Suzuki et al, 1980). However, higher sputtering yields by Ar sputtering than by Ne sputtering have been reported (Fluit et al, 1963). The larger clusters of atoms with respect to the surrounding atoms on the surface of the film may be a reason for the formation of microvoids. XPS measurements showed that the plasmon energy of Si(2p) line of a-Si, prepared by Ne sputtering, is nearly equal to that of c-Si (Fig. 5-15). This suggests a close-packed structure in Ne-sputtered a-Si; with a mass density comparable with that of c-Si.

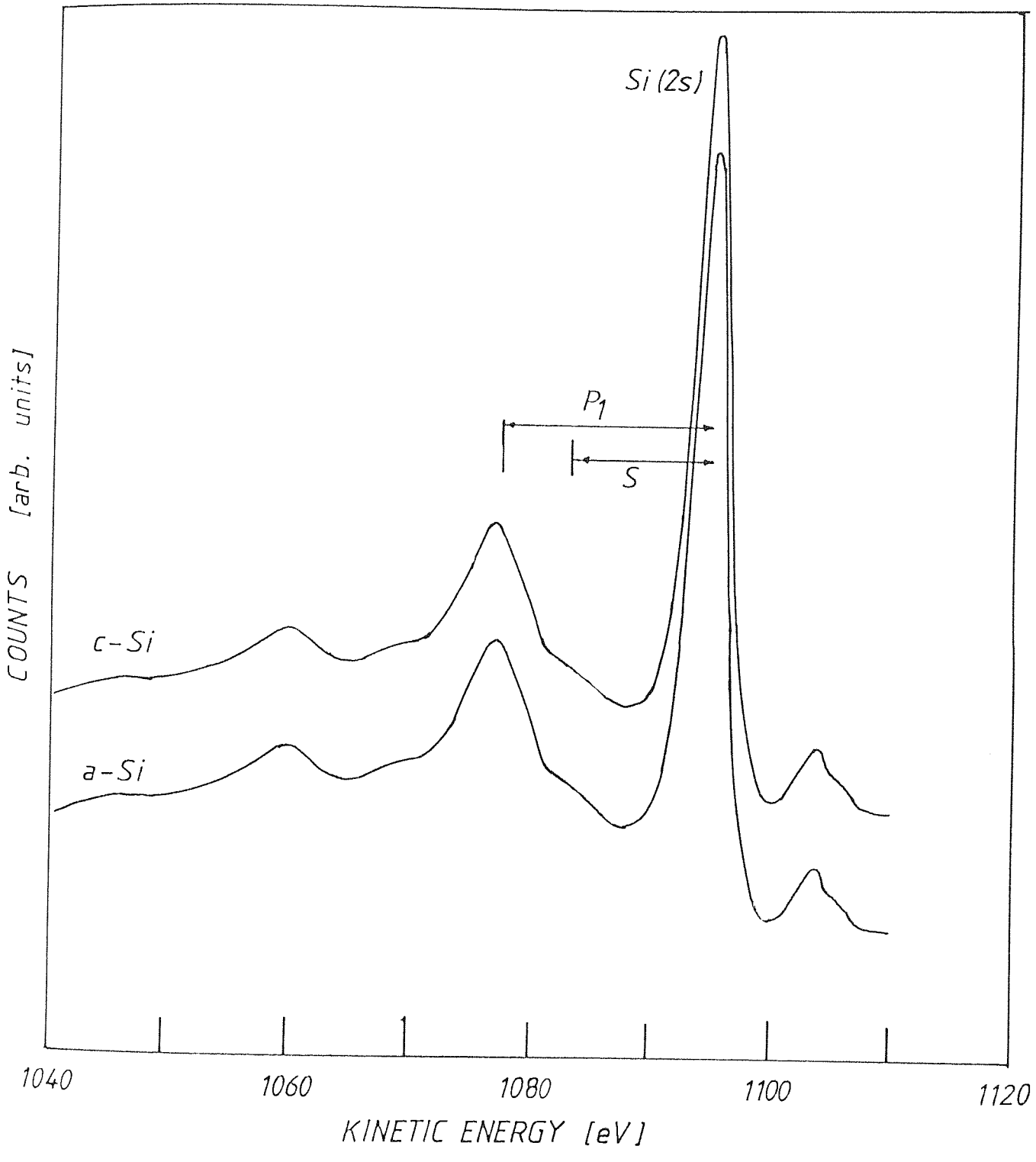

Fig. 5-15: Si(2s) photopeak in the XPS spectra showing the bulk and surface plasmon losses, for a-Si and c-Si. P_1 first bulk plasmon, S surface plasmon .

The dependence of the electronic and optical properties of undoped a-Si, on the substrate temperature, T_s, during the deposition (Fig. 5-8) can be divided into two ranges; one below 300 ^{o}C and the other above 300 ^{o}C. It is worth mentioning that all the results of Fig. 5-8 were for specimens prepared at about Pd/V_{sb}=0.68 mTorr.cm.V^{-1}; a condition near the optimum according to Fig. 5-5 (range II). Well below T_s=300 ^{o}C the sticking coefficient of the arriving particles at the substrate may be relatively high as suggested by the higher deposition rate, and the surface mobility of the atoms is low; this would make it difficult for the atoms to be organised in the appropriate way to produce low defect-states-density films. As T_s approaches 300 ^{o}C the surface mobility of the atoms becomes enough for them to be organised in a more relaxed structure with a low defect-states-density.

Although substrate temperatures higher than 300 ^{o}C are expected to improve the degree of order in the lattice (Cody et al, 1981) and to give a more relaxed structure, it seems that higher temperatures produce more defects in the a-Si network, and subsequently cause a deterioration in the electronic and optical properties. In Fig. 5-8a the deposition rate decreases with increasing substrate temperatures above 300 ^{o}C. This effect has been reported elsewhere and it was suggested that this could be due to a reduction of the sticking coefficient at high T_s (Davidse and Maissel, 1965). This effect would, in turn, produce a higher density-of-states material in a similar way to Pd/V_{sb} values in excess of 0.80 mTorr.cm.V^{-1} (Fig. 5-5, range III). This is suggested by the increase in σ_{RT} and the decrease in σ_{Ph}, E_o and ΔE_a upon increasing T_s above 300 ^{o}C (Figs. 5-8b,c and d).

5.3.2. THE PHOTOCONDUCTIVE PROPERTIES

The high photoresponse of the films prepared at high values of Pd/V_{sb} (Fig. 5-10) suggests a low density-of-states in the mobility gap for these films. The shoulder around 1.2 eV has been attributed to an optical transition from occupied localised states at ϵ_y in the lower half of the band gap (see Fig. 3-3) to the conduction band (Anderson et al, 1980; Moddel et al, 1980). The origin of these states is still unspecified although it has been suggested that they could be natural defect-states. However, the occurrence of this shoulder at approximately the same energy in all the films, suggests that there is a rapid rise in the gap density-of-states at about 1 eV below the conduction-band edge. This rise has been demonstrated by the field-effect measurements of a-Si:H prepared by glow-discharge decomposition of silane (Madan et al, 1976). However, the changes in the height (intensity) of the shoulder with preparation conditions, indicate that the localised states in the mobility gap are controlled by these preparation conditions. The high photosensitivity of films prepared at high Pd/V_{sb} (0.80 $mTorr.cm.V^{-1}$) could be a result of increasing recombination lifetime according to eq.(3-20). On the other hand, when Pd/V_{sb} exceeds 0.80 $mTorr.cm.V^{-1}$ (for example the curve labled 0.95 $mTorr.cm.V^{-1}$ in Fig. 5-10), tne photosensitivity is reduced, suggesting a decreasing recombination lifetime. This is consistent with the electrical and optical properties and the deposition rate results discussed earlier in this chapter.

As mentioned in section 5.2.2.1., it was concluded, from the hot-probe technique, that all the undoped films reported here were n-type. It has been established that in low density-of-states a-Si, the transport of excess carriers (photocarriers) takes place predominantly in the extended electron states (LeComber and Spear, 1970) where the hole mobility is negligibly small compared to electron mobility. Evidence in support of this conclusion is provided by the satisfactory agreement in table 5-3 between the photoconductive threshold $[\Delta E_a^{Ph} = (\epsilon_c - \epsilon_F)_{RT}]$ and the position of the Fermi level $[\Delta E_a = (\epsilon_c - \epsilon_F)_0]$, deduced from the dark conductivity measurements on the same specimens. The onset of the photoconductivity is therefore thought to coincide with transitions from filled states at ϵ_F into extended states at ϵ_c. The slight difference between ΔE_a and ΔE_a^{Ph} could be due to the fact that ΔE_a refers to the extrapolated position of the Fermi level at absolute zero, whereas ΔE_a^{Ph} is measured at room temperature (Spear and LeComber, 1976). Therefore, according to eq. (3-5a),

$$(\epsilon_c - \epsilon_F)_{RT} = (\epsilon_c - \epsilon_F)_0 - \delta T \qquad (3 - 5a)$$

Taking $\delta T \approx 0.07$ eV, the average value deduced from the difference between ΔE_a^{Ph} and ΔE_a in table 5-3, the temperature coefficient $\delta \approx 2.3 \times 10^{-4}$ eV.K^{-1}.

Figs. 5-13 suggest an activated photocurrent with an activation energy between 0.15 and 0.20 eV in the temperature range to the right of the photoconductive maximum.

In this temperature range, $\sigma_{Ph} \gg \sigma$ so that the photo-generated density of carriers at the conduction-band edge ϵ_c (and the valence-band edge ϵ_v), as defined in the model used by Spear and LeComber (1976) and discussed in section 3.2., is larger than that in the dark so that the quasi Fermi levels are separated from the thermal equilibrium Fermi level ϵ_{F0} and move towards the band-tail states at ϵ_A and localised states at ϵ_y (see Fig. 3-3). Consequently, the charge neutrality condition tends towards $n_A \approx n_y$. This will lead to a bimolecular recombination process in which recombination takes place via holes trapped at ϵ_y above the valence band. In this case the photoconductivity may be represented by the relation (3-15). According to this relation, the photoconductivity will be activated and the plots of $\log \sigma_{Ph}$ vs 1/T determine the position of the band-tail edge ϵ_A with respect to ϵ_c (or the band-tail width). From Figs. 5-13a and b and other similar plots (not shown here) it can be concluded that the band-tail width does not change significantly with changing (Pd/V_{sb}). This could mean that no significant change in the degree of disorder has occured upon varying the quantities P, d and V_{sb}. Instead, these quantities are more likely to affect the defect-states-centres as indicated earlier. The agreement betweeen $(\epsilon_c - \epsilon_A)$ values and those reported for a-Si:H prepared by glow discharge (Spear et al, 1974; Ray et al, 1983) is an indirect indication that the films prepared in this laboratory are amorphous.

On the other hand, at high temperatures and/or low light intensities, the photoconductivity becomes less than the dark conductivity. In this case it is believed that the quasi Fermi levels for electrons (and holes) coincide with the thermal equilibrium Fermi level ϵ_{F0}. This leads to a suggestion (Spear et al, 1974) that the monomolecular recombination process is associated with electron recombination via states at the Fermi level (see section 3.6.1.2.). The exponent $p = 1$ indicates that this type of recombination is taking place. Fig. 5-16 shows a schematic representation of the energy levels and the recombination transitions discussed above.

It has been shown that the photoconductivity, when monomolecular recombination is dominating, can be given by eq. (3-18),

$$\sigma_{Ph} = \frac{e\mu_c}{kT} \left(\frac{G}{K_2}\right) \frac{N(\epsilon_c)}{N(\epsilon_F)\, N(\epsilon_A)} \exp\left(-\frac{\epsilon_c - \epsilon_A}{kT}\right) \qquad (3-18)$$

It is worth noticing that this equation predicts that $\sigma_{Ph} \propto 1/N(\epsilon_F)$ at constant temperature for a given generation rate G and constant $[N(\epsilon_c)/N(\epsilon_A)]$ and $(\epsilon_c - \epsilon_A)$. A photoconductivity value of $10^{-6}\Omega^{-1}cm^{-1}$ in a-Si is thought to correspond to a density-of-states around the Fermi level $N(\epsilon_F)$ of between 10^{17} and 10^{18} $cm^{-3}eV^{-1}$ (Spear, private communication). An interesting result, which is consistent with this theory , is the relation betweeen σ_{Ph} and $(\epsilon_c - \epsilon_F)$ shown in Fig. 5-17. Large $(\epsilon_c - \epsilon_F)$ means that ϵ_F moves towards the minimum of the density-of-states distribution

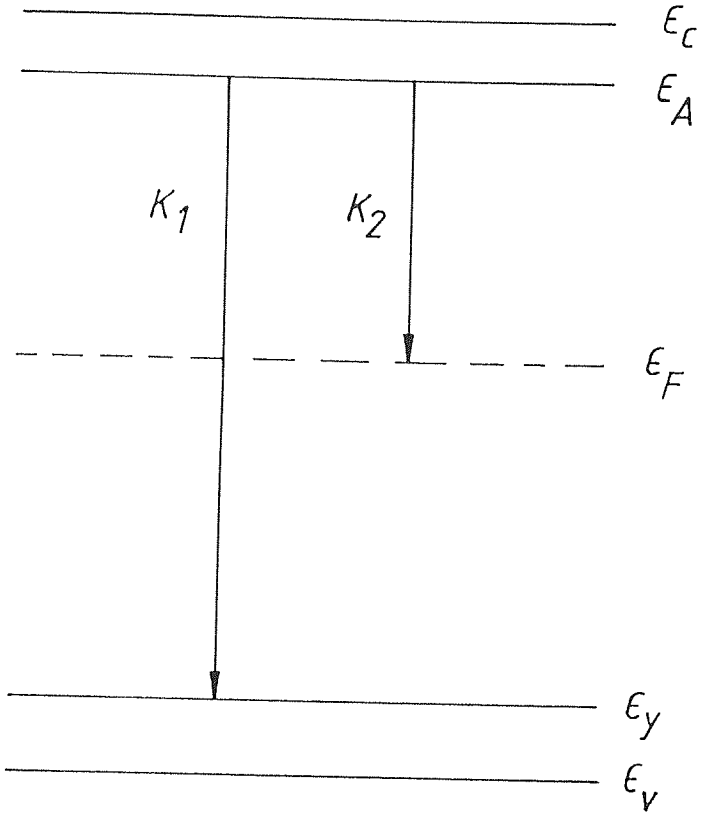

Fig. 5-16: A schematic representation of the energy levels and the recombination transitions in the mobility gap. K_1 and K_2 are as given in eqs. (3-15) and (3-18) respectively.

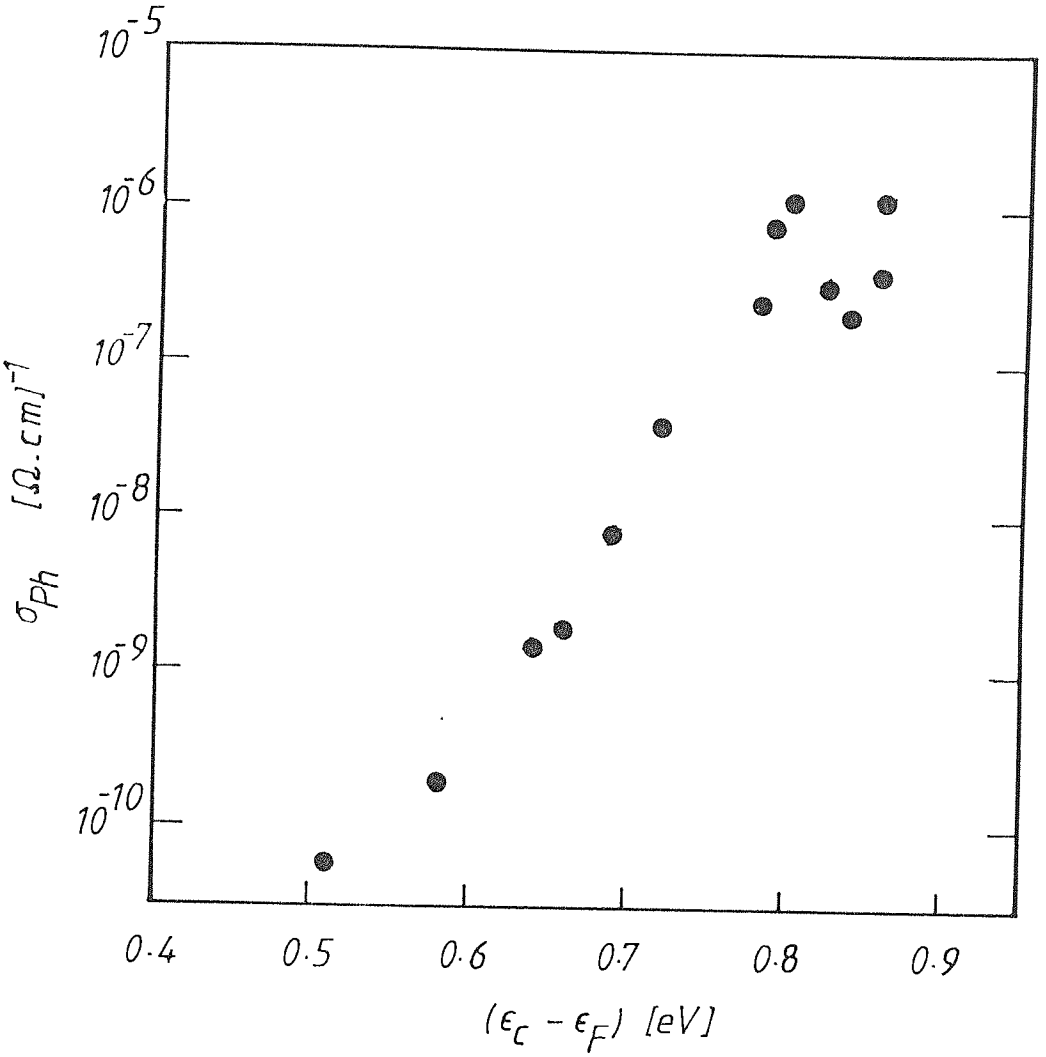

Fig. 5-17: The photoconductivity σ_{Ph} as a function of the Fermi-level position with respect to the conduction-band edge $(\epsilon_c - \epsilon_F)$ for undoped a-Si.

(Fig. 3-3). Therefore the high σ_{Ph} which corresponds to a large $(\epsilon_c - \epsilon_F)$ in Fig. 5-17 is in support of the above argument. It is worth mentioning that the results in Fig. 5-17 are similar to the dependence of σ_{Ph} on the hydrogen content in a-Si:H prepared by r.f. sputtering in Ar/H_2 (Paul and Anerson, 1981), where at low H_2 content ($\lesssim$1 at.%), $(\epsilon_c - \epsilon_F)$ increases with inceasing H_2 concentration in a-Si:H.

The decrease in the light intensity level, at which the recombination changes into bimolecular, with increasing Pd/V_{sb} (Fig. 5-12) may be another indication of the production of a low density-of-states in the mobility gap by controlling the defect states in a-Si network.

From the plots of α vs $\hbar\omega$ for various films prepared under different conditions (Fig. 5-14), it can be seeen that upon increasing the product Pd/V_{sb} the absorption edge between $\alpha = 10^4$ and 10^5 cm^{-1} is displaced to higher energies. Similar changes have been reported for a-Si:H (e.g. Freeman and Paul, 1979), and were attributed to hydrogen satisfying the dangling bonds and relaxing the a-Si network. Furthermore, upon increasing Pd/V_{sb}, lowering the height of the shoulder around 1.2 eV in the optical absorption spectra and the variation of the slope β with the optical gap E_o (Fig. 5-7) are in support of the above argument. In addition the curve marked 0.95 $mTorr.cm.V^{-1}$ (Fig. 5-14) shows that the shoulder is higher than that in the case of 0.79 $mTorr.cm.V^{-1}$, which indicates that the

optimum preparation conditions are approached at about 0.80 mTorr.cm.V^{-1}.

In the light of the electrical and optical results, the optical gap ($E_o = \epsilon_c - \epsilon_v$), the band-tail width ($\epsilon_c - \epsilon_A$) and the position of the localised states represented by the peak at ϵ_y above the valence band can be determined . From these parameters together with the shape of the absorption spectra (Fig. 5-14), the band model suggested by Spear and his collaborators (Fig. 3-3) can be the appropriate model for the Ne-sputtered a-Si prepared in our laboratory, where the results of electronic and optical properties can be consistently interpreted. Fig. 3-3 is redrawn (Fig. 5-18) to show a representation of the energy levels and the recombination transitions discussed earlier.

The absorption spectra could possibly be used to give an idea about the density-of-states level in the mobility gap as pointed out in section 3.6.3.. This method may still need further justification. Therefore α values derived from the photoconductivity measurements, at low energies, will be considered as representing the lower limits to α . It is, however, emphasised that the absorption spectra cannot determine the absolute density-of-states in the mobility gap, but can be used as a basis of comparison for samples prepared under different conditions. In addition, they can be compared with the absorption spectra derived by others (Moddel et al, 1980) for a-Si:H which in

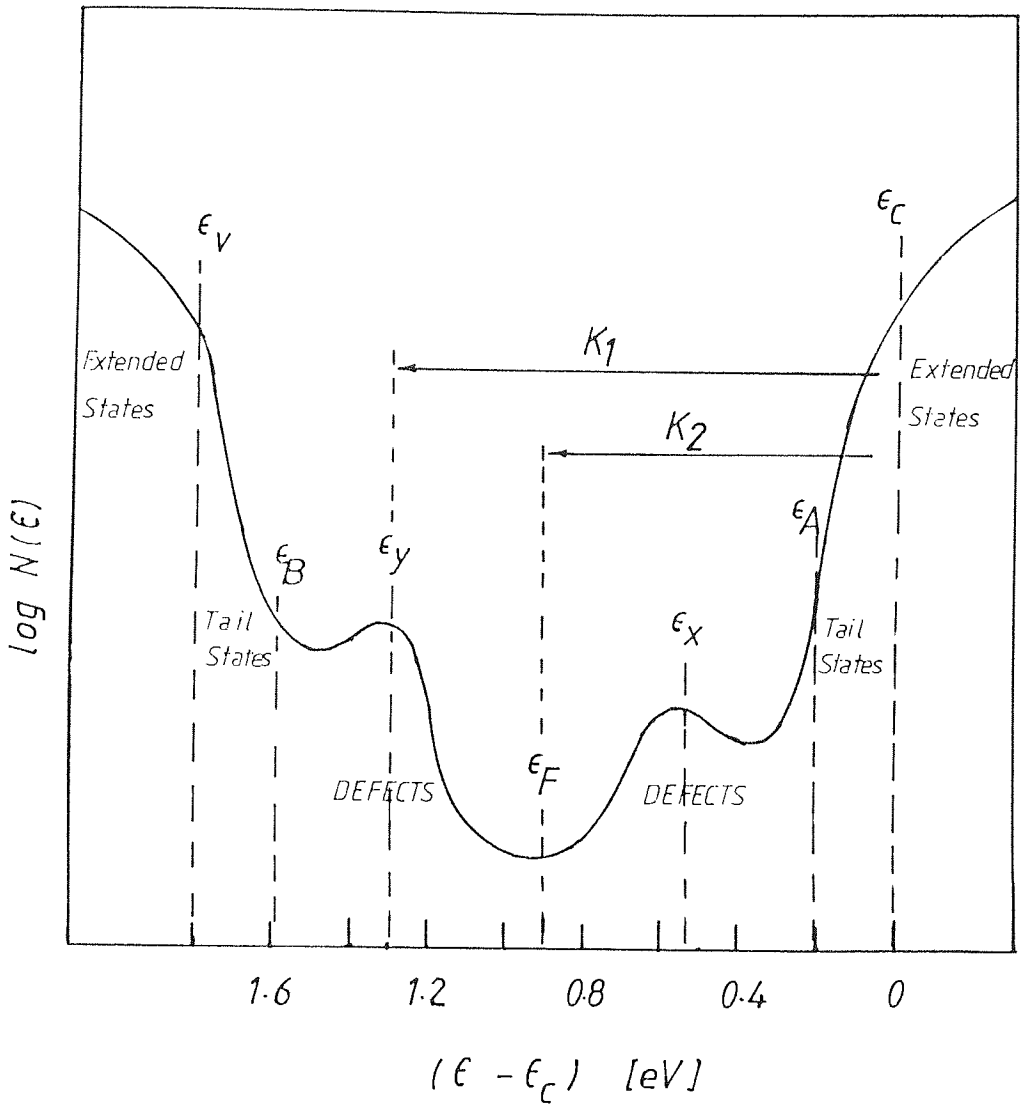

Fig. 5-18: The density-of-states distribution of Fig. 3-3, showing the energy levels and the recombination transitions, in the light of the present results. K_1 and K_2 are as given in eqs. (3-15) and (3-18) respectively.

turn can be compared with direct measurements of the density of states such as field-effect measurements (e.g. Madan et al, 1976).

Therefore, for the purpose of comparison of the density of states of the present material with that of a-Si:H, the same assumptions of those of Moddel et al (1980) will be made. Assuming that $\alpha = 10^4$ cm^{-1} corresponds to band-to-band transitions, that the states density at the band edge is about 10^{20}-10^{21} $cm^{-3}eV^{-1}$, and that the optical matrix element is about the same for the localised-to-band as for the band-to-band transitions, then peaks at about 1.2 eV in Fig. 5-14, would correspond to a gap density-of-states of the order of about 10^{17} $cm^{-3}eV^{-1}$ in films prepared at relatively high Pd/V_{sb} values and T_s=300 ^oC.

CHAPTER SIX

DOPING EFFECTS OF GROUP-III ELEMENTS IN a-Si

6.1. INTRODUCTION

We have seen in chapter five that a low-defect-density-material can be produced by Ne sputtering without hydrogen or a halogen, by optimising the preparation conditions. The high resistivity and the large thermal activation energy of amorphous silicon are characteristics of a semiconductor that has the possibility of being doped. As indicated in chapter three, a high doping efficiency requires a low density-of-states in the gap. To provide evidence for the low density-of-states, p-type doping effects in a-Si have been investigated. In this chapter, the doping effects of Al, B and Ga in a-Si are presented. The results are mainly divided into two parts, one deals with the doping effects when the preparation conditions are near the optimum (section 6.2.), while the other deals with the dependence of doping effects on the preparation conditions. The doping effects were studied in terms of the d.c. dark conductivity, the optical gap and the Fermi level position as functions of the dopant concentration in a-Si. The doping efficiencies of the present technique (sputtering from composite targets or a predoped target) are compared with that for other techniques, such as doping from the gas phase, ion-implantation doping and co-sputtering in Ar or Ar/H_2.

6.2. THE ELECTRICAL AND OPTICAL PROPERTIES

In the following, the variations of the electrical and optical properties of a-Si, on doping with group-III elements, are studied. Different combinations of the preparation conditions were chosen to give a Pd/V_{sb} value near the optimum for relatively low defect-states-density material as described in section 5.2.2.. For all the specimens in this section the substrate temperature, $T_s \approx 300$ °C. The Pd/V_{sb} value was 0.76 mTorr.cm.V^{-1} for Al-doped and Ga-doped specimens and 0.79 mTorr.cm.V^{-1} for B-doped specimens. However, in this range of Pd/V_{sb} the properties of a-Si vary only slowly with P, d and V_{sb} (Fig. 5-5, range II) and consequently a direct comparison of the various dopants is valid.

6.2.1. Al DOPING

The d.c. electrical dark conductivity, σ, was measured for samples with gap-cell configurations with Al electrodes, under vacuum to reduce the surface contamination. The experimental arrangement for these measurements is described in section 4.4.. Al proved to make good ohmic contacts with Al-doped a-Si in the range of applied fields up to 10^4 V.cm^{-1}. However, a field of only 10^2 V.cm^{-1} was applied. The dark conductivity was measured as a function of temperature, T, in the temperature range from about -150 °C to about 140 °C. Fig. 6-1 shows the plots of $\log\sigma$ vs 1000/T for doped a-Si with Al concentrations up to about 12 at.%. The atomic concentration of Al in Si was estimated using the methods described in section 4.7.. The

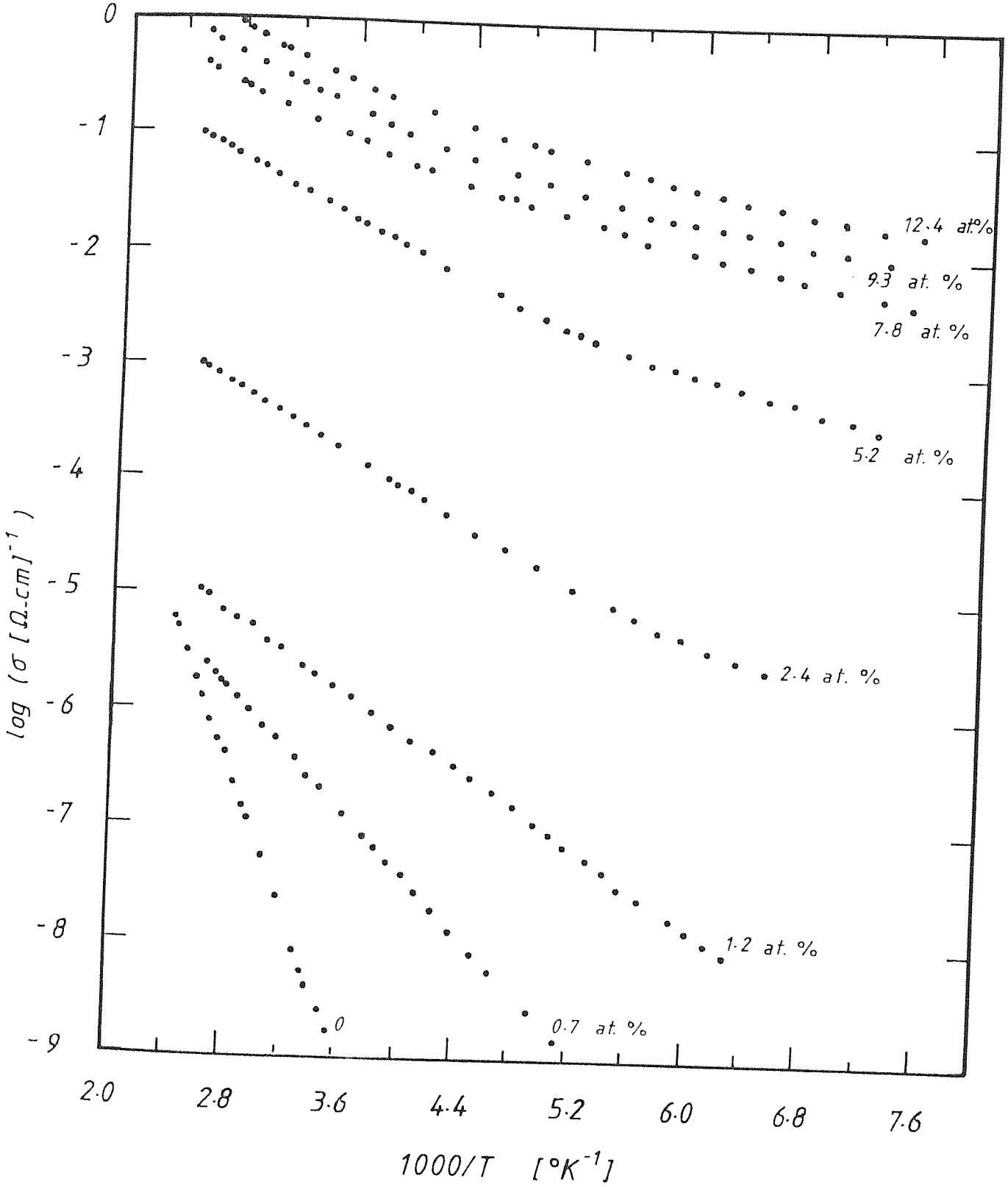

Fig. 6-1: D-C dark conductivity as a function of 1000/T for different Al-doping levels of a-Si as indicated. The films were prepared at Pd/V_{sb}=0.76 mTorr.cm.V^{-1} and T_s=300 °C.

plots of Fig. 6-1 indicate that the conductivity is thermally activated. A common feature of the plots is that thermally activated conduction in the extended states, following eq. (3-4), is dominant even at temperatures far below room temperature. For films with Al content of 2.4 at.% or more the plot is curved in the low temperatures range, indicating a hopping conduction. It can be seen from Fig. 6-1 that the slope of the curves, just above room temperature, decreases with increasing the Al content in the film. This in turn indicates the decrease of thermal activation energy (ΔE_a) with Al concentration in a-Si.

The optical transmission data of Al-doped films was taken using a UNICAM SP-800 spectrophotometer, and the absorption coefficient α was calculated as described in section 4.5.. The optical gap E_o of the films was determined from the intercept of the extrapolation of the straight part of the plot of $(\alpha\hbar\omega)^{\frac{1}{2}}$ vs the photon energy $\hbar\omega$ with the $\hbar\omega$ axis. Fig. 6-2 shows these plots for Al-doped a-Si with different Al concentrations as indicated. It can be seen that the change in the mobility gap is small even for high concentrations of Al, indicating that Al has not appreciably changed the basic band structure of the a-Si network, contrary to other reports on a-Si:H:Al alloys (Thompson and Reinhard, 1980; Xu et al, 1984).

The dependence of the room-temperature conductivity (σ_{RT}), the thermal activation energy (ΔE_a) and the optical gap (E_o) of Al-doped a-Si are listed in Table 6-1 for different Al contents. These values are plotted in Fig. 6-3. This figure shows that, initially, σ_{RT} decreases with increased Al concentration which corresponds to a slight increase in ΔE_a as compensation takes place and the Fermi level moves towards the minimum of

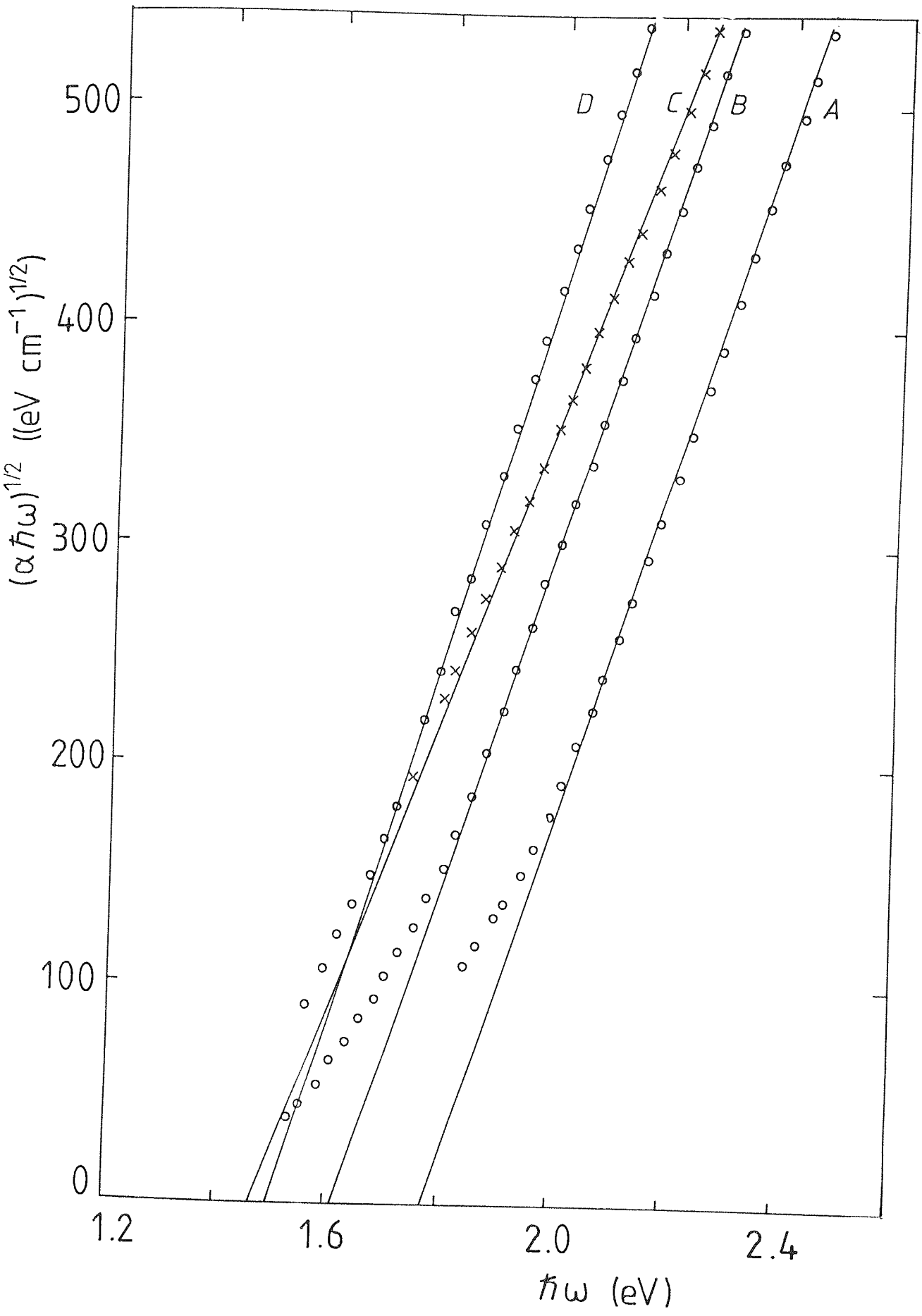

Fig. 6-2: Samples of the plots of $(\alpha\hbar\omega)^{\frac{1}{2}}$ against $\hbar\omega$ for (A) undoped a-Si, (B) 0.7at.% Al, (C) 2.37 at.% Al and (D) 9.33 at.% Al in a-Si. All the films were pepared by co-sputtering in Ne plasma at Pd/V_{sb}=0.76 mTorr.cm.V^{-1} and T_s=300 ^{o}C.

Table 6-1: Summary of various measurements for doped a-Si with a range of Al at.%. The films were prepared by co-sputtering Al with Si at high Pd/V_{sb} (0.76 mTorr.cm/V). σ_{RT} room-temperature conductivity; ΔE_a thermal activation energy; E_o optical gap.

Specimen No.	Al/Si at.%	σ_{RT} (Ω.cm)$^{-1}$	ΔE_a (eV)	E_o (eV)
1	0	5.6×10^{-9}	0.67	1.76
2	0.10	4.0×10^{-9}	0.73	1.73
3	0.25	1.0×10^{-9}	0.75	1.72
4	0.70	3.2×10^{-7}	0.26	1.63
5	1.20	2.2×10^{-6}	0.18	1.55
6	2.40	2.8×10^{-4}	0.15	1.48
7	5.20	2.8×10^{-2}	0.13	1.45
8	7.80	1.3×10^{-1}	0.12	1.37
9	9.30	2.2×10^{-1}	0.12	1.50
10	12.40	3.9×10^{-1}	0.11	1.37

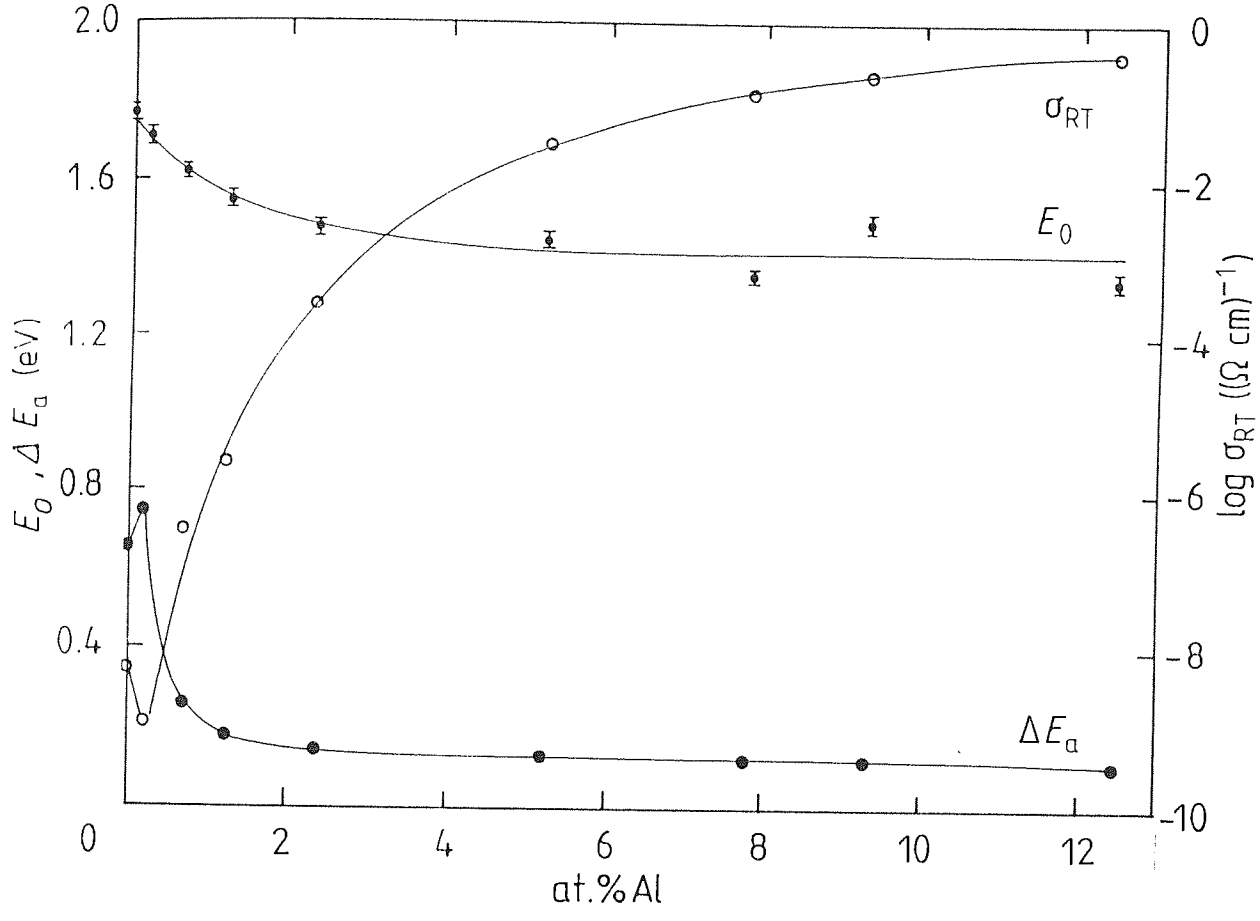

Fig. 6-3: The optical gap E_o, the thermal activation energy ΔE_a and the room-temperature conductivity σ_{RT} as functions of the atomic percentage of Al in a-Si.

the density of states at the centre of the mobility gap according to the Dundee group model (Madan et al,1976). Thereafter, σ_{RT} increases monotonically up to about 0.4 $\Omega^{-1}.cm^{-1}$ with the increased Al atomic concentration up to about 12.4 %. The increase of σ_{RT} is accompanied by a continuous decrease in ΔE_a to a nearly constant value of 0.1 eV. It can be seen from Fig. 6-3 that σ_{RT} changes over about 9 orders of magnitude , and ΔE_a changes by about 0.7 eV. For Al concentrations greater than 4 at.% the change in both σ_{RT} and ΔE_a becomes very slow, which could be attributed to the limit in the solid solubility of Al in Si and to the fact that at these doping levels, the Fermi level lies within the rapidly rising density-of-states region of the gap (see Figs. 3-3 and 5-18). The slight change in E_o with Al atomic concentration, as shown in Fig. 6-3, together with the variations in σ_{RT} and ΔE_a suggest that the Fermi level is not pinned, but rather shifted towards the band edge as the Al content increases.

As a check on the type of doping, some Al-doped films were deposited on various combinations of crystalline n- and p-type Si. The n-crystalline/Al-doped amorphous junction devices showed marked rectification properties similar to those reported by Thompson et al (1978). On the other hand, p-crystalline/Al-doped amorphous devices showed very little rectification which could be due to slight energy difference in the Fermi level position in the two materials. These devices confirm the p-type doping effect of Al in a-Si. Fig. 6-4 shows the I-V characteristic curve of a typical n-crystalline/p-amorphous

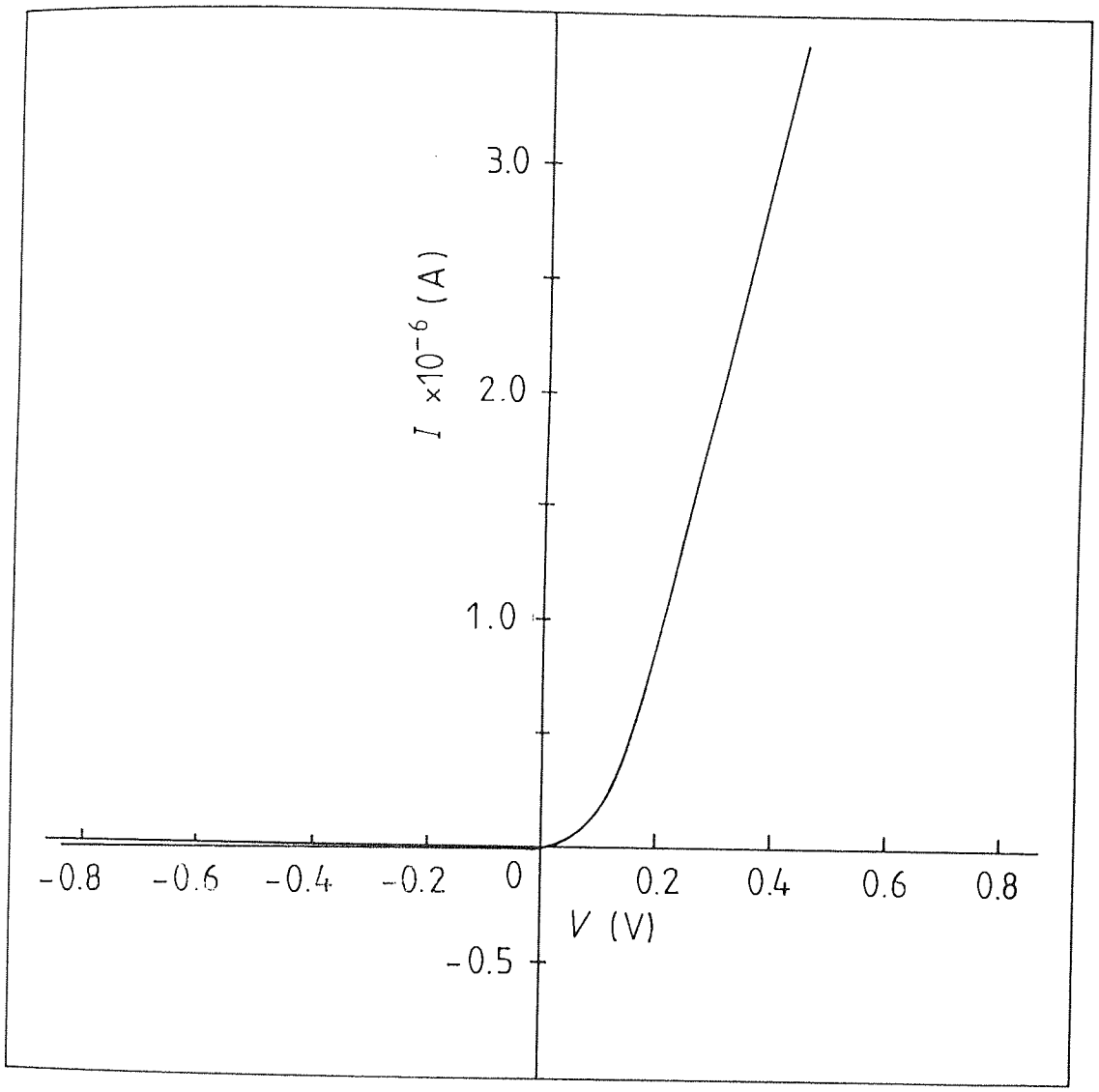

Fig. 6-4: I-V characteristic curve of a typical n-crystalline/p-amorphous Si junction device.

junction device. Also the hot probe thermoelectric technique confirmed that p-doping had taken place by Al/Si co-sputtering in Ne.

6.2.2. B DOPING

The B-doped films were prepared by sputtering from a composite target of Si and B pellet made of B powder as described in section 4.3. . The electrical and optical measurements for B-doped films were made using the same method as described in the case of Al-doped films.

The dark conductivity, σ, was measured as a function of temperature in the range from -100 ^{o}C to about 150 ^{o}C, for B-doped films with B/Si area ratio up to about 2.2%. In fact it was very difficult to determine the B atomic concentration in Si by x-ray photoemission spectroscopy (XPS), since the B(1s) photopeak is superimposed on the plasmon peaks of Si(2p), and B(1s) has a small ionisation cross-section (Scofield , 1976). Moreover, the sputtering yield of B is not available in the literature. Therefore the target area ratio was considered rather than the atomic ratio. It could, however, be estimated from the XPS spectra that the B/Si atomic ratio is less than the area ratio. Small sputtering yields for powder targets, in general, compared to those for solid targets, have been reported (Carter and Colligon, 1968). In addition, since the B atom is lighter than Si atom, it may suffer higher scattering than does Si. Accordingly, the B/Si area ratio could be considered to be the upper limit of the B/Si atomic ratio. Fig. 6-5 shows the plots of $\log\sigma$ vs 1000/T for B-doped specimens with

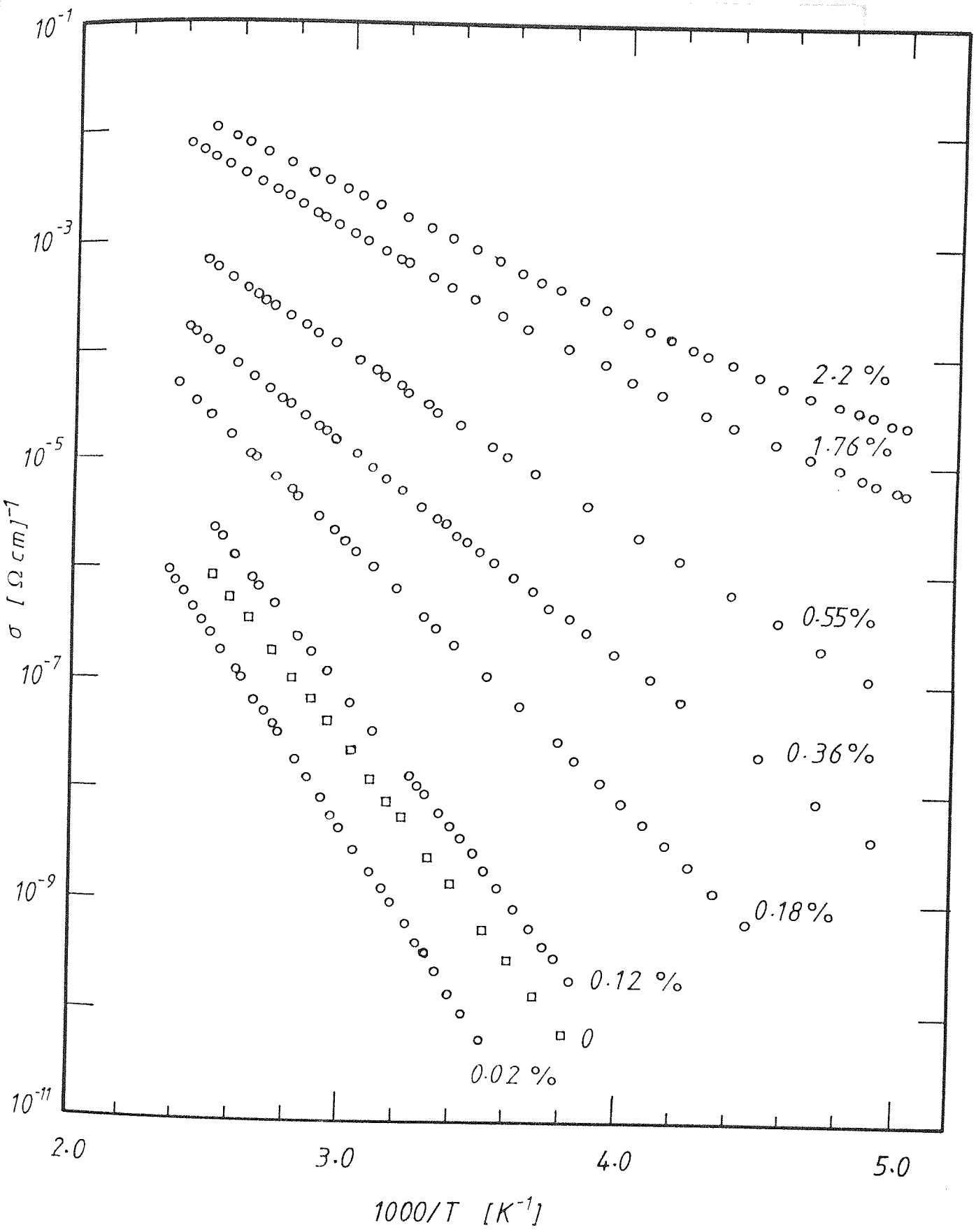

Fig. 6-5: D-C dark conductivity as a function of 1000/T for different B-doping levels of a-Si. Shown on the curves are B/Si area ratios. The films were prepared at Pd/V_{sb}=0.79 mTorr.cm.V^{-1} and T_s=300 ^{o}C.

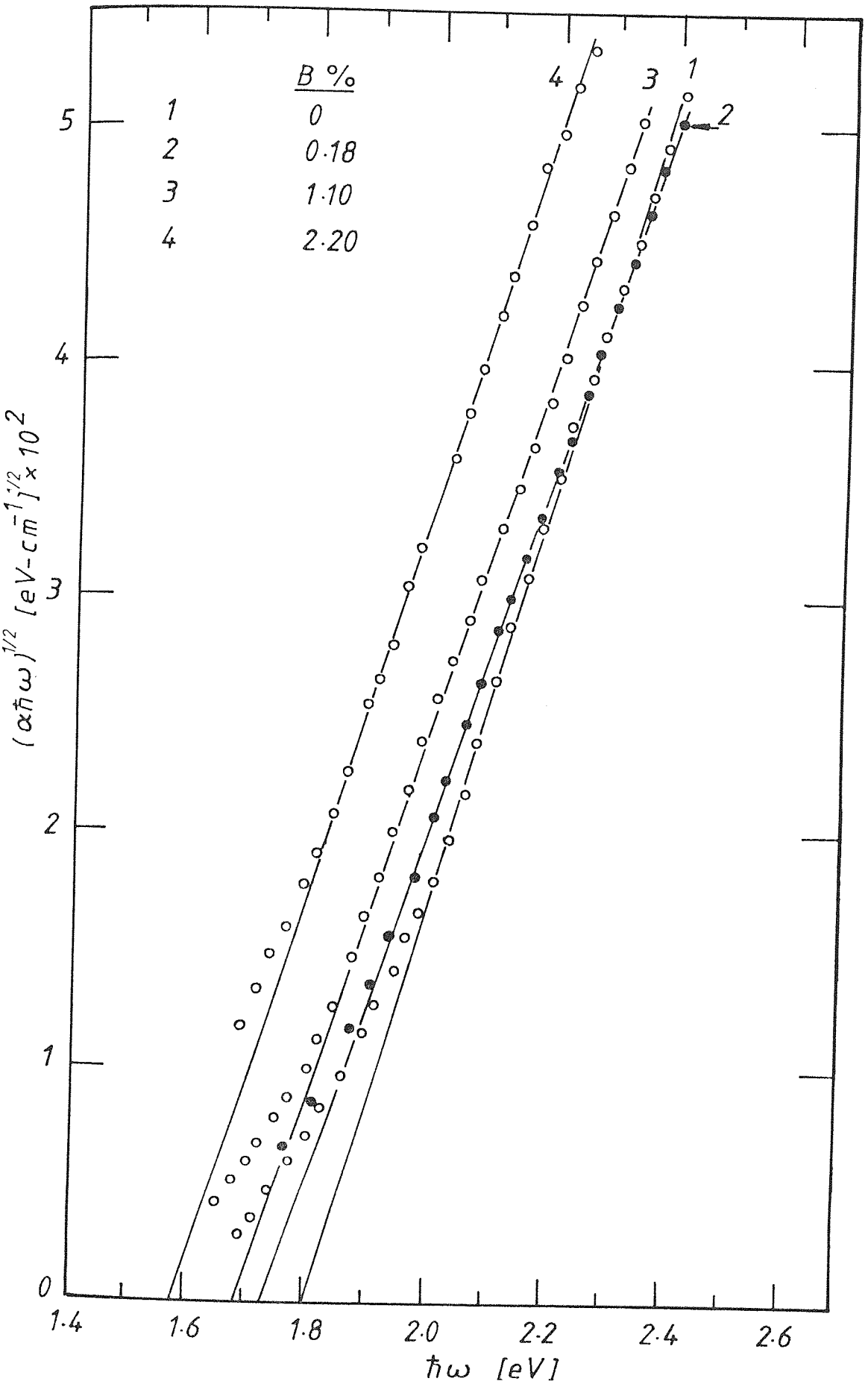

Fig. 6-6: Samples of the plots of $(\alpha\hbar\omega)^{\frac{1}{2}}$ against $\hbar\omega$ for different B/Si area ratios as indicated. All the films were prepared by co-sputtering in Ne plasma at Pd/V_{sb}=0.79 mTorr.cm.V^{-1} and T_s=300 ^{o}C.

Table 6-2: Summary of various measurements for doped a-Si with a range of B% (area ratio). The films were prepared by co-sputtering B with Si at high Pd/V_{sb} (0.79 mTorr.cm/V) and T_s = 300 °C. σ_{RT} room-temperature conductivity; ΔE_a thermal activation energy; E_o optical gap.

specimen No.	B/Si area %	σ_{RT} $(\Omega.cm)^{-1}$	ΔE_a (eV)	E_o (eV)
1	0	2.2×10^{-9}	0.72	1.80
2	0.02	2.5×10^{-10}	0.80	1.79
3	0.12	6.3×10^{-9}	0.65	1.78
4	0.18	3.0×10^{-7}	0.46	1.74
5	0.36	3.2×10^{-6}	0.37	1.74
6	0.55	2.8×10^{-5}	0.31	1.72
7	1.10	2.8×10^{-4}	0.24	1.68
8	1.76	5.0×10^{-4}	0.23	1.62
9	2.20	1.3×10^{-3}	0.19	1.58

B/Si area ratios up tp 2.2 %. From this figure, the decrease in slope can be seen as B/Si increases, which means a change in the thermal activation energy. Furthermore, the thermally activated conduction is clearly dominant even at temperatures well below room temperature, especially for lightly doped films.

The optical gap E_o of B-doped films was determined from the plots of $(\alpha\hbar\omega)^{\frac{1}{2}}$ vs $\hbar\omega$ as described for the case of Al-doped films, where α was determined from the transmission spectra. Fig. 6-6 shows $(\alpha\hbar\omega)^{\frac{1}{2}}$ vs $\hbar\omega$ for a range of B-doped films with different B concentrations. It can be seen from the figure that the change in E_o as B content in Si is increased is relatively small.

The values of σ_{RT}, ΔE_a and E_o for a range of B contnent are listed in Table 6-2. The plots of σ_{RT}, ΔE_a and E_o as functions of B/Si area ratio are shown in Fig. 6-7. Initially, with the addition of a very small amount of B to Si (~ 0.02 %), the conductivity decreases by at least an order of magnitude while the thermal activation energy increases to about 0.8 eV. This is expected where the compensation of the intrinsic n-type material takes place and the Fermi level moves towards the centre of the gap (see Fig. 3-3). Upon increasing the B content the conductivity increases rapidly by over 7 orders of magnitude accompanied by a shift of the Fermi level to within less than 0.2 eV from the valence band. The total shift of the Fermi level within the mobility gap is about 0.7 eV. The increase in conductivity and the decrease in the thermal activation energy,

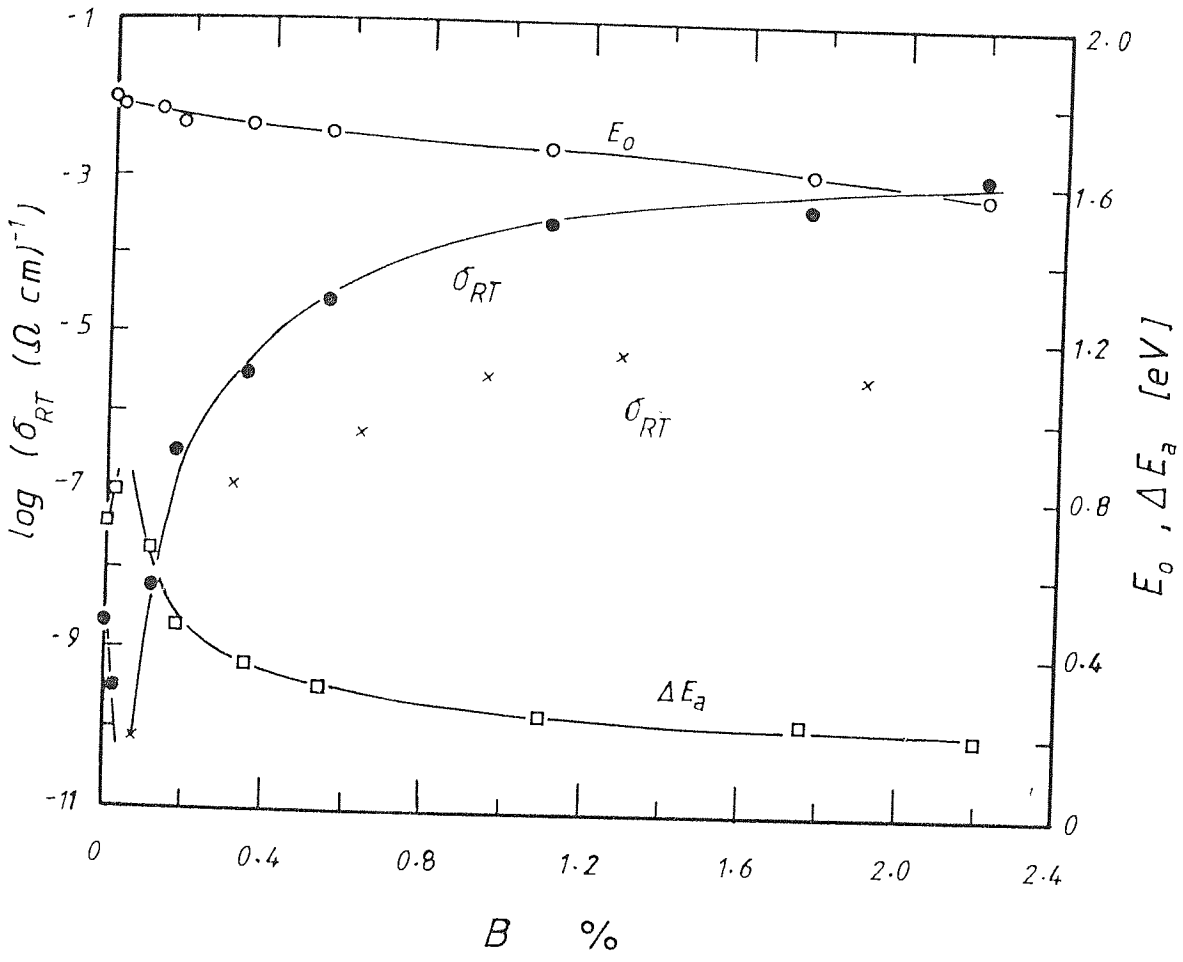

Fig. 6-7: The optical gap E_o, the thermal activation energy ΔE_a and the room-temperature conductivity σ_{RT} as functions of the B/Si area ratio. The points marked (x) are the room-temperature conductivity of B-doped a-Si prepared by co-sputtering in Ar (Suzuki et al, 1980).

together with the negligible change in the optical gap, indicate that substitutional doping has taken place. The dip in σ_{RT} vs B/Si% and the corresponding peak in ΔE_a vs B/Si% are further evidence of the p-type doping effect of B in Si as expected.

Included in Fig. 6-7 is σ_{RT} for B-doped a-Si prepared by Ar sputtering (Suzuki et al, 1980), for the purpose of comparison. It can be seen that σ_{RT} for Ne sputtering is about 2 orders of magnitude higher than that for Ar sputtering. This is indicative of a better quality a-Si prepared by Ne-sputtering than by Ar sputtering as discussed in section 5.3.

Furthermore, sputtering from a B-predoped Si-target with an estimated 1 at.% B, under the same conditions as for sputtering from a composite target, gave a large change in the conductivity and the thermal activation energy. Fig. 6-8 shows $\log\sigma$ vs 1000/T for B-doped film prepared from a predoped Si target, at $Pd/V_{sb} \approx 0.80$ mTorr.cm.V^{-1}, and T_s=300 °C. A conductivity of 10^{-3} $\Omega^{-1}.cm^{-1}$, at room temperature, is comparable with that in the case of co-sputtering B with Si.

6.2.3. Ga DOPING

Since the Ga has a low melting point, it was very difficult to control the required Ga/Si area ratio during sputtering. Accordingly it was difficult to achieve a pre-determined Ga/Si atomic ratio in the film and reproducibility was almost impossible. Therefore, only two specimens of Ga-doped Si are presented here, to show the possibility of p-type doping with Ga. A small Ga ingot was rubbed against the centre of the Si target. During the deposition procdure the Ga melted and formed a small ball hanging on the surface of the target. From the intensity ratio of Ga(3d) and Si(2s) photopeaks in the photoemission spectra, the Ga atomic percent in Si was estimated using eq. (4-3).

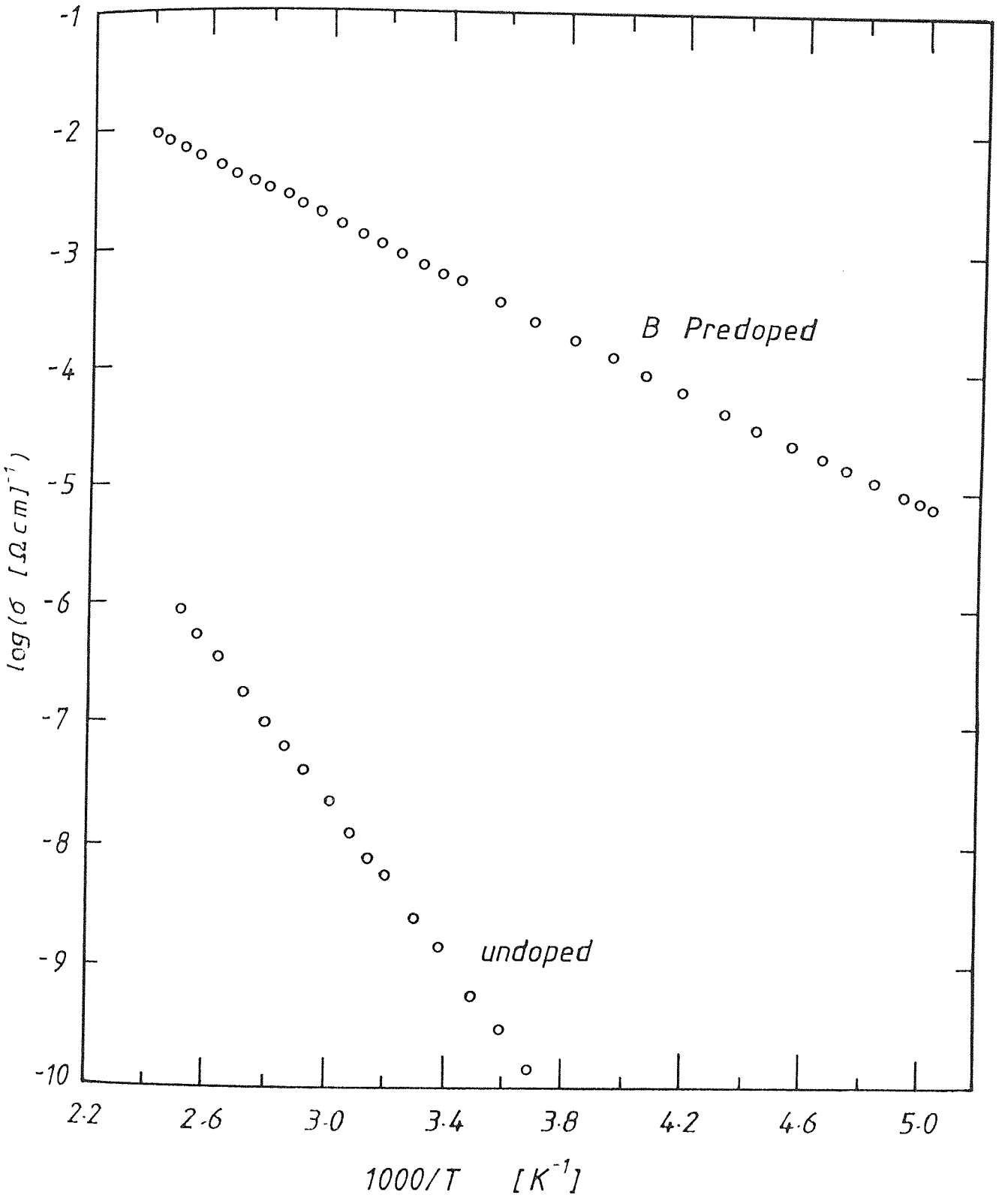

Fig. 6-8: D-C dark conductivity as a function of 1000/T for two films, one undoped a-Si and the other doped by sputtering from a B-predoped Si target. The films were prepared by sputtering in Ne plasma at Pd/V_{sb}=0.79 mTorr.cm.V^{-1} and T_s=300 °C.

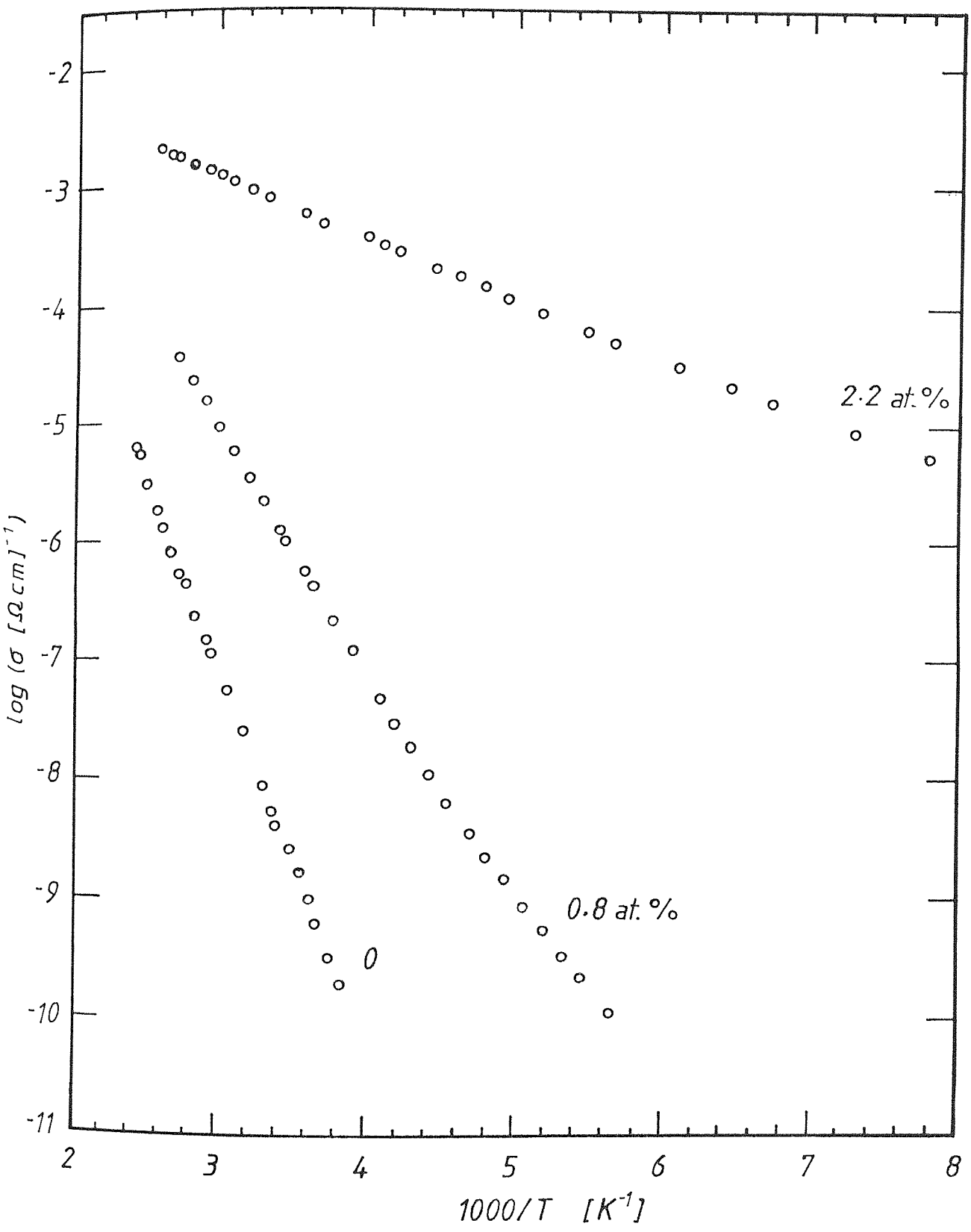

Fig. 6-9: D-C dark conductivity vs 1000/T for two Ga doping levels of a-Si, as indicated, compared with undoped a-Si. The films were pepared by co-sputtering in Ne plasma at Pd/V_{sb}=0.76 mTorr.cm.V^{-1} and T_s=300 ^{o}C.

Fig. 6-9 shows the plots of $\log\sigma$ vs 1000/T for two Ga-doped films; one contains 0.8 at.% Ga and the other 2.2 at.% in Si as indicated. The two plots are compared with that for the undoped a-Si, marked 0. It can be seen from the figure, that the conductivity increases by 6-7 orders of magnitude upon increasing the Ga content up to 2.2 at%. This is accompanied by a change in ΔE_a of about 0.7 eV. The optical absorption measurements (not shown here) again showed little variation in the optical gap upon incorporating Ga into the Si. This indicates that the variations in σ and ΔE_a with Ga content are due to a doping effect. The hot-probe thermoelectric measurements indicated p-type doping, as expected for doping with group-III elements.

6.3. DEPENDENCE OF ELECTRICAL AND OPTICAL PROPERTIES ON PREPARATION CONDITIONS

In section 5.1., it has been shown that different combinations of the gas pressure, P, the target-substrate distance, d and the self-bias voltage, V_{sb}, giving the same product (Pd/V_{sb}) resulted in films with substantially the same electronic and optical properties. Such a result made it more convenient to compare the properties of films prepared at different individual conditions, where the preparation conditions are dealt with as two parameters, (Pd/V_{sb}) and T_s, instead of four parameters. The effects of these conditions on the properties of undoped a-Si were reported in chapter 5. In the following sections the dependence of doping efficiency of Al or B on (Pd/V_{sb}) and T_s will be presented in terms of the electrical conductivity,

the thermal activation energy and the optical gap.

6.3.1. DEPENDENCE OF THE ELECTRICAL AND OPTICAL PROPERTIES ON Pd/V_{sb}

To see the effect of Pd/V_{sb} on the temperaure dependence of the dark conductivity, films prepared at three different values of Pd/V_{sb} were chosen, to represent three regions of Pd/V_{sb} as in the case of undoped a-Si, discussed earlier (Fig. 5-5). Fig. 6-10 shows the plots of $\log\sigma$ vs 1000/T for Al-doped a-Si, with 5.2 at.% Al, for films prepared at a Pd/V_{sb} of (1) o.33, (2) 0.76 and (3) 0.95 $mTorr.cm.V^{-1}$ respectively and a substrate temperature of about 300 ^{o}C. This atomic concentration of Al was chosen as an intermediate value, well above the concentration at which the "dip" in the conductivity occurs (Fig. 6-3). Fig. 6-10 indicates that the conductivity increases, and the thermal activation energy, around room temperature, decreases as the Pd/V_{sb} value is increased up to about 0.80 $mTorr.cm.V^{-1}$. This is accompanied by a small increase in the optical gap (not shown here). Curve 3 of Fig. 6-10 represents a film prepared at a (Pd/V_{sb}) value higher than 0.80 $mTorr.cm.V^{-1}$, where the conductivity is reduced and the thermal activation energy is increased. This is consistent with the variations in σ_{RT}, ΔE_a and E_o with Pd/V_{sb}, for undoped a-Si as discussed in section 5.2.2. (Fig. 5-5).

Similar variations of σ, ΔE_a and E_o with Pd/V_{sb} were found for B-doped a-Si, prepared both by co-sputtering B with Si and by sputtering from a B-predoped target. Fig. 6-11 shows the plots of $\log\sigma$ vs 1000/T for three B-doped films prepared

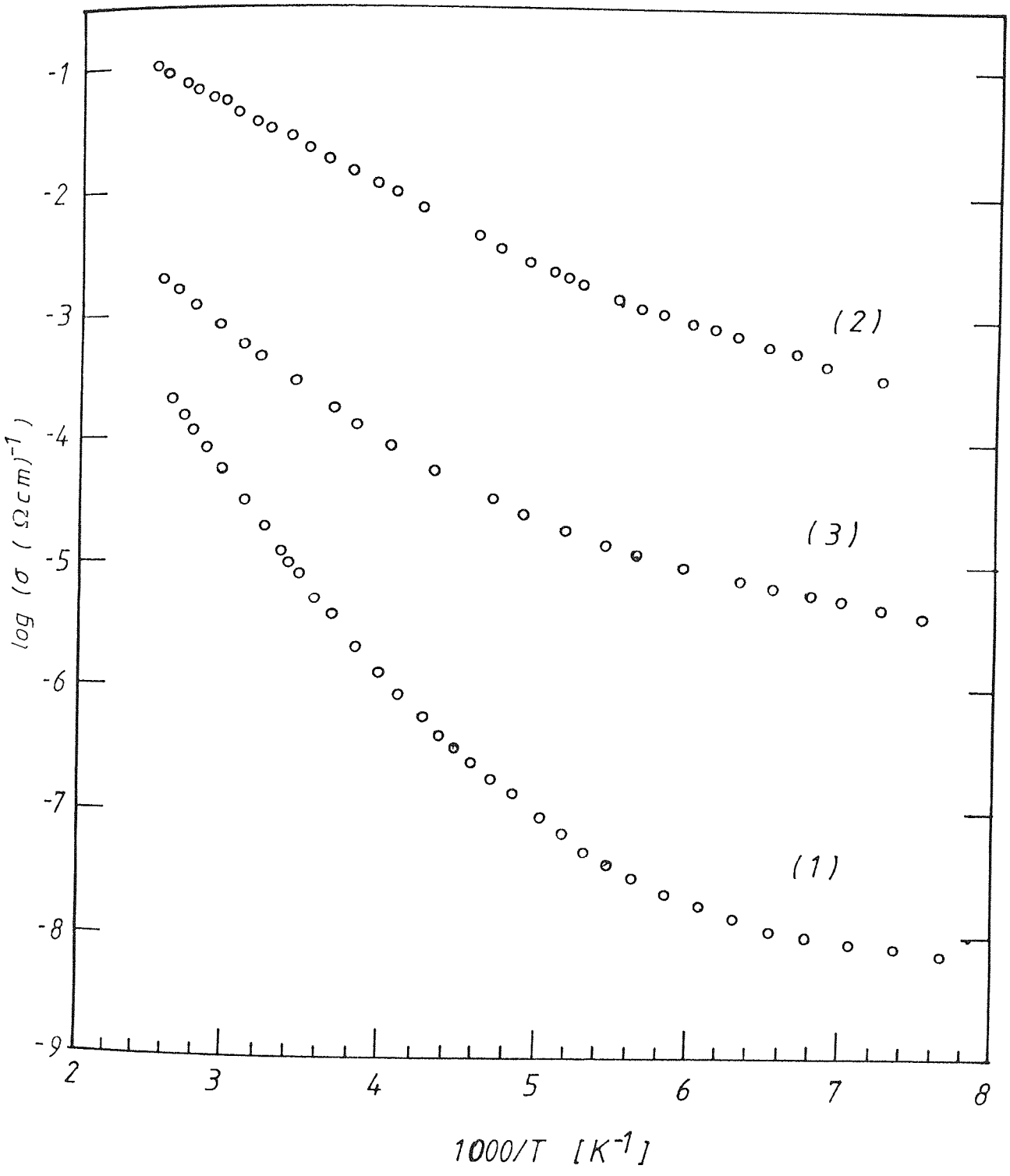

Fig. 6-10: D-C dark conductivity vs 1000/T for Al-doped films with 5.2 at.% Al in Si. The films were prepared at T_s=300 °C and Pd/V_{sb}= (1) 0.33, (2) 0.76 and (3) 0.95 mTorr.cm.V^{-1}.

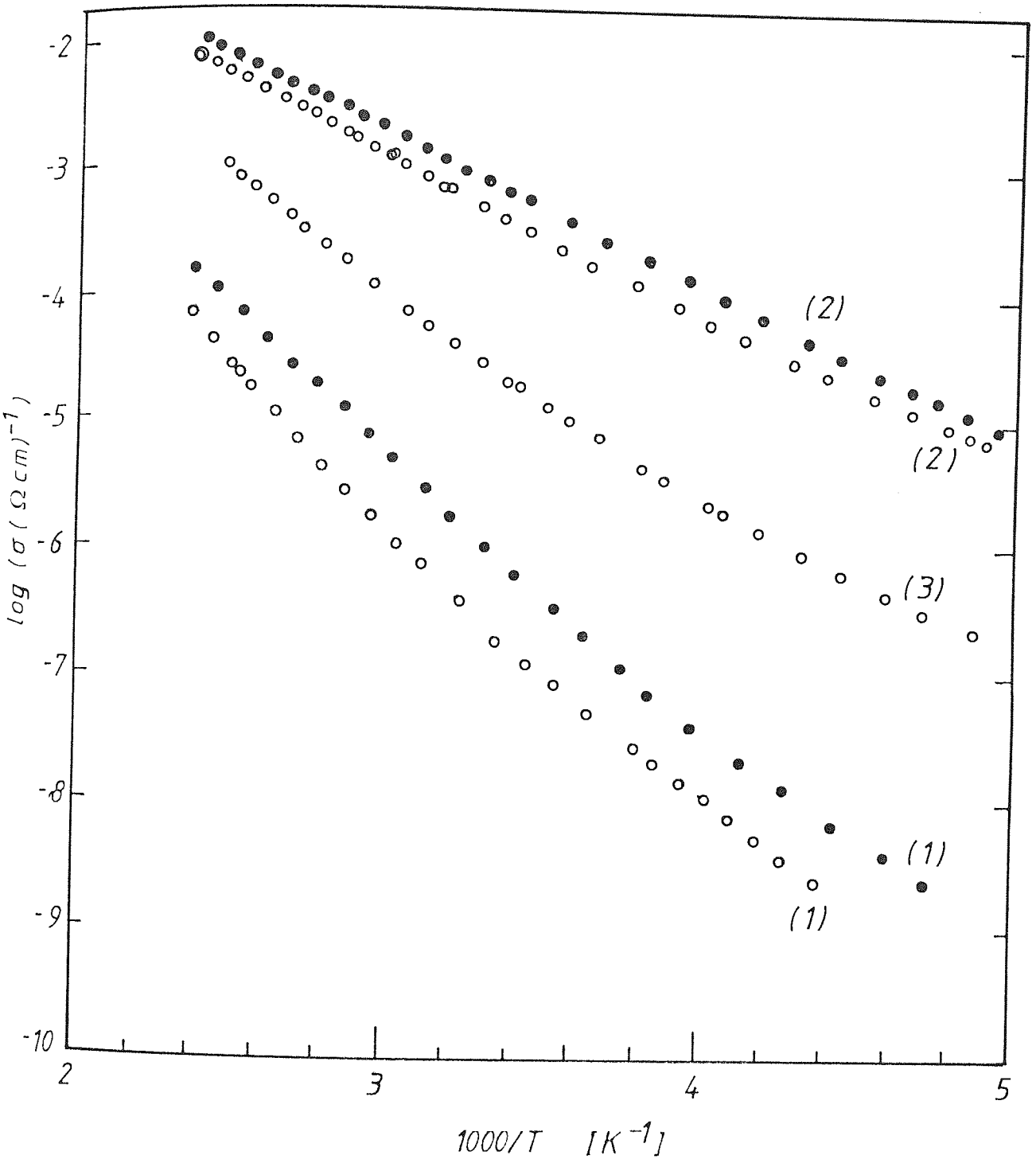

Fig. 6-11: D-C dark conductivity vs 1000/T for B-doped films prepared by sputtering from a composite target (ooo) with 1.76% B, or sputtering from a predoped target (●●●). The films were rpepared at T_s=300 °C and different Pd/V_{sb} values; (1) 0.35, (2) 0.79 and (3) 0.95 mTorr.cm.V^{-1}.

by co-sputtering at three different values of Pd/V_{sb} as indicated, and T_s=300 °C. The concentration of B in the films was 1.76 area%, well above the concentration at which the "dip" in the plots of σ_{RT} vs B area% occurs (Fig. 6-7). The variations in conductivity with Pd/V_{sb}, in the case of B doping by sputtering from a predoped target are also shown. They are qualitatively consistent with the variations in conductivity of specimens doped by co-sputtering with B (Fig. 6-11).

The temperature dependence of d.c. dark conductivity was measured for Al-doped a-Si films with a range of Al concentrations up to about 12 at.%. The films were prepared at a low Pd/V_{sb} value (0.33 mTorr.cm.V^{-1}) and T_s≈300 °C. The plots of $\log\sigma$ vs 1000/T for these films are shown in Fig. 6-12 . It can be seen from this figure that the thermal activation energy of the dark conductivity, ΔE_a, around room temperature, increases initially upon increasing the Al content up to about 1 at.%. When the Al content exceeds 1 at.%, ΔE_a decreases with increasing Al at.%. It is worth noticing that in these plots, the temperature at which the slope changes, i.e. the conduction mechanism changes into phonon-assisted hopping, is higher than the corresponding temperature in the case of Al-doped films prepared by co-sputtering at higher values of Pd/V_{sb} (Fig. 6-1).

Also, the optical gap E_o was determined from the plots of $(\alpha\hbar\omega)^{\frac{1}{2}}$ vs $\hbar\omega$ shown in Fig. 6-13. At low Al concentrations there is no appreciable change in E_o, while, as it can be seen

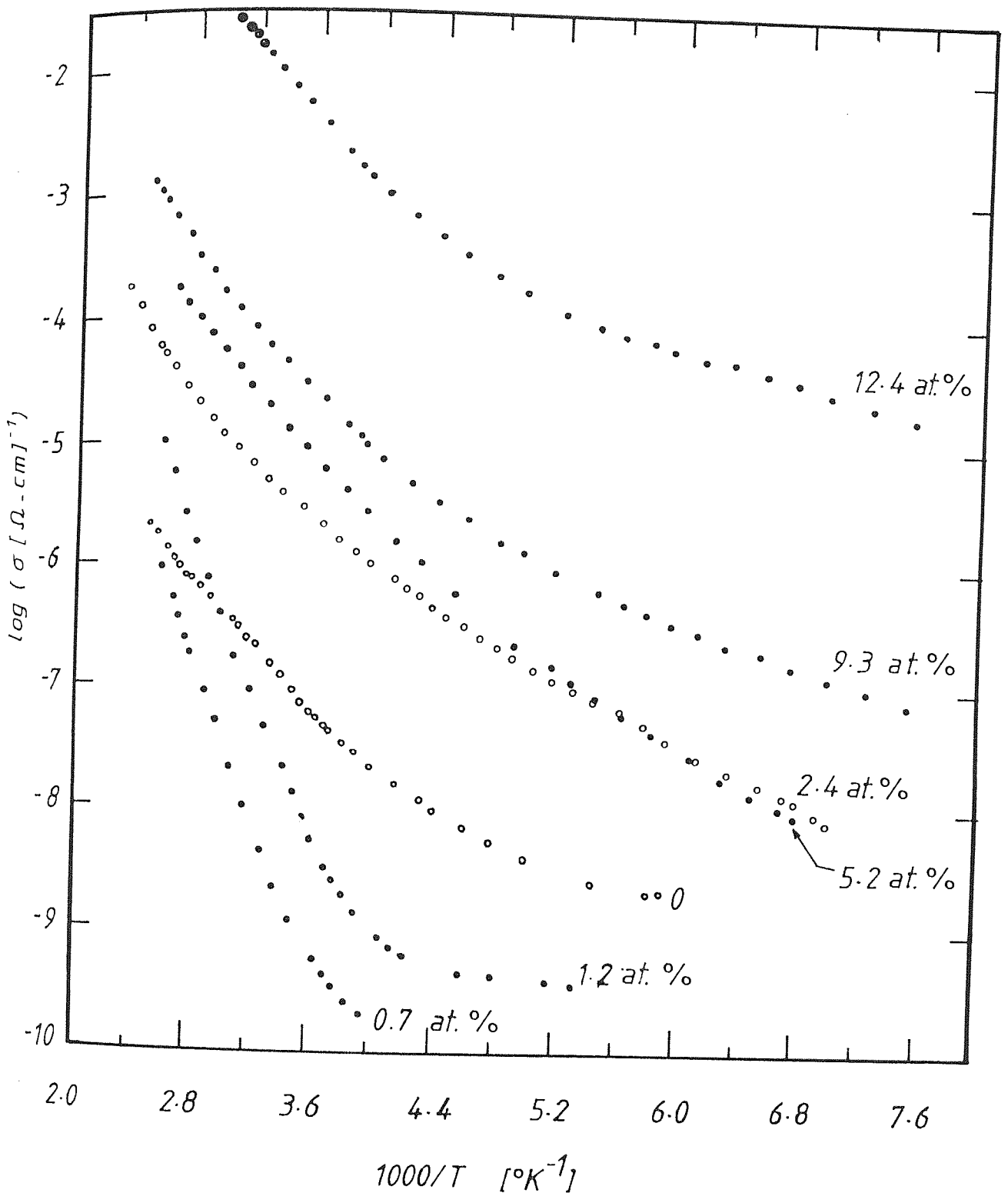

Fig. 6-12: D-C dark conductivity vs 1000/T for different Al-doping levels of a-Si (given in at.% on the figure). The films were prepared at T_s=300 °C and Pd/V_{sb}=0.33 mTorr.cm.V^{-1}.

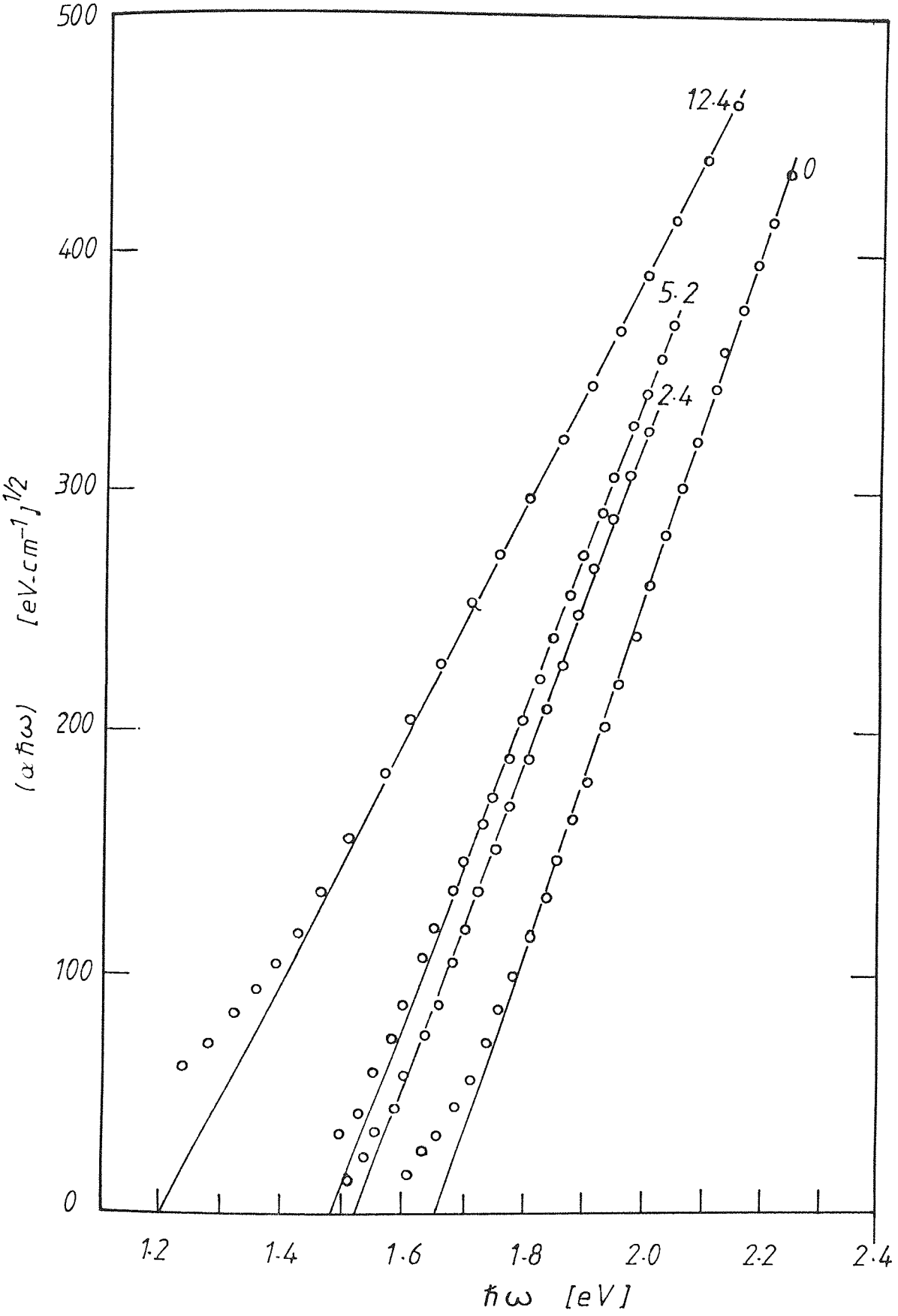

Fig. 6-13: Samples of the plots of $(\alpha\hbar\omega)^{\frac{1}{2}}$ vs $\hbar\omega$ for different Al at.% in Si as indicated. The films were prepared by co-sputtering in Ne at T_s=300 ^{o}C and Pd/V_{sb}=0.33 mTorr.cm.V^{-1}.

from Fig. 6-13, the film containing 12.4 at.% Al exhibits a considerable reduction in E_o down to about 1.2 eV. The slope of the curve marked 12.4 at.% Al is lower than for films with lower Al content. However, the optical gap of low Pd/V_{sb} films is generally lower than for higher Pd/V_{sb} films which is consistent with the dependence of E_o on Pd/V_{sb} in the case of undoped a-Si (section 5.2.2.).

For a better comparison with films prepared at higher Pd/V_{sb} values, the room-temperature conductivity, the thermal activation energy and the optical gap for films listed in Table 6-3, were plotted as functions of Al at.% and shown in Fig 6-14 . In this figure a qualitatively similar behaviour of σ_{RT} and ΔE_a with Al at.% to that in the case of high Pd/V_{sb} (0.76 $mTorr.cm.V^{-1}$)(Fig. 6-3) can be seen. The main features of Fig. 6-14 different from those of Fig. 6-3 are the following;

(i) The "dip" in the conductivity and the peak in ΔE_a occur at the Al concentration of about 1 at.% instead of less than 0.25 at.% in the case of high Pd/V_{sb} (Fig. 6-3).

(ii) Above 1 at.% Al, the addition of Al up to about 10 at.% increases the conductivity monotonically by about 5 orders of magnitude accompanied by a reduction of ΔE_a to about 0.2 eV. This is compared to about 9 orders of magnitude, accompanied by the reduction of ΔE_a down to about 0.1 eV, in the case of high Pd/V_{sb} (Fig. 6-3).

(iii) As the Al content exceeds 10 at.% (Fig. 6-12), σ_{RT} exhibits a rapid increase accompanied by a considerable decrease in the optical gap (about 0.45 eV). On the other hand

Table 6-3: Summary of various measurements for doped a-Si with a range of Al at.%. The films were prepared by co-sputtering Al with Si at low Pd/V_{sb} (0.33 mTorr.cm/V) and T_s = 300 °C. σ_{RT} room-temperature conductivity; ΔE_a thermal activation energy; E_o optical gap.

specimen No.	Al/Si At.%	σ_{RT} $(\Omega.cm)^{-1}$	ΔE_a (eV)	E_o (eV)
1	0	1.6×10^{-7}	0.58	1.65
2	0.70	3.2×10^{-9}	0.70	1.59
3	1.20	1.8×10^{-8}	0.52	1.59
4	2.40	5.0×10^{-6}	0.31	1.52
5	5.20	2.8×10^{-5}	0.31	1.48
6	9.30	6.3×10^{-5}	0.21	1.40
7	12.40	1.0×10^{-2}	0.26	1.20

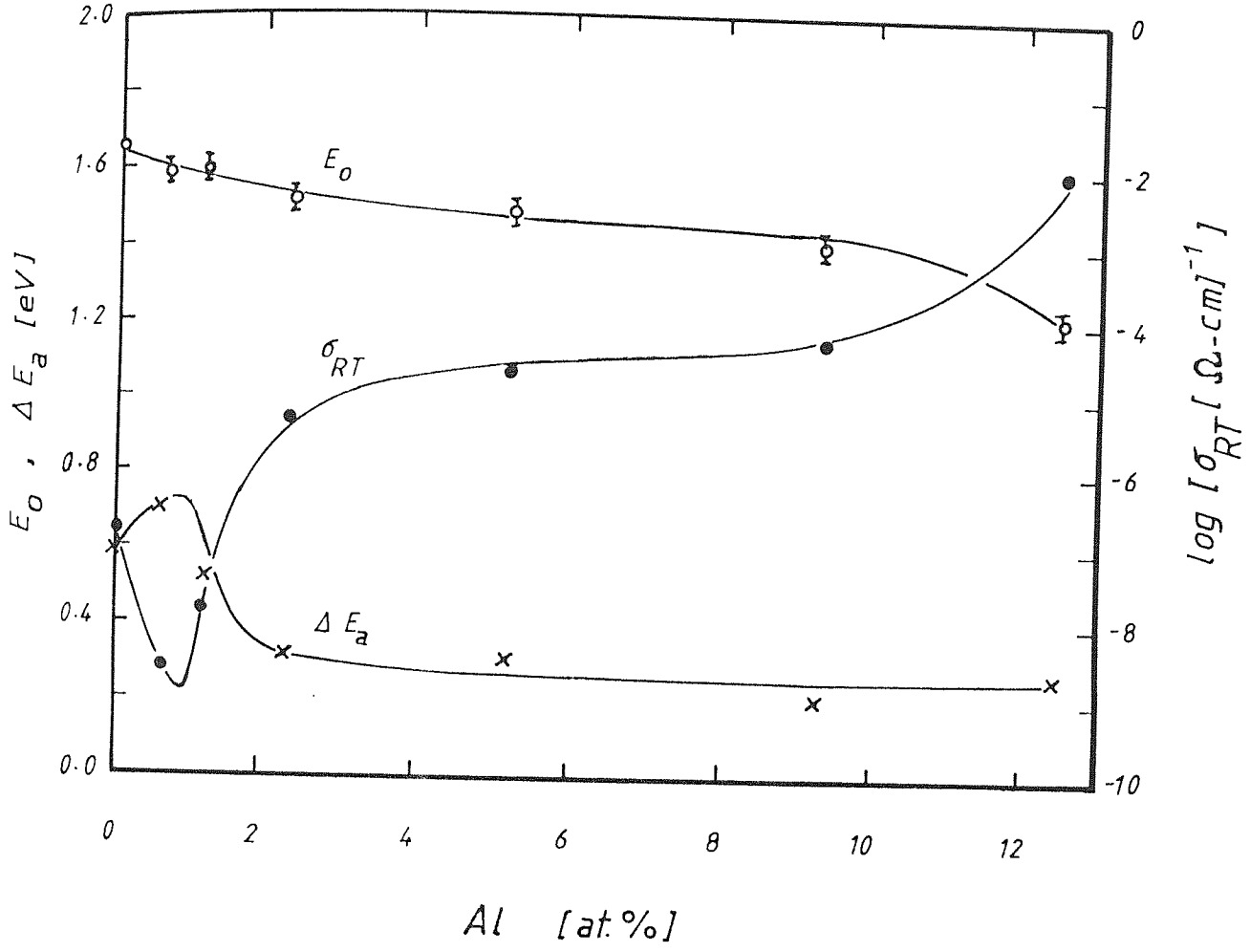

Fig. 6-14: The optical gap E_o, the thermal activation energy ΔE_a and the room-temperature conductivity σ_{RT} as functions of Al at.% in Si. The films were prepared by co-sputtering in Ne at T_s=300 °C and Pd/V_{sb}=0.33 mTorr.cm.V^{-1}.

we have seen that the optical gap changed very little in the case of high Pd/V_{sb} (Fig. 6-3). The rapid increase in the conductivity for high Al concentrations, which is accompanied by a decrease in the optical gap, could be due to a modification in the band structure of the a-Si at this range of Al content, when co-sputtered at low Pd/V_{sb} values.

It should be emphasised that Al-doped films prepared at high Pd/V_{sb} (0.76 $mTorr.cm.V^{-1}$) have conductivities about 4 orders of magnitude higher than films prepared at low Pd/V_{sb} (0.33 $mTorr.cm.V^{-1}$).

6.3.2. DEPENDENCE OF THE ELECTRICAL AND OPTICAL PROPERTIES ON T_s

The doping effects of Al and B were studied for films prepared at substrate temperatures in the range from 150 °C to 460 °C. The Pd/V_{sb} value for all the films was about 0.76 - 0.79 $mTorr.cm.V^{-1}$. The temperature dependence of dark conductivity for Al-doped films prepared at three different substrate temperatures is shown in Fig. 6-15. The Al content in the films was 5.2 at.% and found to be independent of substrate temperature. It can be seen from this figure that at low temperature (150 °C) the conductivity is low and the thermal activation energy is relatively high (0.29 eV) as indicated on the figure. As the substrate temperature increases the conductivity increases and reaches its maximum value at a moderate substrate temperature ($T_s \approx 300$ °C) where ΔE_a decreases to a minimum value of 0.13 eV. Thereafter the conductivity decreases with increasing T_s up to 460 °C. The variations

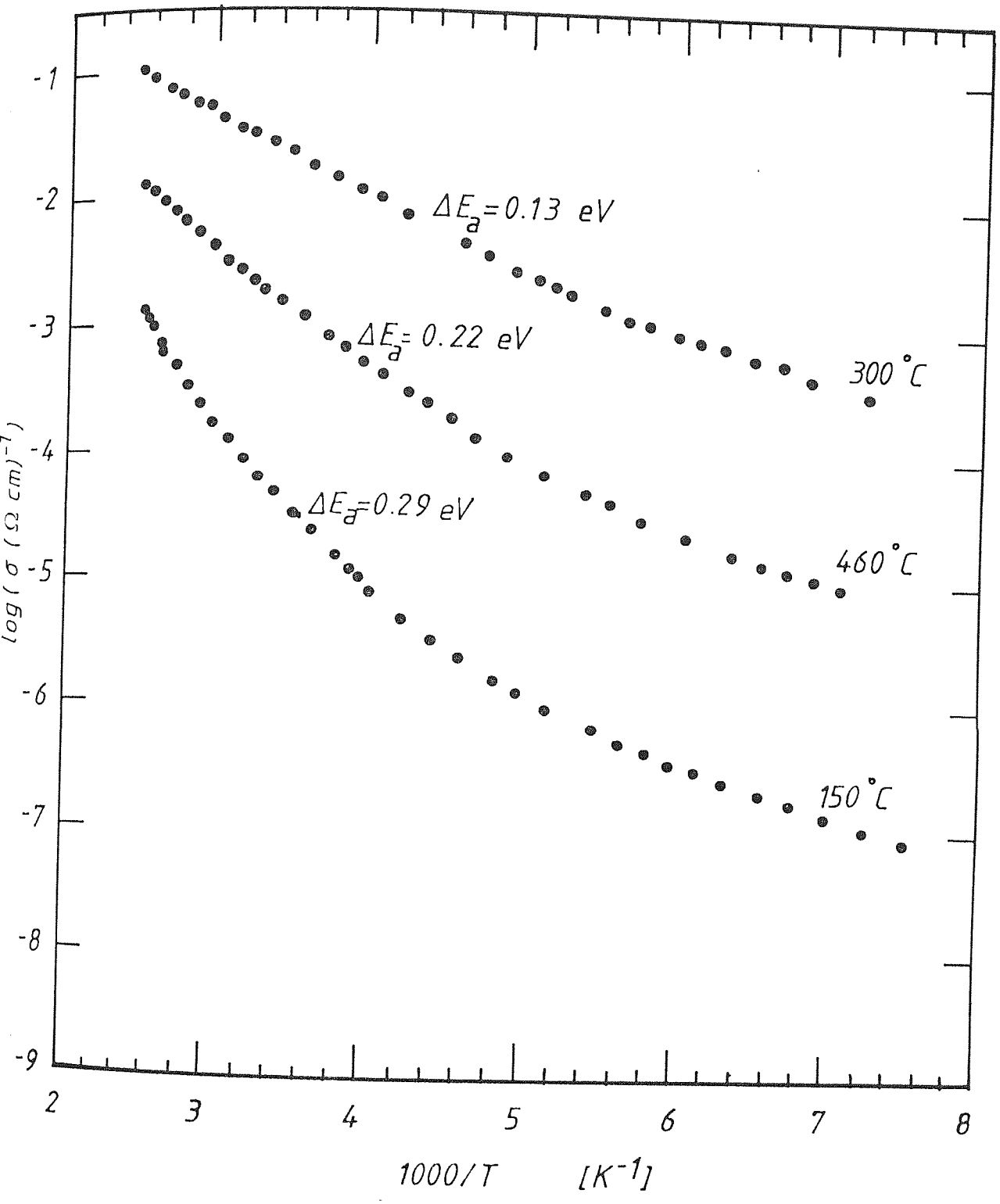

Fig. 6-15: Log σ vs 1000/T for Al-doped a-Si films, with 5.2 at.% Al. The films were pepared by co-sputtering in Ne at Pd/V_{sb}=0.76 mTorr.cm.V^{-1} and different substrate temperaturesas indicated.

in conductivity and thermal activation energy with T_s are consistent with that in the case of undoped a-Si (section 5.2.3.). The variation in the optical gap with T_s (not shown here) was found to be consistent with the variations in σ and ΔE_a, where a maximum optical gap (1.45 eV) was obtained at $T_s \approx 300\ ^{\circ}C$.

The B-doped a-Si prepared by co-sputtering B with Si or by sputtering from a B-predoped target, showed a qualitatively similar behaviour to that of Al-doped a-Si, regarding the variations in the electrical and optical properties with substrate temperature. Fig. 6-16 shows the plots of $\log_{\lambda}\sigma$ vs 1000/T for co-sputtered B/Si films at different substrate temperatures, with B content of 1.76 area% in a-Si. As in the case of Al-doped films, the B-doped films prepared at $T_s \approx 300\ ^{\circ}C$ exhibit the highest conductivity and lowest slope (ΔE_a), while below and above this temperature the conductivity of the films decreases accompanied by the increase of the thermal activation energy. Similar variations of the conductivity with T_s were observed for the films prepared by sputtering a B-predoped target, as can be seen from Fig.6-16.

In general, it can be seen that the effects of substrate temperature on the electrical and optical properties of p-type doped films are similar to the effects of the substrate temperature in the case of undoped a-Si (section 5.2.3.). These effects could be due to the control of the density of defect-states by the substrate temperature as suggested in section 5.2.3., which in turn, would affect the doping efficiency.

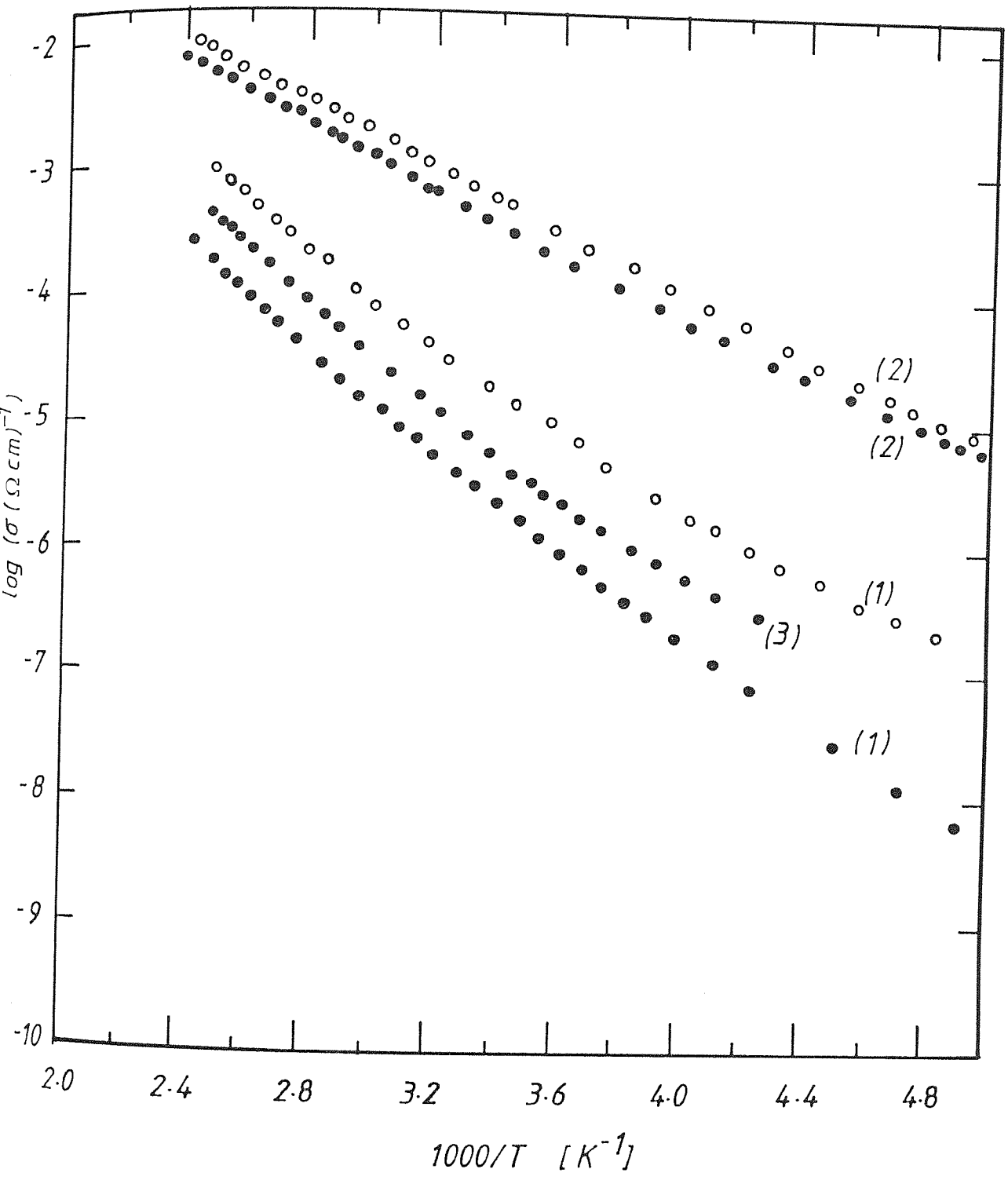

Fig. 6-16: Log σ vs 1000/T for B-doped films, prepared by sputtering from a composite target (●●●) or sputtering from a B-predoped target (ooo), at Pd/V_{sb} 0.79 mTorr.cm.V^{-1}, and different T_s ; (1) 150 °C, (2) 300 °C and (3) 460 °C.

6.4. DISCUSSION

In section 6.2. the results demonstrated a change in the room-temperature conductivity, over about 9 orders of magnitude upon doping with Al up to about 12 at.%, and over 7-8 orders of magnitude upon doping with B up to about 2.2 area%. This change is comparable with the best results reported for doping of hydrogenated a-Si from the gas phase (Spear and LeComber, 1975). In fact, the maximum conductivity reported for our Al-doped films, at about 10 at.% Al, is about one to two orders of magnitude higher than for the gas phase doping. A direct comparison with other work requires information about the number of acceptor impurities actually incorporated into the material. This requires a knowledge of the density of states around the Fermi level, $N(\epsilon_F)$, so that by the use of eq. (3-1) the acceptor concentration n_d^+ may be calculated. The conductivity at low temperatures was used for this purpose. To meet the conditions for using eq. (3-1), lightly doped films were used. Fig. 6-17 shows $\log\sigma$ vs $T^{-1/4}$ for Al- and B-doped films with 0.7 at.% Al and 0.12 area% B respectively. According to eq. (3-8), using the slope of the $\log\sigma$ vs $T^{-1/4}$ curves, $N(\epsilon_F)$ was estimated to be of the order of 10^{17}-10^{18} $cm^{-3}.eV^{-1}$, assuming a wavefunction decay length, a^{-1}, of a few atomic spacings (about 10 Å) (e.g. Shimizu et al, 1980). From x-ray photoemission spectroscopy measurements it could be considered that the B/Si atomic ratio is less than the B/Si area ratio. Therefore, the B/Si area ratio is considered as the upper limit for the atomic concentration of B in a-Si. Thus, in the light of these considerations, and the evaluation of the doping

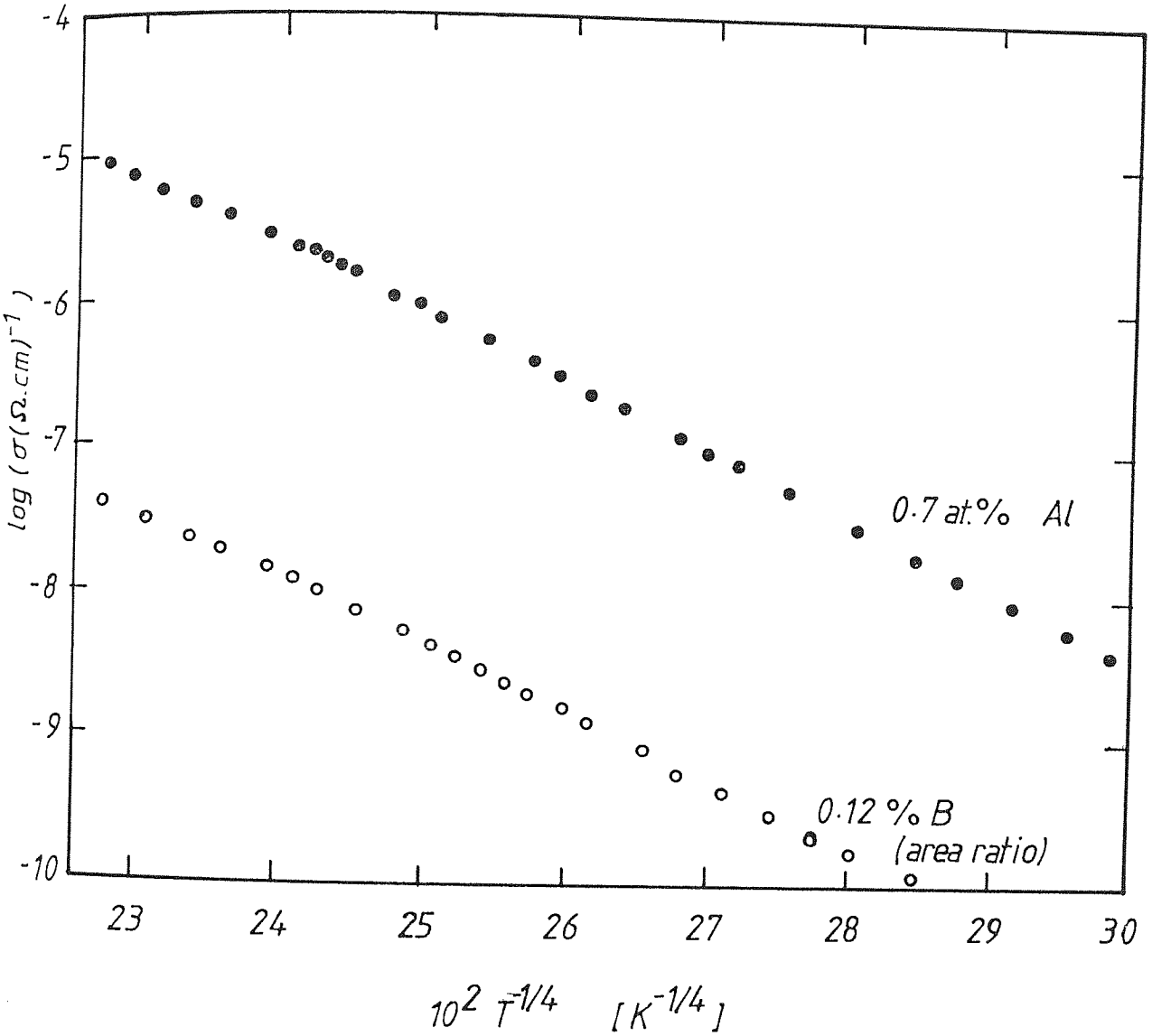

Fig. 6-17: Samples of the plots of $\log \sigma$ vs $T^{-1/4}$ for Al-doped films with 0.7 at.% Al in Si (●●●) and B-doped films with 0.12% B/Si area ratio (ooo). The Al-doped films were pepared by co-sputtering at T_s=300 ^{o}C and Pd/V_{sb}=0.76 mTorr.cm.V^{-1} while B-doped films at T_s=300 ^{o}C and Pd/V_{sb}=0.79 mTorr.cm.V^{-1}.

efficiency, f, from eq. (3-2), it has been estimated that about 1 in 800 Al atoms acts as acceptor centre which is less than that for Al doping by ion implantation (Müller et al, 1977). On the other hand, it was found that about 1 in 150 B atoms contributes to doping, in the case of sputtering from a composite target. This is slightly higher than the doping efficiency of 1/200 for B ion-implantation (Müller et al, 1977). However, sputtering from a predoped target (about 1 at.% B) showed that the doping efficiency of this method (about 1/75) is higher than that for doping by sputtering from a composite target. This could be due to the uniform distribution of B atoms among Si atoms in the case of predoped target.

At low doping levels, both the room-temperature conductivity σ_{RT} and the thermal activation energy ΔE_a changes rapidly upon increasing the dopant concentration (see Figs. 6-3 and 6-7). This is attributed to the fact that in this range of doping, the Fermi level moves towards the bottom of the density-of-states distribution (Fig. 3-3). On the other hand, at high Al concentration the slow increase in σ_{RT} together with slow decrease in ΔE_a are consistent with the shift of ϵ_F to the high density-of-states near the tail states region.

The photoconductivity measurements made by several investigators (e.g. Zanzucchi et al, 1977; Tsai and Fritzsche, 1979; Anderson et al, 1980) have demonstrated that undesirable states are introduced into the mobility gap of a-Si:H when the material is doped with phosphorous or boron, and these states increase as

the amount of doping material increases. Furthermore, it has been suggested that these states are generally associated with defects in the a-Si network (Anderson et al, 1980). Such states would lower the doping efficiency especially at higher doping levels. In addition, these states would affect the optical absorption transitions and hence would slightly lower the measured optical gap as demonstrated by the highly doped specimens (Figs. 6-3 and 6-7).

Fig. 6-18 shows the σ_{RT} vs the atomic concentration for different dopants incorporated by different techniques. In addition, Fig. 6-19 shows the thermal activation energy, ΔE_a, as a function of the atomic concentration of the same dopants as in Fig. 6-18. The atomic concentration of the dopant elements in our films was determined by the methods described in section 4.7.. From Fig. 6-18 we see that σ_{RT} of our Al-doped films is two orders of magnitude higher than the maximum conductivity obtained by boron doping from the gas phase . Furthermore, Fig. 6-19 shows that ΔE_a of Al-doped a-Si prepared by co-sputtering in Ne is lower than that reported for boron-doped a-Si:H (LeComber et al, 1980). This suggests that at high doping levels, less defect-states are created in the co-sputtering case using Ne gas when compared with the case of boron doping from the gas phase. Also Figs. 6-18 and 6-19 show that ion-implantation doping of Al is less efficient than that of B, while the Al doping by co-sputtering is more efficient than that of Al doping by ion implantation. Taking into account that large clusters of Al atoms (or molecules) are expected to be

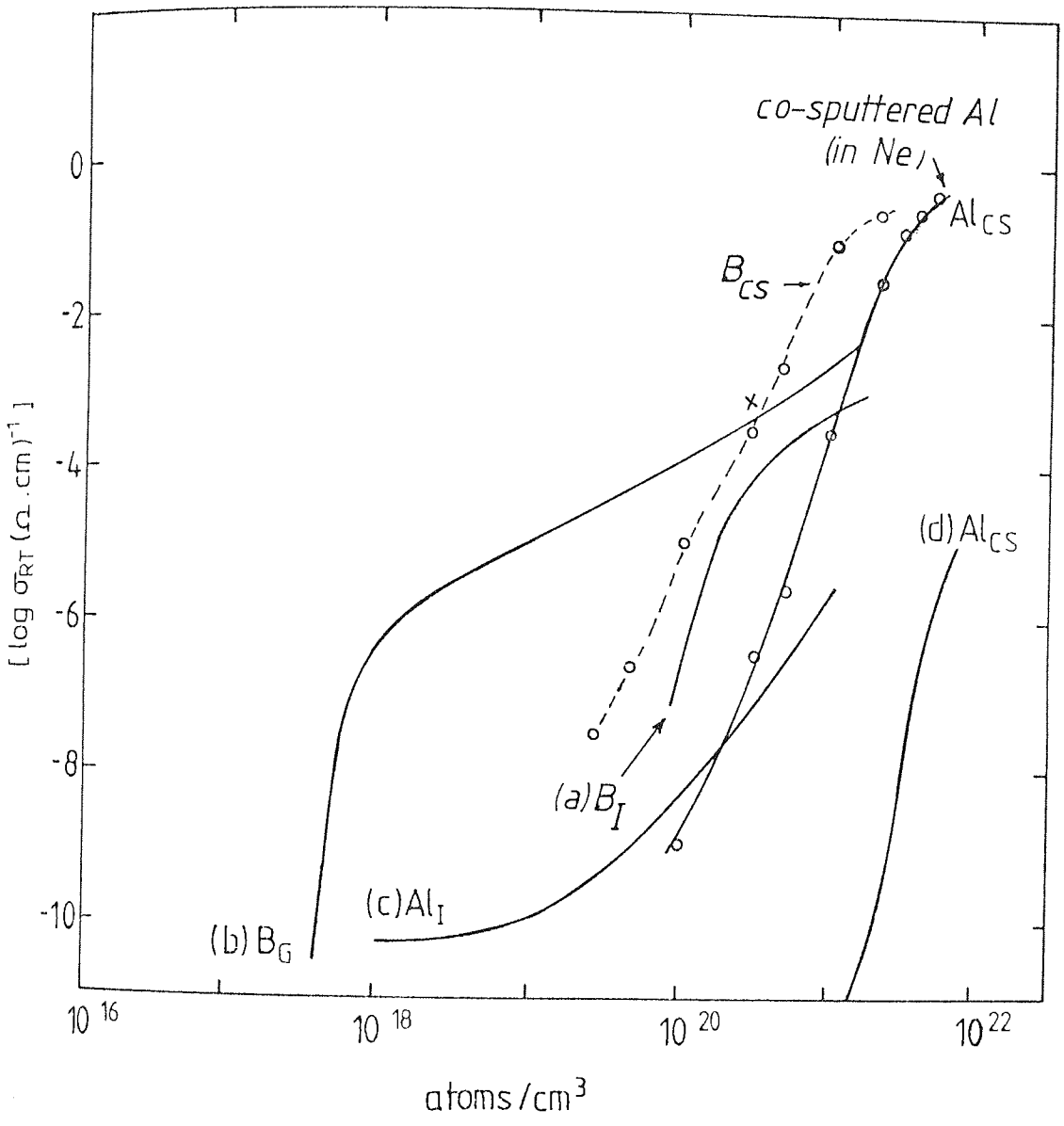

Fig. 6-18: Room-temperature conductivity as a function of Al concentration for co-sputtering in Ne compared with doping by (a) ion implantation of boron B_I, (b) gas phase doping of boron B_G, (c) ion implantation of Al in glow-discharge a-Si:H, Al_I (LeComber et al, 1980) and (d) co-sputtering Al in Ar/H_2 mixture , Al_{cs} (Thompson and Reinhard, 1980). The curve B_{cs} repesents B-doping by co-sputtering in Ne. The point (x) represents B-doping by sputtering from a predoped target.

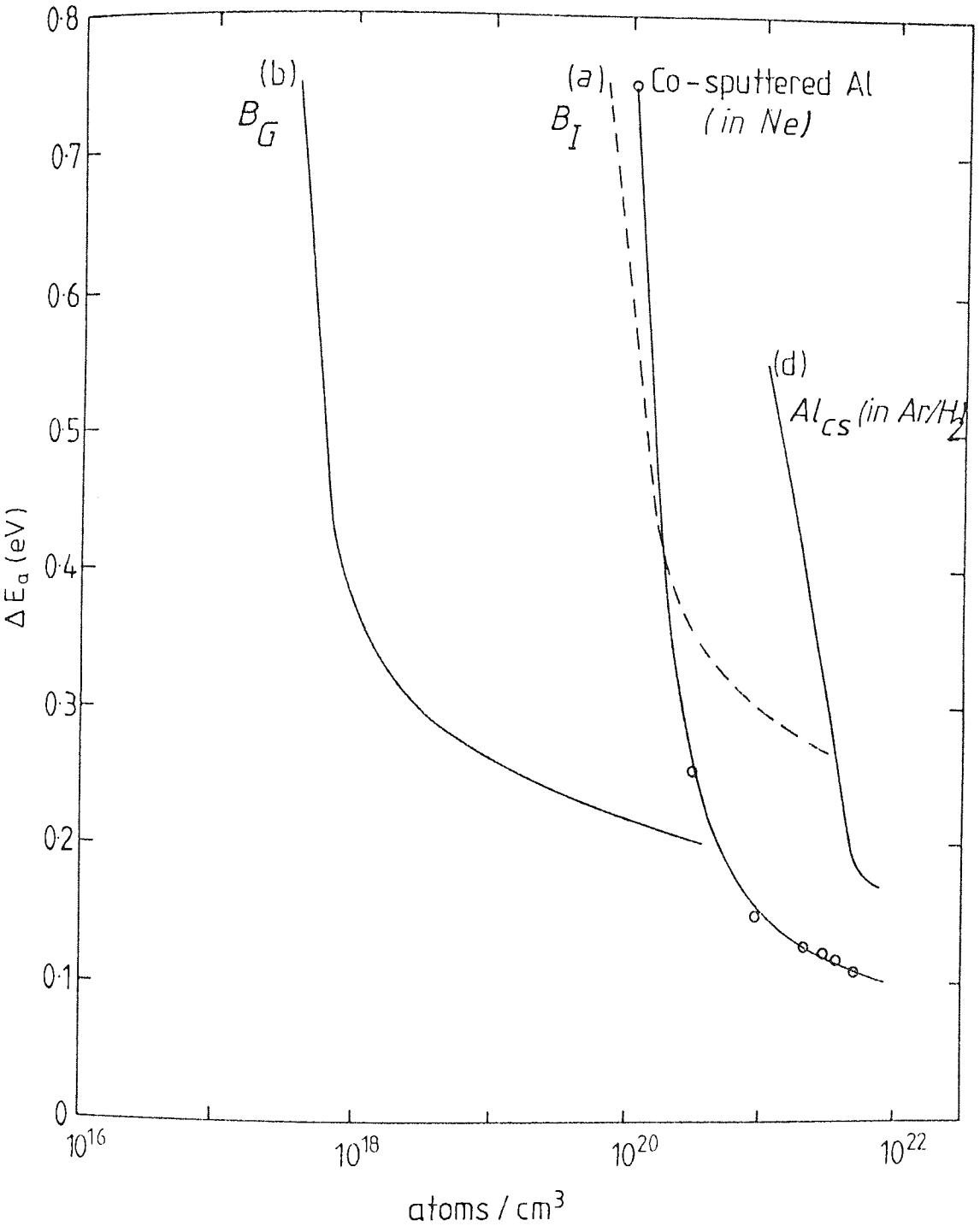

Fig. 6-19: Thermal activation energy ΔE_a as a function of co-sputtered Al atomic concentration compared with doping by other techniques. The notations are the same as in Fig. 6-18.

sputtered (Wehner and Anderson, 1970), which would not contribute to doping, we would then expect the B co-sputtering to be more efficient than the ion implantation of B. The efficiency of such boron doping would then be a closer approach to the gas-phase doping efficiency. In Figs. 6-18 and 6-19, respectively σ_{RT} and ΔE_a of the boron doping by co-sputtering B with Si are shown. It can be seen that the efficiency of boron doping by co-sputtering in Ne is slightly higher than that of boron doping by ion implantation. Also, it can be seen that the efficiency of boron doping by co-sputtering in Ne is more comparable with that of boron doping from the gas phase, than is Al doping by co-sputtering in Ne.

It can be seen clearly from Figs. 6-18 and 6-19 that our Al-doping efficiency is higher than that for co-sputtering Al with Si in Ar/H_2 gas mixture (Thompson and Reinhard, 1980). This could be attributed to lower defect-density in the mobility gap in the case of co-sputtering in Ne.

It is worth mentioning that B doping by co-sputtering in Ne, might give higher efficiencies than those reported here, if a pure clean B could be obtained. The fact that B pellets made of powder were used for doping, makes the presence of oxygen, in the resulted films, inevitable and hence reduces the conductivity. The oxygen content in the B-doped films (by co-sputtering) was estimated from the XPS spectra to be about 2 at.%. However, sputtering from B-predoped target, which is assumed to be free from contamination,

showed that a better doping efficiency can be obtained, as inicated by the point (x) in Fig. 6-18.

Although only results for two films with different Ga content are presented here, the possibility of substitutional p-type doping with Ga using the present technique is demonstrated by the changes in conductivity and thermal activation energy with Ga content. It is estimated that the Ga has a doping efficiency almost equal to that of Al.

The small change in the optical gap demonstrated by the addition of group-III elements, together with the control of conductivity over a wide range, in conjunction with the shift in the Fermi level over about 0.7 eV, suggest that the basic band structure of the a-Si network has not been changed with the addition of group-III elements, provided that sputtering takes place at relatively high Pd/V_{sb} as shown earlier. The photoemission spectra show that the relative intensity and the shape of the plasmon peaks do not change when the dopant material is added (see Fig. 6-20), which supports the view that the band structure of a-Si has been retained. The above discussion leads to the conclusion that it is unlikely that the observed phenomena result from a modification of thea-Si band structure as suggested by other authors (Ovshinsky, 1977; Thompson and Reinhard,1980; Xu et al.1984) but rather the results indicate that substitutional p-type doping has taken place by Al/Si , B/Si or Ga/Si co-sputtering or sputtering from a predoped target, in Ne gas, under the conditions of relatively high

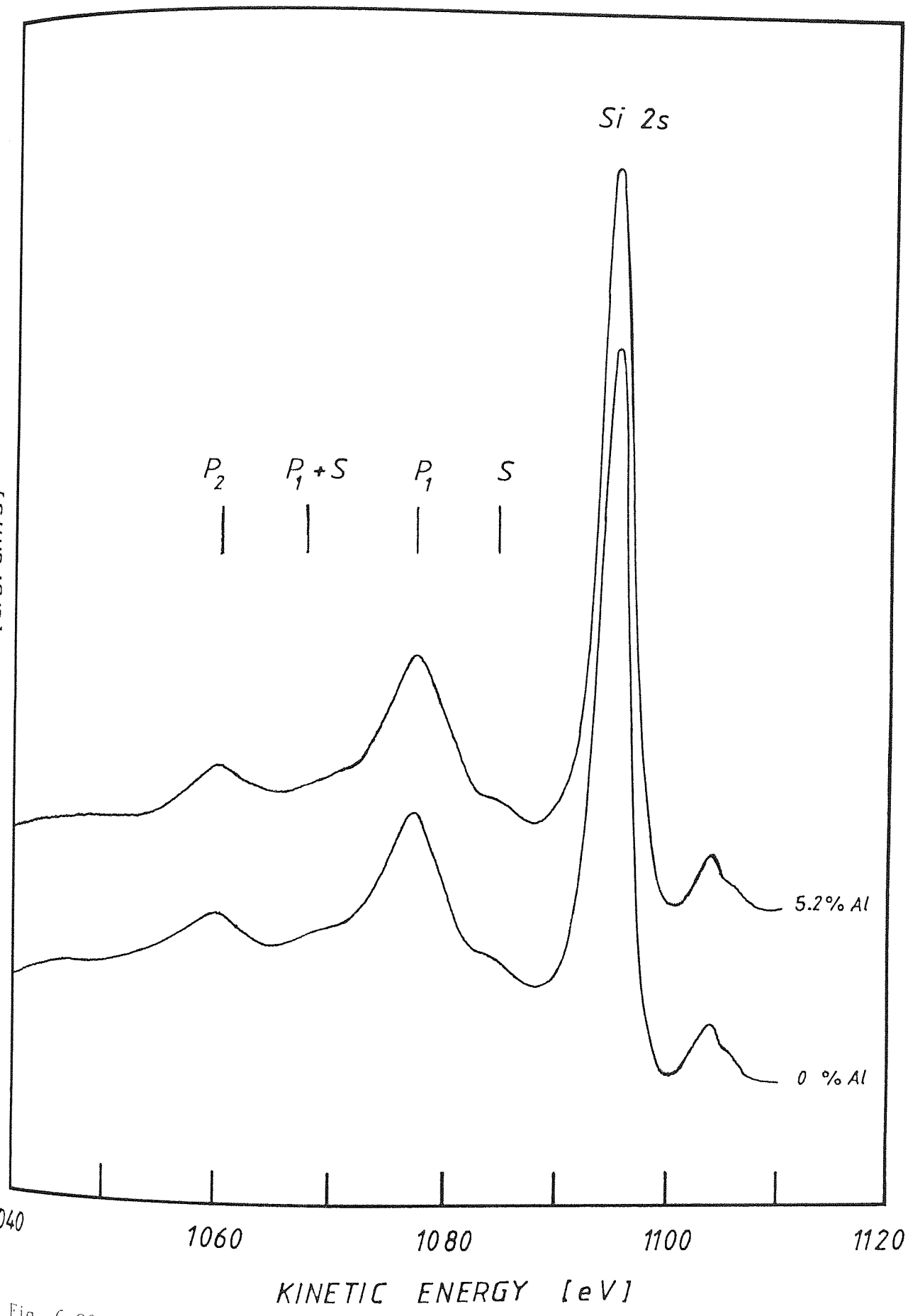

Fig. 6-20: The photoemission spectra of Si(2s) photopeak showing the bulk plasmons (P) and surface plasmons (S), for undoped a-Si and doped a-Si with 5.2 at.% Al.

Pd/V_{sb} values and T_s=300 °C. This conclusion is consistent with that drawn earlier (chapter 5) that a-Si with low defect-states-density can be produced by sputtering in Ne gas at relatively high Pd/V_{sb} and T_s=300 °C. Further evidence for the low defect-density can be drawn from the plots of $\log\sigma$ vs 1000/T (Figs. 6-1, 6-5 and 6-8), where the conduction in the extended states dominates at temperatures well below room temperature, even for high doping concentrations.

It has been established that the optical and electrical properties of amorphous semiconductors are primarily controlled by the density-of-states distribution in the mobility gap . This density-of-states in turn controls the doping efficiency. It has been demonstrated, in chapter 5, that the electrical and optical properties of the undoped a-Si varied over a wide range by varying the preparation conditions. The results given in section 6.3. show that the electrical and optical properties of p-type doped a-Si are controlled to some extent by the preparation conditions such as Pd/V_{sb}. The higher conductivity of Al- or B-doped a-Si, prepared at relatively high Pd/V_{sb} is consistent with the low conductivity and the high photoconductivity of undoped a-Si prepared in the same range of Pd/V_{sb}. It is believed that deposition at low Pd/V_{sb} may produce a base material which possesses a high density-of-defect-states in the gap as indicated by the low photoresponse and high conuctivity. Therefore the low doping efficiency at low Pd/V_{sb} (see Fig. 6-14) is not surprising. The occurrence of the hopping conduction at temperatures around or near

room temperature is another indication that the density-of-states is higher for films prepared by low Pd/V_{sb}.

However, by comparing our results with other work, it can clearly be seen that even at relatively low Pd/V_{sb} (0.33 mTorr.cm.V^{-1}), the doping efficiency of the present technique using composite targets is better than that of other techniques. Fig. 6-21 compares the room-temperature conductivity vs Al at.% for Al-doped films prepared by co-sputtering in Ne gas at (1) high (0.76 mTorr.cm.V^{-1}) and (2) low Pd/V_{sb} (0.33 mTorr.cm.V^{-1}), and by co-sputtering (3) in Ar/H_2 plasma (Thompson and Reinhard, 1980) and (4) in Ar (Suzuki et al, 1980). It can be seen from this figure that the conductivity is controlled over about 9 orders of magnitude in the case of co-sputtering in Ne at high Pd/V_{sb} (curve 1), compared to 5 orders of magnitude in the case of low Pd/V_{sb} (curve 2), 5 orders of magnitude in the case of Ar/H_2 sputtering (curve 3) and 3 orders of magnitude for sputtering in Ar (curve 4). The occurrence of the "dip" in the case of low Pd/V_{sb} (curve 2), at higher Al concentration than that in the case of high Pd/V_{sb} (curve 1), is attributed to a higher density of states in the material of curve 2. Accordingly, the "dips" in the curves of Fig. 6-21 suggest that a-Si prepared by Ne sputtering in high Pd/V_{sb} possesses a lower density-of-states than that prepared by sputtering in Ar or Ar/H_2 plasma. This is consistent with the conclusion made in chapter 5, in the light of optical, electrical and photoconductive properties of undoped a-Si.

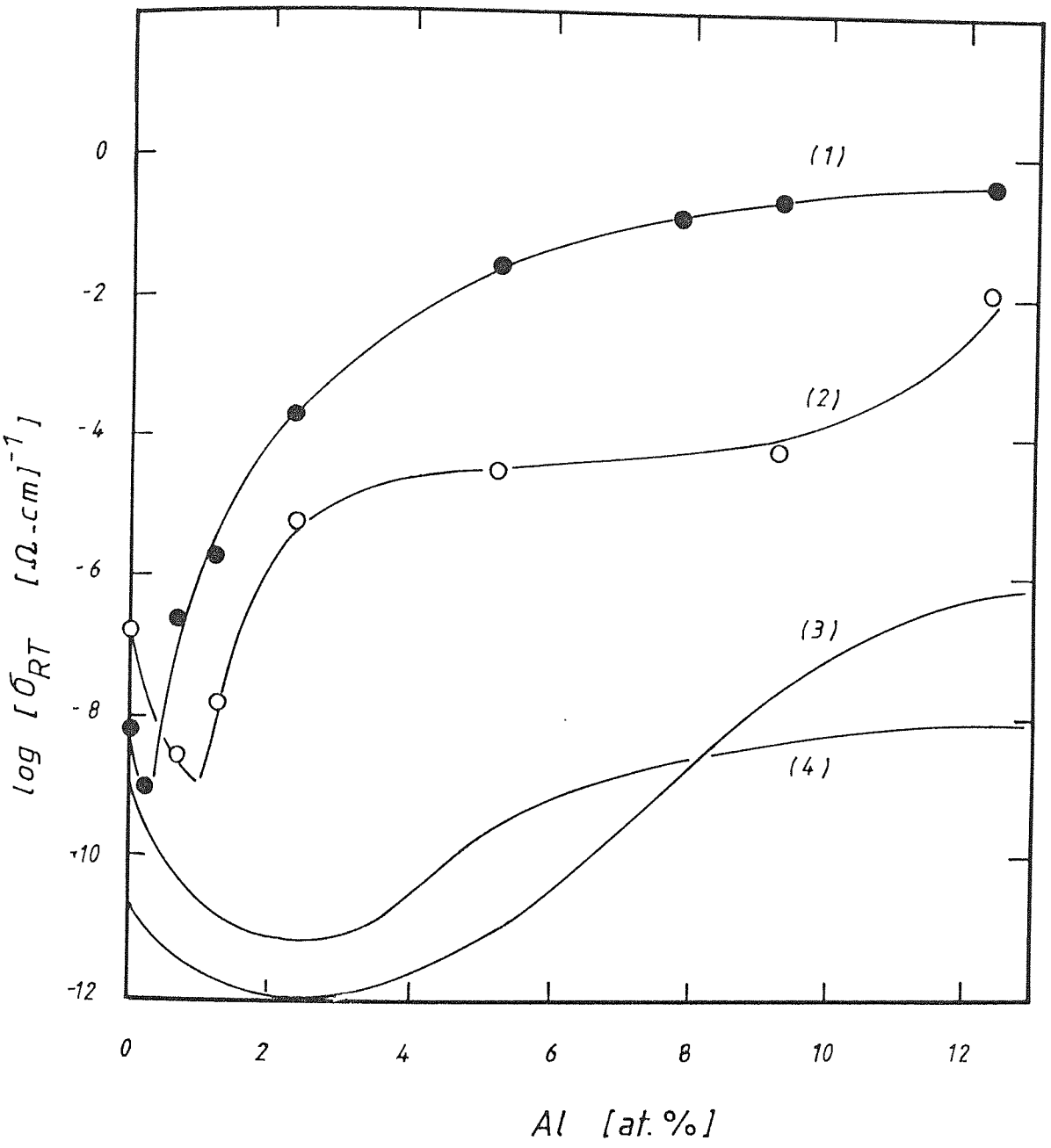

Fig. 6-21: Log σ vs Al at.% for a-Si doped by co-sputtering Al with Si (1) in Ne at Pd/V_{sb}=0.76 mTorr.cm.V^{-1}, (2) in Ne at Pd/V_{sb}= 0.33 mTorr.cm.V^{-1}, (3) in Ar/H_2 plasma (Thompson and Reinhard, 1980) and (4) in Ar (Suzuki et al, 1980).

In addition, comparing the B-doping by sputtering in Ne gas at high Pd/V_{sb}, with that prepared by sputtering in Ar gas (Suzuki et al, 1980), we can see that in the former the doping efficiency is higher than that for the latter case (see Fig. 6-7).

The effect of substrate temperature on doping efficiency, which has been considered in section 6.3.2., for group-III elements, seems to be mainly due to the influence of substrate temperature on the properties of the silicon itself rather than due to activation of the dopants. This conclusion is supported by the fact that the optimum properties for doped films prepared at $T_s \approx 300$ °C, are consistent with those for undoped a-Si (section 5.2.3.).

However, it is obvious that the doping efficiency in the case of co-sputtering in Ne gas is still slightly lower than that of gas phase doping in a glow discharge. Perhaps further optimisation of other parameters, not examined here, should be considered. Since the electronic and optical properties of undoped a-Si, prepared by the present technique, are comparable with those of GD and Ar/H_2 sputtered a-Si, it is most likely that the problem lies in the method of incorporating the dopant into the a-Si.

The p-n homo- and heterojunctions and MS junctions made of a-Si (Fig. 6-22a), a-Si on c-Si (Fig. 6-4) and Metal on a-Si (Fig. 6-22b) respectively, showed marked rectification properties, which imply potential semiconductor applications

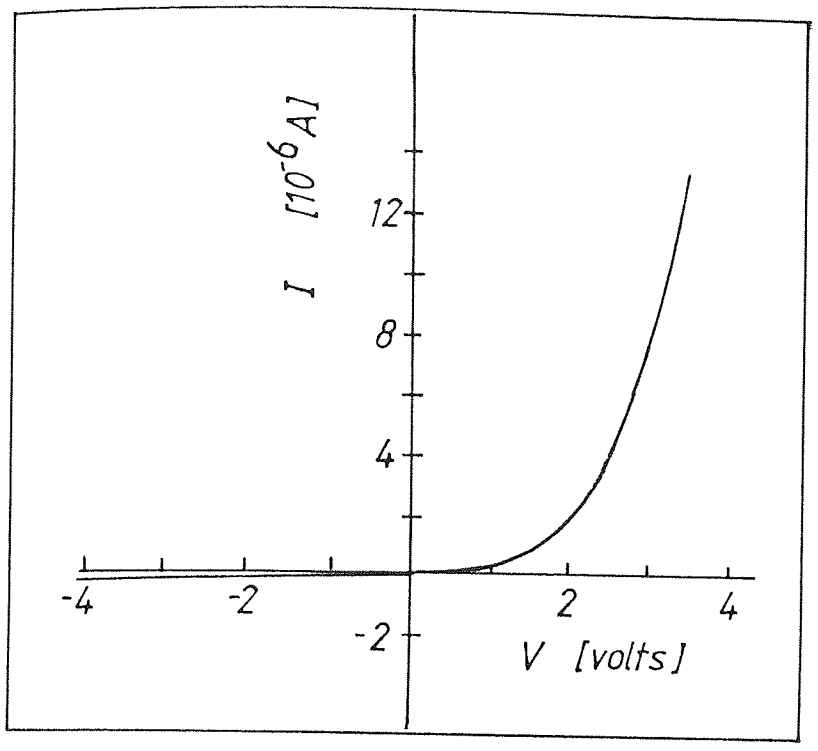

(a)

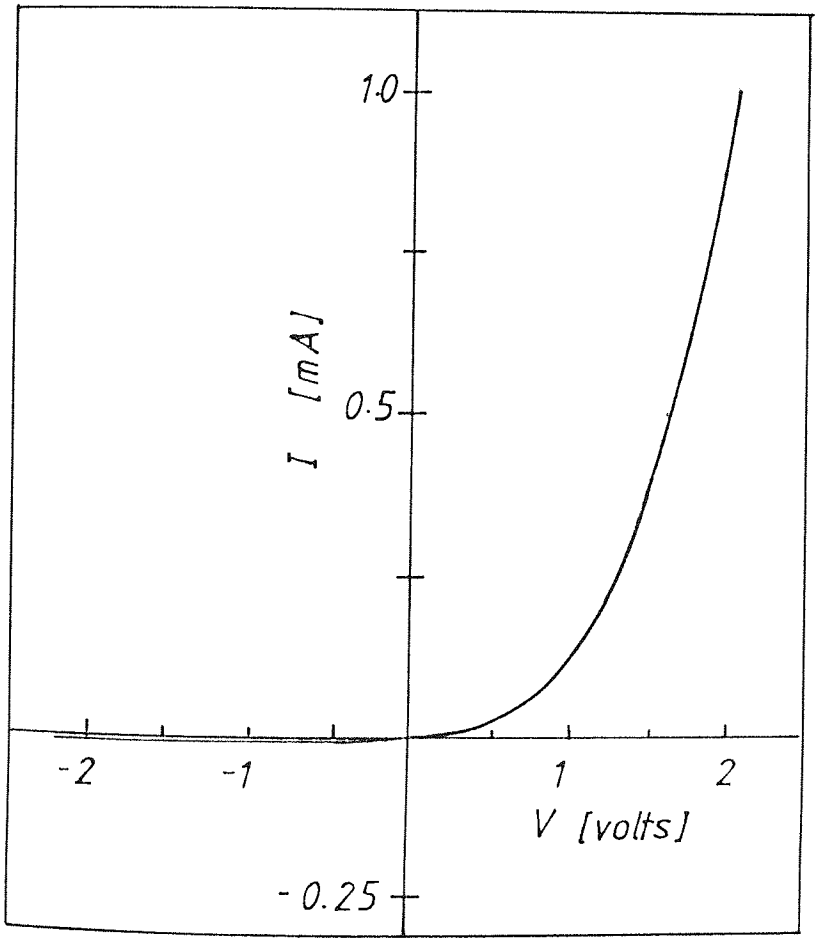

(b)

Fig. 6-22: (a) I-V characteristic curve of a typical p-amorphous/n-amorphous a-Si junction. The p-type layer is Al-doped a-Si while the n-type layer is Ta-doped a-Si, both prepared by co-sputtering in Ne.

(b) I-V characteristic curve of a MS junction made of Au on undoped a-Si prepared by sputtering in Ne.

of this material. However, detailed investigation of these and other possible applications is needed.

Finally, it should be emphasised that the consistency of the results of substitutional doping discussed in this chapter confirms that the production of low density-of-states a-Si by Ne-sputtering without the introduction of hydrogen or a halogen is feasible.

CHAPTER SEVEN

ANNEALING EFFECTS ON DOPING EFFICIENCY

7.1. INTRODUCTION

In this chapter the effects of annealing co-sputtered films on the doping efficiency are studied. The dark conductivity and the position of the Fermi level are investigated. The chapter is mainly devoted to studying doped films, although a few undoped a-Si films are considered to check whether the effects are due to annealing of the basic material or activation of the dopant.

The films described in this chapter, unless otherwise specified, were prepared at Pd/V_{sb}=0.70-0.80 mTorr.cm.V^{-1} and T_s=300 ^{o}C. These conditions are within the optimum range of the conditions as described in section 5.2.2.. The films were annealed in an electric furnace at the appropriate temperatures in a nitrogen atmosphere. The method is described in more detail in section 4.8..

7.2. RESULTS

7.2.1. ANNEALING TIME

The room-temperature conductivity, σ_{RT}, of doped a-Si films was measured as a function of annealing time. It has been found that σ_{RT} of the doped films increased rapidly as the annealing time was increased up to about 90 minutes, when

they were annealed at 470 °C. Further annealing caused a slow increase in conductivity. However, although the general trend of conductivity variation with time, for all the dopants investigated, was similar, it seems from the results that the rate of change of the conductivity is different from one dopant to another. This may be due to different diffusion coefficients. Fig. 7-1 shows σ_{RT} as a function of time for Al-doped films, with Al concentration of about 0.25 at.% . The time, t_a=0, represents the as-deposited films. The annealing temperature, T_a, was about 470 °C, well above the preparation temperature (about 300 °C). It can be seen from the figure that σ_{RT} increased from about 10^{-9} to about $10^{-5}\Omega^{-1}cm^{-1}$ upon annealing for 90 minutes. Any further annealing seems not to have any significant effect on the conductivity . Therefore the rest of the results, presented in this chapter, represent annealing for about 90 minutes. Annealing time had a small effect on the conductivity of the undoped a-Si, prepared under the above conditions. Annealing of undoped a-Si at 470 °C for 90 minutes only produced a four-fold reduction in the room-temperature conductivity.

7.2.2. ANNEALING TEMPERATURE

The effect of annealing temperature, T_a, on the conductivity was studied for Al-doped samples (with 0.25 at.% Al), in the range of T_a from 250 °C to 470 °C. The films were annealed for about 90 minutes. Fig. 7-2 shows σ_{RT} as a function of the annealing temperature for both undoped and Al-doped a-Si films. It is seen from the figure that the conductivity

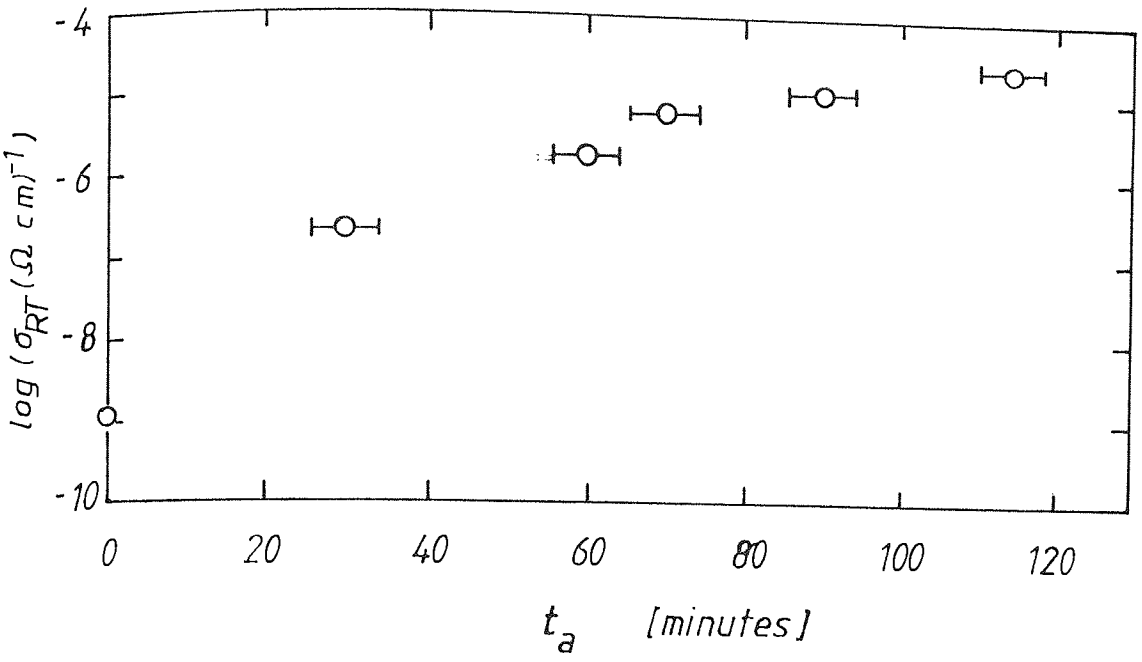

Fig. 7-1: The room-temperature conductivity σ_{RT} as a function of annealing time, t_a, for doped a-Si with 0.25 at.% Al. The films were annealed at 470 °C.

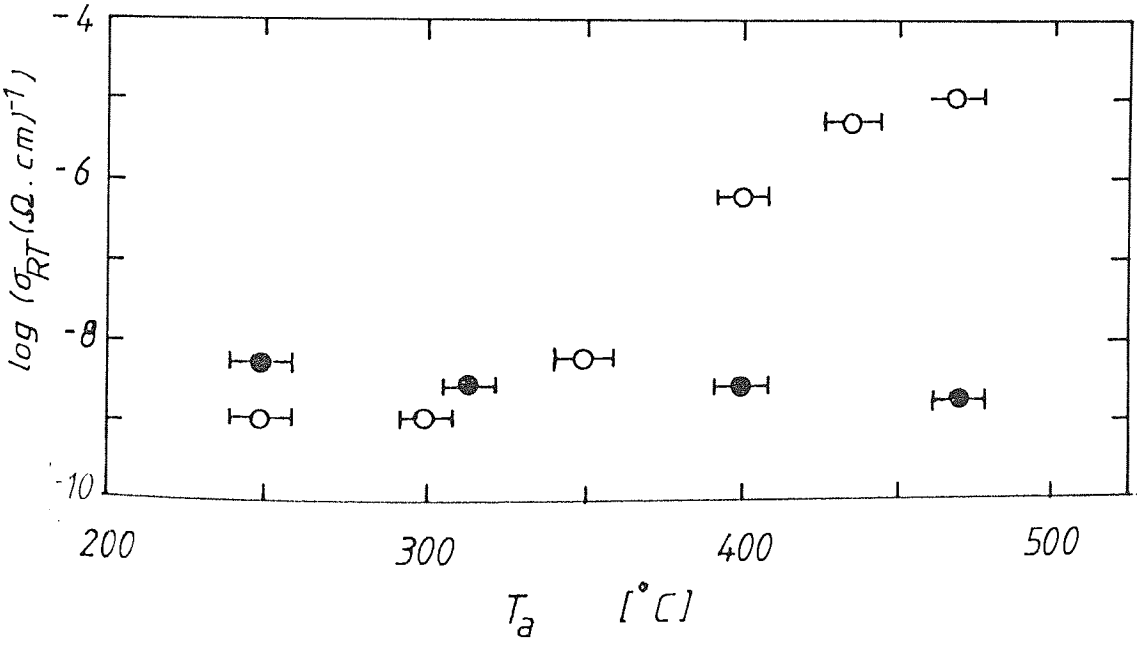

Fig. 7-2: The room-temperature conductivity as a function of annealing temperature T_a for undoped a-Si (●) and doped a-Si with 0.25 at.% Al (o). The films were annealed for about 90 minutes.

remains the same as in the case of the as-deposited films, for temperatures up to about 300 °C. As T_a increases, σ_{RT} of the doped films increases monotonically by 4 orders of magnitude, for T_a increasing up to 470 °C. However, the degree of dependence of σ_{RT} on T_a is reduced as T_a approaches 470 °C. In addition, the optical gap did not vary with T_a within the above range. The increase in σ_{RT} is accompanied by a decrease in thermal activation energy of the dark conductivity, ΔE_a, which inicates the movement of the Fermi level in the mobility gap.

7.2.3. ANNEALING EFFECTS ON VARIOUS DOPANTS

The results presented in this section represent annealing of doped a-Si films at 470 °C for about 90 minutes. Fig. 7-3 shows the plots of $\log\sigma$ vs 1000/T for a few Al-doped a-Si films with Al concentrations up to 5.2 at.%. The open circles represent the as-deposited films while the closed circles are for the annealed films. It can be seen from this figure that for films with low Al-concentration, the conductivity increases by a few orders of magnitude, accompanied by a decreasing slope (thermal activation energy), with annealing. As the Al concentration increases, the increase in conductivity is reduced. This can be seen more clearly in Fig. 7-4, where at 0.25 at.% Al, σ_{RT} increases by about 4 orders of magnitude. On the other hand, at 5.2 at.% Al, σ_{RT} increases only by a factor of 4. In general, as shown in Fig. 7-4, the thermal activation energy, ΔE_a, decreases upon annealing. It is interesting to notice that the conductivity of the undoped

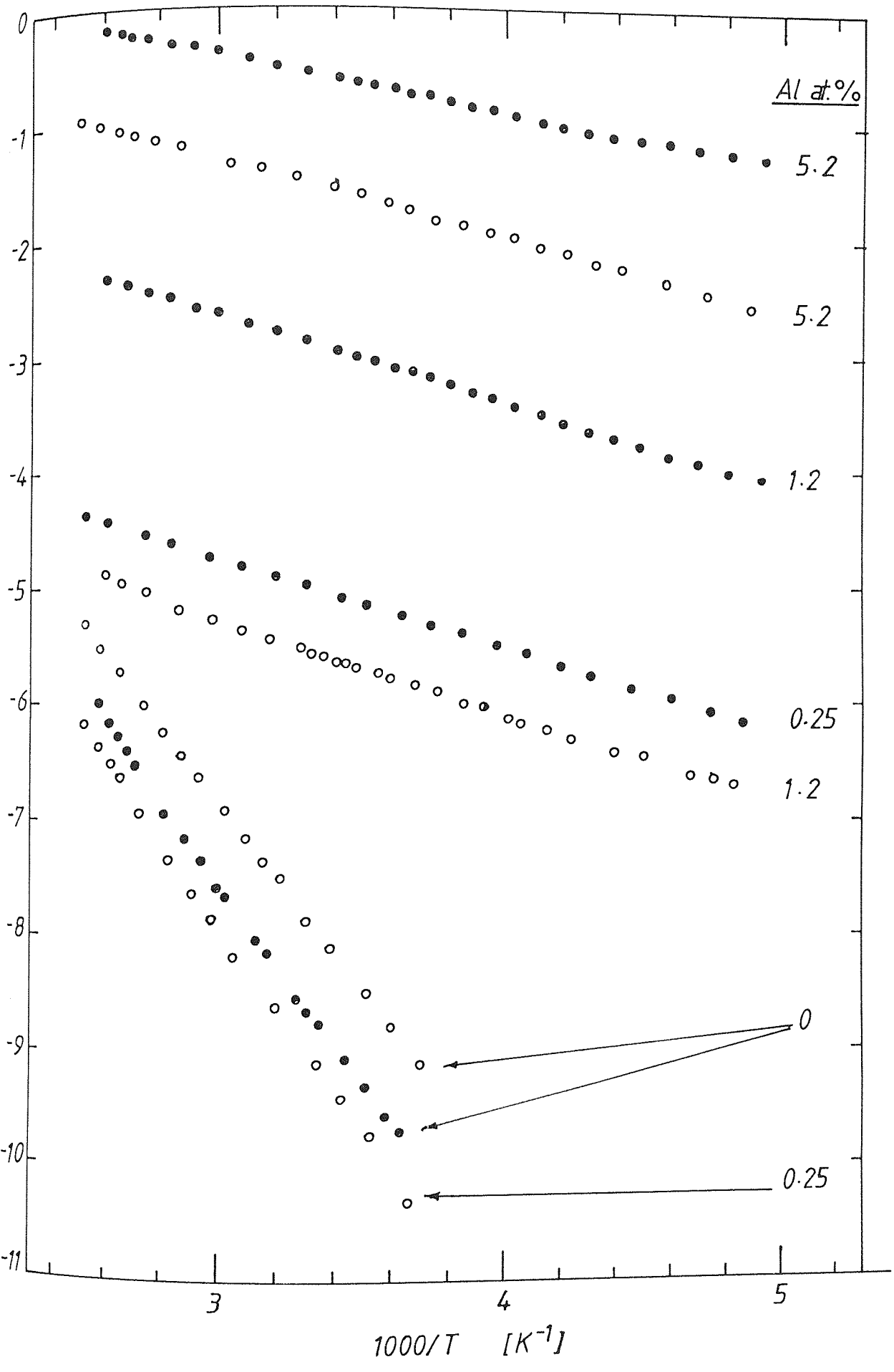

Fig. 7-3: Log σ vs 1000/T for Al-doped films with different atomic contents of Al. The curves marked (ooo) are for as-deposited films while those marked (●●●) are for annealed films at 470 °C for 90 minutes.

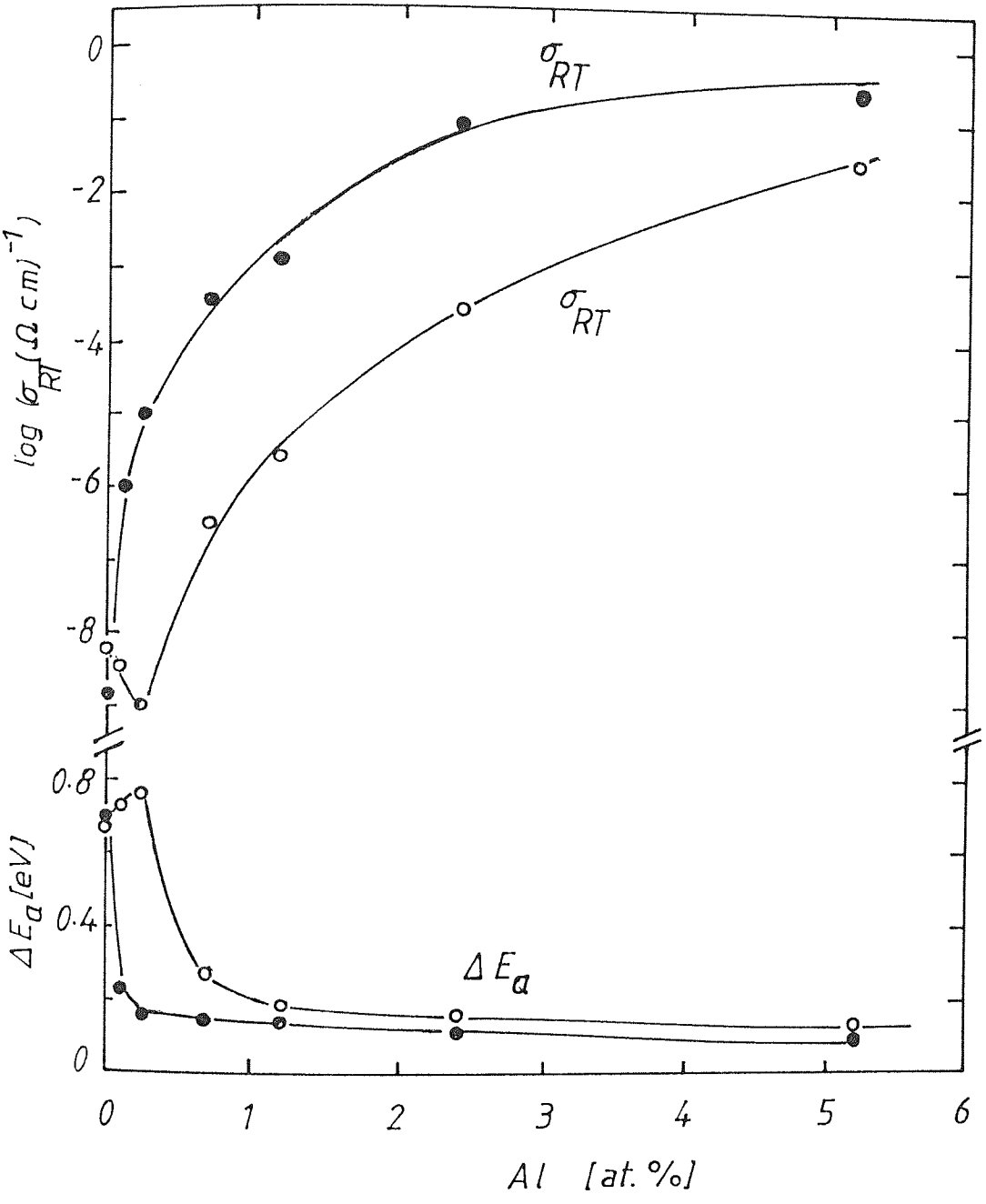

Fig. 7-4: Log σ_{RT} and ΔE_a as a function of Al at.% for as-deposited films (ooo) and annealed films at 470 °C for 90 minutes (●●●).

film (Fig. 7-3) does not suffer a significant change with annealing . The decrease by only a factor of 4 in the conductivity of the undoped film indicates that the structure of the basic material does not change considerably upon annealing. However, this observation is only for films prepared under the conditions mentioned earlier. Annealing undoped a-Si films, prepared at Pd/V_{sb}=0.76 mTorr.cm.V^{-1}, showed that conductivity does slightly decrease with increasing annealing temperature (Fig. 7-3, curves representing 0 at.% Al). This is accompanied by an increase in the thermal activation energy. Therefore, it may be concluded that the increase in conductivity of the doped films by several orders of magnitude is mainly a result of dopant activation rather than annealing the structure of Si itself. However, as mentioned earlier, the optical measurements indicate that the optical gap of the doped films does not change upon annealing, within the above range of temperatures. This may be another indication that activation of the dopants in the films is the major reason for the increase in the conductivity.

Fig. 7-5 shows plots of $\log\sigma$ vs 1000/T for B-doped a-Si films annealed at 470 ^{o}C for 90 minutes. These films were originally doped by co-sputtering techniques as explained in chapter 6. The boron concentration varied between zero and about 2.2 area%. It can be seen, from Fig. 7-5 that, in general, the conductivity of B-doped films increases upon annealing. As in the case of Al-doped films, Fig. 7-6 shows that as the B content increases the increase in conductivity, upon annealing, is reduced. However, this seems to be a general trend for all

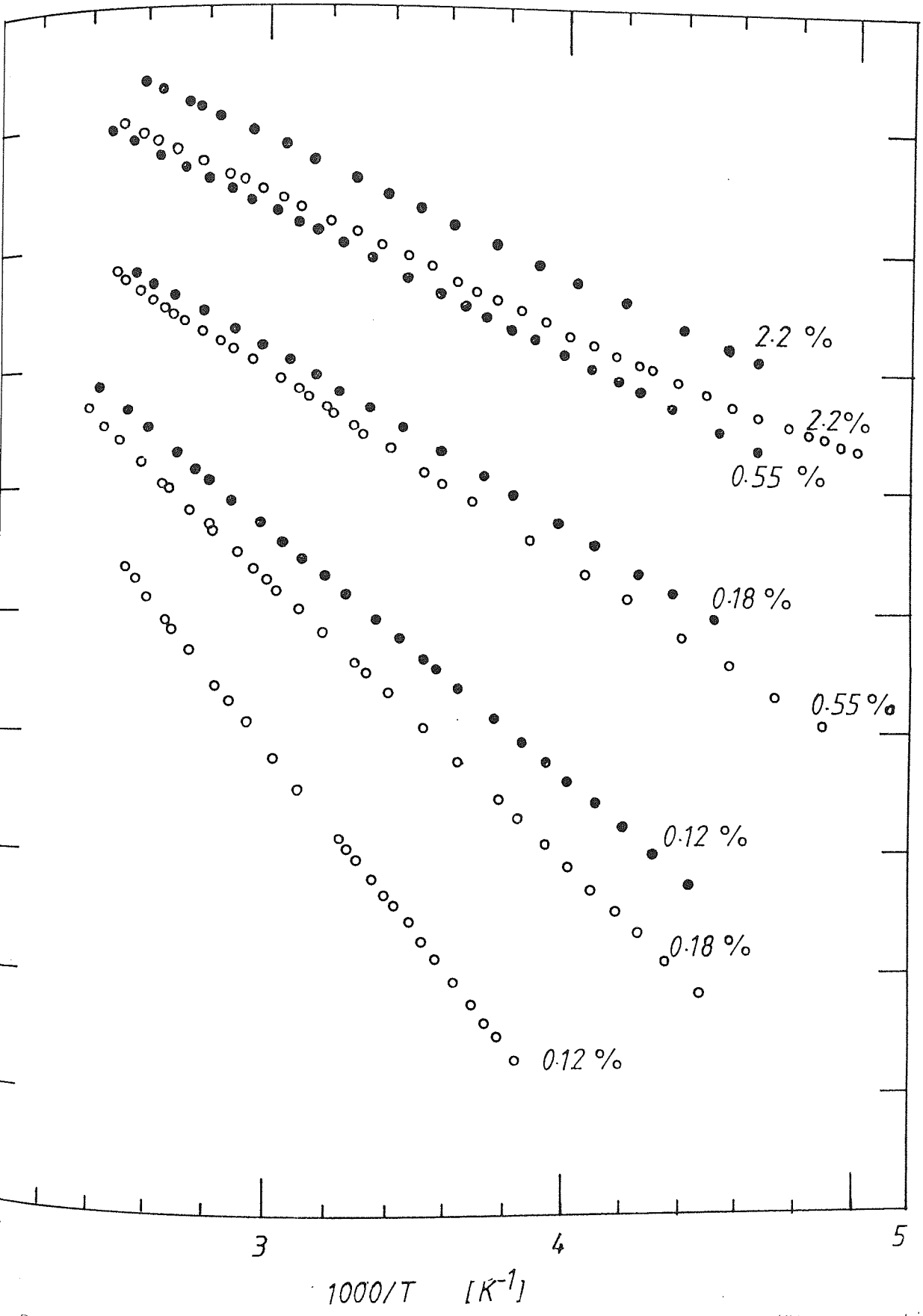

Fig. 7-5: Log σ vs 1000/T for B-doped films with different B/Si area ratios, both for as-deposited films (ooo) and annealed films at 470 °C for 90 minutes (●●●). The films were prepared by sputtering a composite target.

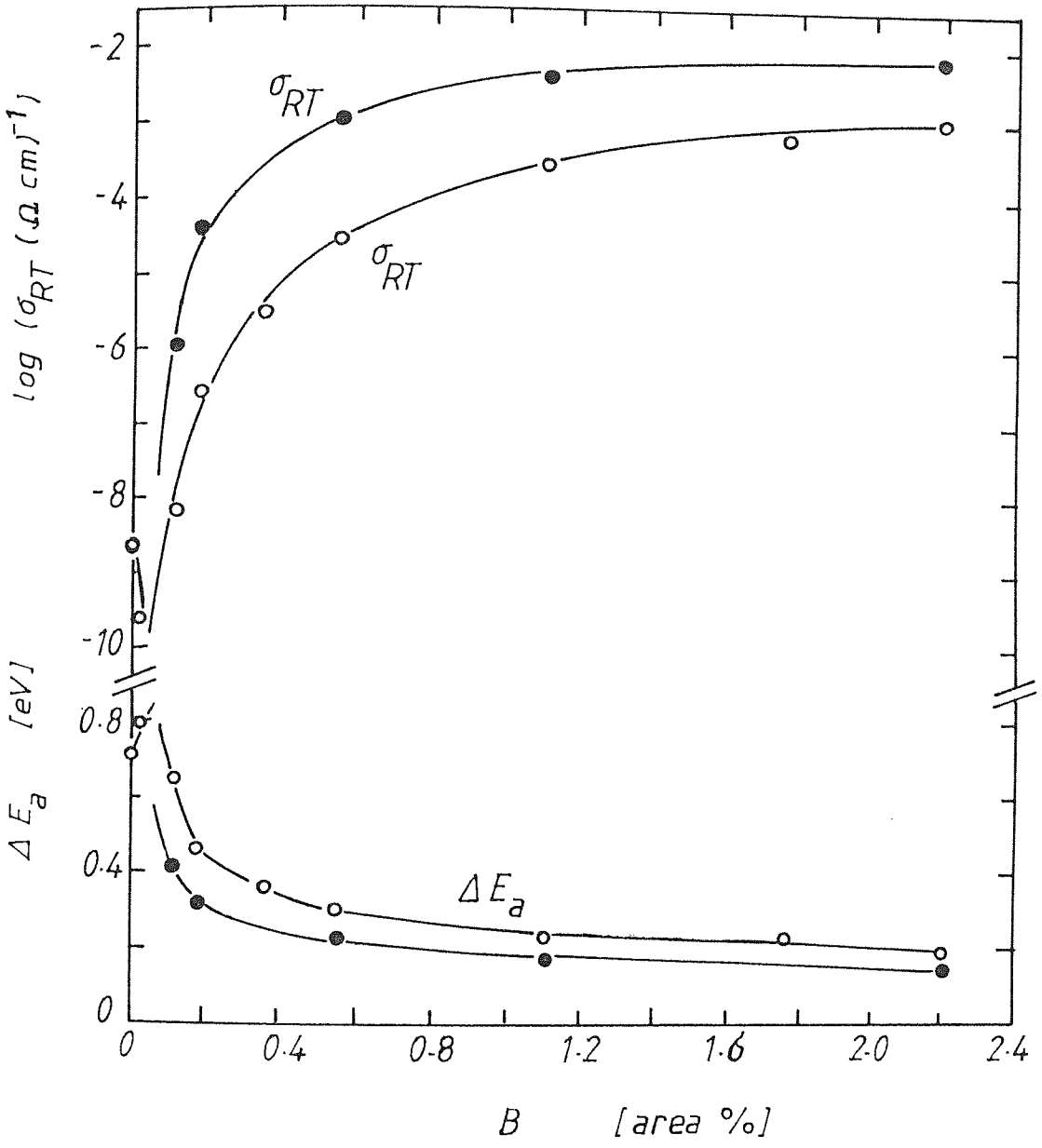

Fig. 7-6: Log σ_{RT} and ΔE_a as functions of B % (area ratio) for as-deposited films (ooo) and annealed films at 470 °C for 90 minutes (●●●). The films were prepared by sputtering a composite target.

the dopants, where annealing is more efficient, in enhancing the doping efficiency, when the dopant concentration is smaller. Fig. 7-7 demonstrates the variation in conductivity upon annealing for two samples of Ga-doped a-Si; as it can be seen, the results are consistent with those above. For the reasons outlined in sections 4.3. and 6.2.3. only two samples of Ga-doped a-Si are presented.

It is worth noticing that activation of the dopants by annealing (at least in the above temperature range) is more efficient in the case of Al-doped a-Si films than in B- or Ga-doped films. A summary of annealing effects on room-temperature conductivity and thermal activation energy, for Al-, B- and Ga-doped a-Si films is given Table 7-1.

7.3. DISCUSSION

In general, the annealing results demonstrate an increase in the conductivity of the doped films, with annealing temperature. On the other hand, the undoped films prepared under conditions near the optimum (section 5.2.2) showed that annealing at temperatures as high as 470^{o}C decreases the conductivity slightly, with no significant change in the thermal activation energy. The above observations indicate that the enhancement of the conductivity of the doped a-Si films is mainly due to activating the dopant rather than to annealing the structure of the basic material (e.g. reconstruction of weak bonds and structure relaxation). The optical gap independence of annealing temperature is in support of

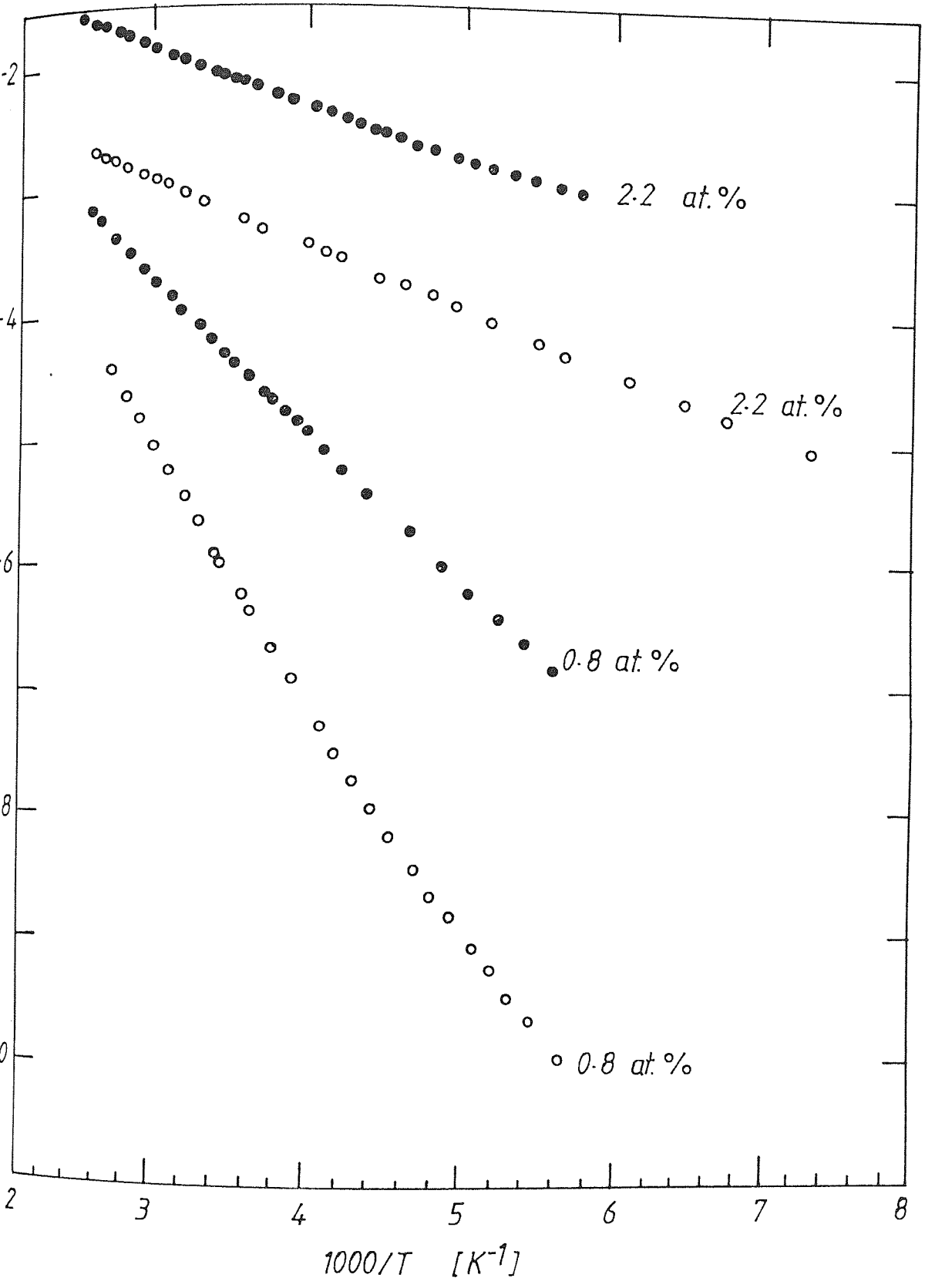

Fig. 7-7: Log σ vs 1000/T for two Ga-doped films with different Ga at.% in Si, both for as-deposited films (ooo) and annealed films at 470 °C for 90 minutes (●●●). The films were prepared by co-sputtering in Ne.

Table 7-1: A summary of the annealing results of doped a-Si with different dopants. σ_{RT} the room-temperature conductivity, ΔE_a the thermal activation energy. The annealing took place at 470 °C for 90 minutes.

Dopant	%	σ_{RT} (Ω.cm)$^{-1}$ as-deposited	σ_{RT} (Ω.cm)$^{-1}$ annealed	ΔE_a (eV) as-deposited	ΔE_a (eV) annealed
	0	5.6×10^{-9}	1.4×10^{-9}	0.67	0.69
	0.10	4.0×10^{-9}	1.0×10^{-6}	0.73	0.22
	0.25	1.0×10^{-9}	1.0×10^{-5}	0.75	0.15
Al	0.70	3.2×10^{-7}	3.5×10^{-4}	0.26	0.14
	1.20	2.2×10^{-6}	1.3×10^{-3}	0.18	0.14
	2.40	2.8×10^{-4}	8.9×10^{-2}	0.15	0.11
	5.20	2.8×10^{-2}	2.5×10^{-1}	0.13	0.10
	0.12	6.3×10^{-9}	1.0×10^{-6}	0.65	0.42
	0.18	3.0×10^{-7}	4.0×10^{-5}	0.46	0.33
B	0.55	2.8×10^{-5}	1.0×10^{-3}	0.31	0.24
	1.10	2.8×10^{-4}	3.5×10^{-3}	0.24	0.17
	2.20	1.3×10^{-3}	7.1×10^{-3}	0.19	0.15
Ga	0.80	2.2×10^{-6}	6.3×10^{-5}	0.42	0.26
	2.20	7.9×10^{-4}	7.9×10^{-3}	0.11	0.10

the above argument. The dopant activation could be due to thermal diffusion of Al, B or Ga atoms in the a-Si network; thus giving the chance for more dopant atoms to act as electrical centres, and hence increase the doping efficiency, instead of, probably, being isolated in a cluster form.

Annealing for a longer time seems to increase the conductivity of the doped films, since it is expected to give the dopant atoms more time to diffuse into a larger volume. However for the relatively high dopant concentration, after a given period of annealing time, the rate of increase in the conductivity is reduced. This may be attributed to the limitation of the solid solubility of the dopant in the basic material.

For low dopant concentration, the change (the increase) in conductivity is greater than that in the case of high dopant concentration. This can be seen from Figs. 7-4 and 7-6. The room-temperature conductivity increases by about 4 orders of magnitude, for a-Si doped with 0.25 at.% Al (about 2 orders of magnitude in the case of 0.18 % B), while it changes only by a factor of 4 for an Al concentration of 5.2 at.%. This might be further evidence for the limitation of the solid solubility of the dopants in a-Si.

One more interesting observation is that the increase in conductivity with annealing, in the case of Al-doping, is greater than that in the case of B- or Ga-oping, for the same

dopant concentration. This may be attributed to the differnce in the diffusion coefficients of different dopants in a-Si. At 470 ^{o}C, the diffusion coefficient of Al in Si is about one order of magnitude greater than that of Ga, and about 2.5 orders of magnitude greater than that of B (Sze , 1979).

Finally, the change in conductivity, upon annealing, of undoped a-Si prepared by sputtering in Ne at relatively high Pd/V_{sb} and T_s=300 ^{o}C (section 5.2.2.), is too small to account for any significant change in the density of states. This result together with the high change in conductivity of doped a-Si, may be an indirect evidence that a-Si produced under the above conditions, exhibits an intrinsically low density-of-defect-states. The results of annealing the undoped a-Si are qualitatively similar to those reported for a-Si sputtered in Ar, with the substrate negatively biased (Suzuki et al , 1982), in the sense that the conductivity is independent of annealing temperature, although the latter exhibited higher dark conductivity.

However, the above discussion does not entirely exclude the possibility of structure annealing of a-Si in some cases. The change in both the conductivity and thermal activation energy, with T_a, of films prepared by sputtering in Ne at low Pd/V_{sb} (lower than o.5 mTorr.cm.V^{-1}) is expected, since the electrical and optical properties of such films indicate that they possess relatively high density-of-states in the gap (see section 5.2.2.)

CHAPTER EIGHT

CONCLUDING REMARKS

It has been seen that the electrical and optical properties of undoped and doped a-Si, prepared by r.f. sputtering in Ne, can be controlled and varied systematically over a wide range, by variation of the preparation conditions. Various combinations of P, d and V_{sb} result in films with similar electrical and optical properties, provided that they are prepared at the same substrate temperature. Relatively high Pd/V_{sb} and a moderate substrate temperature may produce a-Si films with low density-of-states in the gap, as suggested by the high photoresponse, low conductivity, large energy gap and thermal activation energy. The thermal activation energy, the band tail-width, the localised states above the valence band, the shape of the optical-absorption spectral distribution and the consistency of interpretation of the results, suggest that the band model proposed by the Dundee group for a-Si:H is appropriate for the Ne-sputtered a-Si presented in this thesis.

It has been shown (chapter 6) that p-type doping by co-sputtering with group-III elements is possible, as evidenced from the control of the conductivity over many orders of magnitude and the shift of the Fermi level. The doping effects may be another indication that unhydrogenated a-Si with

ntrinsically low density-of-states is produced by r.f. sput-
ering in Ne. Although the doping efficiency of the co-sput-
ering technique is comparable with other techniques, such as
on implantation and doping from the gas phase, sputtering
rom a predoped target could further improve the doping effi-
iency. However, annealing results demonstrated that doping
fficiency may be enhanced by post-deposition annealing of
he doped films as the dopant is activated. It is worth
entioning that co-sputtering at low pd/V_{sb}, high concentration
f the dopant in a-Si may result in modification of the band
tructure rather than doping in the conventional sense.

Preliminary experiments on p-n and M-S devices, together with
ne high photoresponse of undoped a-Si, predict the possibility
f semiconductor and photovoltaic applications of a-Si produced
y the present technique.

It should be emphasised that the scope of this project is
o study the feasibility of the production of intrinsically
w density-of-states a-Si without the addition of hydrogen
a halogen and the possibility of doping this material.
erefore, in the light of this work, the following sugges-
ons could be made for future work.

(1) It is recommended that the density of states should be
udied quantitatively, for example, by field effect technique.

(2) More work is needed to further improve the doping
ficiency, perhaps, by investigating the negative bias of
e substrate and magnetron sputtering, or by investigating

another method of doping, such as ion implantation or possibly doping from the gas phase.

(3) Furthermore, we suggest various devices such as FET, p-n and MS junctions to be investigated in detail for semiconductor and/or photovoltaic applications.

(4) Finally, Detailed experimental work is needed to study the properties of the plasma, to give a better understanding of the sputtering mechanisms that control the properties of the deposited films.

REFERENCES

Abo-Namous S.A. and Sayigh A.A.M., 1982, "Present Assessment of a-Si Technology Through Literature Survey", Technical Report, KISR683, Kuwait Inst. for Sci. Res., KUWAIT

Abo-Namous S.A., Zaka Y. and Fane R.W., 1983, " Dependence of the Electronic and Optical Properties of Unhydrogenated a-Si on Preperation conditions", Phys. Stat. Sol. (a), 79, 477-82

Anderson D.A., 1978, "Transport in Doped sputtered a-Si:H", Bull. Am. Phys. Soc., 23, 249

Anderson D.A., Moddel G., Collins R.W. and Paul W., 1979, "The Effect of Gap State Density on Photoconductivity and Photoluminescence of a-Si:H", Solid State Commun., 31, 677-681

Anderson D.A., Moddel G. and Paul W., 1980, "Characterisation of High Gap State Densities in Heavily Hydrogenated a-Si", J. Non-Cryst. Solids, 35/36, 345-50

Anderson D.A., Moustakas T.D. and Paul W., 1977, "Effect of Hydrogen on Transport Properties of a-Si", Proc. 7th Inter. Conf. Amorphous and Liquid Semiconductors, ed. W.E.Spear (Edinburgh-University of Edinburgh Press), p334-38

Anderson D.A. and Paul W., 1982, "Transport Properties of a-Si:H alloys Prepared by Sputtering II: The Effect of Doping", Phil. Mag. B, 45, 1-23

Bahl S.K., Bhagat S.M. and Glosser R., 1973, "Properties of Amorphous Silicon Films : Dependence on Deposition Rate", Solid State Commun., 13, 1159-63

Batabyal A.K., Chaudhuri P., Ray S. and Barua A.K., 1984, "The Influence of Deposition Parameters on the Properties of Amorphous Silicon with Films Peoduced by the Magnetron Sputtering Method", Thin Dloid Films, 112, 51-59

Beyer W., Barna A. and Wagner H., 1979, "Highly Doped Evaporated Amorphous Silicon by Alkali Implantation", Appl. Phys. Lett., 35, 539-41

Beyer W., Fischer R. and Wagner H., 1979a, "Lithium Doping of Amorphous Silicon", J. Electron. Matter., 8, 127-37

Beyer W., Stritzker B. and Wagner H., 1980, "The Influence of Alkaline

and Halogen Implantation on Electrical Properties of Amorphous Silicon", J. Non-Cryst. Solids, 35/36, 321-26

Booth D., Allred D.D. and Seraphin B.O., 1979, Stabilised CVD a-Si for High Temperature Photothermal Solar Energy Conversion", Solar Energy Materials, 2, 107-24

Brodie I., Lamont L.T. and Myer D.O., 1969, "Substrate Bombardment During RF Sputtering", J. Vac. Sci. Technol., 6, 124-27

Brodsky M.H., 1979, "Topics in Applied Physics: Amorphous Semiconductors", Vol. 36 (Springer-Verlag, Berlin)

Brodsky M.H., Cardona M. and Cuomo J.J., 1977, "Infrared and Raman Spectra of the Silicon Hydrogen Bond in a-Si Prepared by Glow Discharge and Sputtering", Phys. Rev. B, 16, 3556-71

Carasco F. and Spear W.E., 1983, "Photogeneration and Geminate Recombination in a-Si", Phil. Mag. B, 47, 495-507

Carlson D.E., 1980, "Recent Development in Amorphous Silicon Solar Cells", Solar Energy Materials, 3, 503-18

Carlson D.E. and Wronski C.R., 1976, "Amorphous Silicon Solar Cells", Appl. Phys. Lett., 28, 671-73

Carter G. and Colligon J.S., "Ion Bombardment of Solids", (Heinemann Educational Book Ltd., London) p323 (1968)

Cody G.D., Tiedje T., Abeles B., Brooks B. and Goldstein Y., 1981, "Disorder and the Optical-Absorption Edge of Hydrogenated a-Si", Phys. Rev. Lett., 47, 1480-83

Cody G.D., Wronski C.R., Abeles B., Stephens R.B. and Brooks B., 1980, "Optical Characterisation of Amorphous Silicon Hidride Films", Solar Cells, 2, 227-43

Cohen M.H., Fritzsche H. and Ovshinsky S.R., 1969, "Simple Model for Amorphous Semiconducting Alloys", Phys. Rev. Lett., 22, 1065-68

Connell G.A.N., 1979, in "Topics in Applied Physics: Amorphous Semiconductors", Vol 36, ed. M.H.Brodsky, (Springer-Verlag, Berlin), pp73-111

Davidse P.D. and Maissel L.I., 1965, "RF Sputtering of Insulators", Transactions of 3rd Inter. Vacuum Congress, (Stuttgart, Germany) pp651-55

DOE Photovoltaic Program, Module/Array Technology, Price Goal and History (1980), U.S.A.

EMIS, INSPEC, Station House, Nightingale Road, Hitchin, ENGLAND

Fane R.W., 1981, "The Production of Amorphous Silicon Without Hydrgoen", J. Phys. D: Appl. Phys., 14, L113-L116

Fane R.W. and Abo-Namous S.A., 1983, "P-Type Unhydrogenated a-Si Prepared by Ne Sputtering", J. Phys. C: Solid State Phys., 16, 6121-28

Fane R.W. and Zaka Y., 1983, "Highly Doped Sputtered Amorphous Silicon Without Hydrogen", J. Non-Cryst. Solids, 57, 1-7

Fluit J.M., Rol P.K. and Kistemaker J., 1963, "Angular-Dependent Sputtering of Copper Single Crystals", J. Appl. Phys., 34, 690-91

Freeman E.C. and Paul W., 1979, "Optical Constants of RF Hydrogenated Amorphous Silicon", Phys. Rev. B, 20, 716-28

Fritzsche H., 1980, "Characterisation of Glow-Discharge Deposited a-Si:H", Solar Energy Materials, 3, 447-501

Fuhs W., Milleville M. and Stuke J., 1978, "Drift Mobility and Photo-Conductivity in a-Si", Phys. Stat. Sol.(b), 89, 495-502

Gray H.B., 1970, "Chemical Bonds, an Introduction to Atomic and Molecular Structure", (Benjamin/Cummings- California) p46

Gibson R.A., LeComber P.G. and Spear W.E., 1978, "Doped a-Si and its Application in Photovoltaic Devices", Solid State and Electronic Devices (Special Issue), 2, S3-S6

Grigorovici R., 1969, "Short-Range Order in Amorphous Semiconductors", J. Non-Cryst. Solids, 1, 303-25

Hamakawa Y., 1981, " Review of Photovoltaic in Japan", J. De Physique, 42, (C4), 1131-42

Iselborn S., Rübel H., Geiger J. and Schröder B., 1983, "Hydrogenation and Direct-Substitutional Doping of Evaporated a-Si Films", Phil. Mag. B, 48, 561-19

Jackson G.N., 1970, "RF Sputtering", Thin Solid Films, 5, 209-46

Janai M., Allred D.D., Booth D.C. and Seraphin B.O., 1979, "Optical Properties and Structure of a-Si Prepared by CVD", Solar Energy Materials, 1, 11-27

Jang J., Kang J.H. and Lee C., 1980, "Hydrogenation and Doping of Vacuum-Evaporated a-Si", J. Non-Cryst. Solids, 35/36, 313-18

Joannopoulous J. and Lucovsky G., 1983, "The Physics of Amorphous Silicon and its Applications", (Springer-Verlag, Berlin)

Kaplan D., Sol N., Velasco G. and Thomas P., 1978, "Hydrogenation of Evaporated Silicon by Plasma Treatment", Appl. Phys. Lett., 33, 440-42

Kittel C., 1971, "Introduction to Solid State Physics", 4th edition, (John Wiley & Sons Ltd, New York), p277

Kuwano Y. and Ohnishi M., 1981, "Industrialisation of a-Si Solar Cells", J. De Physique, 42, (C4), 1155-64

LeComber P.G., 1979, "Electrical Conduction in Amorphous Semiconductors", Sci. Prog., Oxford, 66, 105-118

LeComber P.G., Madan A. and Spear W.E., 1972, "Electronic Transport and State Distribution in a-Si Films", J. Non-Cryst. Solids, 11, 219-34

LeComber P.G., Madan A. and Spear W.E., 1973, in "Electronic and Strctural Properties of Amorphous Semiconductors", eds. P.G.LeComber and J.Mort (Academic Press, New York) p373

LeComber P.G. And Spear W.E.. 1970, "Electronic Transport in Amorphous Silicon Films", Phys. Rev. Lett., 25, 509-11

LeComber P.G., Spear W.E., Müller G. and Kalbitzer S., 1980, "Electrical and Optical Photoconductive Properties of Ion Implanted a-Si", J. Non-Cryst. Solids, 35/36, 327-32

Loveland R.J., Spear W.E. and Al-Sharbaty A., 1973/4, "Photoconductivity and Absorption in a-Si", J. Non-Cryst. Solids, 13, 55-68

Madan A., LeComber P.G. and Spear W.E., 1976, "Investigation of the Density of Localised States in a-Si using Field Effect Technique", J. Non-Cryst. Solids, 20, 239-57

Mahan A.H. and Stone J.L., 1981, "Amorphous Silicon Bibliography", Solar Cells (Special Issue), 4, part (3)

ibid, 1982, 4 , part (4)

ibid, 1984, 7, part (4)

Malhotra A.K. and Neudeck G.W., 1976, "Evaporation in the Presence of Hydrogen, Effects of Hydrogen Contamination on the Localised States in a-Si", Appl. Phys. Lett., 28, 47-49

Matsushita T., Komoto K., Konagai M. and Takahashi K., 1984, "High Performance a-Si:H Solar Cells With Graded Boron-Doped Intrinsic Layers Prepared From Disilane at High Deposition Rate", Appl. Phys. Lett., 44, 1092-94

McGill J., Wilson J.I.B. and Kinmond S., 1979, "Interfacial Layer in MIS amorphous Silicon Solar Cells", J. Appl. Phys., 49, 548-50

Moddel G., Anderson D.A. and Paul W., 1980, "Derivation of the Low-Energy Optical-Absorption Spectra of a-Si:H From Photoconductivity", Phys. Rev. B, 22, 1918-25

Mort J. and Pai D.M., 1976, "Photoconductivity and Related Phenomena",

(Elsevier Scientific Publ. Co., Amsterdam, North Holland)

Mott N.F., 1969, "Conduction in Non-Crystalline Materials II: Localised States in Pseudogap and Near Extremities of Conduction and Valence Bands", Phil. Mag., 19, 835-52

Mott N.F. and Davis E.A., 1979, "Electronic Proccesses in Non-Crystalline Materials", (Oxford: Clarendon)

Moustakas T.D., 1979, "Sputtered Hydrogenated Amorphous Silicon", J. Electron. Mater., 8, 391-435

Moustakas T.D., 1980, "Photogeneration, Optical Absorption and Transport in Hydrogenated Sputtered Amorphous Silicon", Solid State Commun., 35, 745-51

Moustakas T.D., Anderson D.A. and Paul W., 1977, "Preparation of Highly Photoconductive a-Si by RF Sputtering", Solid State Commun., 23, 155-58

Moustakas T.D. and Paul W., 1977, "Transport and Recombination in Sputtered Hydrogenated a-Ge", Phys. Rev. B, 16, 1564-76

Müller G., Kalbitzer S., Spear W.E. and LeComber P.G., 1977, "Doping of Amorphous Silicon by Ion Implantation", Proc. 7th Inter. Conf. Anorphous and Liquid Semiconductors, ed. W.E.Spear, (Edinburgh-University of Edinburgh Press) pp442-46

Newman R.M., 1972, "The Growth Structure and Optical Properties of Sputtered Barium Titanate Thin Films", Ph.D. Thesis. The University of Aston in Birmingham, U.K.

Niu H., Yoshizawa I., Shikama T., Matsuda T. and Takai M, 1984, "High Conductive P-Type Films of $Si_{100-x}-Al_x$:H Fabricated by co-Sputtering and Subsequent Annealing", Jap. J. Appl. Phys., 23, L18-L20

Ovshinsky S.R., 1977, "Chemical Modification of Amorphous Chalcogenides", Proc. 7th Inter. Conf. Amorphous and Liquid Semiconductors, ed. W.E.Spear (Edinburgh-University of Edinburgh Press)519-23

Paesler M.A. and Paul W,, 1980, "Photoluminescence in Sputtered a-Si:H Alloys", Phil. Mag. B, 41, 393-417

Paul W. and Anderson D.A., 1981, "Properties of a-Si:H with emphasis on Preparation by Sputtering", Solar Energy Materials", 5, 229-316

Paul W., Lewis A.J., Connell G.A.N. and Moustakas T.D., 1976, "Doping, Schottky Barrier and p-n Junction Formation in a-Ge and a-Si by RF Sputtering", Solid State Commun., 20, 969-72

Pawlewicz W.T., 1978, "Influence of Deposition Conditions on Sputter-Deposited a-Si", J. Appl. Phys., 49, 5595-601

Penn D.R., 1976, "Quantitative Chemical Analysis by ESCA", J. Electron Spectroscopy and Rel. Phenom., 9, 29-40

Pierce D.T. and Spicer W.E., 1972, Electronic Structure of a-Si From Photoemission and Optical Studies", Phys. Rev. B, 5, 3017-29

Polk D.E., 1971, "Stuctural Model for Amorphous Silicon and Germanium", J. Non-Cryst. Solids, 5, 365-76

Priestland C. and Jackson G.N., 1968, 1st Inter. Conf. Applications of Vacuum Science and Technology to Coating and Surface Structure, Dijon, (15-19 October) (after Jackson,1970).

Proceedings of 7th Inter. Conf. on Amorphous and Liquid Semiconductors, 1977, ed. W.E.Spear, (Edinburgh, University of Edinburgh Press)

Proceedings of 8th Inter. Conf. on Amorphous and Liquid Semiconductors, 1979, (Cambridge, Mass.) Published as J. Non-Cryst. Solids, (1980), 35/36

Proceedings of 9th Inter. Conf. on Amorphous and Liquid Semiconductors, 1981 (Grenoble, France) Published as J. De Physique, 1981, 42 (C4)

Proceedings of 13th Photovoltaic Specialists Conference, 1978, (IEEE, New York)

Ray S., Chaudhuri P., Batabyal A.K. and Barua a.K., 1983, "Some Properties of Intrinsic and Phosphorous Doped a-Si Thin Films", Jap. J. Appl. Phys., 22, 23-28

Robertson J., 1983, "Electronic Structure of Amorphous Semiconductors", Adv. Phys., 32, 361-452

Rock F.C. and Smith C.W., 1975, "Bell-Jar RF Sputtering System", J. Vac. Sci. Tech., 12, 943-45

Scofield J.H., 1976, "Hartree-Slater Subshell Photoionisation cross-section at 1254 and 1487 eV", J. Electron Spectroscopy and. Rel. Phenom., 8, 129-37

Shimizu T., Kumeda M., Watanabe I. and Kamono K., 1979, "Influence of Oxygen and Deposition Conditions of RF Sputtered a-Si Films", Jap. J. Appl. Phys., 18 , 1923-29

Shimizu T., Kumeda M., Watanabe I. and Kiriyama Y., 1980, "Properties of a-Si Prepared by RF Sputtering with a High Ar Pressure", Jap. J. Appl. Phys., 19, L235-L238

Snell A.J., Spear W.E. and LeComber P.G., 1981, "The Influence of Injected Carriers in a-Si p-n Junctions", Phil. Mag. B, 43, 407-17

Spear W.E., 1977, "Doped Amorphous Semiconductors", Adv. Phys., 26, 811-45

Spear W.E., Allen D., LeComber P.G. and Ghaith A., 1980, "The Interpretation of Transport Results in Amorphous Silicon", J. Non-Cryst. Solids, 35/36, 357-62

Spear W.E., Allen D., LeComber P.G. and Ghaith A., 1980a, " A New Approach to the Interpretation of Transport Results in a-Si", Phil. Mag. B, 41, 419-38

Spear W.E. and LeComber P.G., 1972, "Investigation of the Localised States Distribution in a-Si Films", J. Non-Cryst. Solids, 8-10, 727-38

Spear W.E. and LeComber, 1975, "Substitutional Doping of Amorphous Silicon", Solid State Commun., 17, 1193-96

Spear W.E. and LeComber P.G., 1976, in "Photoconductivity and Related Phenomena", eds. J.Mort and D.M.Pai (Elsevier Scientific Publ. Co., New york) pp185-214

Spear W.E. and LeComber P.G., 1979, in "Topics in Applied Physics : Amorphous Semiconductors", Vol. 36, ed. M.H.Brodsky (Springer-Verlag, Berlin) pp251-85

Spear W.E., Loveland R.J. and Al-Sharbaty A., 1974, "The Temperature Dependence of Photoconductivity in a-Si", J. Non-Cryst. Solids, 15, 410-22

Sterling H,F, and Swann R.C.G., 1965, "Chemical Vapour Deposition Promoted by RF Discharge", Solid State Electron., 8, 653-54

Suzuki M., Maekawa T., Okano S. and Bandow T., 1981, "Effects of RF-Bias on Properties of Sputtered Silicon Films", Jap. J. Appl. Phys., 20, L485-L487

Suzuki M., Nakao A., Maekawa T., Kumeda M. and Shimizu T., 1980,"Doping Effects of Group-III and -V Elements on a-Si Sputtered by High Pressure RF Sputtering", Jap. J. Appl. Phys., 19, (Supplement 19-2), 85-89

Suzuki M., Suzuki Makoto, Kanada M. and Kakimoto Y., 1982,"Thermal Stability of Pure a-Si Films Prepared by RF-Bias Sputtering", Jap. J. Appl. Phys., 21, L89-L91

Sze S.M., 1979, "Physics of Semiconductor Devices", 2nd edition, (Wiley-Interscience, New York), pp31-32

Tauc J., 1970, in "Optical Properties of Solids", ed. F.Abeles, (Amsterdam, North Holland)

Thompson M.G. and Reinhard D.K., 1980,"Modification of a-Si:H by co-Sputtered Aluminium", J. Non-Cryst. Solids, 37, 325-33

Thompson M.J., Allison J. and Al-Kaisi M.M., 1978, "Doping of Sputtered a-Si Solar Cells", Solid State Electronic Devices (Special Issue), 2, S11-S14

Title R.S., Brodsky M.H. and Cuomo J.J., 1977, "Electron Paramagnetic Resonanse Study of a-Si With Low Spin Concentration", Proc. 7th Inter. Conf. Amorphous and Liquid Semiconductors, ed. W.E.Spear, (Edinburgh, University of Edinburgh Press), pp424-28

Treble F., 1977, "
Proc. Photovoltaic Solar Energy Conference, Luxembourg (Holland, Reidel) pp732-44

Tsai C.C. and Fritzsche H., 1979, "Effect of Annealing on the Optical Properties of Plasma Deposited a-Si:H", Solar Energy Materials, 1, 29-42

Tsai C.C., Fritzsche H., Tanielian M.H., Gaczi P.J., Persana P.D. and Vesaghi M.A., 1977, "Plasma Deposited Si-H and Si-B-H Films". Proc. 7th Inter. Conf. Am orphous and Liquid Semiconductors, ed. W.E.Spear (Edinburgh, University of Edinburgh Press) pp339-42

Usami K., Katayama Y. and Shimada T., 1980, "XPS Determination of Amount of Incorporated Rare Gas in Amorphous Silicon Films Produced With Reactive Sputtering Method", Jap. J Appl. Phys., 19, 2065-68

Von Roedern B., Ley L., Cadona M. and Smith F.W., 1979, "Photoemission Studies in situ Prepared Hydrogenated Amorphous Silicon Films", Phil. Mag. B, 40, 433-50

Wakim F.G., Al-Jassar A. and Abo-Namous S.A., 1982, "Amorphous Silicon With Selenium Films: Optical Absorption", J. Non-Cryst. Solids, 53, 11-17

Wehner G.K. and Anderson G.S., 1970, in "Handbook of Thin Film Technology", eds. L.l.Maissel and R.Glang (McGrraw-Hill Book Co., New York) ch. 3

Wronski C.R. and Carlson D.A., 1977, "Electronic Properties of Discharge-Produced a-Si Used in Efficient Solar Cells", Proc. 7th Inter. Conf. Amorphous and Liquid Semiconductors, ed. W.E.Spear, (Edinburgh. University of Edinburgh Press) pp452-56

Xu L., Foiles C.L. and Reinhard D.K., 1984, "Thermopower of Sputtered Amorphous Si(Ga) Alloys", Phil. Mag. B, 49, 249-58

Yacobi B.G., Szadkowski A.J., Zukotynski S. and Corbett J.M., 1980, "Compound Formation Between Amorphous Silicon and Chromium", J. Appl. Phys., 51, 6424-25

Yamasaki S., Matsuda A. and Tanaka K., 1982, " Anomalous Optical and Structural Properties of B-Doped a-Si:H", Jap. J. Appl. Phys., 21, L789-L791

Zachariasen W.H., 1932, "The Atomic Arrangement in Glass", J. Am. Chem. Soc., 54, 3841-51

Zaka Y., Abo-Namous S.A., Crumpton D. and Fane R.W., 1984, "Composition and Properties of Unhydrogenated a-Si Produced by Sputtering in Ar or Ne", Vacuum "84" Conference, York , U.K. (1-4 August)

Zanzucchi P.J., Wronski C.R. and Carlson D.E., 1977, "Optical and Photoconductive Properties of Discharge-Produced a-Si", J. Appl. Phys., 48, 5227-36

Zemek J., Zavetova M. and Kov S., 1980, "On the Role of Hydrogen in a-Si:H", J. Non-Cryst. Solids, 37, 15-22

phys. stat. sol. (a) 79, 477 (1983)

Subject classification: 14.3 and 20.1; 16; 22.1.2

Physics Department, University of Aston, Birmingham[1])

Dependence of the Electronic and Optical Properties of Unhydrogenated a-Si on Preparation Conditions

By

S. A. Abo-Namous[2]), Y. Zaka, and R. W. Fane

J. Phys. C: Solid State Phys., 16 (1983) 6121–6128. Printed in Great Britain

P-type unhydrogenated amorphous silicon produced by Ne sputtering

R W Fane and S A Abo-Namous†
Physics Department, University of Aston in Birmingham, Gosta Green, Birmingham B4 7ET, UK

Aston University

Content has been removed for copyright reasons

J. Phys. C: Solid State Phys., 17 (1984) 1775–1782. Printed in Great Britain

Photoconductive properties of unhydrogenated Ne-sputtered a-Si

S A Abo-Namous† and R W Fane
Physics Department, University of Aston in Birmingham, Gosta Green, Birmingham B4 7ET, UK

Received 18 August 1983

Aston University

Content has been removed for copyright reasons

VACUUM "84" Conference, York, U.K. (1-4 April 1984)

DEPENDENCE OF PHOTOCONDUCTIVE PROPERTIES OF UNHYDROGENATED Ne-SPUTTERED a-Si ON PREPARATION CONDITIONS

S.A.Abo-Namous*, Y.Zaka and R.W.Fane

Physics Department, University of Aston in Birmingham, Birmingham, B4 7ET, U.K.

ABSTRACT

The photoresponse of undoped a-Si films, prepared by r.f. sputtering in Ne without the addition of hydrogen or a halogen, has been investigated as a function of the preparation conditions; gas pressure (P), target-substrate distance (d), self-bias voltage on the target (V_{sb}) and substrate temperature (T_s). Also, the temperature dependence of photoconductivity of these films has been measured as a function of the preparation conditions. High photoresponse of films produced at relatively high values of (Pd/V_{sb}) ratio and moderate temperature T_s suggests a low density-of-states in the mobility gap.

INTRODUCTION

It has been believed, for a long time, that sputtered or evaporated amorphous silicon (a-Si) possesses a high density-of-states in the gap, and consequently could not be doped. On the other hand, hydrogenated amorphous silicon (a-Si:H), prepared by glow-discharge decomposition of silane[1], or r.f. sputtering in Ar/H_2 [2], was found to have a low density-of-states in the gap.

In recent years, attempts have been made to produce a-Si with a low density-of-states, without the addition of hydrogen or a halogen, by sputtering at high Ar pressure [3], or at high Ne pressure [4]. Ar-sputtered a-Si was found to exhibit low doping efficiency and a poor photoresponse. On the other hand, Ne-sputtered a-Si exhibited a higher doping efficiency [5,6] and high photoresponse [7], which were comparable with the properties of a-Si:H.

However, the electronic and optical properties of a-Si seem to depend strongly on the preparation conditions. In this communication, the photoresponse of Ne-sputtered a-Si, without hydrogen or a halogen, is studied as a function of various preparation conditions, such as the gas pressure, the target-substrate distance, the self-bias voltage on the target and the substrate temperature. In addition, the temperature dependence of photoconductivity as a function of these conditions is reported.

---

* Permanent address: Materials Application Department, Kuwait Institute for Scientific Research, KUWAIT.

FILM PREPARATION AND CHARACTERISATION

A radio-frequency diode-type sputtering system, was used to deposit amorphous silicon films. A single crystal wafer of electronic grade was used as a target which was water cooled. The substrate holder could be electrically heated to vary the substrate temperature, T_s, between 150°C and 500 °C. The substrate temperature was measured with a chromel-alumel thermocouple, placed on top of the substrate. A field of about 0.01 T at the centre of the discharge was produced by a Helholtz pair of coils. The base pressure was of the order of 10^{-7} Torr, obtained by a conventional vacuum system of oil diffusion pump with a baffle and liquid nitrogen cooled trap. Corning 7059 glass substrates were ultrasonically cleaned in a detergent, rinsed in distilled water and then boiled in isopropyl alcohol prior to placing in the chamber.

Neon gas (99.999%) was admitted into the chamber via a needle valve, and the pressure, P, in the chamber was varied between 40 and 200 mTorr. The distance, d, between the target and the substrate was varied between 2 and 5.3 cm. The self-bias voltage, V_{sb}, on the target was varied between 650 and 1100 V, measured using a circuit similar to that described by Rock and Smith [8]. It has been found that, at constant T_s, different combinations of P, d and V_{sb}, within the ranges indicated above, giving a fixed Pd/V_{sb} ratio result in films with the same electrical and optical properties. Therefore the preparation conditions are represented here by two parameters, Pd/V_{sb} and T_s. To study the dependence of the properties of a-Si on substrate temperature, Pd/V_{sb} was fixed at about 0.68 mTorr-cm/V, and T_s was varied between 150 °C and 460 °C.

The film thickness was measured using a multiple-beam interferometer with an estimated uncertainty of ± 10%. The deposition rate ranged from about 4 A/s to 1 A/s as Pd/V_{sb} was varied from 0.2 to 1 mTorr-cm/V. In addition, increasing T_s from 150 °C to 460 °C reduced the deposition rate from 1.3 A/s to 0.8 A/s. The results of compositional analysis by x-ray photoemission spectroscopy will be reported elsewhere [9].

MEASUREMENTS AND RESULTS

The results reported here were for films of approximately the same thickness (about 0.5 μm), therefore no correction for the light penetration was needed for comparison. The dark conductivity and photoconductivity were measured under vacuum using gap-cell configurations with Al electrodes 1 mm apart. Al electrodes proved to make good ohmic contacts with a-Si for electric fields up to about 10^4 V/cm. However, a field of 10^2 V/cm was used for all the measurements reported here. The films were illuminated by a tungsten lamp and selective filters were used to give photon energies from 0.8 to 3.5 eV. For the photoresponse spectral distribution, the photocurrent, i_{ph}, defined as the difference between the current under illumination and the dark current, was measured at room temperature, and normalised to 10^{14} photons.cm.$^{-2}$.s^{-1}, where at this range of illumination intensity, it was found that the photocurrent was proportional to the light intensity.

The steady-state photocurrent was measured as a function of photon energy, $\hbar\omega$, for a number of undoped a-Si films deposited at about 300 °C with a range of Pd/V_{sb} values between 0.21 and 0.95 mTorr.cm/V. Fig. 1 shows the steady-state photoresponse represented as $[i_{ph}/eF(1-R)]$,

as a function of $\hbar\omega$ in the range of $0.8 \lesssim \hbar\omega \lesssim 3.5$ eV, for three films prepared at various Pd/V_{sb} values and T_s=300 °C. F(1-R) is the number of photons incident on 1 cm^2 of the specimen per second, corrected for surface reflection. It has been shown [7], that the photoresponse increased as the Pd/V_{sb} value increased up to about 0.80 mTorr.cm/V. The effects of Pd/V_{sb} values higher than 0.80 mTorr.cm/V on the photoresponse are shown in Fig. 1 (curve c). It can be seen from the figure that for Pd/V_{sb}=0.95 mTorr.cm/V, the photoresponse is reduced.

The photoresponse spectral distribution was also measured as a function of T_s, for Pd/V_{sb}=0.68 mTorr.cm/V and is shown in Fig. 2 for three films with T_s=150 °C, 300 °C and 390 °C. It can be seen from this figure that the highest photoresponse is for films prepared at T_s=300 °C, while for temperatures higher or lower than this temperature, the photoresponse is reduced.

In general, the photoresponse curves of Figs. 1 and 2 have common features. They show peaks between 1.8 and 2.15 eV, which may approach, or even exceed, unity if higher fields were applied. The photoresponse drops rapidly at energies lower than 0.8 eV and shows a shoulder around 1.2 eV followed by a rapid rise in the photoresponse above about 1.6 eV. These features are very similar to those reported for a-Si:H prepared by glow-discharge decomposition of silane [10,11] or r.f. sputtering in Ar/H_2 mixture [12].

For the temperature dependence of photoconductivity, the films were illuminated by a monochromatic light with energy 1.89 eV at a flux intensity of about $8x10^{14}$ photons.cm^{-2}.s^{-1} (Figs. 3 and 4). The photoconductivity, σ_{Ph}, was measured as a function of temperature in the range from about -30 °C to about 115 °C, for several films prepared under various conditions of Pd/V_{sb}, with T_s=300 °C. The plots of log σ_{Ph} vs 1/T are shown in Fig. 3. Curves a, b and c are for films prepared at 0.31, 0.76 and 0.95 mTorr.cm/V respectively. The films were excited by $8x10^{14}$ photons.cm^{-2}.s^{-1}. Also, shown in Fig. 3 is the dark conductivity, σ, for the films prepared at Pd/V_{sb}=0.76 mTorr.cm/V.

All the photoconductivity curves of Fig. 3 show maxima in σ_{Ph} at relatively high temperatures, beyond which the photocurrent was difficult to measure with a reasonable accuracy because $\sigma_{Ph} \ll \sigma$.

The log σ_{Ph} vs 1/T data suggest a thermally activated photocurrent with an activation energy between 0.15 and 0.2 eV. There was no systematic dependence of the thermal activation energy of σ_{Ph} on Pd/V_{sb}, or light intensity [7].

The log σ_{Ph} va 1/T plots for films prepared at Pd/V_{sb}=0.68 mTorr.cm/V and different substrate temperatures, T_s, are shown in Fig. 4. In this figure, curves a, b and c represent films prepared at T_s=150 °C, 300 °C and 390 °C respectively . The films were illuminated by monochromatic light of energy 1.89 eV at a flux intensity of $8x10^{14}$ photons.cm^{-2}.s^{-1}. The dark conductivity plot represents a film prepared at 300 °C. It can be seen from Fig. 4 that the dependence of σ_{Ph} on 1/T is similar to the dependence of Pd/V_{sb} shown in Fig. 3. Also, the figure shows that the photoconductivity is improved for T_s=300 °C, while for T_s higher than 300 °C (curve c , Fig. 4), it is reduced. An interesting observation is that the thermal activation energy of σ_{Ph} always lies in the range between 0.15 and 0.2 eV, and does not vary systematically with T_s. This may suggest that, within the experimental errors expected from this type

of measurement, the possibility of a significant change in the degree of order of the films with T_s may be remote in this range of substrate temperatures.

DISCUSSION AND CONCLUSIONS

The high photoresponse of films prepared at Pd/V_{sb} in the range from about 0.6 mTorr.cm/V to about 0.8 mTorr.cm/V suggests a low density-of-states. The shoulder around 1.2 eV has been attributed to an optical transition from occupied localised states at ϵ_y above the valence-band edge to the conduction band [12,13]. It has been suggested that these localised states could be defect states. However, the occurrence of this shoulder at approximately the same energy in all the films, suggests that there is a rapid rise in the gap density-of-states at about 1 eV below the conduction-band edge as demonstrated by the field-effect measurements of glow-discharge a-Si:H [14]. The change in the height of the shoulder with preparation conditions (Figs. 1 and 2) indicates that the localised states in the mobility gap can be controlled by these conditions. The high photosesitivity of the films prepared at Pd/V_{sb}=0.80 mTorr.cm/V and T_s=300 °C (Fig. 1 curve b) could be a result of increasing recombination lifetime. It has been thought that for these preparation conditions, the plasma species are thermalised enough [3] to result in films with less microvids and defect states as indicated by the corresponding optical and electronic properties [7,15], as well as from the doping efficiency [5]. On the other hand, when Pd/V_{sb} exceeds 0.80 mTorr.cm/V and/or T_s exceeds 300 °C, the photosensitivity is reduced, suggesting a decreasing recombination lifetime. This is consistent with the dependence of the electrical and optical properties on Pd/V_{sb} ($\gtrsim$ 0.80 mTorr.cm/V) and T_s ($\gtrsim$ 300 °C) [16].

Taking into consideration that the transport of photocarriers takes place, predominantly, in the extended electron states [17], according to the relation

the position of the band-tail edge, ϵ_A, with respect to c_c, $(\epsilon_c-\epsilon_A)$ can be determined from the slopes of log σ_{Ph} vs 1/T curves on the low temperature side. The detailed meaning of different symbols in this equation can be found elsewhere [18]. From Figs. 3 and 4 and other similar plots (not shown here), the band-tail width $(\epsilon_c-\epsilon_A)$ seems not to change significantly with the parameters Pd/V_{sb} and T_s. This could mean that no significant change in the degree of disorder has occured upon varying the quantities P, d, V_{sb} and T_s within the ranges indicated earlier. Instead, these quantities are more likely to affect the defect-states-centres through the deposition mechanism, as suggested by the change in the height of the localised-states peak at 1.2 eV (Figs. 1 and 2). The consistency between the dependence of the electronic and optical properties of a-Si on the deposition rate and on Pd/V_{sb} has been reported elsewhere [15]. Furthermore it has been found that at substrate temperatures higher than 300 °C the electrical and optical properties deteriorate, increased conductivity is accompanied by a reduction in the photoconductivity, optical gap and thermal activation energy of the dark conductivity. Also, the deposition rate was found to decrease with increasing substrate temperature. More detailed work is required to explain the observed effects of substrate temperature.

The increase in the peak intensity at 1.2 eV in the photoresponse spectral distribution (Fig. 2) with increasing T_s may be interpreted, according to the Dundde Group model [14] as an indication of increasing localised defect-states.

From the present results and the electrical and optical results reported elsewhere [7,15], it can be concluded that films with a low defect-state-density are produced by sputtering in Ne gas at moderate combination of P, d, V_{sb} and T_s. Furthermore, the photoresponse of these films may suggest potential photovoltaic and semiconductor applications. However, investigation of other parameters, such as negative bias of the substrate and, possibly, the use of magnetron sputtering, is worthwhile, to improve further the properties of a-Si films.

The authors would like to thank Mr. R.S.Bassi for technical assistance.

REFERENCES

[1] For example, W.E.Spear and P.G.LeComber, J.Non-Cryst. Solids, 8-10, 727, (1972)
[2] W.Paul, A.J.Lewis, G.A.N.Connell and T.D.Moustakas, Solid State Commun., 20, 969, (1976)
[3] For example, M.Suzuki, A.Makao, T.Mackawa, M.Kumeda and T.Shimizu, Jap.J.Appl.Phys., 19-20, 85, (1980)
[4] R.W.Fane, J.Phys. D: Appl.Phys., 14, L113, (1981)
[5] For example, R.W.Fane and S.A.Abo-Namous, J.Phys. C: Solid State Phys., 16, 6121, (1983)
[6] R.W.Fane and Y.Zaka, J.Non-Cryst.Solids, 57, 1, (1983)
[7] S.A.Abo-Namous and R.W.Fane, J.Phys.C: Solid State Phys., 17, 1775, (1984)
[8] F.C.Rock and C.W.Smith, J.Vac.Sci.Tech., 12, 943, (1975)
[9] Y.Zaka, S.A.Abo-Namous, D.Crumpton and R.W.Fane, Vacuum "84" Conference, York University, York,U.K. (1-4 August 1984)
[10] R.J.Loveland, W.E.Spear and A.Al-Sharbaty, J.Non-Cryst.Solids, 13, 55, (1973/74)
[11] S.Ray, P.Chaudhuri, A.K.Batabyal and A.K.Barua, Jap.J.Appl.Phys., 22, 23, (1983)
[12] D.A.Anderson, G,Moddel and W.Paul, J.Non-Cryst. Solids, 35/36, 345, (1980)
[13] G.Moddel, D.A.Anderson and W.Paul, Phys. Rev. B, 22, 1918, (1980)
[14] A.Madan, P.G.LeComber and W.E.Spear, J.Non-Cryst.Solids, 20, 239, (1976)
[15] S.A.Abo-Namous, Y.Zaka and R.W.Fane, Physica Status Solidi (a), 79, 477, (1983)
[16] S.A.Abo-Namous (unpublished data)
[17] P.G.LeComber and W.E.Spear, Phys.Rev.Lett., 25, 509, (1970)
[18] W.E.Spear, R.J.Loveland and A.Al-Sharbaty, J.Non-Cryst.Solids, 15, 410, (1974)

Fig. 1

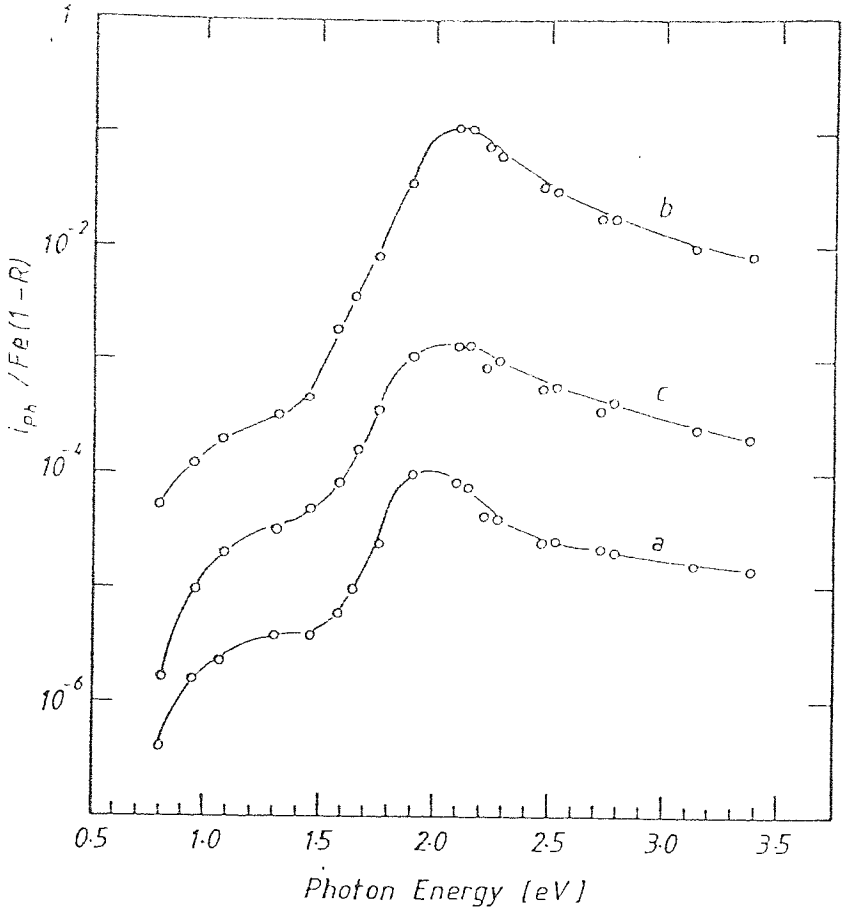

Fig. 2

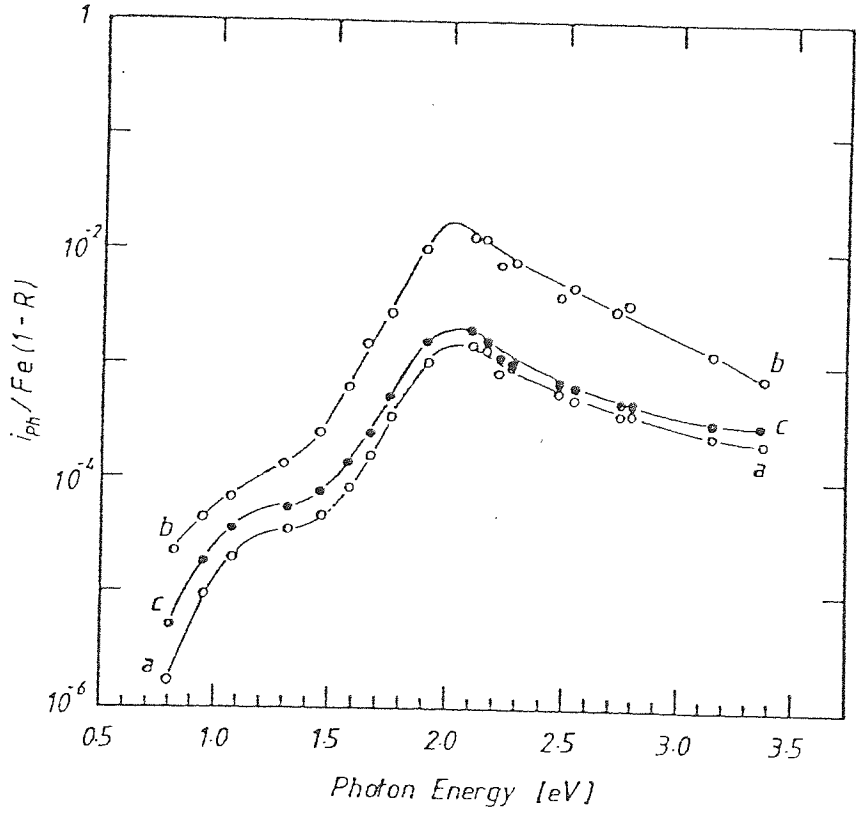

Fig. 1: The photoresponse spectral distribution for films prepared at T_s=300 °C and different Pd/V_{sb} values: (a) 0.31, (b) 0.76 and (c) 0.95 mTorr.cm/V.

Fig. 2: The photoresponse spectral distribution for films prepared at Pd/V_{sb}=0.68 mTorr.cm/V and different substrate temperatures, T_s: (a) 150 °C, (b) 300 °C and (c) 390 °C.

Fig. 3

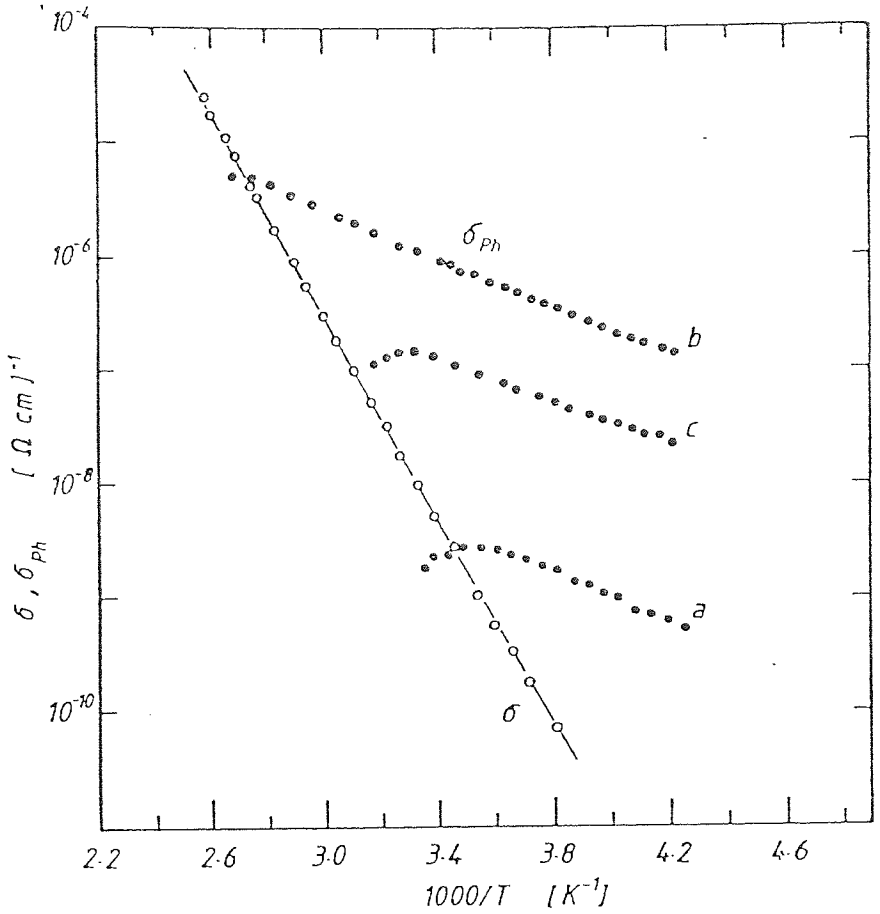

Fig. 4

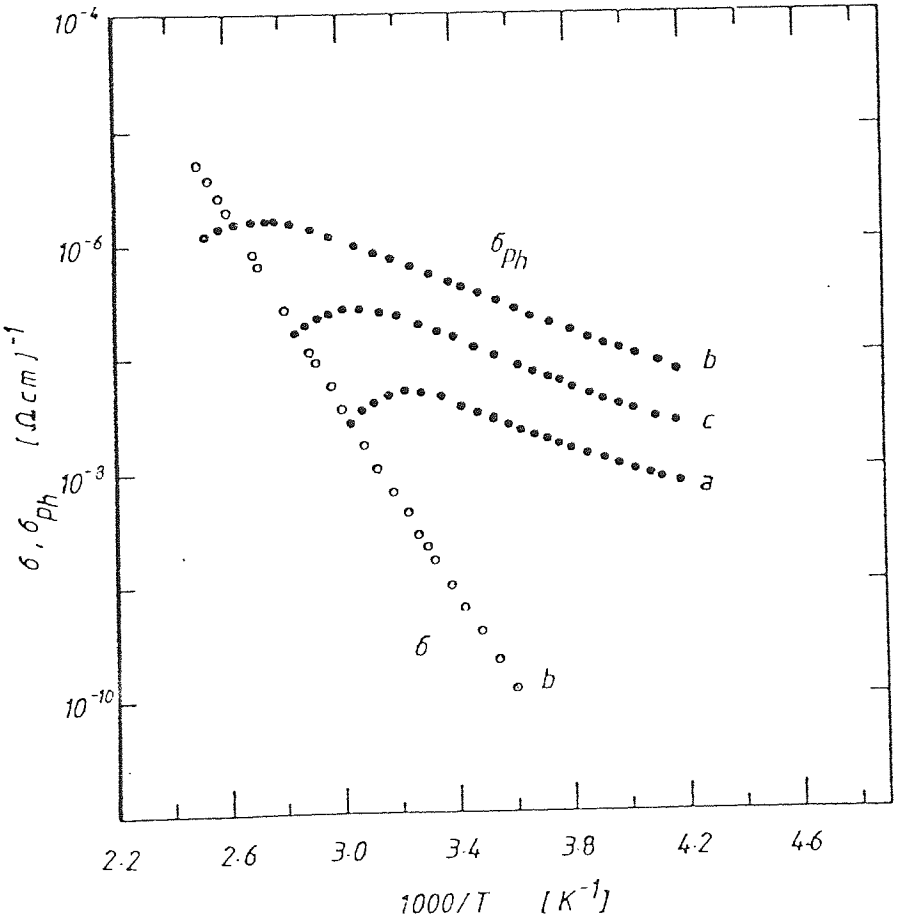

3: The plots of log σ_{Ph} vs 1/T for films prepared at T_s=300 °C and different Pd/V_{sb} values; (a) 0.31, (b) 0.76 and (c) 0.95 mTorr.cm/V

4: The plots of log σ_{Ph} vs 1/T for films prepared at Pd/V_{sb}=0.68 mTorr.cm/V and different T_s; (a) 150 °C, (b) 300 °C and (c) 390 °C.

VACUUM "84" Conference, York, U.K. (1-4 April 1984)

COMPOSITION AND PROPERTIES OF UNHYDROGENATED AMORPHOUS SILICON PRODUCED BY SPUTTERING IN ARGON OR NEON GAS

Y.Zaka, S.A.Abo-Namous*, D.Crumpton and R.W.Fane

Physics Department, University of Aston in Birmingham, Birmingham, B4 7ET, U.K.

ABSTRACT

The electrical and optical properties of amorphous silicon produced by r.f. sputtering in pure argon or neon gas are compared. The effect of varying the inert gas pressure has been investigated. It is shown that the density of defect states can be reduced by sputtering in high pressure neon instead of the conventionally used argon. The composition of the films has been studied by Rutherford backscattering spectroscopy (RBS) and x-ray photoemission spectroscopy (XPS)

INTRODUCTION

Inherent in all methods of producing amorphous silicon (a-Si) films is the presence of large number of dangling bonds and microvoids. These defects introduce localised states in the mobility gap between the conduction and valence bands, thus hindering the control of electrical properties by substitutional doping [1]. Hence a large fraction of research has been directed towards reducing the density of defects to a sufficiently low level to allow efficient doping.

In 1975 Spear et al [2] were the first to dope a-Si produced by the glow-discharge decomposition of SiH_4 with phosphorous and boron. Their method succeeded because the hydrogen present in the plasma attached itself to the dangling bonds thus reducing the density of states in the gap. Soon after, a-Si produced by r.f. sputtering in Ar/H_2 plasma was also doped successfully [3]. The success with doping a-Si:H alloy and the realisation of its potential device capabilities have diverted a lot of attention away from the need to investigate the basic parameters affecting film properties and to optimise them to achieve "pure" a-Si films with a low density-of-defect-states. Instead experimentalists have saturated the silicon with dangling-bond terminators such as hydrogen or the halogens to achieve the desired properties. Concentration of these intentionally incorporated impurities can be as large as 26% [4]. Compensation by hydrogen may remove the gap states, but the interaction of nearby Si-H units may re-introduce gap states near the conduction band [5]. The long term stability of these films is questionable since hydrogen effuses at 350 °C and there is some evidence that hydrogen effuses even at room temperature [6].

---

* Permanent address: Materials application Department, Kuwait Institute for Scientific Research, KUWAIT

It is therefore important to optimise the preparation conditions to give pure a-Si films with a low density-of-defect-states. In this paper we report the effects of varying the sputtering gas and pressure on the composition and electrical and optical properties of a-Si films produced by r.f. sputtering in (99.999%) pure argon and neon gases. The films produced have been characterised by measuring the electrical conductivity over a temperature range of 200 °C. The optical gap has been determined by the transmission measurements in an UV-Vis. spectrophotometer. Compositional analysis has been carried out by Rutherford backscattering spectroscopy (RBS) and x-ray photoelectron spectroscopy (XPS). In particular, the amount of rare gas incorporated into the silicon matrix as a function of gas pressure was investigated. Problems related to the determination of the density of the films from the RBS spectra are also discussed.

EXPERIMENTAL DETAILS

Experimental details have been described elsewhere [7]. Briefly, the apparatus consists of a diffusion pumped, r.f. diode sputtering arrangement with a baffle and liquid nitrogen cooled trap. A Helmholtz pair of coils gives a field of about 0.01 T at the centre of the discharge. The power input is adjusted to give a r.f. self bias on the target of about 900 eV. The target-substrate distance is set at 3.5 cm and the substrate temperature maintained at approximately 200 °C, measured with a chromel-alumel thermocouple. Films were deposited simultaneously on several substrates. Corning 7059 glass was used for electrical and optical measurements, for RBS measurements, carbon, crystalline silicon, alumina and quartz substrates were used while aluminium substrates were used for XPS measurements. The rare gases entered the chamber via a needle valve which controlled the flow rate to achieve the desired pressure.

Film thickness, measured by a multiple-beam interferometer, ranged from about 200 to 1000 nm. Deposition rate varied from about 0.2 nm/s for high pressure argon films to about 0.4 nm/s for low pressure films, for neon-sputtered films the deposition rate decreased from about 0.3 to o.1 nm/s on increasing the sputtering pressure.

ELECTRICAL AND OPTICAL PROPERTIES

The electrical conductivity of the films was measured in the manner described elsewhere [7]. Fig. 1 shows the variation of room-temperature electrical conductivity, σ_{RT}, with sputtering pressure for argon and neon gases. It is seen that by increasing the argon pressure from 0.67 Pa to about 5.3 Pa, σ_{RT} decreases by more than five orders of magnitude, any further increase in pressure has little effect on σ_{RT} other than increasing it slightly at the higher pressure. The highest pressure at which we can operate with argon is limited by the geometry of the system and is about 14.6 Pa beyond which the mean free path of the argon ions becomes comparable to the spacing between the target and the earthed shield surrounding it. For neon this limitation is not so severe and sputtering pressures upto 40 Pa can be tolerated. For neon, an increase in the pressure from 0.67 to 5.3 Pa had a similar effect but an increase in the pressure to about 20 Pa further decreased the conductivity by more than three orders of magnitude. Any further

increase in pressure again, as in the case of argon, produced a reversal in the trend with the conductivity increasing with pressure.

A similar behaviour is observed in the variation of thermal activation energy, ΔE, and the optical gap, E_o, with pressure as illustrated in Fig. 2. For argon ΔE increases from 0.14 eV to about 0.6 eV as the pressure is increased from 0.67 to 8.6 Pa and any further increase in pressure has little effect. For neon, ΔE increases with pressure to a value of about 0.9 eV at 14.6 Pa, higher pressure results in a slight decrease in ΔE. The optical gap was determined from the plots of $(\alpha \hbar\omega)^{\frac{1}{2}}$ vs $\hbar\omega$ according to the relation [8]

$$(\alpha \hbar\omega)^{\frac{1}{2}} = \beta (\hbar\omega - E_o)$$

where β is a constant, $\hbar\omega$ the photon energy and α the absorption coefficient. The optical gap, E_o, increases from about 1.4 eV at low pressure to about 1.7 eV for high-pressure sputtering in argon and 1.8 eV for the neon case.

COMPOSITIONAL ANALYSIS

Fig. 3 shows the ratio of argon and neon atoms to silicon atoms in the films as a function of sputtering pressure. Rutherford backscattering spectroscopy using 2.8 MeV He ions and XPS using Mg Kα radiation were used to determine the argon and neon contents of the films respectively. The ratio of argon to silicon atoms of the films was found to decrease from about 6.0% at low pressure to less than 0.5 % for high pressure . The variation of neon in the films with pressure exhibits a similar trend to that of the argon; however, at any given sputtering pressure the neon incorporated in the films is approximately twice as much as argon. Inspection of RBS spectra readily confirmed that the argon was distributed uniformly throughout the films; however, to verify the uniformity of neon in the silicon matrix, films had to be etched by argon bombardment and spectra taken at various depths.

DISCUSSION AND CONCLUSIONS

The results indicate that the density of defect states in a-Si can be reduced by sputtering at high pressure. For sputtering in pure argon this is evidenced by a decrease in room-temperature electrical conductivity by more than five orders of magnitude and an increase in the thermal activation energy from 0.14 to 0.6 eV as the argon pressure is increased from the conventionally used value of 0.67 Pa to 8.7 Pa.

Similar results for argon sputtering have been reported by others. Pawlewicz [9] decreased σ_{RT} from about 10^{-5} to about 10^{-7} $(\Omega\,\mathrm{cm})^{-1}$ by increasing the argon gas pressure from 3.3 to 20 Pa and there was corresponding increase in the activation energy from 0.2 to 0.3 eV. Van Dong et al [10] sputtered in a d.c. triode system and obtained, under a special condition of heating, a-Si films with $\sigma_{RT} \cdot 10^{-9}$ $(\Omega\,\mathrm{cm})^{-1}$ and activation energy of about 0.8 eV. Shimizu et al [11] secreased the electrical conductivity by more than five orders of magnitude by increasing the product of argon pressure, P, and the target-substrate spacing, d, from 13 to 130 Pa-cm. The original suggestion by Pawlewicz [9], that increasing the sputtering pressure reduced the kinetic energy of the various species bombarding the film thus reducing the number of defects,

seems to be consistent with the above results. However, recently it has been found that the low conductivity of the high pressure argon-sputtered films could be due in part to post-deposition oxidation because the films have a porous structure [12]. This is thought to be due to the fact that although bombardment by high energy species (ions, neutrals, electrons) in the plasma is detrimental to the film properties, some bombardment is beneficial in that it helps to remove loosely bound atoms. Thus a film grown under the condition of high pressure, where the plasma species have become thermalised before reaching the substrate, tends to have a porous structure.

To investigate this hypothesis, the oxygen content of the films was extracted from the relevant RBS spectra. The results are summarised in Fig. 4. From these results it is evident that films produced in argon sputtering pressures upto 3.5 Pa are essentially oxygen free, while films produced at higher pressures contain about 20% oxygen.

Our results appear to support the suggestion that as the gas pressure is increased the electronic and optical properties of the films improve due to the reduction in the kinetic energy of the various species in the plasma which are continuously bombarding the growing film. This is evident from a decrease in σ_{RT} by four orders of magnitude as the pressure is increased from 0.67 to 3.5 Pa, while maintaining essentially oxygen free films. The variations of thermal activation energy, optical gap and the argon content with argon pressure have a similar relationship; ΔE and E_o increase and the argon content decreases sharply as the pressure is increased from 0.67 to 3.5 Pa. Increasing the pressure beyond 3.5 Pa also removes low energy bombardment of the film which is beneficial in that it removes loosely bound material from the surface of the film, thus films produced at high argon pressure tend to be porous and susceptable to post-deposition oxidation as is evident by a sharp increase in the oxygen content of the films produced at pressure higher than 3.5 Pa. The decrease in σ_{RT} as the pressure is increased beyond 3.5 Pa is less sharp, levelling off at pressures of about 8.6 Pa snf is probably due to the oxygenation of the films. Similarly E and E_o increase and the argon content decreases slightly as pressure is increased beyond 3.5 Pa and eventually levels off at about 8.6 Pa.

Another quantity which can be used to support the above argument is the measurement of the density of the films. This could in theory be readily obtained from the RBS spectra and the thickness of the film, measured independently by other means, employing the relation [13],

$$\Delta\epsilon = [\theta] \frac{N_o \rho}{A} t$$

where $\Delta\epsilon$ is the energy difference between the energy of the ions scattered from the front surface of the target and the ions scattered from the back surface of the target, $[\theta]$ is the stopping cross-section, N_o is Avogadro's number, A is the atomic weight of element and ρ and t are the density and thickness of the film respectively. Since $[\theta]$ is tabulated [14] the density can be obtained by measuring $\Delta\epsilon$ and the thickness of the film. We attempted to measure the density by depositing the films on carbon substrates since the carbon edge lies well below the silicon peak, but measurement of $\Delta\epsilon$ and the shape of the peak indicated that carbon and silicon had diffused into each other, resulting in the broadening of $\Delta\epsilon$, and hence an over-estimation of the

density. To voercome this problem, quartz and alumina substrates were employed and although no sign of diffusion seemed apparent, there was a large error in determining $\Delta\epsilon$ due to the overlap of the silicon and the substrate peaks. Thus, so far we have been unable to measure the density of the films but further work to overcome the problem indicated above and to investigate alternative methods is in progress.

It can be seen by inspection of Figs. 1-3 that the variations in properties of neon-sputtered films follow the same general trend as for argon case. However, in this case the region of rapid changes in properties with increase in pressure extends upto 12 Pa. An increase in pressure from 0.67 to 12 Pa results in a decrease in σ_{RT} by more than six orders of magnitude to less than 10^{-9} $(\Omega\,cm)^{-1}$, accompanied by an increase in ΔE and E_o by 0.6 eV and 0.4 eV respectively. The neon concentration in these films decreases to about 1.0 at.% at 12 Pa and levels off at about 0.5 at.% at higher pressures.

The pressure region 0.67 to 12 Pa for neon corresponds to the region 0.67 to 3.5 Pa for argon, in that the improvement in film properties is believed to result from the thermalisation of plasma species. However it is apparent from the results that improvement of film quality is greater for neon-sputtered films. Further increase in pressure leads to contamination by oxygen, although figures for oxygen contnent have only been obtained for argon-sputtered films.

Detailed examination of the sputtering plasma is required to determine the factors which result in an improvement in film quality when using neon as opposed to argon sputtering. Thermalisation as mentioned above, is important but this may be achieved in either case by using the appropriate pressure. Other factors may be important. The higher ionisation potential for neon means that there is less likelihood of doubly charged ions which would result in greater damage to the film. For a given energy the smaller stopping distance for argon ions results in a larger energy dissipation per unit length and consequently more damage to the growing film. Small atomic size could also be important in causing less structural deformation. There is a higher probability for clusters of atoms to be sputtered with argon [15] which could result in film inhomogeneity and also lead to lower doping efficiency as compared to the case of neon sputtering [16,17].

Finally, the effect of magnetic field needs to be assessed and, although this feature is again common to both gases used in our system, the effectiveness of this constraint will be different in the two cases.

ACKNOWLEDGEMENT

The authors are grateful to Mr. J.Sullivan and Mr. A.Abbot for their assistance in the XPS measurements. Also the technical assistance of Mr. R.S.Bassi is highly appreciated. One of the authors (YZ) would like to acknowledge the receipt of a grant from SERC.

REFERENCES

[1] For example, E.A.Davis, in Topics in Applied Physics, ed M.H.Brodsky, Springer-Verlag, Vol. 36, 41, (1979)
[2] W.E.Spear and P.G.LeComber, Solid State Commun., 17, 1193, (1975)
[3] W.Paul, A.J.Lewis, G.A.N.Connell and T.D.Moustakas, Solid State Commun., 20, 969, (1976)

[4] H.Fritzsche, M.Tanielian, C.C.Tsai and P.J.Gaczi, J. Appl. Phys., 50, 3366, (1976)
[5] T.D.Moustakas, D.A.Anderson and W.Paul, Solid State Commun., 23, 155,(1977)
[6] C.C.Tsai, H.Fritzsche, M.H.Tanielian, P.J.Gaczi, P.D.Persans and M.A.Vesaghi, Proc. 7th Inter. Conf. on Amorphous and Liquid Semiconductors, ed. W.E.Spear, University of Edinburgh Press, p339, Edinburgh (1977)
[7] R.W.Fane, J.Phys. D: Appl. Phys., 14, L113, (1981)
[8] N.F.Mott and E.A.Davis, Electronic Processes in Non-Crystalline Materials (Clarendon Press, Oxford) (1979)
[9] W.T.Pawlewicz, J. Appl. Phys., 49, 5595, (1978)
[10] N.Van Dong, J. De Physique, 42, 647, (1982)
[11] T.Shimizu, M.Kumeda, I.Watanabe and K.Kamono, Jap. J. Appl. Phys., 18, 1923, (1979)
[12] For example, T.Shimizu, M.Kumeda, I.Watanabe and Y.Kiryama, Jap. J. Appl. Phys., 19, L235, (1980)
[13] D.G.Simons, C.R.Growe and M.D.Brown, J. Appl. Phys., 53, 3900, (1982)
[14] W.K.Chu, J.W.Mayer and M.A.Nicolet, Backscattering spectroscopy, Academic Press, New York (1978)
[15] G.K.Wehner and G.S.Anderson, in Handbook of Thin Film Technology, eds. L.I.Maissel and R.Glang, McGraw-Hill Book Company, ch. 3, New York (1970)
[16] For example, R.W.Fane and Y.Zaka, J. Non-Cryst. Solids, 57,1,(1983)
[17] R.W. and S.A.Abo-Namous, J. Phys. C: Solid State Phys., 16, 1621, (1983)
[18] S.A.Abo-Namous, Y.Zaka and R.W.Fane, Physica Status Solidi (a), 79, 477, (1983)

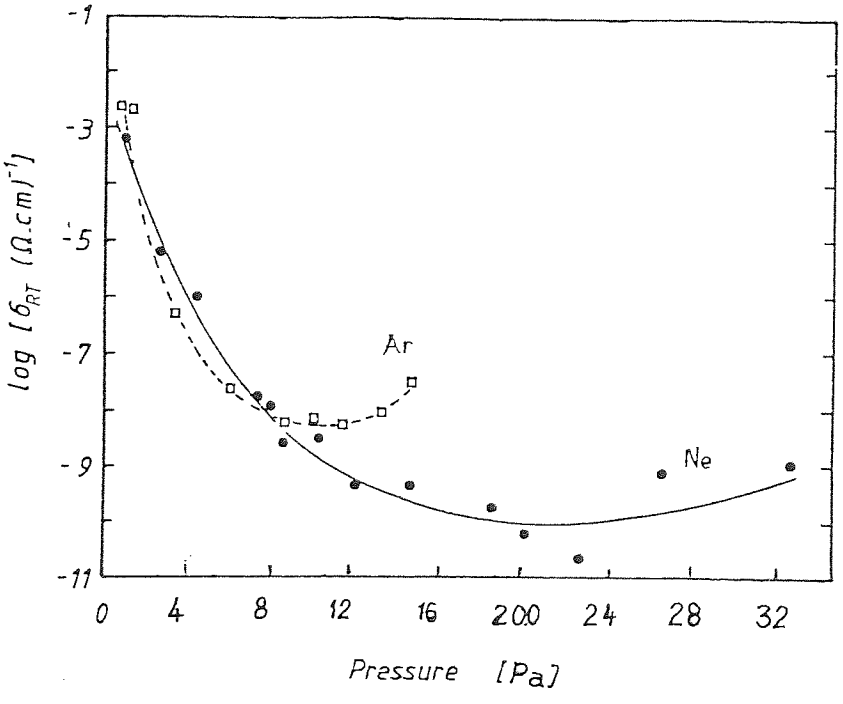

Fig. 1: The room-temperature conductivity, σ_{RT}, as a function of sputtering pressure.

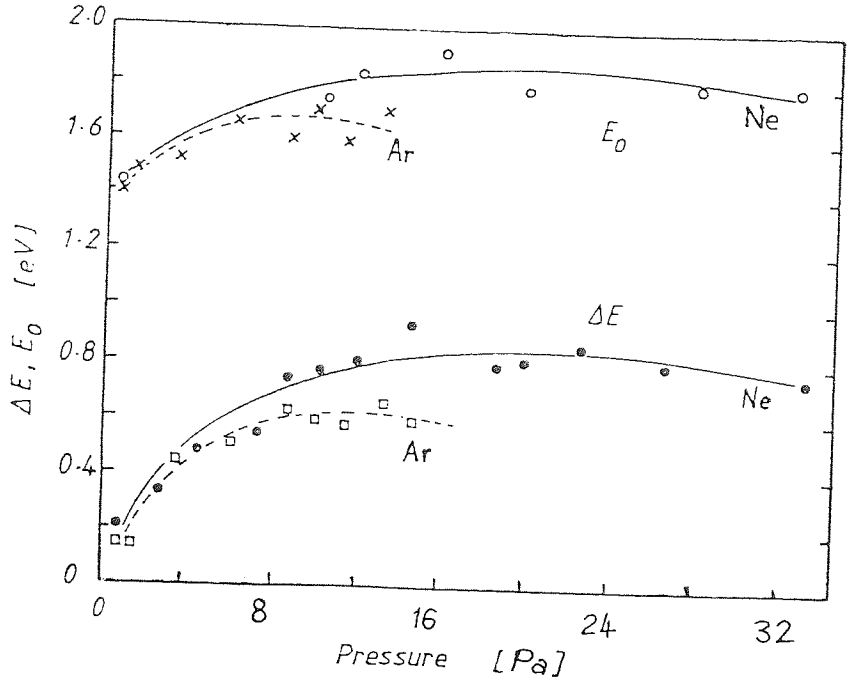

Fig. 2: The variation of thermal activation energy, ΔE, and the optical gap, E_o, with sputtering pressure.

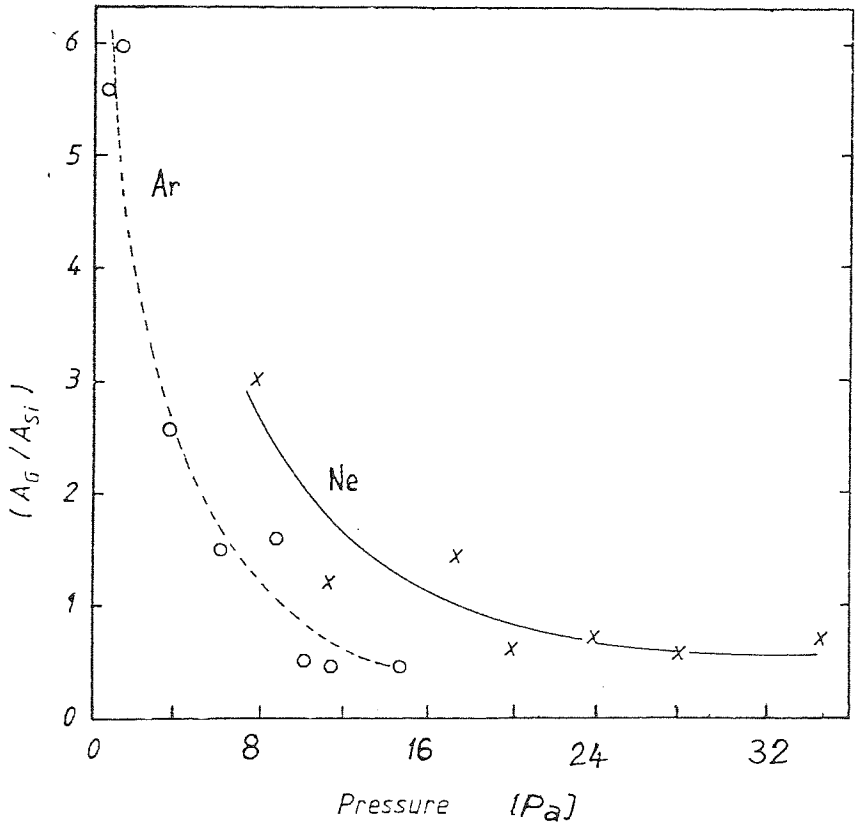

Fig. 3: The ratio of argon and neon to silicon atoms in the film as a function of sputtering pressure.

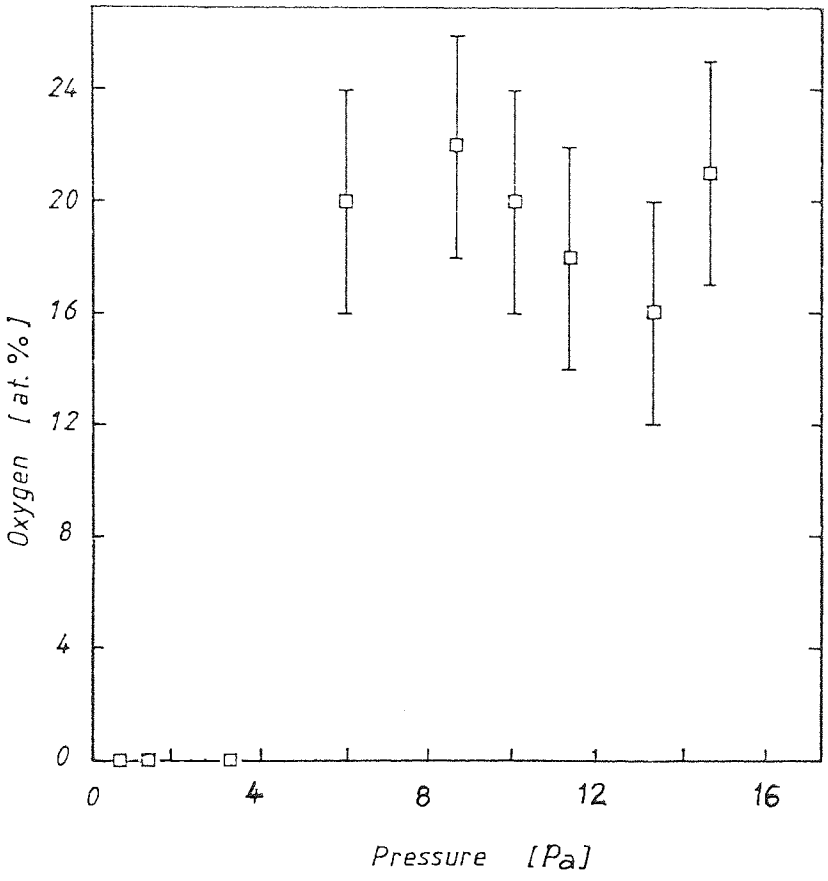

Fig. 4: Concentration of oxygen in argon-sputtered films as a function of sputtering pressure.